

E-Tattoos: Toward Functional but Imperceptible Interfacing with Human Skin

Published as part of *Chemical Reviews virtual special issue "Wearable Devices"*.

Hongbian Li, Philip Tan, Yifan Rao, Sarnab Bhattacharya, Zheliang Wang, Sangjun Kim, Susmita Gangopadhyay, Hongyang Shi, Matija Jankovic, Heeyong Huh, Zhengjie Li, Pukar Maharjan, Jonathan Wells, Hyoyoung Jeong, Yaoyao Jia, and Nanshu Lu*

Cite This: *Chem. Rev.* 2024, 124, 3220–3283

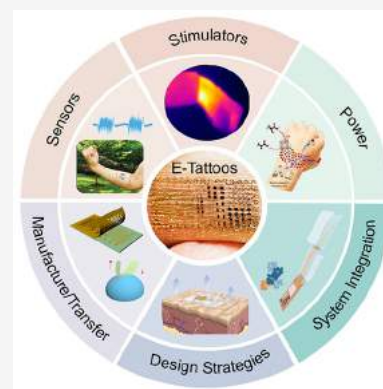
Read Online

ACCESS |

Metrics & More

Article Recommendations

ABSTRACT: The human body continuously emits physiological and psychological information from head to toe. Wearable electronics capable of noninvasively and accurately digitizing this information without compromising user comfort or mobility have the potential to revolutionize telemedicine, mobile health, and both human–machine or human–metaverse interactions. However, state-of-the-art wearable electronics face limitations regarding wearability and functionality due to the mechanical incompatibility between conventional rigid, planar electronics and soft, curvy human skin surfaces. E-Tattoos, a unique type of wearable electronics, are defined by their ultrathin and skin-soft characteristics, which enable noninvasive and comfortable lamination on human skin surfaces without causing obstruction or even mechanical perception. This review article offers an exhaustive exploration of e-tattoos, accounting for their materials, structures, manufacturing processes, properties, functionalities, applications, and remaining challenges. We begin by summarizing the properties of human skin and their effects on signal transmission across the e-tattoo-skin interface. Following this is a discussion of the materials, structural designs, manufacturing, and skin attachment processes of e-tattoos. We classify e-tattoo functionalities into electrical, mechanical, optical, thermal, and chemical sensing, as well as wound healing and other treatments. After discussing energy harvesting and storage capabilities, we outline strategies for the system integration of wireless e-tattoos. In the end, we offer personal perspectives on the remaining challenges and future opportunities in the field.



CONTENTS

1. Introduction	3221	3.3.2. Cut-and-Paste	3233
2. Properties of Human Skin and Desirable Properties of E-Tattoos	3225	3.3.3. Printing Methods	3233
2.1. Skin Structure	3225	3.3.4. On-Skin Fabrication	3234
2.2. Mechanical Properties	3225	3.3.5. Laser Engraving	3234
2.3. Physiological Properties	3225	3.3.6. Electrospinning	3234
2.4. Electrical Properties	3225	3.4. Transfer-on-Skin Technologies of E-Tattoos	3234
2.5. Thermal Properties	3226	3.4.1. Transfer Printing	3235
2.6. Optical Properties	3226	3.4.2. Tattoo-Paper-Assisted Transfer	3235
2.7. Acoustic Properties	3226	3.4.3. Medical-Patch-Assisted Transfer	3235
3. Materials, Design, Manufacture, and Transferring Technologies of E-Tattoos	3227	3.4.4. Substrate-Free Transfer	3235
3.1. Materials for E-Tattoos	3227	4. E-Tattoo Sensors	3236
3.2. Design Strategies of E-Tattoos	3228	4.1. Biophysical Sensors	3238
3.2.1. Stretchability	3228	4.1.1. Biopotential Recording Electrodes	3238
3.2.2. Adhesiveness	3230		
3.2.3. Breathability	3231		
3.3. Manufacturing Technologies of E-Tattoos	3233		
3.3.1. Microfabrication	3233		

Received: September 1, 2023

Revised: January 17, 2024

Accepted: February 8, 2024

Published: March 11, 2024



4.1.2. Bioimpedance Sensors	3241
4.1.3. Strain Sensors	3243
4.1.4. Pressure Sensors	3246
4.1.5. Photodetectors and Displays	3248
4.1.6. Temperature Sensors	3251
4.2. Biochemical Sensors	3253
4.2.1. Body Fluid Analysis	3253
4.2.2. Wound Sensing and Treatment	3256
5. E-Tattoo Stimulators	3256
6. E-Tattoos for Energy Harvesting and Storage	3258
6.1. Energy Harvesting E-Tattoos	3258
6.1.1. Triboelectric Nanogenerators	3258
6.1.2. Piezoelectric Nanogenerators	3260
6.1.3. Biofuel Cells	3260
6.1.4. Thermoelectric Energy Harvesting	3260
6.1.5. Photovoltaic Cells	3260
6.1.6. Wireless Energy Harvesting	3260
6.2. Energy Storage E-Tattoos	3262
6.2.1. Rechargeable Batteries	3262
6.2.2. Supercapacitors	3262
7. System Integration of E-Tattoos	3262
7.1. Integration of Components	3262
7.2. Encapsulation	3263
8. Challenges and Prospects	3264
Author Information	3266
Corresponding Author	3266
Authors	3266
Author Contributions	3266
Notes	3267
Biographies	3267
Acknowledgments	3268
Abbreviations	3268
References	3268

1. INTRODUCTION

The human body continuously emits electrical,¹ mechanical,² thermal,³ optical,⁴ and chemical information⁵ through the skin. Some unique properties of the skin, such as electrical conductivity and sweat secretion, facilitate the transmission of certain signals, e.g., electrical and chemical signals, respectively, while other properties of the skin pose challenges that must be overcome.² For example, the roughness, hairiness, and stretchiness of the skin are obstructive to the establishment of stable interfaces between devices and the skin. This barrier must be overcome for noninvasive yet accurate collection of signals from various internal systems of the human body, including the brain,⁶ heart,⁷ muscles,⁸ blood vessels,⁹ and tissues under the skin.¹⁰ Many of these signals are already measurable by state-of-the-art wearable devices, which are also capable of signal processing and wireless transmission.^{11,12} The digitization of the human body through wearable technologies can potentially revolutionize many different fields.¹³ In healthcare, disease management, prediction, and prevention have reached new heights by leveraging wearables.^{14,15} In fitness tracking and physical training, wearables are widely used for movement quantification¹⁶ and injury mitigation.¹⁷ In human-machine interface, digitized human motions or intentions can be used to control prosthetics or robots.^{18,19} In addition, wearable technologies are also transforming the fashion²⁰ and beauty industries.²¹

Traditional skin-interfaced medical devices typically require expert operation and are bulky and expensive, and thus they are

incompatible with at-home or ambulatory monitoring. Commercial wearable electronics such as smart watches, smart glasses, and headbands have been developed for monitoring human motion, heart rate, blood oxygen saturation, temperature, and brain activity in everyday life.²² However, as they rely on rigid hardware, motion artifacts and skin chafing are prominent challenges due to the mechanical mismatch with the soft human skin.²³ Additionally, the bulkiness, discomfort, and lack of self-adhesiveness of current commercial products limit their application to specific anatomical locations such as the wrist and forehead. This limitation severely restricts the types of acquired signals and prevents the comprehensive digitization of the human body. To overcome these obstacles, wearable electronics with thin film sensors and circuits fabricated on thin and flexible polymer substrates have been developed. These devices exhibit a significantly improved device–skin interface and signal quality when compared to conventional wearables, as summarized in several recent review papers.^{11,18,24–26} However, there are still some gaps to fill when interfacing these devices with human skin. Specifically, the epidermis is microscopically rough and hairy and therefore, moderately thin and soft wearable electronics have limited conformability to human skin at the microscale.²⁷ In addition, the mechanical mismatch between these polymer substrates and soft skin can prevent these polymer substrates from perfectly matching the deformation of the skin. As a result, the skin–device interface can be easily disturbed by motion, resulting in unreliable signals, particularly in ambulatory settings. Generally, these devices require medical tapes or additional adhesives to attach to the skin, limiting the breathability and deformability of the skin.

Electronic tattoos (e-tattoos), also known as epidermal electronics, present a class of ultrathin and ultrasoft wearable electronics that can conform well to the skin surface without obstructing skin deformation (Figure 1).²⁸ The conformable

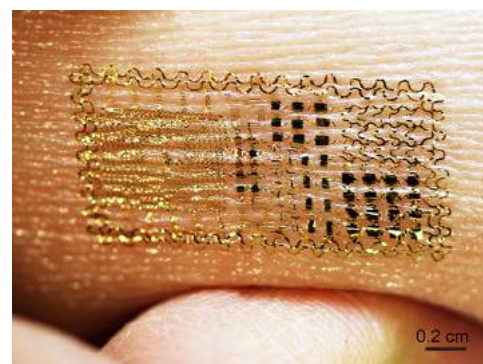


Figure 1. First e-tattoo ever created can conform to the microscale surface textures of human skin. This innovative device features multimodal sensing, wireless charging, and light-emitting diode (LED) signaling capabilities. Copyright attribution is due to Prof. John A. Rogers.

interface with human skin is a unique feature that differentiates e-tattoos from other forms of wearable electronics.^{28–32} It enables better electrical, thermal, optical, deformation, and mass transfer across the skin–tattoo interface; it suppresses detachment and minimizes relative motion between the skin and the e-tattoo, reducing motion artifacts during skin deformation; it does not affect natural skin functionalities such as deformation or touch sensation. Since Rogers group reported the first e-

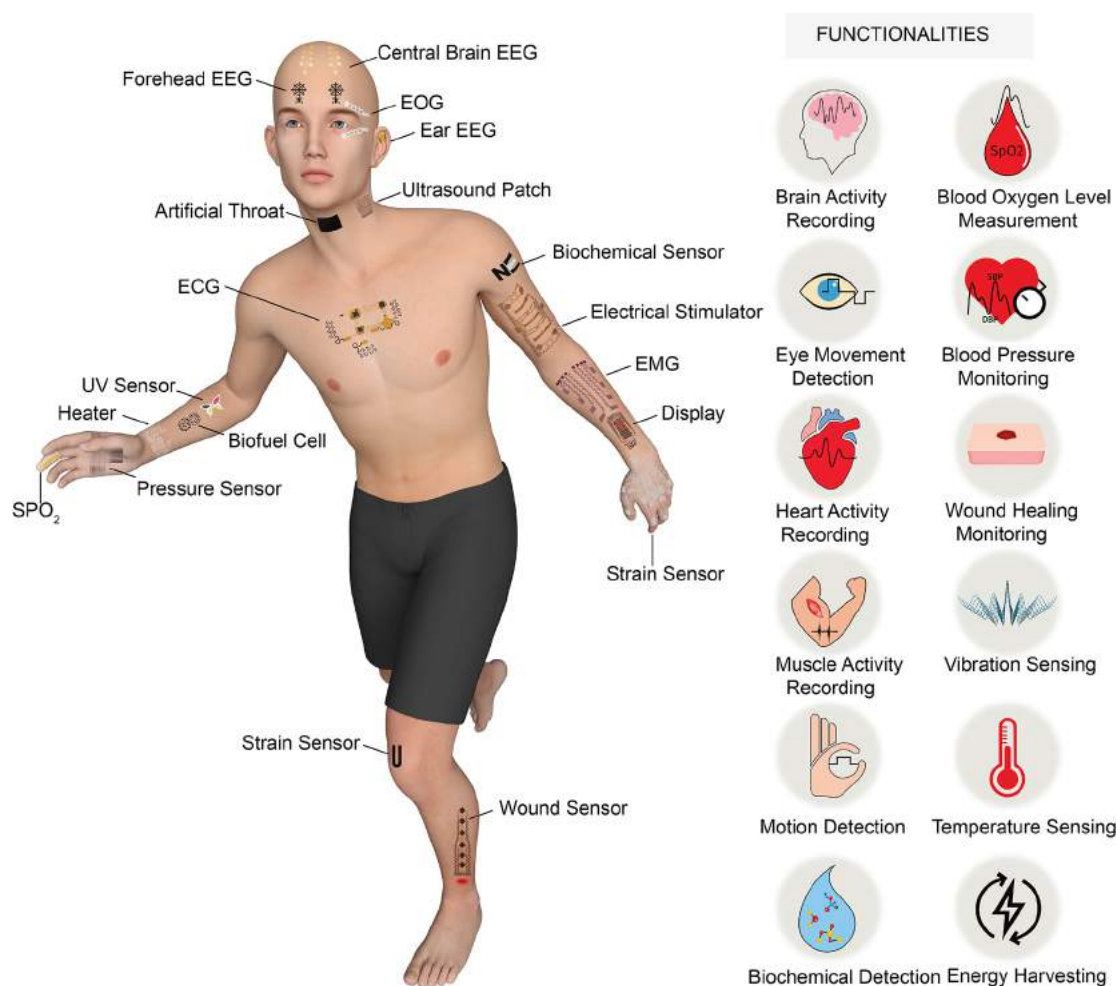


Figure 2. A variety of e-tattoos displayed on different anatomical locations of human skin, each showcasing its unique functionality.

tattoo in 2011,²⁸ a range of e-tattoos with diverse functionalities have been developed and applied to various anatomical locations, with representative examples depicted in Figure 2.

Over the past 13 years, the field of e-tattoos has witnessed significant advancements in materials and properties, thereby enabling a broad spectrum of applications (Figure 3). The first generation of e-tattoos mainly utilizes noble metals as electrical materials.²⁸ While being highly conductive and chemically inert, these noble metals have high cost and poor intrinsic stretchability. Consequently, various soft conductive materials have emerged. Carbon-based nanomaterials and nanocomposite particles³³ have been extensively explored. Similarly, silver nanoparticles and nanowires have been widely used in e-tattoos.³⁴ Conducting polymers, represented by poly(3,4-ethylenedioxythiophene) polystyrenesulfonate (PEDOT:PSS),³⁵ and semiconducting rubbery electronic composites³⁶ have been successfully integrated on e-tattoos. Hydrogels have also emerged as a promising material for e-tattoos owing to their combined conductivity, softness, and adhesion to human skin.³⁷ Two-dimensional (2D) semiconductors, such as MoS₂, have been successfully used for submicrometer-thick e-tattoos.³⁸ Liquid metal has also been utilized for e-tattoos with proper encapsulation.³⁹ These new materials have enabled e-tattoos to achieve more skin-synergistic or skin-mimetic properties than just conformability,²⁸ such as imperceptibility,⁴⁰ breathability,⁴¹ self-adhesivity,⁴² self-healing,⁴³ noninterference with touch,⁴⁴ and even living.⁴⁵ Moreover, advanced properties that surpass

the natural functionalities of skin, such as antibacterial capability,⁴⁶ have been incorporated into e-tattoos. These enhanced characteristics have enabled new unique applications for e-tattoos. Initial e-tattoos served as an integrated platform for biopotential recording, temperature monitoring, strain sensing, and skin heating.^{28,47} Chemical sensing of different biomarkers³³ and energy harvesting with chemical reactions with sweat⁴⁸ were introduced with the advent of carbon-based e-tattoos with large surface area. Wound sensors⁴⁹ were implemented by monitoring changes in the thermal properties of the skin with e-tattoos. E-Tattoos have since advanced from just sensing to also providing therapeutics through drug delivery⁵⁰ and electrical stimulation.⁵¹ With advancements in optical materials and device structures, e-tattoo-based display platforms have been realized.⁵² From the first e-tattoo strain sensor introduced in 2011 to the first e-tattoo pressure sensor introduced in 2018,⁵³ e-tattoos can provide mechanical sensation just like the skin. A breakthrough e-tattoo ultrasonic device was developed for wearable imaging of central blood pressure waveforms.⁵⁴ A chip-less surface acoustic wave (SAW) sensor array was also developed to monitor human glucose concentrations, blood pressure, heart rate, and activities, and transmit signals wirelessly.⁵⁵ As the development of new materials and properties continues, the range of applications uniquely achievable with e-tattoos continues to expand.

In this article, we provide a comprehensive review of e-tattoos, covering materials, structures, manufacturing, skin interfacing,

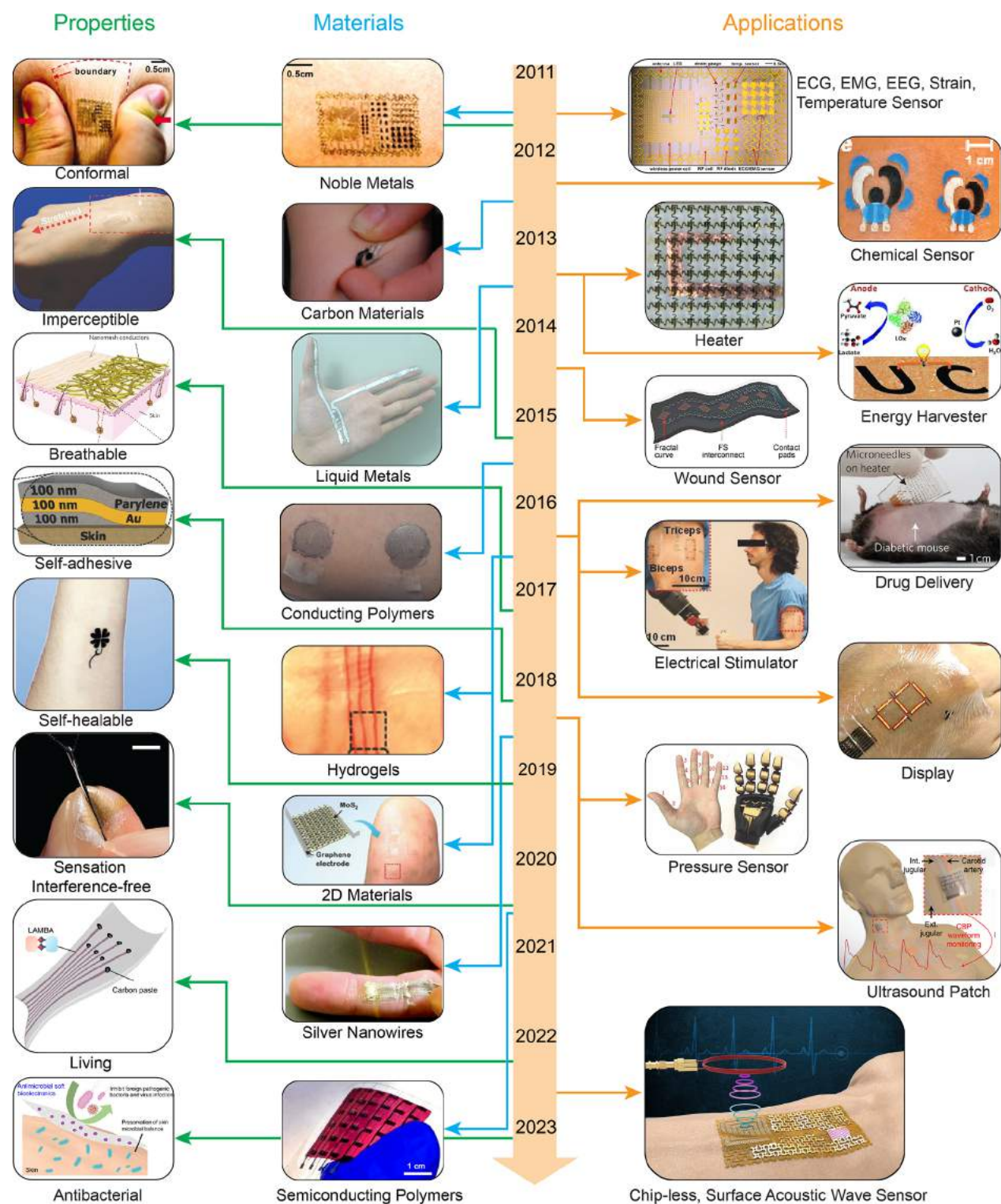


Figure 3. A chronological overview of the evolution of e-tattoos, highlighting advancements in materials, properties, and applications. Materials: Reproduced with permission from refs 28, 33–39. Copyright 2011, 2021 AAAS; 2015, 2016, John Wiley and Sons; 2018, MDPI; 2012, 2019 Royal Society of Chemistry; 2013 The Public Library of Science. Properties: Reproduced with permission from refs 28, 40–46. Copyright 2011, 2020, 2023 AAAS; 2017, 2022 Springer Nature; 2015, 2018, 2019 John Wiley and Sons. Applications: Reproduced with permission from refs 28, 33, 47–55. Copyright 2011, 2016 AAAS; 2012 Royal Society of Chemistry; 2013, 2014, 2016, 2018 John Wiley and Sons. The copyright for the chip-less, wireless, surface acoustic sensor is attributed to Professor Jeehwan Kim.

functionalities, and system integration. We first discuss how the diverse properties of human skin can act as either obstacles or facilitators for sensing and stimulation. Subsequently, we summarize the materials, structures, manufacturing, and transfer

processes used in e-tattoos that provide the requisite stretchability, functionality, breathability, and adhesiveness to overcome this barrier. Following this, we discuss the applications of e-tattoos in different sensing and therapeutic modalities, as

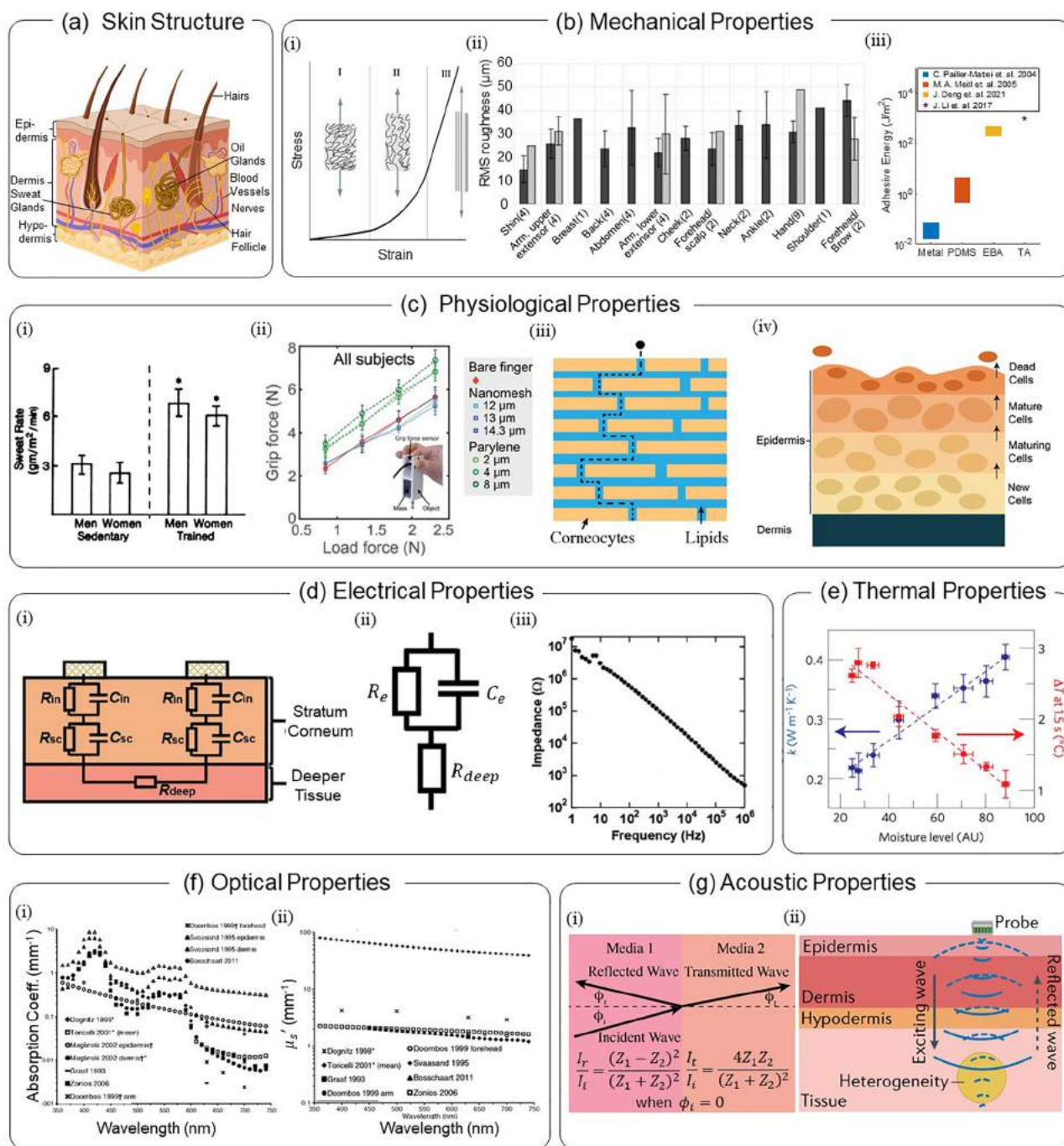


Figure 4. Summary of basic properties of human skin. (a) Schematic of human skin structure, showing its rough surface, layers (epidermis, dermis, and hypodermis), sweat glands, and hairs. Created with [BioRender.com](#). (b) Mechanical properties: (i) stress–strain curve; (ii) root-mean-square (RMS) roughness at different body anatomical locations; (iii) compiled data of the adhesion energy between skin and various materials (metal,⁶⁵ polydimethylsiloxane (PDMS),⁶⁸ electrical bioadhesive (EBA),⁶⁹ and slug-inspired tough adhesive (TA)).⁷⁰ (i) and (ii) Reproduced with permission from refs 61 and 64. Copyright 2001 Elsevier and 2010 IntechOpen. (c) Physiological properties: (i) typical sweat rate at rest and during exercise; (ii) gripping force versus object weight for bare finger and finger attached with nanomesh, and parylene thin films with various thicknesses; (iii) cross-sectional structure of stratum corneum illustrating its limited water permeability; (iv) schematic of epidermal cell turnover. (i) and (ii) Reproduced with permission from refs 44 and 74. Copyright 2020 AAAS and 1988 The American Physiological Society. (d) Electrical properties: (i,ii) equivalent circuit for impedance measurement and its simplified model; (iii) frequency-dependent skin impedance. Reproduced with permission from ref 84. Copyright 2020 John Wiley and Sons. (e) Thermal conductivity as a function of moisture level. Reproduced with permission from ref 47. Copyright 2013 Springer Nature. (f) Optical properties: (i) light absorption coefficient; (ii) scattering coefficient at different wavelengths of light. Reproduced with permission from ref 85. Copyright 2013 Institute of Physics and Engineering in Medicine and 2012 SPIE. (g) Acoustic properties: (i) acoustic impedance and its effect on acoustic wave reflection and transmission; (ii) schematic of ultrasound probing subcutaneous tissue. Reproduced with permission from ref 89. Copyright 2022 Springer Nature.

well as their use in displays and energy harvesting or storage. We then discuss how e-tattoos can be integrated into wireless and

long-term systems. Finally, we summarize the current challenges and prospects of e-tattoos for imperceptible, smart, and comprehensive digitization of the human body.

2. PROPERTIES OF HUMAN SKIN AND DESIRABLE PROPERTIES OF E-TATTOOS

2.1. Skin Structure

Human skin consists of three layers from the outermost to the innermost: the epidermis, dermis, and hypodermis (Figure 4a).⁵⁶ This unique structure defines a multitude of properties and functions of human skin, necessitating meticulous consideration in the design of e-tattoos. For example, the outermost epidermis, which is in direct contact with e-tattoos, has a microscopically rough surface and is often covered by hair. Therefore, e-tattoos should be designed to conform to the microscale surface textures of the skin to maximize the skin–tattoo contact area. The dermis has various structures and cells, including blood vessels, nerves, and sweat glands, which can be interrogated mechanically, thermally, optically, electrically, and chemically by e-tattoos. The hypodermis, also known as the subcutaneous layer, contributes to the mechanical and physiological properties of the skin.

2.2. Mechanical Properties

The Young's modulus of human skin, indicative of its stiffness, varies greatly from 1 kPa to 1.12 MPa, depending on the anatomical location and the individual's age.^{57,58} Additionally, the skin is stretchable, as characterized by a three-stage stress–strain curve (Figure 4b-i).^{59–61} During daily activities, the skin can undergo strains up to 50%.³¹ Therefore, two primary mechanical requirements for the e-tattoo upon adhesion to the skin are as follows: it should be capable of enduring skin deformation without any fractures or delamination to ensure its functionality, and it should impose minimal mechanical constraints on the skin to ensure comfort during daily wear. When no delamination is considered, naively, the e-tattoo should match the modulus and stretchability of the skin. However, when an e-tattoo is comprised of stiff devices placed over a soft substrate, the soft substrate could limit the strain transfer from the skin to the device due to so-called shear lag effects. In this case, the stretchability of the device does not necessarily need to reach 50%, nor does its modulus have to be as low as that of the skin.^{62,63} To avoid delamination, a simple energy-based argument is that the total elastic energy of the e-tattoo and the skin cannot exceed the work of separation of the tattoo–skin interface. The elastic energy of an e-tattoo consists of both bending energy and membrane energy. The bending energy of an e-tattoo is proportional to its flexural rigidity which scales with Eh^3 , whereas the membrane energy of an e-tattoo is proportional to its tensile rigidity, Eh , where E is the Young's modulus of the e-tattoo and h is the thickness of the e-tattoo. As a result, e-tattoos should be sufficiently soft and thin to avoid delamination under skin deformation. At the microscale, skin surfaces are not smooth, with the valleys and ridges varying between 10 and 100 μm . Similar to skin modulus, the roughness of the skin depends on the anatomical location and age of the individual (Figure 4b-ii).⁶⁴ To achieve accurate sensing or efficient stimulation, e-tattoos must establish intimate contact with the rough texture of the skin, a characteristic known as conformability. Several factors govern this conformability, including skin modulus and roughness, the adhesion between the e-tattoo and skin, and the stiffness of the e-tattoo. The adhesion energy between abiotic materials and skin can range

from 0.1 J/m^2 for a skin–metal interface to 1000 J/m^2 for a skin–bioadhesive interface (Figure 4b-iii).^{65–70} 2D plain strain elasticity models have revealed that Ecoflex, with a modulus of 70 kPa, must be less than 7.5 μm in thickness to achieve full conformability with the skin without adhesives. Once Ecoflex exceeds a thickness of 7.5 μm , its conformability can drastically decrease to below 25% due to mechanical instabilities.⁷¹ For a graphene e-tattoo, whose mechanical property is dominated by poly(methyl methacrylate) (PMMA) with a Young's modulus of 2.9 GPa, the critical thickness for full conformability reduces to 510 nm.⁷² When skin deforms, conformability tends to enhance under-skin stretch and reduce under-skin compression.⁷³ While the elasticity models are well established, there is no closed-form solution. In the most simplified view that only the bending energy is considered, the conformability is dictated by e-tattoo flexural rigidity. When the flexural rigidity is high ($>10^{-10}$ $\text{N}\cdot\text{m}$), the device needs additional adhesives to attach to the skin. When the flexural rigidity is low (10^{-12} – 10^{-10} $\text{N}\cdot\text{m}$), the device can adhere to the skin without additional adhesive but may not be able to fully conform to the microscale texture of the skin. When the flexural rigidity of the device is ultralow ($<10^{-12}$ $\text{N}\cdot\text{m}$), it can effortlessly conform to the skin's microscale texture.^{71,73} Achieving full conformity to the microscopic roughness of the skin requires e-tattoos to be submicrometer in thickness, which poses a great challenge in e-tattoo fabrication and skin transfer. In this review, e-tattoos refer to those that can either perfectly or partly conform to the skin surface.

2.3. Physiological Properties

The skin has diverse physiological functions, including thermo-regulation, sensation, protection, self-healing, and self-renewal. This provides opportunities for e-tattoos to digitize the human body while also posing challenges in forming a long-term stable e-tattoo–skin interface for reliable signal recording. For example, the skin regulates body temperature through sweating (Figure 4c-i),⁷⁴ which provides a rich source of chemical biomarkers.^{74,75} However, sweat accumulation can disrupt the device–skin interface, leading to reading failures and irritation during prolonged wear. Therefore, e-tattoos should be designed with breathability to ensure stable signal quality and comfort during long-term wear.^{76–79} Moreover, e-tattoos should be designed not to interfere with the skin's tactile sensing ability enabled by receptors and nerves (Figure 4c-ii).^{44,80} E-Tattoos must also withstand the same environmental conditions that the human body encounters, such as extreme temperature variations, water, and electromagnetic interference. This can be achieved through encapsulation, which will be discussed in detail in section 7.2. The outermost layer of the epidermis is a dense and insulated stratum corneum, serves as a mechanical skin barrier that protects the underlying skin layers and tissues. However, it also poses a significant challenge for transdermal drug delivery (Figure 4c-iii).^{81,82} At last, the epidermis and dermis undergo a renewal process known as turnover every 40–56 days (Figure 4c-iv),⁸³ which limits the duration of e-tattoo use.

2.4. Electrical Properties

The skin is electrically conductive, allowing for the noninvasive and passive recording of various electrophysiological signals, including electroencephalogram (EEG), electrocardiogram (ECG), and electromyography (EMG).¹ Additionally, the bioimpedance of the skin can be actively measured with bioimpedance sensors, providing insights into skin hydration, perspiration, and even blood flow. Parts d-i and d-ii of Figure 4

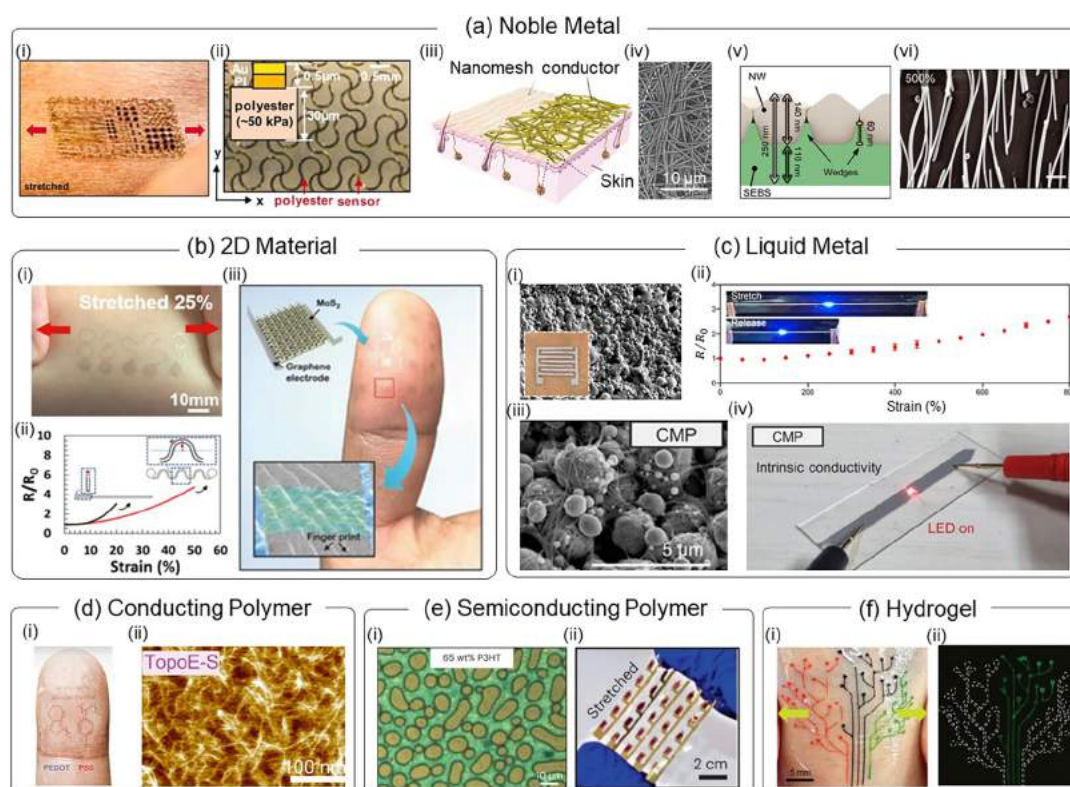


Figure 5. Materials used for e-tattoos. (a) Noble metals: (i) epidermal electronic system with filamentary serpentine-shaped gold nanomembranes for electrophysiological sensing; (ii) the system on human skin under stretching; (iii) schematic of gold nanomesh; (iv) scanning electron microscope (SEM) image showing the stretchability of the gold nanomesh; (v) schematic of the teeth-embedded-in-gum structure of silver nanowires; (vi) SEM image of the silver nanowire film under 500% strain; scale bar: 100 nm. Reproduced with permission from refs 28, 41, 99. Copyright 2011, 2021 AAAS, 2017 Springer Nature. (b) 2D materials: (i) graphene e-tattoo stretched on a skin; (ii) comparison of the stretchability between graphene e-tattoos with straight and serpentine designs; (iii) MoS₂ e-tattoo conforming to the fingerprint ridges. Reproduced with permission from refs 72 and 38. Copyright 2017 American Chemical Society and 2016 John Wiley and Sons. (c) Liquid metal: (i) SEM image of liquid metal particles with a printed e-tattoo on human skin (inset); (ii) electrical resistance changes from 0% to 800% tensile strain; (iii) SEM image of liquid metal particles with platinum-decorated CNTs; (iv) liquid metal e-tattoo lighting up an LED. Reproduced with permission from refs 130 and 132. Copyright 2022 American Chemical Society and 2022 John Wiley and Sons. (d) Conducting polymer: (i) transparent, stretchable PEDOT:PSS e-tattoo on a fingertip; (ii) atomic force microscope (AFM) phase image of the TopoE film post acid treatment. Reproduced with permission from ref 133. Copyright 2022 AAAS. (e) Semiconducting polymer: (i) optical image of bicontinuous P3HT/SEBS film; (ii) stretched P3HT/SEBS transistor array. Reproduced with permission from ref 143. Copyright 2022 Springer Nature. (f) Hydrogel: (i) 3D-printed living hydrogel e-tattoo under stretching; (ii) detection of smeared isopropyl β -D-1-thiogalactopyranoside (IPTG) with the living e-tattoo. Reproduced with permission from ref 151. Copyright 2018 John Wiley and Sons.

depict a typical equivalent circuit and its simplified model for measuring skin impedance with two electrodes placed on the skin.⁸⁴ The skin impedance measured can vary by several orders of magnitude, depending on the frequency at which it is measured (Figure 4d-iii).⁸⁴ The key components include the interface impedance (R_{in} , C_{in}), the impedance of the stratum corneum (R_{sc} , C_{sc}), and the resistance of the deeper tissues (R_{deep}). To achieve a high signal-to-noise ratio, a lower interface impedance, that is, a higher C_{in} and a lower R_{in} , is preferred. Therefore, an e-tattoo electrode with low resistance and high conformability to the skin is crucial for reducing contact impedance and enhancing signal quality.

2.5. Thermal Properties

Skin temperature reflects information associated with blood flow and infection. Additionally, the thermal conductivity of the skin changes with skin conditions (Figure 4e).⁴⁷ Therefore, measurement of the thermal conductivity of the skin allows for monitoring of wound-healing process. To achieve an accurate measurement of temperature and thermal conductivity, the sensing materials of e-tattoos should possess high thermal

conductivity. In addition, the conformal contact of e-tattoos and the skin is essential for efficient heat transfer from the skin to the recording units.

2.6. Optical Properties

The unique optical properties of skin and tissue allow for sensitive detection of various molecules inside the body.^{4,85} The absorption coefficient of different tissues is wavelength dependent (Figure 4f-i),⁸⁵ and different molecules can be characterized by their optical absorption spectrometry. A notable example is oxyhemoglobin and deoxyhemoglobin characterization in pulse oximetry⁸⁶ and near-infrared spectroscopy (NIRS).⁸⁷ While most optical e-tattoos are concerned with absorption changes in tissue, scattering is the dominating optical interaction in tissue (Figure 4f-ii).⁸⁵ Scattering-based methods, including tissue contrast for tumor characterization, have been employed in traditional biomedical devices and hold potential for future incorporation into e-tattoos.⁸⁸

2.7. Acoustic Properties

Traditionally, electrical, thermal, and optical methods are only able to interrogate relatively superficial tissues, with some

notable exceptions like EEG and NIRS. In contrast, ultrasonography offers a direct imaging modality for deep tissues and anatomical structures.⁸⁹ Acoustic impedance is a critical property in ultrasound imaging. Mismatches in acoustic impedances result in the reflection of acoustic waves (Figure 4g-i),⁸⁹ thus enabling the characterization of the anatomical and mechanical properties of deep tissues by detecting the time-of-flight of the reflected waves (Figure 4g-ii).⁸⁹ The skin has an acoustic impedance of approximately 1.53 MRayls.⁹⁰ To maximize the transmission of acoustic energy at the device–skin interface, the acoustic impedance mismatch between the e-tattoo transducers and the tissue should be minimized. Additionally, given that the acoustic impedance of air is nearly 4 orders of magnitude lower than that of tissue, e-tattoos that conform well to the skin can facilitate efficient transmission of the ultrasonic signal.

3. MATERIALS, DESIGN, MANUFACTURE, AND TRANSFERRING TECHNOLOGIES OF E-TATTOOS

To achieve a long-term, imperceptible interface with the skin, e-tattoos must be flexible, stretchable, and breathable. This necessitates a careful material selection and structural design. The ultrathinness of e-tattoos also calls for specialized manufacturing and transfer-on-skin technologies. This section discusses the optimization of e-tattoo characteristics through material and structural choices, as well as the technologies for skin interfacing.

3.1. Materials for E-Tattoos

Materials are essential for e-tattoos to seamlessly integrate onto the human body's soft, curved surfaces and to collect signals.^{91,92} Due to their ultrathin nature, e-tattoos undergo more mechanical deformation during manufacturing and application compared to other wearable electronics. This makes the selection of functional materials crucial. Noble metals, such as gold, are commonly used in e-tattoos due to their high electrical conductivity (4.11×10^7 S/m), corrosion resistance, and biocompatibility.²⁸ Yet, gold is intrinsically stiff and brittle, losing conductivity under strains below 5% due to crack propagation.⁹³ Specific structural designs, such as serpentine structures (Figure 5a-i,a-ii),²⁸ are employed to improve the stretchability of gold films. Noble metal films compromised of nanoribbons (Figure 5a-iii,a-iv)⁴¹ and nanowires⁹⁴ offer increased stretchability, as the microstructures can rotate and align under mechanical strain. These porous structures, coupled with a porous substrate, make e-tattoos permeable to sweat, ensuring stable device–skin interfaces even under sweaty conditions.⁹⁵ Nanocomposites with noble metal fillers embedded in elastomers are also popular in e-tattoos. The elastomers in these nanocomposites help dissipate strain while maintaining the conductivity of the metal fillers.^{96–99} For example, embedding compact-assembled silver nanowires in elastomers creates a teeth-embedded-in-gum structure (Figure 5a-v) that maintains conductivity even under large strains (Figure 5a-vi).⁹⁹ These films exhibit conductivities of 1.03×10^7 S/m along and 3.29×10^6 S/m across the direction of nanowire alignment. Additionally, these films remain highly conductive at strains of 200% in the parallel direction and over 1000% in the vertical direction. This approach presents a promising method for fabricating metal conductors with combined high conductivity and stretchability.

Carbon materials, including carbon micro/nanoparticles, carbon nanotubes (CNTs), and graphene, are highly attractive

for e-tattoos due to their excellent electrical conductivity and mechanical strength.^{100,101} Printed conductive carbon e-tattoos, for instance, are extensively used in detecting biochemicals in sweat.¹⁰² When carbon particles are dispersed in elastomers like PDMS, they can measure strains up to 150%.¹⁰³ CNTs, known for their high conductivity, mechanical strength, chemical stability, and large surface area, are another popular choice. A single-walled CNT (SWCNT) network grown by chemical vapor deposition (CVD) exhibits a conductivity of 2.64×10^4 S/m.¹⁰⁴ Ink-sprayed CNT films show reduced conductivity due to CNT cleavage in preprocessing steps like ultrasonication, which leads to shorter CNTs and more junctions, thereby impeding electron transport.¹⁰⁵ Nevertheless, ink-sprayed CNT films are more popular due to their cost-effectiveness and scalability of fabrication. Graphene, a 2D carbon nanomaterial with atomic thinness and good conductivity, is particularly interesting for submicrometer-thick e-tattoos.^{106–108} Monolayer graphene, with conductivity up to 3×10^6 S/m and transmittance of 97.6%,¹⁰⁹ is ideal for ultrathin, imperceptible e-tattoos.⁷² Graphene has an intrinsic stretchability of up to 25%.¹¹⁰ With a filamentary serpentine design, graphene e-tattoos can remain conductive up to 50% strain (Figure 5b-i,b-ii).⁷² Other 2D materials, such as transitional metal dichalcogenides (TMDs)¹¹¹ and MXenes,^{112–114} have also been explored for e-tattoos.¹¹⁵ For example, monolayer MoS₂ films can conform to fingertip ridges, enabling the mapping of pressure distribution (Figure 5b-iii).³⁸ TMDs like multilayer PtSe₂ and PtTe₂ exhibit metallic behavior, with 6 nm thick PtTe₂ showing a low sheet resistance of only ~ 31 Ω /sq, making it suitable for biopotential recording electrodes.¹¹⁶ However, 2D materials grown by CVD are often expensive and complex to transfer to the skin, potentially affecting electrical properties due to contamination and cracking during the release process.^{117,118} In contrast, liquid-exfoliated 2D materials offer low-cost, scalable fabrication,¹¹⁹ making them suitable for printed electronics in various applications like strain sensing,¹²⁰ biopotential recording,⁴³ chemical sensing,^{50,121} drug delivery,¹²² and energy storage.^{123,124} However, they typically exhibit lower electrical and thermal conductivities than CVD-grown 2D materials due to smaller grain or flake size and defects induced by exfoliation,¹²⁵ limiting their performance in optoelectronics, integrated circuits, and printed circuit boards.

Both noble metals and 2D materials have high Young's moduli, limiting their use in highly stretchable electronics.³¹ In contrast, liquid-phase metals, like gallium and its alloys are intrinsically stretchable due to their fluidity.¹²⁶ EGaIn, the most commonly used liquid metal, exhibits over 500% stretchability and high conductivity of $\sim 10^6$ S/m,^{127,128} along with good biocompatibility and self-healing ability.^{39,46} Liquid metal-based electronics are typically fabricated by injecting and encapsulating the liquid metal into microfluidic channels, leading to a thickness ranging from submillimeter to millimeter.¹²⁹ To fabricate ultrathin printed e-tattoos, liquid metal is sonicated in solvents to form micro/nanoparticles (Figure 5c-i,c-ii).¹³⁰ However, the surfaces of the particles are typically covered with an insulating Ga₂O₃ layer, which impedes electron transmission between particles. Therefore, mechanical activation processes like scrubbing, tensile straining, or chemical etching are required to rupture or remove this oxide layer to enhance the electrical conductivity.¹³¹ A recent study achieved intrinsically conductive liquid metal tattoo circuits by coating liquid metal particles with platinum-decorated CNTs (Figure 5c-iii),¹³² where the platinum nanoparticles induce gallium to

extrude from the insulated Ga_2O_3 layer, forming a continuous conductive layer (Figure 5c-iv). Leakage, a common issue in these e-tattoos due to the fluidity of liquid metals, has been addressed by Xu et al. by incorporating liquid metal micro/nanoparticles into porous polyurethane, significantly reducing leakage through minimizing mechanical deformation.¹⁴⁶

Conducting polymers, such as PEDOT:PSS, are extensively used in e-tattoos for their good electrical conductivity, solution processability, and biocompatibility.¹³³ Notably, PEDOT:PSS exhibits unique electronic-ionic conductivity, which reduces the contact impedance with the skin compared to metals,¹³⁴ making it an ideal choice for biopotential recording electrodes. However, pristine PEDOT:PSS has a conductivity of less than 100 S/m.¹³⁵ This conductivity can be significantly enhanced by introducing dopants such as ethylene glycol (EG), dimethyl sulfoxide (DMSO), polyethylene glycol (PEG), polyethylenimine (PEI), ionic liquids, and deep eutectic solvents.^{136–139} In addition, the stretchability of PEDOT:PSS can be improved by introducing additives like Triton X-100, xylitol, glycerol, and ionic liquids.¹⁴⁰ For example, an ionic liquid-doped PEDOT:PSS exhibited a conductivity of approximately 3.1×10^5 S/m and maintained a conductivity of above 1×10^4 S/m at 600% strain.¹³⁹ However, these additives may wash away in aqueous environments, posing limitations for implantable applications. To address this issue, Jiang et al. developed a photo-cross-linkable dopant termed TopoE, composed of a PEG backbone and PEG methacrylate (PEGMA) functionalized cyclodextrins (Figure 5d-i).¹³³ When blended with PEDOT:PSS and subjected to cross-linking and acid treatment, the resulting film formed interconnected nanofibers (Figure 5d-ii), exhibiting a conductivity of 2.7×10^5 S/m and a stretchability of 150%. The stretching process induced chain alignment, increasing conductivity to 6×10^5 S/m at 100% strain. This development enhances the potential of PEDOT:PSS to possess both mechanical robustness and high conductivity, making it well-suited for use in dynamic biological environments.

Semiconducting polymers, such as poly(3-hexylthiophene-2,5-diyl) (P3HT), are used in various electronic applications, including transistors and photodetectors.^{141,142} P3HT has a Young's modulus of approximately 1 GPa. When it is dispersed in an elastomer matrix with a low Young's modulus, such as polystyrene-*block*-poly(ethylene-*ran*-butylene)-*block*-polystyrene (SEBS), and subsequently spin-coated onto a substrate, a phase separation occurred. This results in the formation of a bicontinuous P3HT/SEBS film (Figure 5e-i) with high mechanical stretchability and carrier mobility (Figure 5e-ii).¹⁴³

Hydrogels are attractive materials for e-tattoos, offering tissue-like compliance (with a Young's modulus in the range of 1–100 kPa), ionic conductivity, and good biocompatibility.^{144,145} They can also be self-adhesive and self-healable, owing to reversible hydrogen bonding and interactions like π - π stacking.¹⁴⁶ However, a significant challenge for the long-term application of hydrogels is their tendency to dehydrate and consequently lose performance over time.¹⁴⁷ To address this issue, various strategies have been explored, such as coating hydrogels with an elastomer layer to serve as a barrier¹⁴⁸ and introducing alcohols or salts to create interpenetrating polymer networks that retain water.¹⁴⁹ For example, a poly(acrylamide-*co*-maleic anhydride) (P(AM-*co*-MAH)) hydrogel treated with glycerol–water solution can retain 70% of its liquid content and maintain mechanical properties after being heated at 60 °C for 24 h.¹⁵⁰ The high mechanical compliance and biocompatibility of hydrogels also render them suitable as scaffolds for cells, leading

to the development of living tattoo devices capable of detecting smeared chemicals on the skin (Figure 5f-i,f-ii).¹⁵¹ Another approach to preserving the mechanical and electrical properties of hydrogels over time involves reducing their water content. In a recent work, Niu et al. developed a poly(vinyl alcohol) (PVA) encapsulated inositol hexakisphosphate (IP6) ionic-conductive elastomer, known as an ionic-tattoo (i-tattoo), which contains only 2.6 wt % water content at a room humidity of 30%.¹⁵² This elastomer maintains its conductivity and stretchability for up to 150 days.

A summary of the electrical and mechanical properties of the materials discussed above can be found in several review papers.^{5,18,31,153} The selection of materials for e-tattoos depends on their intended applications. Gold, with its high conductivity and chemical stability, is well-suited for biopotential recording electrodes,^{28,29,41} temperature sensors,¹⁵⁴ and strain sensors.¹⁵⁵ However, gold films produced via conventional thermal deposition or electron beam deposition methods typically have limited surface areas, leading to low sensitivities in biochemical sensing due to few available functional bonding groups for the target biochemicals. Therefore, an additional coating with high-surface-area materials is required for gold-based e-tattoos in biochemical applications. Carbon nanomaterials, known for their good conductivity and large surface area, are ideal for chemical sensing,¹⁰² biopotential recording,^{43,132} and energy storage in e-tattoos.¹⁵⁶ PEDOT:PSS, notable for its low skin contact impedance, is particularly attractive for biopotential recording e-tattoos¹⁵⁷ and is also suitable for temperature sensing due to its stable response to temperature.¹⁵⁸ Additionally, both carbon nanomaterials and PEDOT:PSS, with their high charge capacity, are suitable for electrical stimulation. Liquid metal, characterized by its high conductivity and intrinsically stretchability, is appropriate for connectors and biopotential electrodes in e-tattoo.^{130,132,159} Hydrogels, known for their softness, self-healing properties, and water retention, hold promise for living e-tattoos and electronics in aqueous biological environments.¹⁴⁴

3.2. Design Strategies of E-Tattoos

Besides rational material selection, achieving skin-mimic properties in e-tattoos relies heavily on their structural design.^{31,160} As discussed in section 2, the softness, stretchability, and breathability of the skin are crucial considerations. The establishment of a conformal and stable interface between the skin and e-tattoos necessitates a high adhesion force, which is achieved through structural engineering, and optimal breathability for long-term wear comfort. The following subsections discuss the design strategies employed to impart stretchability, adhesion, and breathability to e-tattoos.

3.2.1. Stretchability. One common design strategy to enhance e-tattoo stretchability involves introducing wrinkles into functional materials.¹⁶¹ This approach is based on the concept that wrinkles function as mechanical “folds,” enabling materials to accommodate more strain before failure. Several mechanics models predict the stretchability of wrinkled e-tattoos based on wrinkle geometry (e.g., amplitude and wavelength) and material properties of the film and substrate.^{162–165} Various methods have been employed to introduce wrinkles, including transferring prestrained thin films onto an elastomeric substrate,¹⁶⁶ depositing conductive material onto a prestretched elastomer,¹⁶⁷ or inducing surface tension-driven wrinkling through heating.¹⁶⁸ For instance, a gold film on a plasticized silk layer can form micro-sized wrinkles after

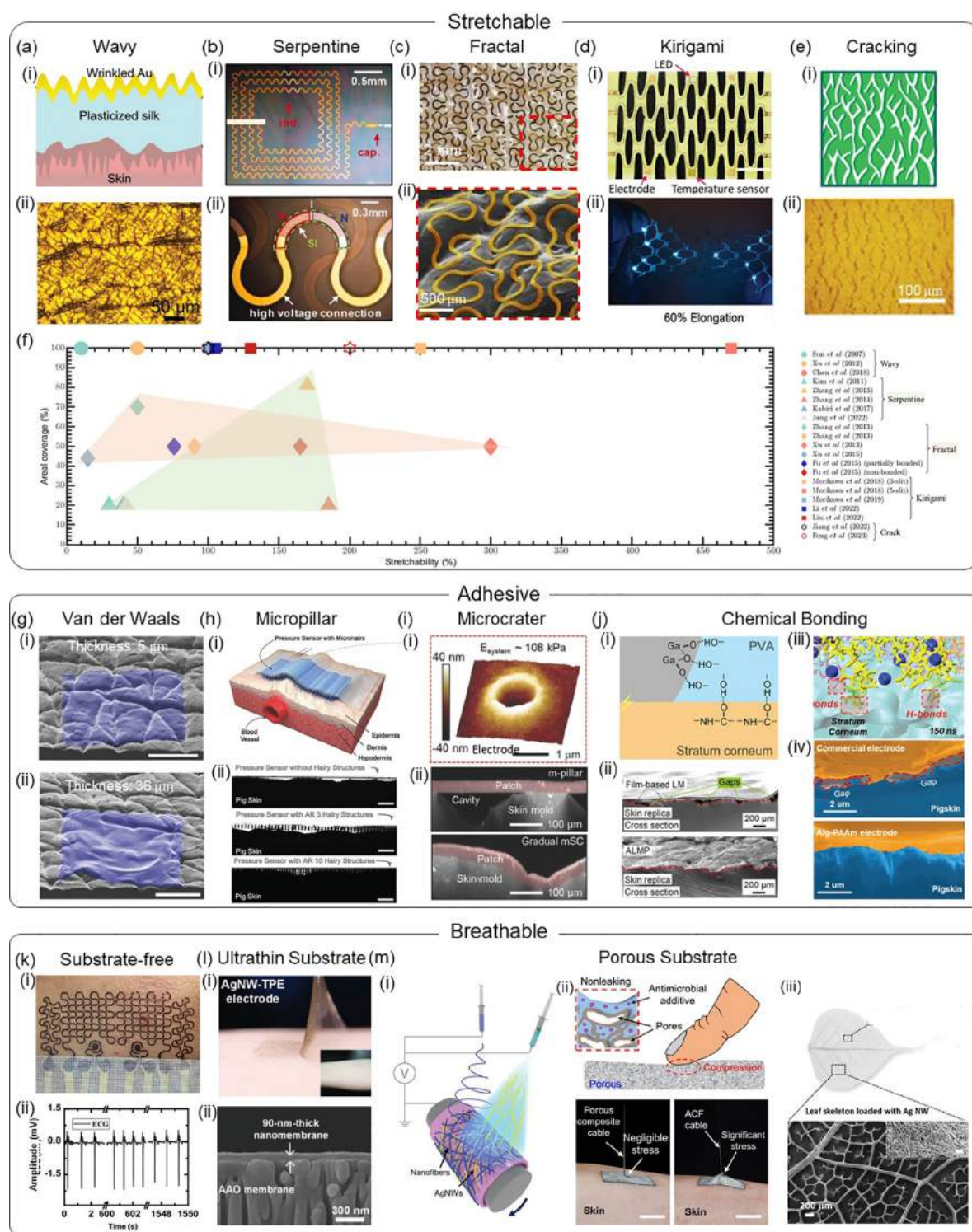


Figure 6. Strategies for achieving stretchability (a–f), adhesiveness (g–j), and breathability (k–m) in e-tattoos. (a) Wrinkled thin films: (i) cross-sectional illustration and (ii) top-down optical image of the wrinkled gold film on plasticized silk under 40% tensile strain. Reproduced with permission from ref 169. Copyright 2018 John Wiley and Sons. (b) Filamentary serpentine design: (i) optical image of a filamentary serpentine inductor connected to a capacitor for radio frequency operation; (ii) optical image of a filamentary serpentine silicon solar cell. Reproduced with permission from ref 28. Copyright 2011 AAAS. (c) Fractal design: (i) optical and (ii) SEM images of Peano-based wires on a skin replica. Reproduced with permission from ref 93. Copyright 2014 Springer Nature. (d) Kirigami design: (i) Kirigami membrane with integrated multifunctional electronics, including LED, bioelectrodes, and temperature sensors, scale bar: 10 mm; (ii) stretched kirigami e-tattoo. Reproduced with permission from ref 182. Copyright 2022 John Wiley and Sons. (e) Engineered cracks: (i) schematic and (ii) optical image of venation-mimicking crack patterns in a stretched gold film. Reproduced with permission from ref 189. Copyright 2023 John Wiley and Sons. (f) An Ashby plot of areal coverage versus stretchability for wavy,^{161,167,169} serpentine,^{28,71,107,172,174} fractal,^{179–181} kirigami,^{182–186} and cracking^{189,190} designs. (g) vdW interactions: SEM images of e-tattoo membranes (blue) with the thickness of (i) 36 μm and (ii) 5 μm placed on a skin replica without added adhesives. Reproduced with permission from ref 191. Copyright 2013 John Wiley and Sons. (h) Micropillared surfaces: (i) schematic of micropillared e-tattoo on the human's neck to detect a pulse;

Figure 6. continued

(ii) cross-sectional images of the micropillared e-tattoos with different aspect ratios attaching to a pig skin, scale bar: 1 mm. Reproduced with permission from ref 193. Copyright 2015 John Wiley and Sons. (i) Microcratered surfaces: (i) 3D AFM image of a miniaturized suction cup; (ii) confocal microscope images showing the cross-section and 3D structure of the contacting interface between a patch with surface miniaturized suction cup array and a skin replica. Reproduced with permission from ref 199. Copyright 2016 John Wiley and Sons. (j) Chemical bonding: (i) schematic of the hydrogen bonding between PVA-functionalized liquid metal and stratum corneum; (ii) comparison of the SEM images between adhesive liquid metal particles on a skin replica and a film-based liquid metal electrode on a skin replica; (iii) molecular interaction simulation depicting the bonding between an adhesive Alg-PAAm hydrogel and the stratum corneum; (iv) comparison between Alg-PAAm–skin interface and commercial electrode–skin interface. Reproduced with permission from refs 130 and 203. Copyright 2022 American Chemical Society and 2020 John Wiley and Sons. (k) Substrate-free design: (i) filamentary serpentine-shaped e-tattoo without substrate; (ii) ECG signals measured under sweating. Reproduced with permission from ref 212. Copyright 2018 Springer Nature. (l) Ultrathin e-tattoos: (i) ultrathin silver nanowire–thermoplastic elastomer e-tattoo applied to human skin and (ii) cross-sectional SEM image of the ultrathin e-tattoo. Reproduced with permission from ref 214. Copyright 2020 John Wiley and Sons. (m) Porous structures: (i) schematic of a nanofiber-reinforced silver nanowire network as a breathable electrode; (ii) breathable and porous liquid-metal elastomer composite; (iii) porous leaf skeleton loaded with silver nanowires. Reproduced with permission from refs 218, 46 and 225. Copyright 2023 AAAS; 2019, 2020 John Wiley and Sons.

hydrating the silk substrate (Figure 6a-i,a-ii),¹⁶⁹ maintaining good electrical conductivity under 100% strain. Other wrinkled films, including graphene,¹⁷⁰ CNT,¹⁷¹ and silver nanowires,¹⁶⁷ also exhibit improved stretchability compared to their planar counterparts. However, it is worth noting that the wrinkled structure may reduce film conductivity due to stress-induced cracks.

Filamentary serpentine designs are more popular for e-tattoos, offering maintained conductivity but greater stretchability compared to linear designs.^{28,71,107,172,173} According to Zhang et al., a nonbonded serpentine copper ribbon can achieve elastic stretchability of up to 50%, facilitated by in-plane rigid rotation and minor out-of-plane buckling.¹⁷⁴ To further enhance stretchability, various mechanics models have been developed to optimize geometric parameters, including aspect ratio, distance between adjacent turns, and crest angle.^{175,176} This design approach has been successfully applied to various e-tattoos, such as interconnected filamentary serpentine inductors and capacitors for efficient radio frequency (RF) operation (Figure 6b-i) and silicon solar cells (Figure 6b-ii).²⁸ Despite these improvements, filamentary serpentine designs still face challenges such as limited areal coverage and difficulties in applications involving miniature devices¹⁷⁷ or a large number of channels.¹⁷²

In contrast to serpentine structures, fractal designs have the potential to enhance both the areal coverage and stretchability of e-tattoos, thanks to their intricate self-similar pattern.^{93,178,179} Parts c-i and c-ii of Figure 6 illustrate a fractal-based structure with repeating Peano layouts that can be scaled to desired dimensions and patterns.⁹³ These fractal designs can withstand strains up to 300% without significant changes in resistance, maintaining structural integrity through multiple stretching and releasing cycles.¹⁸⁰ They distribute stress over a large area, mitigating stress concentration, and enhancing adhesion and signal transport efficiency by increasing the interface area.¹⁸¹ Additionally, fractal designs are scalable, offering high conformability to human skin even at the microscale. However, they come with certain limitations, including a more complex fabrication process, potential challenges in achieving consistent geometries, and nonreusability due to large areas, which may hinder widespread adoption.¹⁸⁰

Kirigami designs, which involve periodic cuts in thin sheets, offer a simpler fabrication process compared to other structural design strategies (Figure 6d-i).¹⁸² Similar to the serpentine design, the kirigami design also enhances stretchability through in-plane rotation and out-of-plane deformation (Figure 6d-ii). Devices with kirigami designs can withstand over 100% strain

without mechanical failure and provide the largest areal coverage among structural design strategies, gaining popularity in stretchable tattoo devices for conductors,¹⁸² sensors,^{183–186} energy storage devices,¹⁸⁷ and displays.¹⁸² However, the cuts in kirigami designs may weaken the material, reducing overall strength and durability.

Cracks have been strategically incorporated into continuous films to enhance their stretchability.^{188–190} For instance, Feng et al. recently developed an ultrastretchable conductor by introducing venation-mimicking cracks into metal films (Figure 6e-i,e-ii),¹⁸⁹ achieving a remarkable stretchability up to 200% through control of defect density and crack patterns. However, several challenges remain, including the precise control of crack patterns during fabrication, structural instability due to cracks, and the suitability of this approach for nonmetal conductive materials such as conducting polymers and hydrogels.

The Ashby plot in Figure 6f provides a comprehensive comparison of different design strategies in terms of areal coverage versus stretchability. While the wavy design provides nearly complete areal coverage within a 100% stretchability range,¹⁶⁹ it requires substrates that increase e-tattoo thickness, potentially compromising adhesion, breathability, and signal transfer. The serpentine design achieves superior stretchability (~185%) but restricts areal coverage to 20%.¹⁷² Despite efforts to enhance coverage to approximately 80% through the adoption of an island-serpentine bridge design, stress concentration at connection points hampers the overall durability.¹⁷⁴ The fractal design provides an average areal coverage of 50–70% with stretchability reaching up to 300% through a complex hierarchical pattern.¹⁸⁰ Kirigami and cracking designs, on the other hand, exhibit the highest areal coverage (~100%) and stretchability (~470%).¹⁸⁶ However, ensuring durability in these designs requires precise control of crack propagation. These trade-offs underscore the need for advanced design strategies to concurrently achieve high areal coverage and stretchability.

3.2.2. Adhesiveness. Ultraconformable e-tattoos achieve full adherence to the human body solely through van der Waals (vdW) interactions.^{28,29,41} However, the strength of these interactions reduces rapidly with an increase in device thickness or stiffness due to reduced contact area between the film and the skin.¹⁸⁸ Figure 6g illustrates this effect, showing that a 5 μm thick e-tattoo fully conforms to a skin replica (Figure 6g-i), while the same material with a thickness of 36 μm only achieves partial conformation (Figure 6g-ii).¹⁹¹ Despite the capability of the ultrathin e-tattoos for full conformal contact, the vdW interactions are relatively weak. For instance, the adhesion

strength of a PDMS/skin interface is 3–9 kPa,¹⁹² and this value may degrade over time.⁷³

To address this issue, researchers have developed surface textures, such as micropillars, to enhance vdW interactions between the e-tattoo and the skin (Figure 6h-i).¹⁹³ Micropillars, which are small hairy structures that conform to the curved surface of the skin, increase contact area, and enhance adhesion compared to a flat geometry (Figure 6h-ii). The adhesion force of micropillars is based on vdW interactions and can be scaled using^{194,195}

$$F_{\text{ad}} \sim \sqrt{A/C}$$

where A is the actual contact area and C is the system compliance in the loading direction. For example, the micropillar structure in a PDMS tattoo can increase its skin contact area to 3.3 times higher than that of a planar device, resulting in an adhesion strength of approximately 10 kPa.¹⁹³ Optimal designs of micropillar tips, such as mushroom-shaped tips, can further increase the contact area, improving adhesion strength to 18 kPa.¹⁹⁶ However, the high aspect ratio of micropillars can lead to buckling, entanglements, and fracture during mechanical deformation.¹⁹⁷ Additionally, the practical limit on achievable adhesion is influenced by manufacturing difficulties and costs when scaling the pillar size down to nanometer level. Furthermore, the interaction between e-tattoos and the skin with vdW force can be easily destroyed by water, posing a challenge for e-tattoos to maintain adhesiveness on wet skin.¹⁹⁸

Microcraters present a promising strategy for enhancing e-tattoo adhesion to the skin in both dry and wet environments (Figure 6i-i,i-ii).¹⁹⁹ In dry environments, microcraters create a robust suction force exceeding that of vdW interactions, preventing e-tattoos from detaching due to mechanical stress. The adhesion strength of microcraters is determined by^{200,201}

$$\sigma_c = \left(1 - \frac{V_1}{V_2}\right) p_0 \frac{A_2}{A_0}$$

which considers the initial projected area (A_0), volume under preload (V_1), inner pressure (p_0), projected area (A_2), and volume preload release (V_2). Studies have shown that the maximum adhesion strength between microcratered surfaces and dry skin can reach 20 kPa.³¹ In wet environments, microcraters enhance e-tattoo adhesion through increased surface tension and wettability, resulting in more effective adhesion compared to flat pads. Specifically, microcraters with protuberances have demonstrated adhesion strengths up to 12 kPa underwater.²⁰²

In addition to vdW interactions, chemical bonding mechanisms like hydrogen bonding and covalent bonding provide stronger adhesion between e-tattoos and human skin due to their higher energy and specificity. E-Tattoos can incorporate compatible functional groups to form hydrogen bonds with the skin, which is abundant in hydroxyl ($-\text{OH}$), carboxyl ($-\text{COOH}$), amine ($-\text{NH}_2$), amide ($-\text{CO-NH}-$), and epoxy ($-\text{O}-\text{CH}_2-\text{CH}_2-\text{O}-$) groups in the epidermis.²⁰³ For instance, the hydroxyl groups on PVA-functionalized liquid metal particles form stable hydrogen bonding with the amide groups on the stratum corneum of the skin (Figure 6j-i),¹³⁰ enabling direct and intimate attachment to the skin even under sweaty conditions (Figure 6j-ii). Elastomers rich in functional groups, such as polydiacetylene-coated PDMS, exhibit significantly higher adhesion energy with the skin (up to 0.5 J/m²) compared to pristine PDMS (up to 0.1 J/m²), making them

promise in adhesive e-tattoos.¹⁵⁹ These adhesive e-tattoos offer advantages over traditional tapes, including improved breathability, flexibility, reduced irritation upon removal, and extended wear time (over 1 month). However, hydrogen bonding is susceptible to water, posing challenges for e-tattoos to maintain stable adhesion underwater. In contrast, covalent bonding provides a stable connection in both dry and wet environments. Dopamine, for instance, can form chemical bonds with tissue proteins (e.g., amino groups), offering a promising adhesive layer for e-tattoos to maintain their performance underwater.²⁰⁴ For example, Ji et al. developed an ionic-conductive dopamine-containing polymer (pDMA), which serves as an adhesive layer for an Au/PDMS electrode, maintaining high adhesion strength (around 1 kPa) underwater and enabling stable ECG recording during swimming.²⁰⁵

Unlike polymeric adhesives with higher Young's modulus, hydrogel adhesives exhibit tissue-like Young's modulus, making them preferable for unobstructive e-tattoos.^{150,206,207} Hydrogel adhesives, with their permeability to water, are suitable for wet environments like wet skin, providing breathability and reducing the risk of skin irritation.²⁰⁸ The multimaterial characteristic of hydrogel adhesives allows for multiple interfacial integration mechanisms, including diffusion-cross-linking⁷⁰ with an adhesion energy up to 1000 J/m² and dry-cross-linking⁶⁹ with an adhesion energy up to 450 J/m². Particularly, the dry-cross-linking interface exhibits an instantly tough bioadhesive with a triggerable benign detachment mechanism. Figure 6j-iii illustrates near instant (150 ns) attachment between an alginate-polyacrylamide (Alg-PAAM) hydrogel adhesive and the stratum corneum, achieving an adhesion force of up to 90 N/m.²⁰³ Therefore, the hydrogel forms a seamless interface with the skin replica (Figure 6j-iv). However, the adhesion strength of the hydrogel may rapidly decrease with the dehydration process, necessitating the use of low-evaporation solvents or operation in a wet environment (e.g., underwater). Additionally, encapsulating the hydrogel surface with other materials, such as elastomers, can reduce water evaporation.

3.2.3. Breathability. The vdW interactions between e-tattoos and the skin can be compromised by sweat secretion, thereby impacting their stable long-term operation. To mitigate this, e-tattoos should prioritize breathability to facilitate moisture evaporation.²⁰⁹ A breathable device typically requires a water vapor transmission rate (WVTR) higher than the perspiration rate of human skin, which is approximately 20 g·m⁻²·h⁻¹ at rest and exceeds 1000 g·m⁻²·h⁻¹ during moderate exercise.²¹⁰

One approach to enhance breathability is adopting a substrate-free design with minimal coverage of e-tattoos on the skin (Figure 6k-i).^{211,212} A substrate-free gold electrode, for instance, enables stable ECG recording without sweat artifacts (Figure 6k-ii).²¹² However, ultrathin e-tattoos often lack mechanical strength, posing challenges for direct skin transfer without a supporting substrate. Another strategy involves reducing the thickness of supporting substrates in e-tattoos, potentially to a submicrometer scale (Figure 6l-i,l-ii).^{213–215} Yet, the WVTR achieved with nanoscale polymer membranes remains below the perspiration rate of human skin during exercise.

Porous materials, including nanofiber mats and nanomeshes, offer a widely used solution for fabricating breathable electronics.²⁰⁹ Nanofiber mats, produced by electrospinning a polymer solution, can incorporate conductive materials like metal nanowires,^{216–219} graphene,^{220–222} CNT,²²³ and liquid

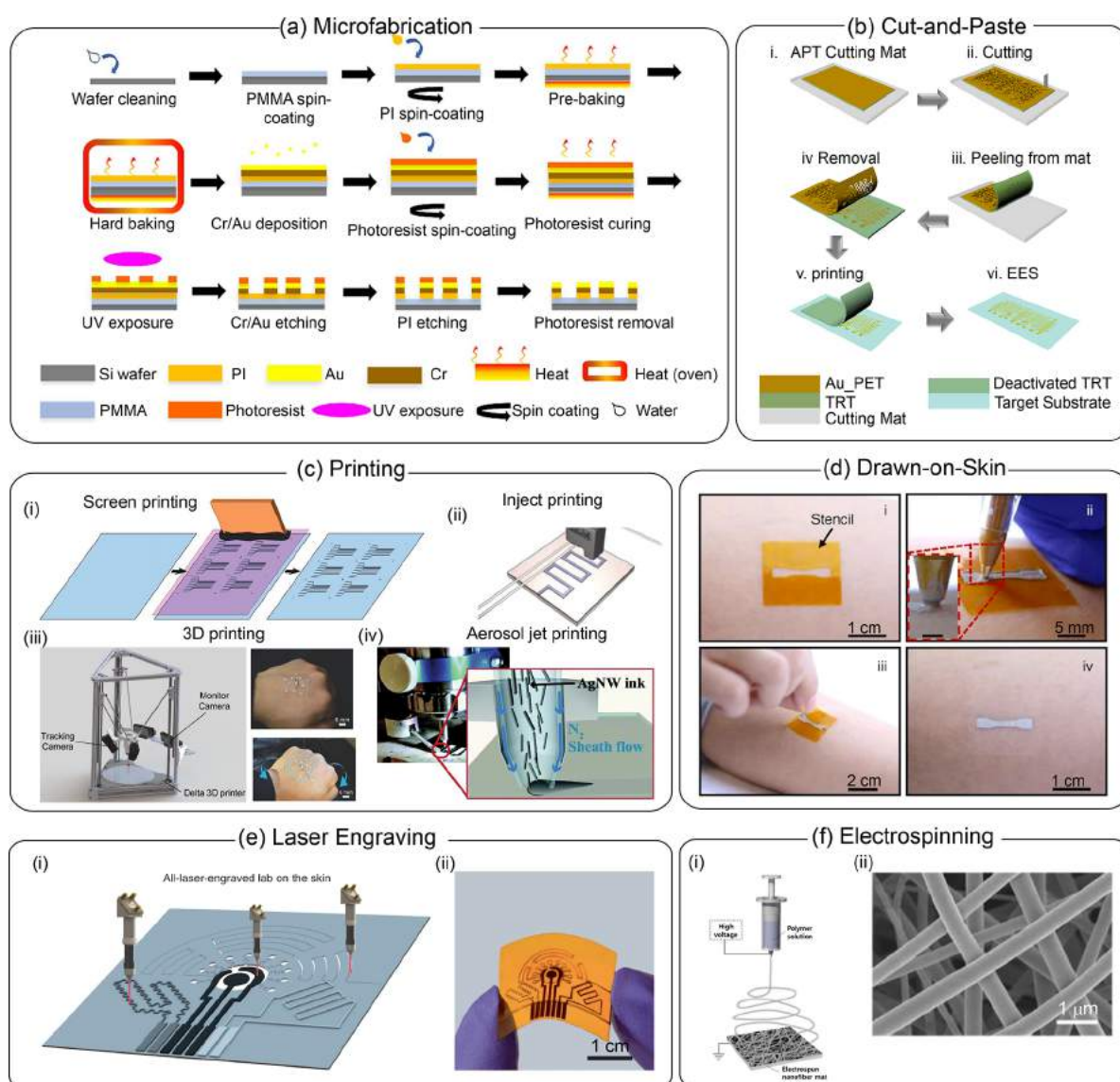


Figure 7. Manufacturing technologies of e-tattoos. (a) Standard microfabrication process for e-tattoos. Reproduced with permission from ref 227. Copyright 2020 American Chemical Society. (b) Schematics illustrating the cut-and-paste manufacturing of e-tattoos. Reproduced with permission from ref 234. Copyright 2015 John Wiley and Sons. (c) Printing e-tattoos: (i) screen printing; (ii) inkjet printing; (iii) 3D printing; (iv) aerosol jet printing. Reproduced with permission from refs 239, 35, 258, and 34. Copyright 2015, 2021, and 2018 John Wiley and Sons; 2019 Royal Society of Chemistry. (d) Drawn-on-Skin (DoS) e-tattoos. Reproduced with permission from 141. Copyright 2020 Springer Nature. (e) Laser engraving e-tattoos: (i) schematic of the laser engraving process; (ii) a multiplexed graphene sensor fabricated by laser engraving. Reproduced with permission from ref 274. Copyright 2020 Springer Nature. (f) Electrospinning process for fabricating porous e-tattoo substrates: (i) schematic of the electrospinning process; (ii) SEM image of an electrospun polymer nanofiber mat. Reproduced with permission from ref 282. Copyright 2016 American Chemical Society.

metal²²⁴ during or after the spinning process. A 125 nm thick epidermal electrode fabricated by simultaneously electrospinning polyamide nanofibers and electrospaying silver nanowires (Figure 6m-i) exhibits minimal hindrance to water vapor transmission due to the large void area in the network.²¹⁸

Another method involves sintering or postetching a composite precursor to create a porous structure. For instance, a porous liquid metal–elastomer composite can be fabricated through mechanical sintering, utilizing phase separation during mixing and curing (Figure 6m-ii).⁴⁶ Alternatively, selective removal of thermoplastic polyurethane (TPU) by water droplets can create a pore array on the substrate, which enhances breathability.⁹⁶ Biomass-derived skeletons, such as leaves and

rose petals, can also work as substrates for loading conductive materials to fabricate breathable e-tattoos (Figure 6m-iii).²²⁵

Innovative design strategies are emerging to develop highly stretchable, adhesive, and breathable e-tattoos for full conformity to the human body. Designers face competing requirements, such as balancing stretchability, conductivity, adhesiveness, and breathability. Wrinkled e-tattoos offer high stretchability but may reduce conductivity due to strain-induced cracks. Chemical bonding enhances adhesiveness, but pain-free detachment is essential. Substrate-free strategies enhance breathability but present potential limitations in fabrication, mechanical durability, and component selection. In conclusion, designers must navigate these trade-offs, balancing thickness for conformability and rupture resistance, size for comfort and

function integration, and adhesiveness for device stability and pain-free removal. The optimal design of an e-tattoo will ultimately depend on the intended use case and desired user experience.

3.3. Manufacturing Technologies of E-Tattoos

Offering unobtrusive, ultraconformal, and comfortable long-term wear on the skin, e-tattoos necessitate unique fabrication strategies that integrate distinctive functional materials and structural designs. These manufacturing methods can be broadly classified into subtractive manufacturing and additive manufacturing. Subtractive manufacturing includes microfabrication and cut-and-paste methods. Additive manufacturing encompasses various printing technologies, Drawn-on-Skin methods, laser engraving, and electrospinning, all of which will be discussed in this section.

3.3.1. Microfabrication. Thanks to decades of development in the semiconductor industry, microfabrication techniques have enabled the design and production of high-resolution electronics (down to sub-10 nm) on silicon wafers with high-throughput mass production.²²⁶ Typical steps in this method include deposition, photolithographic patterning, and etching (Figure 7a).²²⁷ Submicrometer-thick, disposable e-tattoos have been developed using this manufacturing paradigm through precise and intricate patterning and layering of materials. The resulting highly complex tattoo-like devices can be seamlessly integrated with the skin for diverse applications such as health monitoring and drug delivery.^{227–233} Besides silicon, other substrate materials like polyimide (PI), polyethylene terephthalate (PET), and PDMS have also been utilized in the microfabrication of e-tattoos, employing standard metal and metal nanoparticle-based materials, including gold,²²⁷ silver,²²⁸ copper,²²⁹ and gold nanowires.^{230,231} Microfabrication has also proven effective in microfluidics, allowing for precise control of fluid flow for drug delivery and biofluid analysis.^{232,233} However, microfabrication is associated with high costs and necessitates specific electrode materials that are chemically stable under high temperatures, posing challenges in fabricating devices with thermally sensitive and organic solvent-soluble electrode materials.

3.3.2. Cut-and-Paste. In contrast to expensive and time-consuming microfabrication approaches, the cut-and-paste method allows for rapid and low-cost prototyping of large-area e-tattoos. A benchtop programmable cutting machine patterns a planar conductive film with circuit layouts or electrodes. Excess material is then removed, resulting in a stretchable, structurally engineered e-tattoo (Figure 7b).²³⁴ The entire fabrication can be completed in approximately 10 min and is repeatable for integrating multiple layers and materials onto a single substrate. A series of studies have detailed cut-and-paste-based e-tattoos utilizing versatile conductive materials such as graphene and gold on diverse substrates like Tegaderm medical dressing, PVA, PET, and temporary tattoo paper.^{72,107,234–238} The cut-and-paste method holds promise in realizing distinct e-tattoo platforms by incorporating various materials, including carbon-based nanomaterials and fibers, metals, and conductive polymer thin films. As a rapid, cost-effective, and roll-to-roll manufacturing approach, it has the potential to be scalable for future e-tattoo commercialization. However, the cut-and-paste method is challenged by waste generation due to the subtractive fabrication process.

3.3.3. Printing Methods. Solution-processable materials allow the fabrication of tattoo-like electronics through various

printing-based additive manufacturing technologies. The selection of printing methods is based on design complexity, resolution, film thickness, and ink rheological properties. Screen printing, inkjet printing, 3D printing, and aerosol jet printing are conducive to e-tattoo fabrication and will be discussed in the following sections.

3.3.3.1. Screen Printing. Screen printing is a popular contact-based printing method for fabricating e-tattoos by transferring ink through a screen mesh onto the substrate. A squeegee is then used to push the ink through the mesh, creating a predetermined pattern on the substrate (Figure 7c-i).²³⁹ Screen printing typically achieves a resolution of 20–100 μm , depending on ink properties, mesh characteristics, and squeegee specifications.^{240,241} It has been employed for various e-tattoos utilizing materials such as PEDOT:PSS,²³⁹ carbon particles,^{33,242,243} graphene,⁴³ silver nanoparticles,²⁴⁴ silver nanowires,²⁴⁵ and liquid metal.¹²⁸

3.3.3.2. Inkjet Printing. Inkjet printing is a digital, mask-free, noncontact method to release droplets of liquid ink from a printhead onto a substrate to form a specific pattern (Figure 7c-ii).³⁵ It achieves features down to 20 μm resolution. Inkjet printing includes continuous inkjet and drop-on-demand inkjet, each with unique mechanisms. In continuous inject, droplets (typically with a size in the range of 150 μm) are continuously ejected from all nozzles of the printer. A piezoelectric transducer attached to the printhead provides periodic excitation. Once the droplets exit the nozzle, their trajectory is determined and controlled by an electrostatic field, ensuring precise landing on the substrate. In drop-on-demand inkjet printing, a single droplet (with a size as small as 20 μm) is ejected from the printhead only when activated. This printer consists of several injector nozzles in the printhead, and droplets are ejected in parallel to each other with each pulse. Subcategories of drop-on-demand inkjet are defined by the mode used to generate pulses, including acoustic, electrostatic, thermal, and piezoelectric methods.^{246,247} The success of inject printing depends on the rheological properties of the ink, assessed by the ink's Z parameter, defined as the inverse of the Ohnesorge number (Oh), further expressed in terms of the Weber number (We) and Reynolds number (Re). Numerical computations widely accept the optimum range for printing a stable droplet to be $1 < Z < 10$.²⁴⁸ Jetting voltage, drop spacing, stand-off distance, and substrate topography are additional parameters affecting printing success and resolution. Several studies have demonstrated the potential of inkjet printable ultrathin e-tattoos using versatile functional inks comprising PEDOT:PSS,^{35,249,250} silver nanowires,²⁵¹ silver nanoparticles,²⁵² graphene,^{253,254} CNTs,²⁵⁵ and MXene.²⁵⁶

3.3.3.3. 3D Printing. 3D printing technology has transformed personalized wearable manufacturing, enabling on-demand fabrication of tattoo-like sensors tailored to patient-specific geometries. The process begins by creating the printing geometry through computer-assisted design (CAD), followed by 3D scanning of the target substrate. This information is then fed into the printer to generate the resulting e-tattoo structure.²⁵⁷ This process can further be extended to “adaptive 3D printing”, integrating sampled geometric data of the e-tattoo with real-time estimation of the target surface's rigid-body motion. The entire information is fed back to the motion controller to enable printing (Figure 7c-iii).²⁵⁸ For biosensor fabrication, common techniques include material jetting and material extrusion, including direct ink writing on the skin.²⁵⁸ Typical horizontal resolution of 3D printing ranges from 20 to

250 μm and vertical resolution ranges from 1 to 100 μm , influenced by factors such as printer type and mechanism, material, thermal conditions, ink viscosity, and nozzle diameter.²⁵⁷ 3D printing has been applied in wearable biosensing e-tattoos using soft, biocompatible functional inks based on silver flakes,²⁵⁸ graphene oxide,²⁵⁹ and CNTs.²⁶⁰ Biological tissues, which are sensitive to heat, solvent, mechanical forces, and compliance, require a fast curing process for the printed ink. Wan et al. recently developed a flexible 3D printing system with an elastic injection chamber containing embedded LEDs.²⁶¹ These LEDs emit light that penetrates through the ink for fast curing, reducing the curing time to a rapid period of 5 min.

3.3.3.4. Aerosol Jet Printing. Aerosol jet printing for e-tattoo fabrication is an emerging technology known for its compatibility with inks featuring a broader viscosity range (1–1000 cP) compared to other printing paradigms. This method avoids nozzle clogging and excels in printing on nonplanar surfaces.²⁶² Additionally, aerosol jet printing is relatively simple and nontoxic. In this process, ink is atomized through a pneumatic or ultrasonic mechanism and directed to the substrate by a sheath gas flow.³⁴ Aerosol jet printing has shown the capability of printing silver nanowires on various curved surfaces, such as an apple, and directly onto the uneven inset surface of the finger (Figure 7c-iv).³⁴ Subsequently, aerosol jet printing has been used to fabricate related epidermal electronics, such as carbon lactate sensor²⁶³ and graphene histamine sensor.²⁶⁴

Highly efficient printing technologies have paved the way for a new generation of epidermal electronics applications. In summary, screen printing, inkjet printing, 3D printing, and aerosol jet printing each have distinct advantages and limitations in e-tattoo fabrication. Screen printing is a cost-effective and scalable process suitable for high-volume production, while inkjet printing excels in producing thinner, higher-resolution patterns with precise features and generates no waste. 3D printing enables the creation of complex and customized structures with high accuracy, while aerosol jet printing is a versatile and flexible process capable of printing on a wide range of substrates and geometries. The choice of the printing technique depends on the specific application and requirements of the e-tattoos.

3.3.4. On-Skin Fabrication. On-skin fabrication primarily involves the direct application of conductive inks onto the skin. The inks solidify on the skin, allowing for exceptional microscale conformability and potential compatibility with hairs. A well-known on-skin fabrication technique is the Drawn-on-Skin method, which uses a modified ballpoint pen or brush to apply functional ink within a stencil that is attached to the skin.¹⁴¹ Once the ink solvent evaporates at room temperature, the stencil is removed, leaving the final e-tattoo on the skin (Figure 7d).¹⁴¹ Defects and device thickness can be corrected by reapplying ink to the same area, and the ultimate resolution is influenced by the stencil design, pen/brush dimensions, and functional inks. Drawn-on-skin e-tattoos have been fabricated using various materials like PEDOT:PSS,^{141,265,266} liquid metal particles and composites,^{130,132} and semiliquid-metal.²⁶⁷ Stencil-guided on-skin fabrication allows for the drawing of well-patterned e-tattoos. However, the stencil is not fully compatible with thick or dense hairs. As a result, stencil-free ink painting technique was developed to directly apply e-tattoos to a hairy scalp, ensuring that the e-tattoos form conformal contact with the skin despite the hairs.^{268–271} However, the resolution of these painted e-tattoos is generally limited. Furthermore, the selection of

conducting materials for on-skin fabrication requires careful consideration due to the limitations of on-skin postprocessing.

3.3.5. Laser Engraving. Laser engraving, also known as laser scribing or laser direct writing, plays a unique role in realizing functional devices due to its distinct ability to tune material properties (e.g., carbonization or reduction) in a rapid and mask-free manner. Porous graphene can be directly engraved on various synthetic and natural carbon precursor substrates under ambient conditions, either through laser-induced direct carbonization of polymeric substrates (including PI, polyethylenimine, Kevlar, and some natural carbon precursors like wood, bread, and potatoes) or laser-induced reduction of graphene oxide.^{120,272–274} Different laser parameters, such as wavelength, power, pulse width, and scanning speed, influence the final graphene structure formation and resolution. Adjusting these parameters allows obtaining graphene with different structures on the same patch for multiplexing applications (Figure 7e-i,e-ii).²⁷⁴ Laser engraving has recently extended to other materials, such as silicon carbide^{275,276} and transition metal oxide.²⁷⁷ Thanks to its speed and high resolution, laser engraving holds great promise for future in situ fabricated e-tattoos.

3.3.6. Electrospinning. Electrospinning is a cost-effective and efficient method for fabricating porous nanofiber mats. To transform these nonwoven fiber mats into breathable, conductive e-tattoos, various methods can be employed. This includes stabilizing and carbonizing polymer nanofibers, electrospinning a blend solution of conductive polymers and metal salts into composite fibers, or depositing conductive materials through sputtering or spraying them over the fiber mat substrate. The resulting conductive porous membranes are ideal for on-skin biosensing due to their thinness, shape conformability, and breathability.^{278,279} A typical electrospinning setup consists of a high-voltage power supply, a polymer solution reservoir connected to a spinneret, and a grounded metal collector.²⁸⁰ The applied electrical field forms the Taylor cone,²⁸¹ causing the polymeric fluid to eject from the cone edge, resulting in the formation of micro/nanofibers (Figure 7f-i,f-ii).²⁸² Key parameters influencing the process include solution parameters (polymer type, concentration, viscosity), process parameters (flow rate, collecting distance, voltage), and ambient parameters (temperature, humidity). Studies have demonstrated electrospinning-based e-tattoos utilizing nanofiber mat of poly(vinylidene fluoride-co-trifluoroethylene),²⁸² porous silk nanofiber (SNF),¹⁰⁵ PVA nanomesh,⁴¹ electrospun thermoplastic elastomers,²⁸³ as well as MXene reinforced nanofibers.²⁸⁴ To enhance yield and address intermittent nozzle clogging in electrospinning, multineedle spinnerets, and needleless electrospinning²⁸⁰ hold significant promises, encouraging further exploration of this technology in e-tattoo manufacturing.

The field of innovative electronic tattoo fabrication is rapidly evolving with promising prospects. Table 1 summarizes state-of-the-art fabrication techniques for e-tattoos, highlighting their functional materials, typical resolution, and notable advantages and disadvantages. Ongoing research is exploring new materials and techniques for highly precise and scalable fabrication processes, enabling the creation of e-tattoos with a wide range of features and functionalities.

3.4. Transfer-on-Skin Technologies of E-Tattoos

Following fabrication, e-tattoos must be transferred to human skin, demanding precision to avoid folding, wrinkles, or tears. This task becomes more intricate with thinner and softer e-

Table 1. Summary of Different Manufacturing Technologies of E-Tattoos^a

manufacturing technologies	functional materials	resolution	advantages	disadvantages	ref
microfabrication	noble metal (Au, Ag, Cu) films, Au nanowires	sub-10 nm; ref233	high resolution; reproducibility; high throughput	high cost; time-consuming	227–233
cut-and-paste	versatile conductive materials such as graphene, carbon film, Au, Al	10 μm according to the cutter	cost-effective; large-area production; fast	limited resolution; waste generation	71, 107, 212, 234–238
screen printing	PEDOT:PSS, carbon particles and fibers, graphene, Ag/AgCl, Ag nanowires, Ag nanoparticles, liquid metal	22–100 μm ; ref237	fast and efficient; scalable	limited lateral resolution; waste of materials	33, 43, 239–245
inkjet printing	PEDOT:PSS, Ag nanowires, Ag nanoparticles, graphene, CNT, MXene	~20 μm ; ref250	high resolution; mass producible	strict ink rheology requirement; wetting issues	35, 249–256
3D printing	Ag flakes, graphite, CNTs	horizontal: 20–250 μm ; vertical: 1–100 μm ; ref254	fast prototyping; easy customization	restricted printable material; limited resolution	258–260
aerosol jet printing	Ag nanowires, carbon, graphene	line width: 20–40 μm , refs 260, 261 spacing: 100 μm , ref261	wide viscosity range for print ink; rapid prototyping	requiring substrate treatment; air pollution and waste generation	34, 263, 264
drawn-on-skin	PEDOT:PSS, liquid metal, semiliquid-metal	line width: 300 μm ; spacing: 200 μm ; ref138	simple fabrication; deposition on dynamic surfaces	hard for batch production; limited postprocessing	130, 132, 141, 267
laser engraving	graphene, silicon carbide, transition metal oxide	12 μm ; ref265	high throughput; high yield	limited scope of materials	120, 272–277
electrospinning	polymers, conducting filler/polymers composite	–	efficient and cost-effective; optimal breathability	harder patterning; difficult in thickness control	41, 105, 282–284

^aNote: “–” means not available. Resolution is the smallest reported line width or spacing.

tattoos. Moreover, self-adhesive e-tattoos can pose challenges by sticking to themselves or unintended surfaces. To address these issues, various standard transfer procedures, including transfer printing, tattoo-paper-based transfer, medical patch-assisted transfer, and substrate-free transfer, have been developed and will be discussed in the following sections.

3.4.1. Transfer Printing. Transfer printing is a versatile method for precisely arranging micro- and nanostructures onto diverse substrates. It employs an elastomeric stamp to transfer devices from their original substrate to a different receiver substrate (Figure 8a-i).²⁹ To transfer e-tattoos to the skin, the adhesion force between the stamp and the e-tattoos must be stronger than that between the device and the handling substrate but weaker than that between the device and the skin. Successful transfer also relies on the viscoelasticity of the stamp and the peeling rate.^{68,285} PDMS has been utilized to pick up devices from silicon wafers and transfer them to the skin.²⁹ However, elastomer-based transfer printing faces challenges with large-area e-tattoos due to the nondevelopable shape of human skin.²⁸⁶ Cartan Transfer Printing (CTP), minimizing transfer-induced strain using a mathematical Cartan connection, ensures point-by-point nonslippery contact, and can facilitate complete transfer over large areas (Figure 8a-ii).²⁸⁷ However, Cartan Transfer Printing is time-consuming. Further exploration of the link between surface physics/chemistry and adhesion can enhance the precision and yield of transfer printing for e-tattoos.

3.4.2. Tattoo-Paper-Assisted Transfer. Water slide decal transfer paper, commonly known as temporary tattoo paper, has emerged as a unique substrate for body-conformable electronics. The desired e-tattoo pattern is printed on a submicrometer-thick transferrable liner, which adheres to a paper backing via a water-soluble adhesive. When the tattoo paper with the device is pressed against the skin, the liner is released from the support paper by dissolving the intermediate water-soluble adhesive with water, and the final e-tattoo with liner backing adheres to the skin via vdW force (Figure 8b).²⁸⁸ Ferrari et al. extensively studied different tattoo paper compositions, comparing them with conventional substrates for tattoo-like devices.²⁸⁹ Electronics with various conductive layers, such as gold²¹² and PEDOT:PSS^{238,289} have been readily fabricated onto tattoo paper and transferred onto the skin for numerous biointegrated applications. While tattoo paper is an inexpensive and versatile substrate for skin-conformable electronics, the liner has limited adhesion on the skin, necessitating additional adhesives, such as a liquid band, to secure the e-tattoos for long-term use.

3.4.3. Medical-Patch-Assisted Transfer. Utilizing an adhesive medical epidermal patch, such as Tegaderm, can enhance the lifespan of temporary ultrathin tattoo electrodes on the skin by providing additional adhesion force and protection. Tegaderm is a polyurethane film-based transparent adhesive medical patch with exceptional breathability (WVTR $\sim 14.47 \pm 0.30$ g·m⁻²·h), thinness (~ 47 μm), strong adhesion (~ 5.93 N/cm), and notable mechanical properties (modulus ~ 7 MPa).^{236,290} Tegaderm can serve as either substrate for the electronics or surface encapsulation to protect preskin-laminated e-tattoos (Figure 8c).^{291–293} Despite enabling robust lamination and extending the endurance of e-tattoos on the skin, Tegaderm is nonreusable, limiting the multiple uses of the e-tattoos.

3.4.4. Substrate-Free Transfer. Substrate-free transfer involves the transfer of electronics without additional substrate support, ensuring a clean device surface. For example, self-adhesive electrodes with robust mechanical strength can be

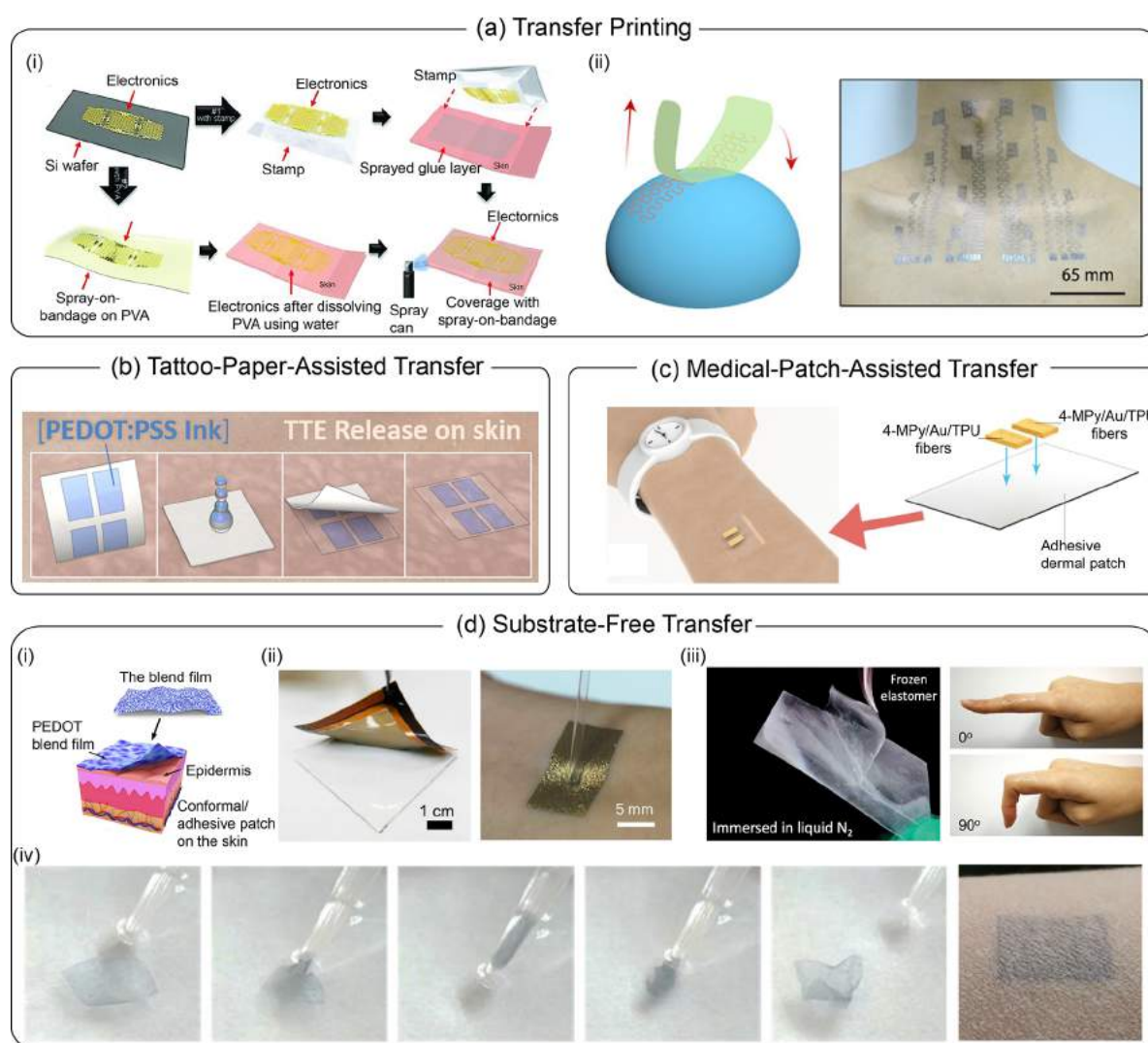


Figure 8. Transfer-on-skin technologies of e-tattoos. (a) Transfer printing: (i) releasing and picking up an epidermal electronic system from its handling wafer and printing it onto human skin via an elastomeric stamp; (ii) large-area tattoo-like electrodes laminated on the neck through rolling contacts, named Cartan Transfer Printing. Reproduced with permission from refs 29 and 287. Copyright 2013 John Wiley and Sons and 2020 AAAS. (b) Temporary tattoo-paper-assisted transfer: attaching temporary tattoo paper with electronics and releasing the liner with e-tattoos on the skin. Reproduced with permission from ref 288. Copyright 2021 MDPI. (c) Medical patch-assisted transfer: attachment of Au/TPU fiber electrode to a transparent adhesive dermal patch and attachment of a wearable pH sensor to the human's arm. Reproduced with permission from ref 291. Copyright 2021 American Chemical Society. (d) Substrate-free transfer: (i) direct transfer, schematic of directly transferring an adhesive PEDOT:PSS film to human skin; (ii) frame-assisted transfer, frame-held ultrathin PDMS-Au conductor (left), and optical image of the electrode on human skin (right); (iii) cryo-assisted transfer, the ultrathin film detached from the substrate when immersed in liquid nitrogen (left) for transfer, and photos of the transferred e-tattoo conformably attached to a finger knuckle at different bending angles (right); (iv) pipette-assisted transfer, a water drop containing the freestanding 230 nm thick PEDOT:PSS/silver nanowire/PEDOT:PSS hybrid electrode delivered on human skin by a pipet, and the electrode self-deployed on the skin due to water surface tension. Reproduced with permission from refs 294, 190, 296, and 297. Copyright 2020, 2022 Springer Nature; 2020 John Wiley and Sons; 2020 American Chemical Society.

directly transferred onto the skin for biopotential recordings (Figure 8d-i).^{294,295} To transfer ultrathin and substrate-free e-tattoos, frame-assisted transfer minimizes mechanical stresses, allowing precise alignment and manipulation during the transfer process (Figure 8d-ii).¹⁹⁰ Additionally, the cryo-assisted transfer method can temporarily maintain a high elastic state when immersed in liquid nitrogen. The resulting gripping force promotes the delamination of the tattoo-like electrode from the substrate for on-skin transfer (Figure 8d-iii).²⁹⁶ Water surface tension can also be leveraged for e-tattoo transfer. For example, a 230 nm thick PEDOT:PSS/silver nanowire/PEDOT:PSS film can be delivered to the skin with a pipet containing water and

then self-deployed on the skin due to water surface tension (Figure 8d-iv).²⁹⁷

4. E-TATTOO SENSORS

With the described material, structural design, manufacturing, and transfer-on-skin technologies, e-tattoos can seamlessly adhere to the skin, enabling long-term, unobstructive monitoring of biosignals. Various sensing modalities have been incorporated into e-tattoos for a wide range of health monitoring and human-machine interface applications. In this section, we discuss how the intended function of the e-tattoo shapes critical design considerations for both biophysical and biochemical sensors.

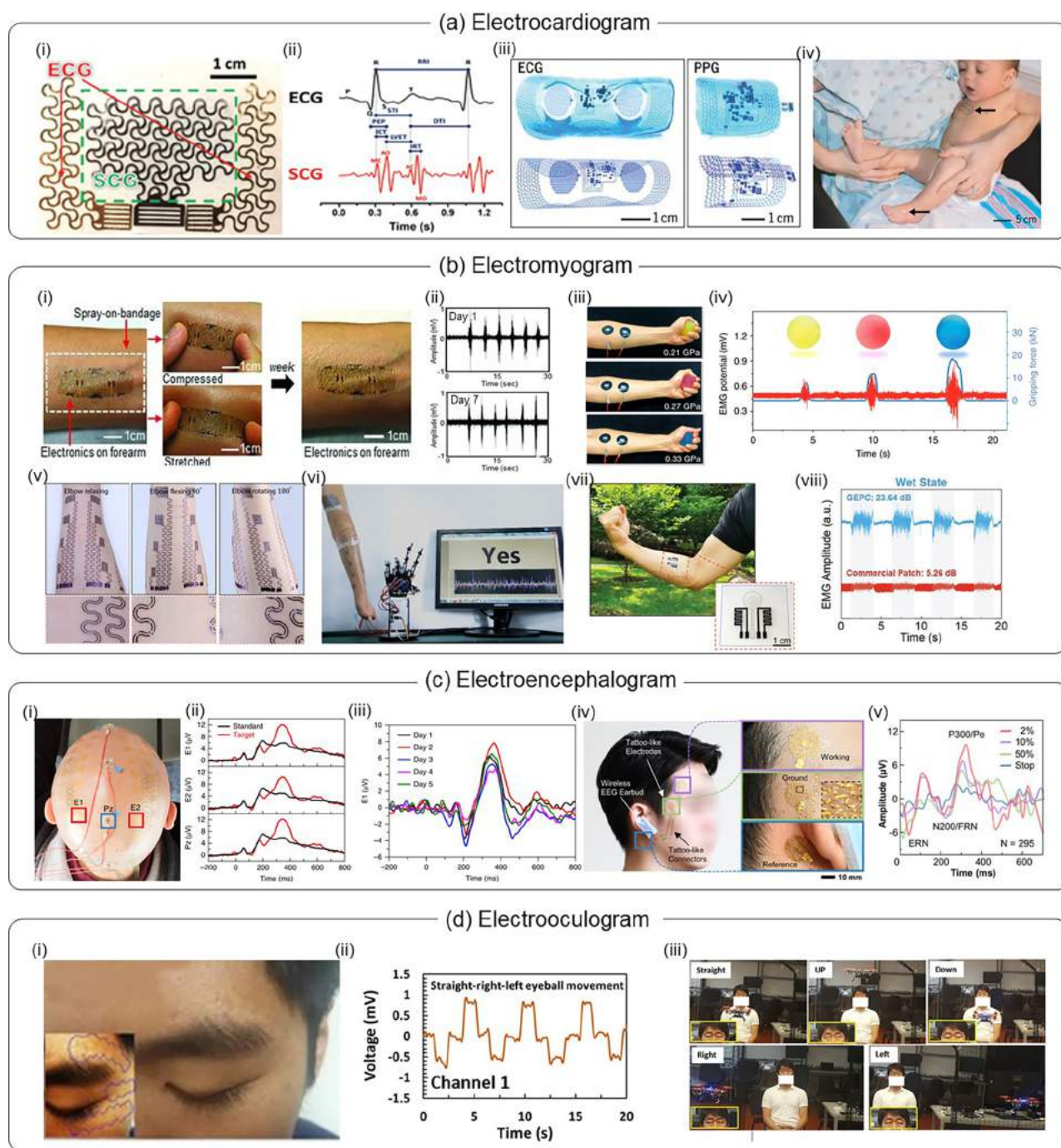


Figure 9. E-Tattoos for electrophysiological recording. (a) E-Tattoos for ECG: (i) photograph of the chest laminated electro-mechano-acoustic e-tattoo; (ii) synchronous ECG and SCG signals acquired by the e-tattoo; (iii) illustration of ECG and PPG e-tattoo for neonatal care; (iv) neonatal care e-tattoo applied onto the baby's chest and foot. Reproduced with permission from refs 236 and 325. Copyright 2019 John Wiley and Sons and 2019 AAAS. (b) E-Tattoos for EMG: (i) photos of the e-tattoo directly printed on the skin that remained on the skin for a week; (ii) EMG recorded on day 1 and day 7 after continuous wear; (iii,iv) EMG signals recorded from a fully organic, self-adhesive dry electrode while gripping balls with different moduli; (v) photos of a large-area, multichannel, and breathable e-tattoo placed on the skin through Cartan Transfer Printing; (vi) a robotic hand controlled through the e-tattoo in (v); (vii) photos of a wearable e-tattoo with the transparent copolymer substrate and electrode; (viii) the EMG acquired by the e-tattoo in (vii) (blue) and commercial electrodes on wet skin. Reproduced with permission from refs 29, 294, 287, and 327. Copyright 2013, 2019 John Wiley and Sons; 2020 AAAS; 2020 Springer Nature. (c) E-Tattoos for EEG: (i) photograph of the large-area MRI-compatible e-tattoo electrodes (E1 and E2) vs conventional EEG cup electrodes (Pz) on the scalp of a bold subject; (ii) P3 event-related potentials recorded using the e-tattoo and the cup electrodes for comparison; (iii) E1 event-related potentials recorded with the e-tattoo electrodes for 5 days of continuous wear; (iv) photograph of a human wearing an earbud-like wireless EEG device and zoomed-in images showing the recording (top), ground (middle), and reference (bottom) e-tattoo electrodes mounted on the mastoid, temple, and forehead of the volunteer, respectively; (v) error-related potentials captured by (iv) with characteristic peaks under different error rates. Reproduced with permission from refs 286 and 329. Copyright 2019 and 2022 Springer Nature. (d) E-Tattoos for EOG: (i) photograph of the transparent graphene e-tattoo applied to human skin; (ii) EOG acquired by the e-tattoo during vertical eye movements; (iii) control of a drone by the EOG signals collected in (ii). Reproduced with permission from ref 211. Copyright 2018 Springer Nature.

4.1. Biophysical Sensors

Biophysical sensors utilize nonreactive processes to interrogate the body, encompassing categories like biopotential, bioimpedance, strain, pressure, optical, and others. E-Tattoos that utilize these modalities have demonstrated the extraction of vital health parameters, including blood pressure, ECG, EMG, EEG, blood oxygenation, and respiration, as discussed in the following sections.

4.1.1. Biopotential Recording Electrodes. Innately flexible and conformable e-tattoos can record bioelectric signals at various anatomical locations, providing valuable information about cardiac, muscular, and neural activities.^{1,56,153} The evolution of e-tattoos has been primarily motivated by the imperative to reduce the electrode–skin contact impedance and artifacts from movements and environmental changes, while simultaneously improving comfort during long-term wear. Lowering the electrode–skin contact impedance can improve the signal-to-noise ratio.^{1,298–300} Metals with a high innate conductivity (e.g., noble metals),^{28,169,301–305} conducting polymers with a high ionic mobility and a high charge transfer rate (e.g., PEDOT:PSS),^{140,306–310} and carbon nanomaterials with both good conductivity and large surface area (e.g., graphene,^{43,311,312} CNTs³¹³), and 2D dichalcogenides with ultrathin thickness¹¹⁶ have been used to reduce the contact impedance of the electrodes on the skin. Minimizing artifacts is crucial for accurate diagnostic monitoring because these artifacts can be falsely interpreted as signals or even mask the actual bioelectric signal. These artifacts are caused by motion, sweat, and electromagnetic interference (EMI).^{314–316} Fully skin-conformal electrodes,^{71,311–313,317,318} self-adhesive electrodes,^{42,157,203,294,307,319} sweat-resistive designs,^{96,212} and proper electromagnetic shielding for circuitry components of e-tattoos^{320–322} can reduce these artifacts by improving skin conformability, ensuring secure adhesion under dynamic motion, preventing excessive sweating-induced skin-electrode sliding, and blocking EMI, respectively. Additionally, adopting a more breathable^{41,96,284,323} and even substrate-free design^{41,141,211,287,294,324} can further enhance the comfort of e-tattoos, encouraging their long-term use. Although fundamental requirements are met, the development of biopotential recording e-tattoos is still in the early stages, especially in design optimization for specific sensing modalities.

Cardiac activity measurement with e-tattoos holds significant value in intensive care monitoring and cardiovascular health assessment. For instance, arrhythmias can be easily detected by observing the timing of the ECG waveform. Additionally, coupling ECG with other modalities like seismocardiography (SCG) allows for a more comprehensive diagnosis of underlying cardiac abnormalities. Ha et al. introduced an electro-mechano-acoustic (EMAC) e-tattoo capable of capturing both the electrical signal and mechanical vibrations from the heart (Figure 9a-i).²³⁶ The ECG electrodes consist of a 13 μm thick gold-deposited PET film (Au/PET film), while the SCG sensor was made of 28 μm thick metalized polyvinylidene fluoride (PVDF). Valve-induced vibrations caused strain in the PVDF, generating voltages used to construct the SCG waveform (Figure 9a-ii). Extracting features from both ECG and SCG waveforms allows for the estimation of various cardiac time intervals, subsequently used for beat-to-beat blood pressure estimation. Another example of synergy between ECG and other modalities is a binodal, wireless e-tattoo developed for neonatal intensive care (Figure 9a-iii).³²⁵ The tattoo-like sensors were directly laminated onto the chest and foot of a neonate to

measure ECG and photoplethysmography (PPG), respectively (Figure 9a-iv). Noninvasive estimation of blood pressure variations was achieved by measuring the time the pulse takes to travel from the heart to the periphery. Additionally, the PPG sensor and a digital thermometer were used to estimate peripheral perfusion and hypothermia risks. Heart and respiratory rates extracted from e-tattoo measurements were comparable to those from a gold standard reference. In summary, future cardiac monitoring e-tattoos will deliver more compact multimodal sensing capabilities for comprehensive information. Beyond cardiovascular disease detection, their applications will extend to various human state estimations, such as stress monitoring and polysomnography.

Continuous and mobile muscle activity tracking through EMG is used in enhancing sports performance, aiding rehabilitation, enabling motion tracking, and facilitating control of robotic exoskeletons. Yeo et al. introduced a multifunctional e-tattoo directly printed on the skin.²⁹ The e-tattoo incorporates gold electrodes for EMG, silicon nanomembranes for strain, and a platinum layer for temperature sensing (Figure 9b-i).²⁹ With a thickness of only 800 nm and high conformality to the skin topography, the device demonstrated mechanical robustness without delamination, enabling high-quality and stable EMG signal acquisition for 1 week (Figure 9b-ii). In recent years, several EMG sensors with unique properties, such as self-adhesiveness,²⁹⁴ large-area conformable designs,²⁸⁷ gas-permeability,^{41,213,326} and sweat tolerance^{157,327} have been developed. Self-adhesive electrodes can enhance device–skin interface stability and prevent skin irritations associated with chemical adhesives. For instance, an EMG electrode consisting of PEDOT:PSS, water-borne PU (WPU), and D-sorbitol can adhere to the skin without additional chemical adhesives (Figure 9b-iii).²⁹⁴ D-Sorbitol enhances electrode adhesiveness due to its strong interaction with the stratum corneum. The electrode enables clear differentiation of EMG signals when gripping balls with different moduli (Figure 9b-iv). Moreover, its self-adhesiveness reduced motion artifacts, improving reliability for long-term use with daily activities. In another example, Wang et al. proposed a large-area, soft, breathable, substrate- and encapsulation-free e-tattoo for EMG-based human-machine interface (Figure 9b-v).²⁸⁷ EMG signals of different hand gestures were collected by the entire forearm covering e-tattoo and decoded to successfully control a robotic hand (Figure 9b-vi). Miyamoto et al. presented an inflammation-free and gas-permeable e-tattoo electrode with gold nanomeshes.⁴¹ The electrode, which is less than 100 nm thick, exhibited excellent conformability with the skin, enabling clear EMG signal acquisition. As discussed in section 2.3, human sweat poses a challenge for e-tattoos, particularly during vigorous physical exercise. Sweat accumulation can reduce device adhesion to the skin, resulting in reduced performance. To address this issue, Zhang et al. introduced a silver nanowire-based e-tattoo with a genetically engineered plasticized copolymer (GEPC) as the substrate (Figure 9b-vii).³²⁷ The copolymer, comprising silk fibroin as the framework, genetically engineered resilin protein as the modifier, and glycerol as the plasticizer, was designed for high sweat tolerance by controlling glycerol molecular replacement under wet conditions without significantly altering electrical and adhesion properties. The e-tattoo maintained a higher signal-to-noise ratio compared to commercial EMG patches under both clean and sweat-infused states (Figure 9b-viii).

Table 2. Summary of E-Tattoo Electrodes for Biopotential Recordings^a

application	materials	conductivity/ resistance	skin contact impedance	stretchability	thickness	recording period	wireless system	ref
ECG	Cu, silicone elastomer	–	–	16% (below skin sensation)	100–150 μm	–	yes	325
ECG	Au–PI, polyurethane	–	–	100%	122 μm	–	no	236
ECG	PEDOT:PSS + DMSO + PVA, substrate-free	16,000 S/m (dry), 46 S/cm (gel)	65.3 k Ω at 10 Hz (dry)	25%	3–5 μm (dry), 18–30 μm (gel)	–	no	324
ECG	Au, PU–PDMS nanofilm	–	500 k Ω at 10 Hz	34%	195 nm	1 week	no	213
EMG	gold nanomesh, substrate-free	$5.3 \times 10^{-7} \Omega\text{-m}$	140 k Ω at 100 Hz	40%	70–100 nm	–	no	41
EMG	copper, polyurethane	–	–	20%	8.64 μm	–	no	305
EMG	carbon/ppEDOT, double-sided adhesive layer	–	20 k Ω at 100 Hz	–	102 μm	–	no	310
EMG	alginate-polyacrylamide/LiCl, substrate-free	–	20 k Ω at 1 Hz	50% (without performance degradation)	–	–	no	203
EMG	Au, plasticized silk	7 Ω /sq	200 k Ω at 1 Hz	100%	~200 μm	–	no	169
EEG	Au/PI, elastomeric film	–	–	50%	1.5–3 μm	2 weeks	no	303
EEG	Au/PI, tattoo paper	–	40 k Ω at 10 Hz	–	900 nm	–	yes	329
EEG	PEDOT:PSS, polyurethane/allyl resin-based decal transfer film	–	1.6 M Ω at 10 Hz	–	2.5 μm	–	no	309
EOG	graphene, substrate-free	–	–	50%	2.35 μm	–	no	211
ECG, EMG	Au, spray-on-bandage	–	35 k Ω at 37 Hz	30%	800 nm	1 week	no	29
ECG, EMG	Au, parylene	–	44 k Ω at 1000 Hz	60%	300 nm	10 h	no	42
ECG, EMG	Cr/Au, substrate-free	–	–	18%	1.2 μm	–	no	287
ECG, EMG	PEDOT:PSS, ethylcellulose	50 Ω /sq	294 k Ω at 60 Hz	5%	0.6–1.2 μm	–	no	249
ECG, EMG	AgNW/TPU, spray-on-bandage	7.3 Ω /sq	2 M Ω at 10 Hz	45%	4.6 μm	–	no	96
ECG, EMG	PEDOT:PSS + Ag nanowires, substrates	70 Ω /sq	20 k Ω at 1 Hz	30%	1.2 μm + substrate	–	no	318
ECG, EMG, EEG	porous graphene, gas-permeable elastomer composite	10.96 Ω /sq	17 k Ω at 100 Hz	500%	520 μm	1 day	no	323
ECG, EMG, EEG	Ag/Ti, Ecoflex, hydrogel, or PU film	–	120 k Ω at 20 Hz	40%	5 μm + substrate	–	yes	304
ECG, EMG, EEG	Cr/Au, adhesive silicone + Ecoflex	–	30 k Ω at 30 Hz	18% (26% with gel)	198 μm	5 days	no	286
ECG, EMG, EEG	MoCl ₅ -intercalated bilayer graphene, SEBS + Tegaderm	40 Ω /sq	–	80%	247 μm	–	no	311
ECG, EMG, EEG	PEDOT:PSS/WPU/D-sorbitol	40 000 S/m	13 k Ω at 10 Hz	30%	22 μm	1 week	no	294
ECG, EMG, EEG	porous carbon nanofibers, biomedical tape + gas-permeable PDMS	4 Ω /sq	23.59 k $\Omega\text{-cm}^2$ at 10 Hz	5%	50 μm + substrate	24 h	no	284
ECG, EMG, EEG	PEDOT:PSS + SDS + LiTFSI + graphene, SEBS or tattoo paper	45 Ω /sq	32 k Ω at 100 Hz	40%	80 nm + substrate (SEBS 50 μm)	12 h	no	312
ECG, EMG, EOG	Ag nanowire/genetically engineered plasticized copolymer	9.66 Ω /sq	–	50%	30 μm	–	no	327
ECG, EMG, EOG	PI/Au/PI (capacitive), silicone elastomer	–	–	~30%	5.8 μm	–	no	314
ECG, EMG, EEG, EOG	Pt-TMDC/PMMA or PI, polyurethane	31 Ω /sq	4 k Ω at 10 kHz	–	0.2–25 μm	–	no	116

^aNote: “–” means not available.

Long-term EEG monitoring offers valuable insights for diagnosing and treating neurological disorders, as well as enabling imperceptible brain–computer interfaces.³²⁸ The high temporal resolution of EEG and the high spatial resolution of magnetic resonance imaging (MRI) have sparked interest in simultaneous recording to provide a more comprehensive view of neural activity and enhanced diagnosis accuracy. Traditional metal EEG electrodes, however, are incompatible with MRI due to the risk of heating, displacement, and distortion caused by strong magnetic fields, posing dangers to patients and leading to inaccurate EEG measurements. Tian et al. reported large area and MRI-compatible e-tattoos for full-head EEG recordings (Figure 9c-i).²⁸⁶ They designed a unique open mesh structure to

minimize heating and electromagnetic interference. As a result, the e-tattoo captured event-related potentials (ERP), such as the P300 on a bold subject (Figure 9c-ii), even after 5 days of wear (Figure 9c-iii). Shin et al. introduced an e-tattoo electrode connected to an earbud-like data acquisition platform to enhance accessibility for daily EEG (Figure 9c-iv).³²⁹ The tattoo-like electrode minimized motion artifacts for EEG recording in ambulatory settings through gradually increasing in thickness from ultrathin electrodes to thick flexible printed circuit connectors and exhibited stable ErrP recording capability (Figure 9c-v). Current tattoo EEG electrodes are mostly employed in hairless regions. However, most brain regions are covered with hair and cannot be measured with conventional e-

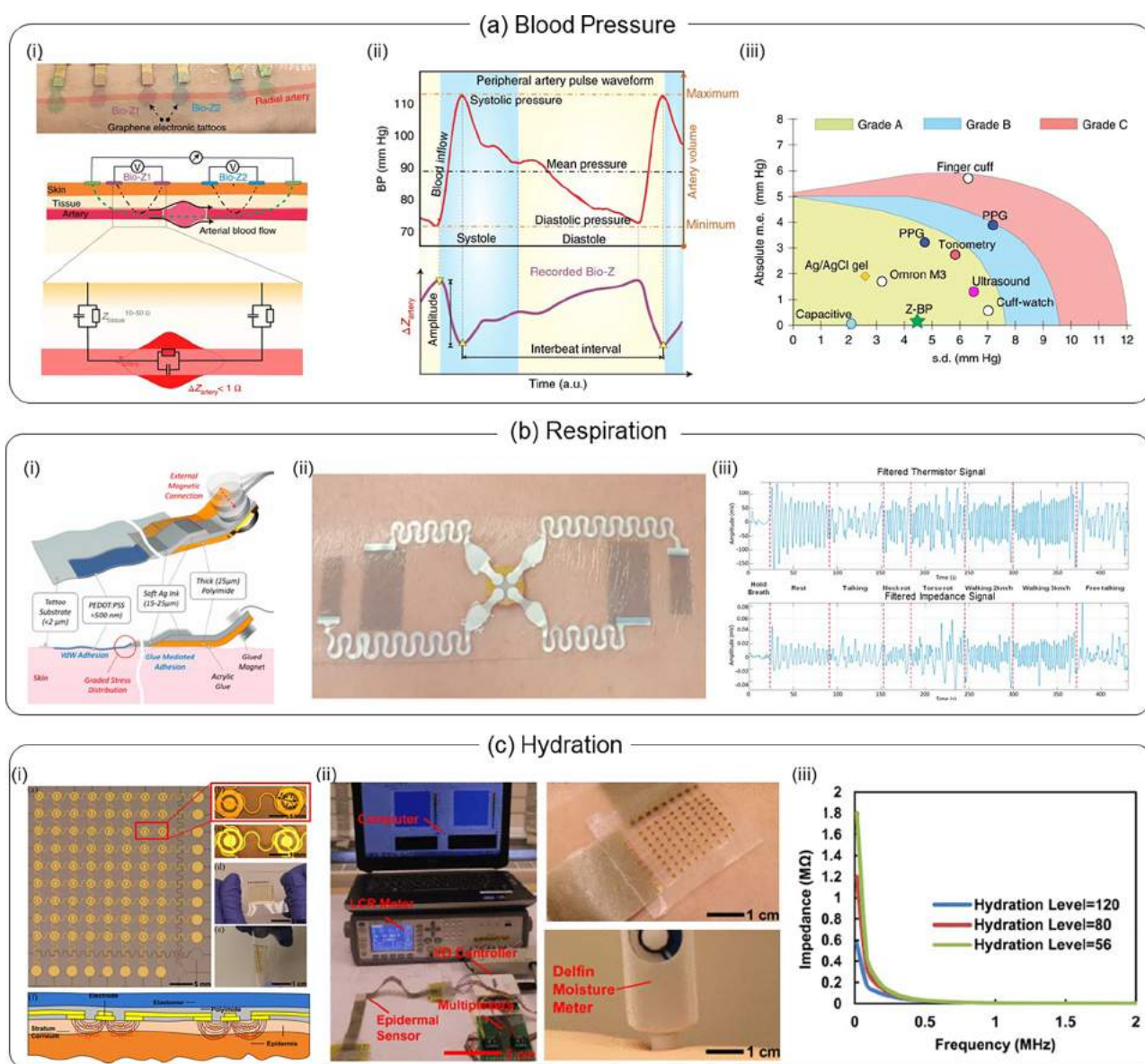


Figure 10. E-tattoo bioimpedance sensors. (a) Graphene electronic tattoos for noninvasive and continuous blood pressure monitoring: (i) images of bioimpedance (Bio-Z) sensing using the e-tattoo in a tetrapolar configuration laminated over the radial artery; (ii) temporally aligned blood pressure and Bio-Z waveforms corresponding to a single heartbeat with labeled fiducial points for systolic, diastolic, and mean arterial blood pressure; (iii) absolute mean error and standard deviation of various blood pressure sensing systems and modalities (circles), including the graphene e-tattoo (star). Reproduced with permission from ref 238. Copyright 2022 Springer Nature. (b) Inkjet-printed PEDOT:PSS tattoo sensor for respiration monitoring: (i) tattoo sensor design and on-body conception; (ii) image of the tattoo sensor laminated on the human chest for data acquisition; (iii) the e-tattoo shows similar performance to a standard thermistor in monitoring respiration. Reproduced with permission from ref 288. Copyright 2021 MDPI. (c) E-tattoo bioimpedance sensor for skin hydration monitoring: (i) an array of embedded impedance sensors featuring chromium/gold dot-ring electrodes interconnected by serpentine ribbons; (ii) characterization of skin hydration using a commercial LCR meter and a commercial hydration sensor; (iii) impedance as a function of injection frequency at different levels of skin hydration. Reproduced with permission from ref 342. Copyright 2013 IEEE.

tattoos. Direct writing of e-tattoos with hydrogels has been recently reported.^{268,269,271} Yet, the long-term recording capability of these e-tattoos needs consideration as hydrogels tend to dehydrate over time.

Electrooculography (EOG) is a noninvasive technique that measures the potential change generated by eye movements. Electrodes can be placed near the eyes to detect these electrical signals and provide precise, real-time measurement of eye movements. This method can be employed to monitor alertness while driving or to determine where the player is focusing during video game play. Because eye movements can induce significant

artifacts in EEG recording, combining EOG with EEG allows for effective artifact removal. Moreover, EOG signals can serve as input for a human–machine interface. For example, Ameri et al. developed a human–machine interface using a graphene e-tattoo as the EOG electrode.²¹¹ This ultrathin, ultrasoft, transparent, and breathable device is visually and mechanically imperceptible (Figure 9d-i). It accurately captured eye movements with an angular resolution of 4° (Figure 9d-ii). As a result, the collected EOG signals successfully controlled the movements of a drone (Figure 9d-iii).

Table 2 provides a summary of e-tattoos for electrophysiological sensing, including target applications, electrode materials, substrates, conductivity/resistance, contact impedance, stretchability, thickness, and long-term recording capabilities. Despite significant advancements, current e-tattoos for biopotential recordings have primarily focused on electrode materials and device design, integration of these e-tattoos into standalone sensing systems is still not well developed.

4.1.2. Bioimpedance Sensors. Bioimpedance (Bio-Z) is a noninvasive bioelectric sensing technique employed for various applications, including arterial pulse extraction,³³⁰ radial arterial compliance monitoring,³³¹ heart rate monitoring,³³² respiratory and cardiac activity assessment,³³³ and skin hydration tracking. Bio-Z is defined as the ability of biological tissue to impede or obstruct the flow of electric current.³³⁴ Its measurement relies on stimulating human tissue with a small amplitude electric current and sensing the corresponding voltage response across the tissue using pairs of electrodes. Bio-Z can be measured in either a bipolar configuration, where the current injection and voltage sensing paths share a single pair of electrodes, or a tetrapolar configuration, where the current injection and voltage sensing paths use different pairs of electrodes (Figure 10a-i).²³⁸ Tetrapolar measurements are typically performed over bipolar measurements as they minimize the impact of skin–electrode contact impedance and enable easier separation of the target signal. However, bipolar configurations are employed for capturing impedance when skin or the skin–electrode interface is a primary concern. Compared to other modalities, Bio-Z sensing offers deep tissue information due to the deep penetrating ability of the high-frequency signal into human skin. Traditional Bio-Z-based sensing systems utilize non-adhesive, rigid, and planar sensors, hindering conformal contact between the skin and sensor and causing sensor displacement and motion-induced signal artifacts. For applications requiring the tracking of minute (i.e., mΩ range) changes in the Bio-Z waveform, mitigating the effects of motion noise is crucial. E-Tattoos, with their flexible, ultrathin, and body-conformal characteristics, can form a stable interface with the skin, ensuring reliable long-term signal acquisition. In this section, we will review recent bioimpedance-based e-tattoos for the assessment of blood pressure, respiration, and skin hydration.

As the pulse propagates through the arterial tree, the volume change in the artery can be detected as a small decrease in Bio-Z. Previous studies have leveraged machine learning algorithms to convert features of the Bio-Z pulse waveform to an estimation of blood pressure.³³⁵ To combat the issues of traditional Bio-Z instrumentation discussed above and offer more accurate blood pressure estimation, Kireev et al. introduced a submicrometer-thick graphene e-tattoo for continuous blood pressure measurement through monitoring bioimpedance variation during pulse wave propagation.²³⁸ Pairs of graphene e-tattoos were placed in line with the radial and ulnar arteries of the wrist (Figure 10a-i), and a high-frequency (10 kHz) small-amplitude alternating current (0.2–1 mA) was injected into the skin to capture the resulting Bio-Z waveform. The graphene e-tattoo offered low skin–electrode impedance for current injection and low skin–electrode impedance variability, ensuring stable long-term operation. The transparent nature of the graphene e-tattoos enabled easy alignment with the artery when laminating onto human skin (Figure 10a-i). The study incorporated a separate low-noise multichannel Bio-Z data acquisition system on a rigid printed circuit board. Extracted features, such as pulse transit time and interbeat-interval (Figure 10a-ii), were input to a

supervised machine-learning algorithm to estimate systolic (SBP), diastolic (DBP), and mean arterial (MAP) blood pressure values. The blood pressure from the graphene e-tattoos achieved good agreement with that captured by a medical-grade BP monitoring device (Finapres NOVA) (mean errors = 0.2 ± 4.5 , 0.2 ± 5.8 , and 0.1 ± 5.3 mmHg for systolic, diastolic, and mean arterial blood pressure values, respectively), achieving a grade A classification (Figure 10a-iii), the highest accuracy level awarded by IEEE. Compared to other sensing systems and modalities, such as a wristband-based approach with an array of silver electrodes³³⁶ and a ring-based solution using a single Bio-Z channel,^{337,338} the graphene e-tattoos achieved the highest accuracy. While these results are promising, they are highly dependent on the precise alignment of the graphene e-tattoos over the radial and ulnar arteries, as misalignment will affect the extracted Bio-Z signal morphology and signal-to-noise ratio.³³⁶ Moreover, the results reported are based on data collected in a static laboratory setting, raising uncertainties about performance in ambulatory environments. Levit et al. proposed screen-printed carbon electrodes in an e-tattoo format that offered robust arterial pulse extraction from the ulnar artery of the wrist even during muscle contractions induced by fist clenching.³³⁹ These results are attributed to the electrodes' ability to conform to the skin and maintain alignment with the artery under motion. Furthermore, Namkoong et al. proposed moldable and transferable conductive nanocomposites consisting of an interpenetrating network of silver nanowires and PEDOT:PSS.³¹⁸ The silver-PEDOT:PSS film exhibited 2.8 and 1.7 times lower contact impedances than commercial Ag/AgCl gel electrodes at 1 and 100 Hz, respectively, resulting in higher quality pulse waveforms for electrophysiological sensing applications.

Just as an influx of blood induces changes in tissue impedance, the respiratory-induced movements of the chest wall can also induce changes in a Bio-Z signal, making it applicable for extracting respiration rate. Accordingly, Bio-Z-based e-tattoos have been developed for long-term continuous respiration monitoring to assist physicians in diagnosing various chronic or respiratory diseases, such as sleep apnea and hypopnea. As one example, Taccola et al. proposed an inkjet-printed PEDOT:PSS tattoo sensor for real-time respiration monitoring based on transthoracic impedance measurements.²⁸⁸ Stretchable soft silver ink traces with serpentine structures interfaced the PEDOT:PSS electrodes to conductive silver-coated PI pads containing neodymium magnets for electrical connections to external electronics via magnetic docking (Figure 10b-i,b-ii). The tattoo sensors achieved a respiration detection accuracy of 92% relative to ground truth measurements obtained from a thermistor placed in a subject's nose during various human activities (e.g., holding breath, talking, walking, etc.) (Figure 10b-iii). However, the presence of a substrate layer in the tattoo sensors may hinder sweat evaporation, potentially leading to PEDOT:PSS electrode delamination over time and degraded or loss of sensing performance. On the other hand, the magnetic docking mechanism enables the tattoo sensors to be employed for other physiological sensing applications in a quick and easy “plug-and-play” manner. For instance, the tattoo sensors demonstrated the ability to monitor EMG and ECG signals with different interface electronics. In another example, Sel et al. introduced ultrathin and flexible gold Bio-Z-based e-tattoos that captured respiration from the wrist.³⁴⁰ These e-tattoos feature an array of six 25 mm² gold electrodes, each interfacing with external electronics via gold serpentine structured traces.³⁴¹ The

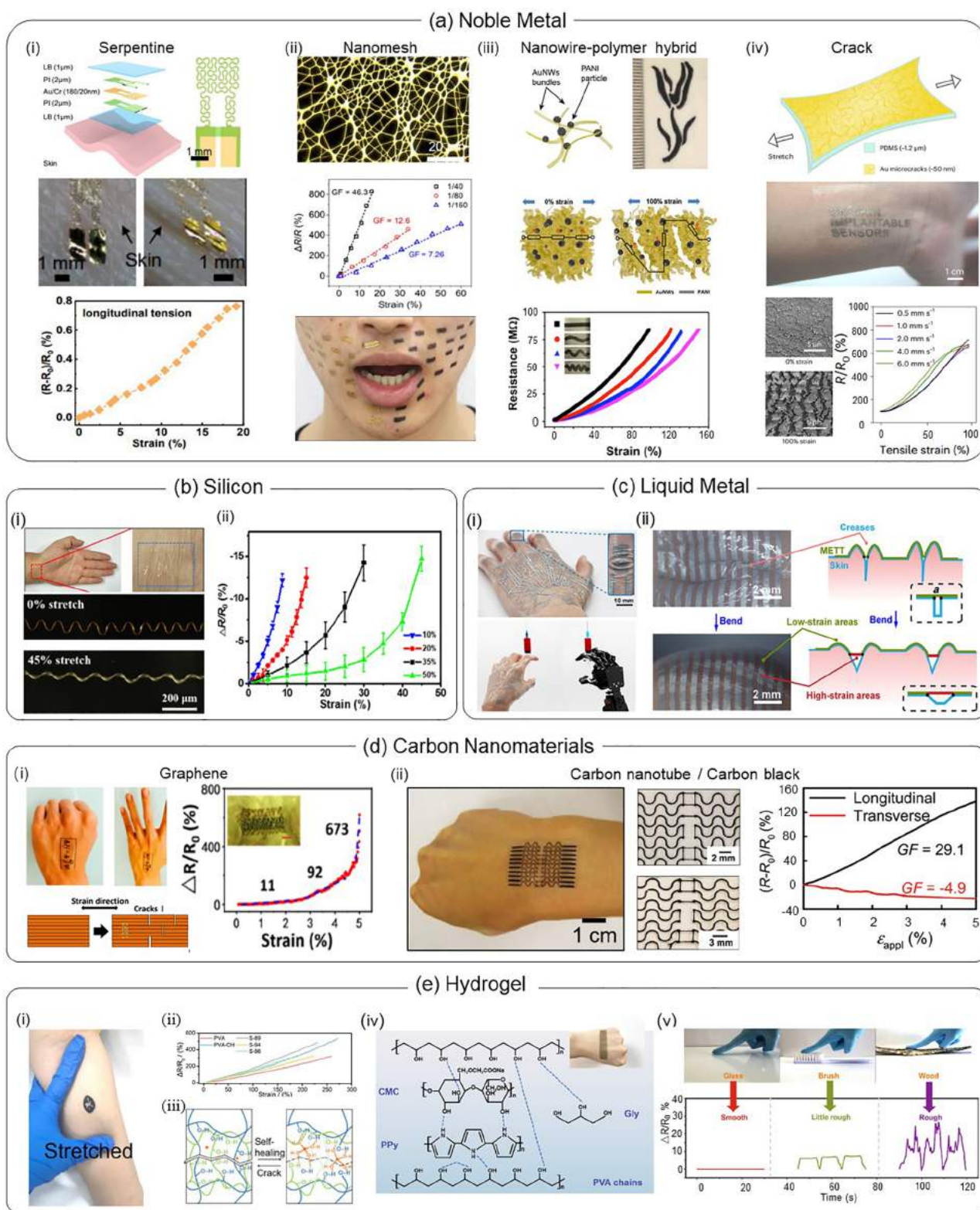


Figure 11. E-tattoo strain sensors. (a) Noble metal e-tattoos for strain sensing: (i) schematic (top), optical image (middle), and strain sensing performance (bottom) of the serpentine gold e-tattoo strain sensor; (ii) microscopic image (top), sensing performance (middle), and application of gold mesh strain sensors in the strain mapping of facial skin deformations during speech (bottom); (iii) top, schematic and a picture of the AuNW-PANI hybrid strain sensor, middle, schematic of the sensing range increasing mechanism of the sensor, bottom, the change in resistance with the strain; (iv) top, schematic of the crack-based gold e-tattoo strain sensor, middle, the ultrathin e-tattoo attaching on a human wrist; bottom, SEM images of the gold film under different strains and the change of the strain sensor as a function of tensile strain. Reproduced with permission from refs 155, 346, 347, and 190. Copyright 2021 Soft Science; 2020 AAAS; 2015 American Chemical Society; 2022 Springer Nature. (b) Silicon e-tattoos for strain sensing: (i) optical images of the silicon sensor laminated on human skin and the optical images of a silicon nanowire under 0% and 45% strain; (ii) relative resistance changes as a function of the strain. Reproduced with permission from ref 352. Copyright 2020 American Chemical Society. (c) Liquid metal

Figure 11. continued

e-tattoos for strain sensing: (i) optical image of the e-tattoo laminated on human skin and robotic hand application; (ii) illustration of crease amplification effects. Reproduced with permission from ref 128. Copyright 2021 AAAS. (d) Carbon-nanomaterial e-tattoos for strain sensing: (i) optical image of the graphene-tattoo laminated on human skin (left top), the cracking mechanism (left bottom), and the relative resistance changes as a function of strain (right); (ii) optical images of the carbon nanotube/carbon black e-tattoo (left) and the e-tattoo before and after being stretched to 150% (middle, right), change of the resistance of the e-tattoo at longitudinal and transverse directions. Reproduced with permission from refs 120 and 103. Copyright 2018 American Chemical Society and 2012 John Wiley and Sons. (e) Hydrogel e-tattoos for strain sensing: (i) optical images of the hydrogel tattoo sensor laminated on the skin under stretching; (ii) sensing performance of the hydrogel; (iii) schematic of the self-healing mechanism of the hydrogel tattoo; (iv) schematic of the structure of ultrathin hydrogel tattoo sensor, inside image shows an ultrathin e-tattoo attaching on the backside of a hand; (v) surface texture recognition with the ultrathin hydrogel e-tattoo. Reproduced with permission from ref 361 (i-iii) and 362 (iv,v). Copyright 2022 Springer Nature and 2021 American Chemical Society.

e-tattoos are supported by a layer of Tegaderm to provide adhesion to the skin and to impart additional mechanical stability and flexibility. Each electrode is separated by 3 mm, creating an effective sensing area of 35 mm × 5 mm along the radial artery of the wrist. The gold e-tattoos achieved an average root-mean-square-error of less than 13% and an average mean error of 0.3% in detecting the start of each respiration beat across five human subjects, relative to a commercial Capnograph (RespSense II, Nonin, USA).

Skin hydration is another health parameter that can be determined by monitoring changes in bioimpedance values. As water leaves the extra- and intracellular tissue, the overall Bio-Z of the tissue increases. E-Tattoos have been utilized to capture skin hydration levels from individuals based on Bio-Z sensing, although these studies are limited. As one example, Huang et al. outlined a hydration monitor utilizing an array of embedded impedance sensors to quantify variations in skin hydration.³⁴² The impedance sensors are 2 μm thick and feature chromium–gold electrodes that are interconnected by chromium–gold serpentine patterned structures (Figure 10c-i). The mechanics of the sensors allowed direct lamination on the skin through vdW interactions alone, conforming with the motions of the skin and enabling repeatable impedance measurements. The high-density, matrix-like format allowed multiplexing electrode pairs for impedance and hydration measurement with high spatial resolution across a large area of skin at both uniform and variable skin depths. To characterize their hydration sensors, a commercial LCR meter, with multiplexing measurement capability, served as the system for quantifying the response of the e-tattoo relative to a commercial hydration sensor (Figure 10c-ii). The array of impedance sensors tracked decreases in impedance amplitude for increased hydration, with more prominent impedance changes occurring at lower frequencies (Figure 10c-iii). Results suggest that increased spacing between electrodes enables greater effective measurement depth and thus partial measurement of hydration levels below the stratum corneum, which can provide more comprehensive skin and tissue health information. Furthermore, Matsukawa et al. found that nanomesh electrodes with high water vapor permeability can prevent artificial, e-tattoo-induced increases in skin hydration (i.e., moisture buildup at the sensing site due to low permeability).⁸⁴ Particularly, the device exhibited a trans-epidermal water loss comparable to bare skin. The skin impedance measured using the nanomesh electrodes and LCR meter correlated negatively with skin hydration levels recorded by a commercial skin hydration sensor (Corneometer CM825), with correlation coefficients ranging from −0.59 to −0.91 across subjects.

While significant advancements have been made toward soft Bio-Z sensors for electrophysiological sensing, many of these

systems still face challenges. Future e-tattoos that utilize these sensing paradigms still face obstacles, including (1) lack of transparent, low contact impedance, and reusable e-tattoo materials for blood pressure and respiration monitoring, (2) lack of intrinsically breathable e-tattoo materials to prevent e-tattoo-induced increases in skin hydration, and e-tattoo delamination, (3) the design of custom motion-artifact reduction algorithms for the elimination of noise introduced at the skin–sensor interface. Addressing these key challenges will undoubtedly contribute to the wider adoption of bioimpedance e-tattoos for human health monitoring in both clinical and ambulatory environments.

4.1.3. Strain Sensors. Strain sensors transduce mechanical motions into electrical signals. Over the past two decades, wearable strain sensors mounted onto joints or muscles have significantly advanced prosthetics and robotics by providing new modalities for human–machine interactions.^{51,343} However, accurate measurement of skin deformation demands strain sensors to genuinely follow skin deformation without causing mechanical constraints. As a result, e-tattoos are ideal for such purposes given their conformability and deformability enabled by their softness and thinness.

Noble metals are widely employed in strain sensors due to their intrinsic sensitivity to strain, high electrical conductivity, and chemical stability.³⁴⁴ However, as discussed in section 3.2, noble metal strain sensors usually exhibit a limited sensing range due to their high Young's moduli.^{93,345} To overcome this limitation, noble metal films have been designed with different patterns to reduce stress concentration, thereby enhancing stretchability. As an example, Wong et al. developed a tattoo sensor with serpentine-shaped gold films as the sensing layer and a 2 μm thick PI as the substrate and insulation layer (Figure 11a-i, top and middle).¹⁵⁵ The serpentine design effectively reduced stress concentration in the gold films, resulting in a sensing range of 20% and a gauge factor of 3.8 and 3.0 in longitudinal and transverse directions, respectively (Figure 11a-i, bottom). With the assistance of a waterproof liquid bandage, the device conformally attached to human skin for over 12 h without delamination, demonstrating applications in monitoring finger bending, pulse vibration, and walking. In contrast to noble metal films, networks of noble metal nanowires exhibit higher stretchability as they tend to rotate under strain. Wang et al. developed a submicrometer thick strain sensor by depositing gold on a polyurethane/PDMS core–shell mesh (Figure 11a-ii, top).³⁴⁶ The strain sensor exhibited a sensing range of 60% with a linear gauge factor of 7.26 (Figure 11a-ii, middle), enabling strain mapping of skin deformations on the face during speech (Figure 11a-ii, bottom). Additionally, the mesh structure possesses sufficient water and gas permeabilities, facilitating sweat evaporation through the pores.^{96,346} Similarly, Gong et al.

Table 3. Summary of the Representative E-Tattoos for Strain Sensing^a

materials	gauge factor (strain range)	sensing range	thickness	application	ref
Au/PI	3.8 (longitudinal) (0–20%) 3.0 (transverse) (0–20%)	20%	2 μm	motion detection	155
gold/PU nanomesh	7.26 (0–60%)	60%	430 ± 18 nm	facial expression monitoring	346
Au-SWCNTs/PDMS	7.1 × 10 ⁴ (0–70%) 3.1 × 10 ⁶ (70%–100%)	100%	36 μm	facial muscle movement monitoring	348
V–Au nanowires/PDMS	1035 (0–20%)	20%	–	pulse detection	231
Au nanowires-PANI/latex rubber	20.4 (0–30%) 61.4 (100%)	149.6%	–	robotic arm control	347
silicon film	–	30%	<8 μm	facial monitoring during silent speech	349
silicon nanowire	0.075 (0–30%)	45%	200 μm	throat motion recognition	352
liquid metal/styrene–butadiene–styrene	1 (0–160%)	800%	22–114 μm	robotic hand manipulation	128
graphene/transfer tape	11 (0–2.5%); 92 (2.5–4.5%); 673 (4.5–5%)	5%	–	respiration detection	120
carbon black/PDMS	29 (0–5%)	23%	300 μm	wrist motion detection	103
carbon black/TPU film	17.5(0–70%); 8962.7 (140–160%)	160%	50 μm	muscle tremor detection	354
CNT/TPU	0.36 (0–1000%)	1000%	100 μm	drinking detection	104
PVA-Ppy	2.1 (0–400%)	500%	110 μm	texture recognition	362
PVA-S/hydrogel (PP film)	1.8 (0–270%)	270%	300 μm	strain sensing	361

^aNote: “–” means not available; sensing range is defined as the maximum stretchability of the sensor before losing electrical integrity.

developed a strain sensor by directly drawing a conductive ink of gold nanowires and polyaniline (PANI) microparticles on the skin (Figure 11a-iii, top).³⁴⁷ The gold nanowires formed a continuous network with PANI particles as the conductive bridge (Figure 11a-iii, middle). Therefore, the device exhibited a sensing range of 99.7% and a gauge factor of 15 (Figure 11a-iii, bottom). Programmed crack formation provides another structural engineering method to increase the sensing range of strain sensors.^{189,231,348} As an example, Jiang et al. developed a 1.3 μm thick e-tattoo by thermal evaporating gold nanofilm onto an ultrathin PDMS film supported by a thick PDMS film on a glass substrate (Figure 11a-iv, top and middle).¹⁹⁰ The thick PDMS underwent thermal expansion during the thermal evaporating process, resulting in numerous microcracks on the gold film (Figure 11a-iv, top). The programmed crack design enabled the sensor to achieve a stretchability of 100% (Figure 11a-iv, bottom). Despite significant progress in the development of noble metal-based strain sensors, the high cost associated with materials and their deposition fabrication processes limit their widespread adoption.

Compared to metals, semiconductors exhibit a much larger resistance change under strain due to bandgap shift-induced carrier redistribution.³⁴⁹ Single-crystalline silicon strain sensors are reported to have a high GF of 50–200.³⁵⁰ However, it has limited stretchability, preventing its use for high strain sensing.³⁵⁰ To address this limitation, Kim et al. patterned the silicon nanomembrane into a serpentine structure and achieved a sensing range of 30%.³⁴⁹ Silicon nanowire springs provide another type of strain sensor with high stretchability.³⁵¹ As an example, Huang et al. developed an ultraminiaturized and transparent silicon strain sensor by buckling single centimeter-long silicon nanowires on a prestrained substrate (Figure 11b-i, top).³⁵² The buckled strain sensor can be stretched under strain (Figure 11b-i, bottom), resulting in a sensing range of 45% (Figure 11b-ii). While significant progress has been made with silicon-based strain sensors, the microfabrication process or high-temperature growth of silicon nanowires hinders their large-scale fabrication for wider applications.

Liquid metal exhibits intrinsic stretchability thanks to its fluidic nature.^{128,130,131,159,353} Therefore, it can function as both

the active and interconnect material, providing a seamless interface with improved mechanical stability. Liquid metals can be dispersed in organic solvents for low-cost and large-area printing fabrication. For example, Tang et al. found that liquid metal dispersed in polyvinylpyrrolidone solution can be directly printed onto a styrene–butadiene–styrene substrate, forming an ultrathin liquid-metal-based strain sensor (Figure 11c-i, top) to control a robotic hand (Figure 11c-i, bottom).¹²⁸ The device formed a partially conformed contact on the wrinkled surface of the skin (Figure 11c-ii). When the device bends, the nonconformed area undergoes higher strain, amplifying the signal due to the crease amplification effect. The sensing area of the sensors have a multilayer structure of thin and long strips of liquid metal to increase sensitivity, while the connection comprises wide strips for good stretchability. Because wrinkles mainly form on the joints, resistance changes are localized in the sensing area and not the connectors. This sensor exhibited a wide sensing range up to 800%. However, liquid metal-based strain sensors usually have limited sensitivity due to the fluidity of the liquid metal, restricting their applications in monitoring subtle movements.

Carbon nanomaterials, including carbon particles,^{102,354} CNTs,^{171,355,356} and graphene^{118,357} are widely employed in strain sensing e-tattoos due to their low cost and good electrical conductivity. Graphene, in particular, exhibits a rapid increase in resistance under stretching due to the formation of cracks in the graphene film, making it an ideal sensing material for high-sensitivity strain sensors. For example, a laser-induced graphene tattoo (Figure 11d-i, top left) generates cracks under strain (Figure 11d-i, bottom left).¹²⁰ The opening and closing of these cracks make the strain sensor exhibit a gauge factor of 673 and a sensing range of 5% (Figure 11d-i, right). CNTs and carbon black are another two candidates for strain sensors and are generally doped within an elastomeric matrix with rigid metal as the connections. However, the connection between the sensing layer and the connectors tends to detach under stretching due to their mechanical mismatch. To address this issue, a multilayer device was designed, with a strain-sensitive carbon-black-doped PDMS layer as the sensing layer and a strain-insensitive CNT-doped-PDMS as the connectors (Figure 11d-ii, left).¹⁰³ This

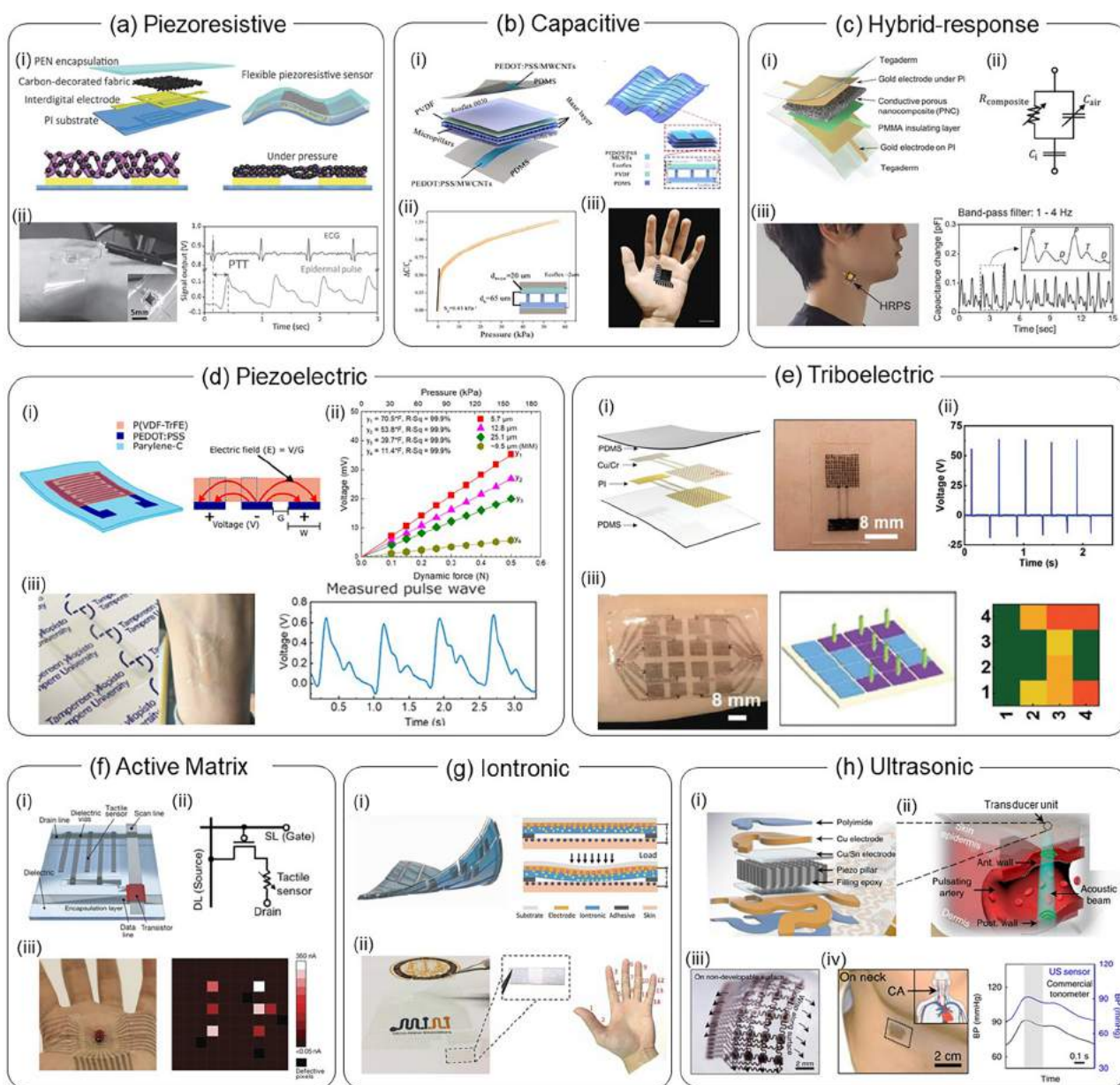


Figure 12. E-tattoo-based pressure sensors. (a) Piezoresistive pressure sensor: (i) schematic of a piezoresistive pressure sensor; (ii) photograph of the piezoresistive pressure sensor attached to a wrist and the measured surface pulse signals. Reproduced with permission from ref 363. Copyright 2016 John Wiley and Sons. (b) Capacitive pressure sensor: (i) schematic diagram presenting the multilayers of a single capacitive pressure sensor; (ii) the sensor's response to the applied pressure; (iii) photograph of an 8×8 capacitive pressure sensor array attached to the palm. Reproduced with permission from ref 367. Copyright 2021 American Chemical Society. (c) HRPS: (i) schematic of an HRPS; (ii) simplified equivalent circuit of the HRPS; (iii) photograph of an HRPS attached to the skin over the carotid artery and the measured and filtered carotid arterial pulse. Reproduced with permission from ref 385. Copyright 2021 John Wiley and Sons. (d) Piezoelectric pressure sensor: (i) schematic of a piezoelectric pressure sensor with interdigitated electrodes (IDE) after the poling process; (ii) output voltage as a function of the applied dynamic force in the normal compression mode; (iii) photographs of the sensor placed on a flat substrate and attached to the wrist, and the recorded arterial pulse waveform. Reproduced with permission from ref 373. Copyright 2021 American Chemical Society. (e) Triboelectric pressure sensor: (i) schematic and photograph of a skin-integrated triboelectric nanogenerator (TENG); (ii) open-circuit voltage produced by the TENG under five cycles of finger hitting; (iii) photograph of a 4×4 sensor array mounted on human skin, and the pressure mapping result. Reproduced with permission from ref 376. Copyright 2020 John Wiley and Sons. (f) Active matrix-type pressure sensor: (i) diagram of a tactile sensor array made from a stretchable active matrix; (ii) circuit diagram of one pixel in the stretchable active-matrix tactile sensor array; (iii) photograph of an array adhering and conforming to a human palm, and the pressure mapping of a synthetic ladybug with six conductive legs. Reproduced with permission from ref 380. Copyright 2018 Macmillan Publishers Limited. (g) Iontronic pressure sensor: (i) schematic of the iontronic pressure sensor; (ii) optical image of microfabricated sensor arrays amounting onto a human hand. Reproduced with permission from ref 53. Copyright 2017 John Wiley and Sons. (h) Ultrasonic pressure sensor: (i) schematic of an ultrasonic pressure sensor device in a flat state; (ii) working principle of the stretchable ultrasonic e-tattoo; (iii) photograph of the device conforming to a complex surface; (iv) blood pressure measurement with the ultrasonic device attached to a human neck, and the collected carotid artery blood pressure waveforms. Reproduced with permission from ref 54. Copyright 2018 Springer Nature.

design has a seamless connection between the sensing layer and the connectors, achieving a sensing range of 50% (Figure 11d-ii, middle) and good sensitivity along both the longitudinal (29.1) and traverse directions (-4.9) (Figure 11d-iii, right). In another work, Yamada et al. fabricated a strain sensor by laying vertically aligned SWCNT side-by-side to form an accordion-like structure, with PDMS serving as the substrate and encapsulation layer. Under stretching, the suspended SWCNT bundles formed bridges for the gaps, enabling the strain sensors to have a sensing range of up to 280%.³⁵⁸

In addition to the inorganic material-based strain sensors described above, organic materials, such as conducting polymers³⁵⁹ and hydrogels,^{360,361} have been employed in strain sensing e-tattoos due to their softness, biocompatibility, and self-healing properties. Liu et al. fabricated a hydrogel strain-sensing e-tattoo with an impressive sensing range of 500%.³⁶⁰ Recently, Wang et al. developed a self-healable hydrogel strain sensing e-tattoo with a PVA and hydroxypropyl cellulose stretchable matrix doped with CNTs (Figure 11e-i).³⁶¹ The ternary heterogeneous polymer network increased the fatigue threshold, exhibiting a stretchability up to 250% (Figure 11e-ii). Additionally, the hydrogel sensor demonstrated fast self-healing capability due to the rapid reformation of hydrogen bonds between the tetrafunctional borate ions and $-OH$ groups from both PVA and hydroxypropyl cellulose (Figure 11e-iii). In another work, Zhang et al. developed a 110 μm thick hydrogel e-tattoo with PVA as the matrix and polypyrrole (PPy) as the conductive filler, which can conformally attach onto human skin (Figure 11e-iv).³⁶² The strain sensor exhibited a sensing range of $\sim 400\%$ with a gauge factor of 2.1. Notably, the ultrathin nature enabled the strain sensor to detect the texture of objects (Figure 11e-v). Despite the excellent stretchability and self-healing capability, it remains challenging for hydrogel-based strain sensors to monitor strains over extended periods due to dehydration issues.

Table 3 summarizes representative strain sensing e-tattoos, including their materials, designs, sensing performance, and applications. There is typically a trade-off between sensitivity and sensing range.²⁶ Further efforts should focus on developing e-tattoo strain sensors with high sensitivity, wide sensing ranges, good stability, long-term operation, and high spatial resolution to comprehensively capture motion from various parts of the human body.

4.1.4. Pressure Sensors. Pressure-sensing e-tattoos allow for long-term monitoring of diverse physiological parameters, including blood pressure, respiration and heart rate, and physical activities. These e-tattoos can be categorized into eight types based on working principle: piezoresistive,^{363–366} capacitive,^{367–371} piezoelectric,^{372–375} triboelectric,^{229,376–379} active matrix,^{380–382} iontronic,^{53,383,384} hybrid-response,^{385–387} and ultrasonic devices.^{54,388,389} Figure 12 provides an overview of some representative pressure-sensing e-tattoos.

Piezoresistive pressure-sensing e-tattoos utilize materials whose resistance changes with pressure-induced deformation.^{363–366} These e-tattoos can outperform other pressure sensors owing to their high sensitivity and easy readout. For instance, Luo et al. developed a flexible piezoresistive sensor comprising carbon-black-decorated fabric as the piezoresistive material and gold interdigital electrodes for cuffless blood pressure measurement (Figure 12a-i, left).³⁶³ When pressure is applied to the sensor, the contact resistance between the rough contact surface of the fabric and the gold electrode changes (Figure 12a-i, right), resulting in a linear sensing range of 0–35

kPa and a sensitivity of 0.585 kPa^{-1} . Further demonstrations showed that the device can be attached to the wrist (Figure 12a-ii, left) to monitor the surface pulse wave with high reliability (Figure 12a-ii, right). However, piezoresistive pressure sensors often exhibit limited sensing ranges and temperature-dependent signal drift, thereby affecting measurement accuracy.

Capacitive pressure-sensing e-tattoos are based on a parallel-plate capacitor architecture, where the electrode distance or the dielectric constant of the sensor is modulated with pressure, resulting in a corresponding change in capacitance. Compared to piezoresistive pressure-sensing e-tattoos, capacitive ones demonstrate relatively weak sensitivities to temperature.³⁷⁰ Scalable matrix-addressed capacitive sensors can be easily developed by arranging top and bottom electrodes into row and column structures.^{369,370} Various strategies, such as utilizing soft dielectric layers and microengineering pressure-sensitive materials,³⁹⁰ have been employed to enhance the sensitivity of capacitive pressure sensors. For instance, Luo et al. developed a capacitive pressure-sensing e-tattoo using a micropillar PVDF (MP) dielectric layer (Figure 12b-i).³⁶⁷ The optimized capacitive e-tattoo exhibited a sensitivity of 0.43 kPa^{-1} for pressures less than 1 kPa (Figure 12b-ii), a minimum-pressure detection limit of 3.4 Pa, and a pressure sensing range of 0–50 kPa, as well as fast response and relaxation times of 33 ms. The image in Figure 12b-iii displays an 8×8 capacitive pressure sensor array based on the MP film and electrode array without external wires under the PDMS package, attached to the palm with a total thickness of about 300 μm . However, sensitivity enhancements through geometric microengineering designs are effective only at low-pressure ranges (e.g., up to 3 kPa). High sensitivity cannot be maintained at large-pressure ranges because compression quickly eliminates the air gaps, leaving a solid that further stiffens due to hyperelasticity and boundary confinement. To overcome the trade-off between sensitivity and pressure range, Ha et al. devised a flexible hybrid response pressure sensor (HRPS) comprising a piece of barely conductive porous nanocomposite (PNC), sandwiched between two flexible Au/PI film electrodes, with an ultrathin PMMA dielectric layer added between the PNC and one side of the electrodes (Figure 12c-i).³⁸⁵ The barely conductive PNC made of CNT-doped Ecoflex exhibited both piezoresistivity and piezocapacitance, providing a hybrid response to pressure changes. The equivalent circuit for the HRPS with barely conductive PNC is shown in Figure 12c-ii. The HRPS with an optimal CNT doping concentration (0.5 wt %) exhibited significantly enhanced sensitivity over wide pressure ranges, from 3.13 kPa^{-1} within 0–1 to 0.43 kPa^{-1} within 30–50 kPa. Further demonstrations showed that the HRPS can be placed on the neck to effectively measure the carotid arterial pulse waveform (Figure 12c-iii).

Piezoresistive and capacitive pressure sensors typically necessitate an external power source for generating electrical signals to characterize sensor impedances. In contrast, piezoelectric pressure sensors produce their own electric signals through charges generated by potential differences in the separation of positive and negative dipoles in response to mechanical deformation, eliminating the need for an external power supply.^{372,373} These sensors can operate across a broad frequency range, making them suitable for measuring dynamic pressure fluctuations.³⁷⁰ To make them more unobtrusive for on-skin health monitoring, Montero et al. demonstrated a fabrication process for fully printed, biocompatible, and ultrathin piezoelectric pressure-sensing e-tattoos (Figure

Table 4. Summary of Representative E-Tattoos for Pressure Sensing^a

application	materials	principle	sensitivity	sensing range	detection limit	thickness	stability	ref
blood pressure monitoring	PEN/Carbon-decorated fabric/Au/PI	piezoresistive	0.585 kPa ⁻¹	0–35 kPa	1 kPa	–	5000 cycles	363
blood pressure monitoring, pressure mapping	PDMS/CNT/Ag-coated fabric/G-nWF/PI	piezoresistive	6.417 kPa ⁻¹	0–800 kPa	1.2 kPa	–	1750 cycles	364
pressure mapping	PDMS/PEDOT:PSS/MWCNTs/PVDF	capacitive	0.43 kPa ⁻¹	0–50 kPa	3.4 Pa	300 μm	1000 cycles	367
human physiological monitoring	Ag ink	capacitive	–	0–200 Pa	<10 Pa	1180 μm	10 cycles	368
blood pressure monitoring	Tegaderm/PI/Au/CNT/Ecoflex 00–30/PMMA	combined piezoresistive and capacitive	3.13 kPa ⁻¹	0–50 kPa	0.07 Pa	700 μm	5000 cycles	385
blood pressure monitoring	PEDOT:PSS/GOPS/PVDF-TrFE/parylene C	piezoelectric	1703 pC/N	2.99–6.56 kPa	–	4.2 μm	1188000 cycles	372
blood pressure monitoring	PEDOT:PSS/P(VDF-TrFE)/parylene C	piezoelectric	275.8 mV/N	0–160 kPa	–	7 μm	657000 cycles	373
tactile sensing, energy harvesting	PDMS/Cu/Cr/PI	triboelectric	–	0–60 kPa	–	342 μm	2000 cycles	375
energy harvesting, human-machine interface	PDMS/PI/Cu/liquid bandage	triboelectric	–	0–16.67 kPa	<0.67 kPa	48.2 μm	3000 bending cycles	376
tactile sensing, pressure mapping, and human-machine interface	PDMS/PI/Cu	triboelectric	0.367 mV/Pa	0–50 kPa	<3 kPa	350 μm	2500 cycles	377
acoustic biometrics applications	TPU/DMF/EMIM/TFSI	combined Iontronic and triboelectric	165 mV/dB	>100 kPa	–	2.5 μm	20000 cycles	387
blood pressure monitoring, pressure mapping	CNT/SEBS H1052/SEBS H1221	active matrix	–	>40 kPa	–	200 μm	1000 cycles	380
blood pressure monitoring, breath signal recording, muscle activity recording, pressure mapping	ITO/nafion/PET/PEDOT:PSS	iontronic	5 nF·kPa ⁻¹	0–30 kPa	–	125 μm	10000 cycles	53
blood pressure monitoring	PI/Cu/Sn/piezo pillar/epoxy	ultrasonic	32% at –6 dB bandwidth	0–21.3 kPa	–	240 μm	–	54

^aNote: “–” means not available.

12d).³⁷³ The device consists of a highly uniform interdigitated electrode (IDE) structure made of PEDOT:PSS and an active piezoelectric layer made of P(VDF-TrFE) with an overall thickness of about 7.3 μm (Figure 12d-i, left). To align the dipoles and enhance piezoelectric performance, the device required high electric field poling (Figure 12d-i, right) by specialized equipment. Characterization revealed that the IDE structure with a sample thickness of 12.8 μm exhibited 4.7 times higher voltage sensitivity compared to the conventional metal–insulator–metal (MIM) structure with a similar sample thickness. The performance of this ultrathin and transparent sensor was demonstrated in monitoring arterial pulse waveforms (Figure 12d-iii). Although the sensor is self-powered, an external device, such as an amplifier or an analogue-to-digital converter (ADC), is still necessary for processing, measuring, and interpreting the signal. Furthermore, piezoelectric pressure sensors exhibit hysteresis in response to external pressure due to the inherent characteristics of piezoelectric materials.^{372,373}

Another approach to self-powered pressure-sensing e-tattoos involves leveraging the triboelectric effect, which is rooted in the mechanism of contact electrification and electrostatic induction.²²⁴ By employing materials with different electron affinities, electrical signals are generated as the contact areas between the functional materials change with applied pressure. Compared to piezoelectric pressure sensors, triboelectric pressure sensors offer higher pressure sensitivity and stability.^{229,390} Liu et al. introduced a thin and stretchable triboelectric e-tattoo for tactile sensing (Figure 12e-i, left).³⁷⁶ The fabricated triboelectric device exhibited excellent flexibility and stretchability (Figure 12e-i, right) and could discern a wide range of pressures associated with normal body motions. For instance, under the pressure of finger hitting (≈ 59.8 kPa), the open-circuit voltage

of the device was measured to be 60.4 V (Figure 12e-ii). Moreover, a 4 × 4 sensor array device was demonstrated for electric skin applications (Figure 12e-iii). Triboelectric pressure-sensing e-tattoos have also been employed for measuring pulse waveform, blood pressure, and respiration.^{391,392} Despite the advantages of triboelectric pressure-sensing e-tattoos, they are responsive only to dynamic pressures, limiting their use as static pressure sensors. Additionally, triboelectric sensors are sensitive to humidity,³⁹³ posing challenges in maintaining their output current in humid environments.

Real-time data acquisition from large-scale, high-resolution pressure sensor arrays is an outstanding challenge due to the large number of pixels that need to be read out simultaneously or sequentially. Passive and active matrices are two types of addressing schemes used for the readout circuitry.³⁸² In a passive-matrix circuit, a matrix of row and column wires is used to address individual pixels, with each pixel connected to both a row and a column interconnect. The simplicity of passive-matrix addressing, however, leads to crosstalk issues, where each pixel is influenced by its adjacent pixels. In contrast, active matrix addressing employs a separate transistor to switch each pixel within that array, resulting in higher precision and faster response time. Wang et al. proposed a scalable fabrication method to manufacture intrinsically stretchable transistor arrays (Figure 12f-i).³⁸⁰ This array utilized CNT as stretchable electrodes and data/scan lines, cross-linked SEBS as the dielectric, and a “conjugated polymer/elastomer phase separation induced elasticity” (CONPHINE) film as the semiconductor, achieving a high device density of 347 transistors per square centimeter. The circuit diagram of one pixel in the sensor array illustrates the connection between the transistor and the corresponding tactile sensor (Figure 12f-ii). The sensor

array maintained a charge-carrier mobility of $0.98 \text{ cm}^2 \cdot \text{V}^{-1} \cdot \text{s}^{-1}$, even at a 100% tensile strain. A 10×10 array of intrinsically stretchable resistive tactile sensors utilizing these transistors demonstrated sensitivity sufficient to detect a small artificial ladybug with six conductive legs when attached to a human palm (Figure 12f-iii).

Iontronic pressure sensors, consisting of two electrodes separated by an ion-conducting material and utilizing ion movement to measure pressure, differ from traditional capacitive pressure sensors. They offer ultrahigh unit area capacitance and sensitivity, remarkable signal-to-noise ratios, and excellent optical transparency.^{53,384} For example, Zhu et al. introduced an epidermal–iontronic interface by incorporating both a single-sided iontronic layer and the skin itself as the pressure-sensing elements (Figure 12g-i, left).⁵³ Under external pressure, the ionic electrode deformed and formed electronic–ionic contact with the skin (Figure 12g-i, right), establishing iontronic capacitance. The device, with a thickness of $125 \mu\text{m}$, achieved a sensitivity of $5 \text{ nF} \cdot \text{kPa}^{-1}$ and could be configured on various parts of human skin for pulse sensing, respiration tracking, muscle activity monitoring, and human hand pressure mapping (Figure 12g-ii). However, the epidermal–iontronic interface is significantly influenced by skin conditions such as body temperature and hydration levels, and it is challenging to make it insensitive to stretch.

Although pressure-sensing e-tattoos can be configured at peripheral sites to monitor peripheral pulse waveforms, emerging clinical evidence suggests that central arterial and venous pulse waveforms hold greater predictive value for cardiovascular events than peripheral waveforms. However, the aforementioned pressure-sensing e-tattoos are limited to accessing superficial peripheral vasculature. In contrast, ultrasonic acoustic pressure waves can penetrate human tissues up to a depth of 4 cm.⁵⁴ Ultrasonic transducers typically employ piezoelectric materials like lead zirconate titanate (PZT) and 1–3 composite.³⁸⁸ Wang et al. developed an approach to integrate ultrasonic transducers in a wearable format (Figure 12h-i).⁵⁴ The ultrasonic device conformed to the skin and could capture vessel diameter waveforms at deeply embedded arterial and venous sites using pulse-echo measurements (Figure 12h-ii). The active elements consist of standard rigid 1–3 piezoelectric composites connected with copper serpentine, used to convert voltage into mechanical vibration and vice versa. The device was ultrathin ($240 \mu\text{m}$) and stretchable (up to 60% strain) (Figure 12h-iii) and allowed for noninvasive, continuous, and accurate monitoring of the pulse waveforms from multiple body locations, such as the carotid artery waveform on the neck (Figure 12h-iv). Unfortunately, this device still relies on a large desktop data acquisition system to control acoustic emission and process received echoes.

Table 4 summarizes representative pressure-sensing e-tattoos with their materials and thickness, working principles, and performance. Despite advancements in pressure-sensing e-tattoos, challenges persist. For piezoresistive and capacitive pressure-sensing e-tattoos, achieving ultrathinness, stretchability, and conformability with good linearity and high sensitivity across a wide sensing range remains challenging due to the need for a certain degree of device compression to generate a significant signal. In the case of piezoelectric and triboelectric e-tattoos, they are unsuitable for measuring static pressures as they only output pulse signals when the pressure changes. Moreover, environmental factors like temperature and humidity can impact the performance of these e-tattoos, necessitating compensation

strategies such as advanced structural design and data processing algorithms. Lastly, there is a need for pressure-sensing e-tattoos with enhanced performance, featuring hybrid or multimodal responses, low power consumption, and wireless communication for robust long-term health or physical activity monitoring.

4.1.5. Photodetectors and Displays. Although humans have found uses for over 20 magnitudes of wavelengths of the electromagnetic spectrum, optical radiation ($100 \text{ nm} < \lambda < 1 \text{ mm}$) is uniquely defined by and used due to its adherence to the laws of optics (e.g., focusing with lenses). One of the greatest advantages of using optical wavelengths in modern electronic measurements, however, is the great availability of semiconductors with appropriate bandgap energies. For absolute imperceptible optical sensing of the body, flexible, and/or stretchable LEDs and photodetectors have been introduced. Organic semiconductors are very popular functional materials due to their inherent flexibility. However, a major challenge for ultrathin organic optoelectronics is that high-energy fabrication processes, such as plasma deposition can easily deform ultrathin substrates. Critical defects will emerge in the active layer if there is excessive roughness. Organic optoelectronics are also limited by their susceptibility to generating hole traps after exposure to oxygen and moisture, thus necessitating ample encapsulation from the outside environment. Despite active layers being very thin ($< 1 \mu\text{m}$), substrates and encapsulations tend to be orders of magnitude thicker to provide effective protection. The susceptibility to water also makes water-assisted transfer methods difficult. Therefore, ultrathin wearable organic LEDs and photodetectors are an outstanding challenge in the field. As an early example of solely using low-temperature processes to achieve ultrathin optoelectronics, Yokota et al. formed an ultraflexible (bending radius $< 10 \mu\text{m}$) e-tattoo with organic LEDs (OLEDs) and photodetectors by annealing the active layers at only $150 \text{ }^\circ\text{C}$ and forming the passivation layers with CVD.⁵² Thanks to the encapsulation provided by multiple layers of SiON and parylene, the device demonstrated an increased half-life from 2 to 29 h at a humidity of 60%. In another example, Barsotti et al. reported an encapsulation-free OLED on a tattoo paper substrate using water-assisted transfer.³⁹⁴ An insulating layer of PMMA was spin-coated on the tattoo paper followed by inkjet printing PEDOT:PSS electrode/hole injection layer. Then, the active layer (F8BT) is spin-coated and is followed by the final electrode (Al) deposition. To transfer to the skin, the tattoo is released from the backing paper using water. Although their achieved equivalent quantum efficiency (EQE) was significantly lower (0.0162–0.0104%) than traditional devices, the device is completely encapsulation-free, and the resulting thickness is extremely low ($2.3 \mu\text{m}$). Unfortunately, the devices failed after several minutes due to exposure to air and water. As encapsulation is necessary for long-term organic optoelectronic operation, significant research is ongoing to develop ultrathin encapsulations.³⁹⁵

One notable application of photosensitive measurement of the body is PPG. As the heart pumps, a pressurized pulse travels through the body and causes blood vessels to expand. The pulse can be observed by shining light (typically with an LED) into a region of tissue and measuring the amount of transmitted or backscattered light. Given that the optical absorption coefficient of blood is significantly higher than that of surrounding muscle (as discussed in section 2.6), the increase in the volume fraction of blood in the tissue leads to greater light attenuation and a decrease in detected light (typically measured with a photodetector). Although now commonplace due to its simplicity,

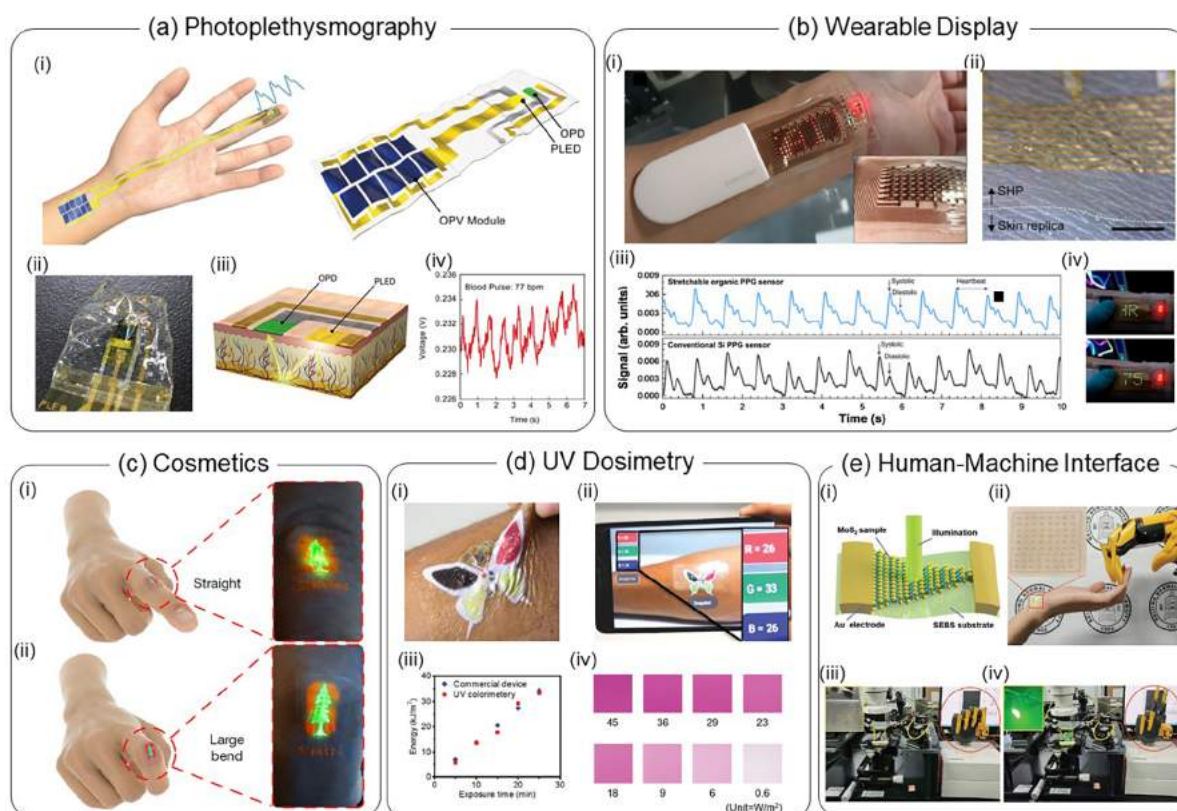


Figure 13. E-Tattoos for photodetection and display. (a) Self-powered organic PPG sensor: (i) device overview; (ii) the e-tattoo is ultraflexible and soft; (iii) diagram of PPG sensing; (iv) pulse waveform and extracted heart rate collected from the PPG e-tattoo. Reproduced with permission from ref 402. Copyright 2021 Springer Nature. (b) Stretchable, wearable e-tattoo display and pulse oximeter: (i) photograph of the e-tattoo on the wrist; (ii) ultrathin microcracked Au stretchable interconnects; (iii) pulse waveforms from the stretchable e-tattoo and a commercial PPG sensor; (iv) HR displayed in real-time. Reproduced with permission from ref 410. Copyright 2021 AAAS. (c) High-brightness cosmetic tattoo LEDs: (i) photographs of the LEDs on a finger without and (ii) with bending, respectively. Reproduced with permission from ref 411. Copyright 2022 Springer Nature. (d) Ultra-soft, tattoo-like personal UV dosimeter: (i) the e-tattoo on the arm demonstrates high adhesion and deformability; (ii) after exposure to UV, the e-tattoo changes color; (iii) the color change can be quantified using a custom mobile app; (iv) detected UV exposure agrees well with a commercial device. Reproduced with permission from ref 415. Copyright 2017 John Wiley and Sons. (e) Stretchable photodetectors for human-machine interface: (i) schematic of the stretchable MoS₂ photodetectors; (ii) photograph of the stretchable photodetector array on the wrist. (iii, iv) robot control by light illumination on the photodiode array. Reproduced with permission from ref 419. Copyright 2022 John Wiley and Sons.

PPG faces challenges in various situations due to its extreme sensitivity to motion. One important contributing factor is the relative motion between the device and the skin.³⁹⁶ Tattoo sensors, due to their skin-like properties, can deform with the skin and minimize relative motion. Lee et al. introduced a soft PPG sensor with light polarizers to further reduce sensitivity to motion.³⁹⁷ First, polarized light is used to illuminate the tissue. The light becomes more randomly polarized the deeper it penetrates the tissue. Therefore, light that only penetrates too shallow to reach the blood vessels will be biased toward the original polarity and can be filtered out with a cross polarizer on the detector. To make a tattoo-like PPG sensor, commercial-off-the-shelf (COTS) rigid optoelectronics may be sufficient. Because the mismatch between the relevant air and tissue optical properties ($n = 1$ and 1.4 , respectively) is not as severe as electrical ($\sigma = 10^{-14}$ to 10^{-17} S/m and 0.01 – 0.5 S/m, respectively) and ultrasonic ($Z = 400$ Rayls and 1.7 MRayls, respectively) properties, ultraconformability of the active elements is not required. Therefore, rigid COTS LEDs and photodetectors have been used with stretchable and thin interconnects for global conformability, stretchability, and comfort. Lo et al. employed inkjet-printed PEDOT:PSS as a stretchable conductor for rigid COTS red LEDs and photo-

detectors.³⁹⁸ Stretchable interconnects can also be achieved through structural engineering. Li et al. designed a multi-PPG system to extract pulse wave velocity with COTS red and green LEDs and photodetectors with a “watch chain” interconnect design.³⁹⁹ By placing the photodetector along the artery, the pulse wave can be measured at two locations and the corresponding pulse wave velocity can be extracted by dividing the distance by the time delay of the two signals and correspondingly estimating blood pressure.

When measuring the PPG signal with multiple wavelengths of light, blood oxygen saturation (SpO₂) can be extracted due to differences in the absorption spectra of oxygenated and deoxygenated hemoglobin (HbO₂ and Hb, respectively). Jeong et al. utilized copper serpentines to connect COTS red and IR LEDs, a photodetector, and ICs to create a modular e-tattoo with a pulse oximeter configuration.⁴⁰⁰ Because the LED consumes the most power in a PPG system, minimizing LED power consumption is advantageous. One approach is to arrange the detectors to receive more light and increase the surface area of the photodetectors. photodetectors can also surround the LEDs, as demonstrated in an ultralow-power ($24 \mu\text{W}$), concentric pulse oximeter introduced by Lee et al.⁴⁰¹ Self-powered LEDs, as seen in the organic–photovoltaic powered

photonic skin demonstrated in Figure 13a-i, could also be utilized.⁴⁰² All three optoelectronic devices (LED, photo-detector, organic–photovoltaic) and the substrate (polyethylene) are ultraflexible, leading to impressive imperceptibility (Figure 13a-ii). With the light emitted from the PLED penetrating the finger, the organic photodetector can detect the reflected light (Figure 13a-iii), and a clear pulse waveform was measured with the system (Figure 13a-iv). Another alternative is to use multiple photodetectors with narrow spectral responses and only a single, broadband light source. Han et al. designed an LED-free flexible pulse oximeter using only ambient light and photodetectors tuned for green, red, and IR light.⁴⁰³ They achieved high spectral sensitivities (~ 100 nm) due to the relatively narrow sensitivities of organic absorbers⁴⁰⁴ and the addition of optical filters. PPG signals were acquired with sunlight and ambient fluorescent, LED, and incandescent light.

While PPG is solely concerned with arterial blood volumetric changes, the same principles of absorption spectrometry are used in several other applications. NIRS extends beyond PPG by analyzing nonpulsatile changes in tissue absorbance, aiming to detect absolute changes in Hb and HbO₂ concentrations. Kim et al. introduced a battery-free epidermal optoelectronic system capable of PPG, NIRS, UV dosimetry, or skin spectrometry using COTS optoelectronics and an island-serpentine structure.⁴⁰⁵ The tattoo could detect changes in the concentration of deoxyhemoglobin, oxyhemoglobin, and total hemoglobin (Hb, HbO₂, and tHb, respectively) using NIRS and agreed well with a commercial NIRS device. This optoelectronic system could be reconfigured into a skin spectrometer using four LEDs (red, IR, orange, and yellow) to construct a four-wavelength spectrogram of skin color. Diseases such as jaundice or Addison's disease can be detected by observing changes in the color of the skin (i.e., tissue absorption spectra). The entire optoelectronic system is powered and transmits data through near-field communication (NFC).

The human eye is estimated to process up to 4.3 Mbps of information⁴⁰⁶ with a resolution of 8.6 μm .⁴⁰⁷ Tremendous efforts have been made to develop high-density visible light emitters for electronic optical displays. On-skin devices (e.g., ECG, PPG) need ways to convey their acquired signals (e.g., HR, SpO₂) to the user. On-skin electronic displays offer a seamless interface between bioinstrumentation and the user. Choi et al. demonstrated a flexible, full-color (i.e., red–green–blue or RGB pixel) on-skin display tattoo with ultrathinness (< 7 μm).⁴⁰⁸ Each pixel consists of RGB OLEDs directly fabricated on MoS₂ thin film transistors. Each LED can be turned on by applying a control signal to the gate and drain of its respective thin film transistor. For high-resolution (e.g., 2460 pixels per inch), deformable, and full-color displays, a stamp-based transfer method dubbed “*intaglio transfer printing*” was introduced to transfer quantum dots from a donor substrate to ultrathin (total device thickness ~ 2.6 μm) substrates.⁴⁰⁹ In addition to high pixel density, the display size should be large enough to convey information easily to the user. This large area necessitates either stretchable interconnects between light-emitting elements and/or stretchable light emitters. Unfortunately, OLED and polymer light-emitting diode performances typically degrade from cracking under stretching. Serpentine interconnects are not conducive for high-density display as these structures require larger dimensions than the active elements to achieve high stretchability. To overcome this, a stretchable optical healthcare patch with an OLED display was designed using stretchable microcracked gold interconnects and stress relief layers (Figure

13b-i).⁴¹⁰ The gold interconnects and stress relief layers reduce stress accumulation on the pixel and the chance of mechanical fracture of the interconnect to the active elements and are ultraconformable (Figure 13b-ii). The acquired waveforms with the optical healthcare patch have comparable signal quality to a traditional silicon-based PPG sensor (Figure 13b-iii) and are used to extract heart rate. The extracted heart rate can be displayed in real time on the organic LED array (Figure 13b-iv).

In addition to conveying information, tattoo-like VIS emitters can serve as a form of self-expression or as cosmetics, harkening back to some of the intended purposes of actual tattoos. Zhang et al. demonstrated a highly bright (7450 cd per square meter) and stretchable (100% strain) LED pattern (Figure 13c-i, c-ii).⁴¹¹ The active layer consists of SuperYellow (SY) nanofibers in a polyurethane soft elastic matrix, and the LED could be wirelessly powered through an NFC chip on a flexible printed circuit board. While displays typically use RGB pixels as combinations of these wavelengths stimulate the cones in the human eye to mimic any other color, cosmetic devices can employ a single LED with any color. Furthermore, tuning the color of the LED can be used as a form of aesthetic signal visualization. For example, Koo et al. developed a multifunctional sensing and display platform combining wearable ECG electrodes, a CNT amplifier, and a color-tunable OLED (CTOLED).⁴¹² A LabVIEW program analyzed the ECG waveform and adjusts the brightness of the OLED based on the waveform's amplitude, allowing the CTOLED to “beat” with the detected ECG signal. The color of the CTOLED will also change if an abnormal ECG signal (e.g., pathological Q wave) is detected, allowing for a quick and intuitive interpretation of a patient's cardiovascular state.

Optical e-tattoos are not limited to measurements only with semiconducting devices. Other photosensitive materials have found uses in UV exposure monitoring. Personal UV dosimetry provides valuable insight into the increased carcinogenic risks an individual may experience, considering skin tone, workplace, and lifestyle, which prevent public UV indices from being universally translatable. Plastics such as polysulphone and polyphenylene oxide were found to darken upon exposure to UV light⁴¹³ and remain the most used materials for chemical UV dosimeters.⁴¹⁴ However, they are rigid and require pins, bands, or tape for attachment to the skin or clothing. To overcome this, Araki et al. introduce a skin-like tattoo that changes color based on UV exposure.⁴¹⁵ The tattoo contains a photosensitive activator that induces color changes in a dye when exposed to UV light (Figure 13d-i). Both the dye and photosensitive activator are embedded in a soft PDMS matrix. Sensitivities for UV-A and UV-B light are achieved by integrating optical filters. The color changes are quantified by taking a picture and are calibrated for ambient illumination with on-device color references (Figure 13d-ii, d-iv). The tattoo demonstrated comparable performance to a commercial UV dosimeter. The tattoo can communicate over NFC thanks to an in-built copper coil and NFC chip. Specifically, it will automatically launch the image capture and analysis application on a mobile phone and measure the skin temperature for calibration. The e-tattoo evolved into a commercial UV exposure patch (My UV Patch by L'Oréal).⁴¹⁶ A battery- and chip-free UV light detector was designed around a gallium nitride (GaN) surface acoustic wave resonator.⁴¹⁷ Absorption of UV light by GaN induces a change in the resonant frequency of the surface acoustic wave and the connected antenna, enabling wireless and battery-free communication. However, the GaN surface acoustic wave is also

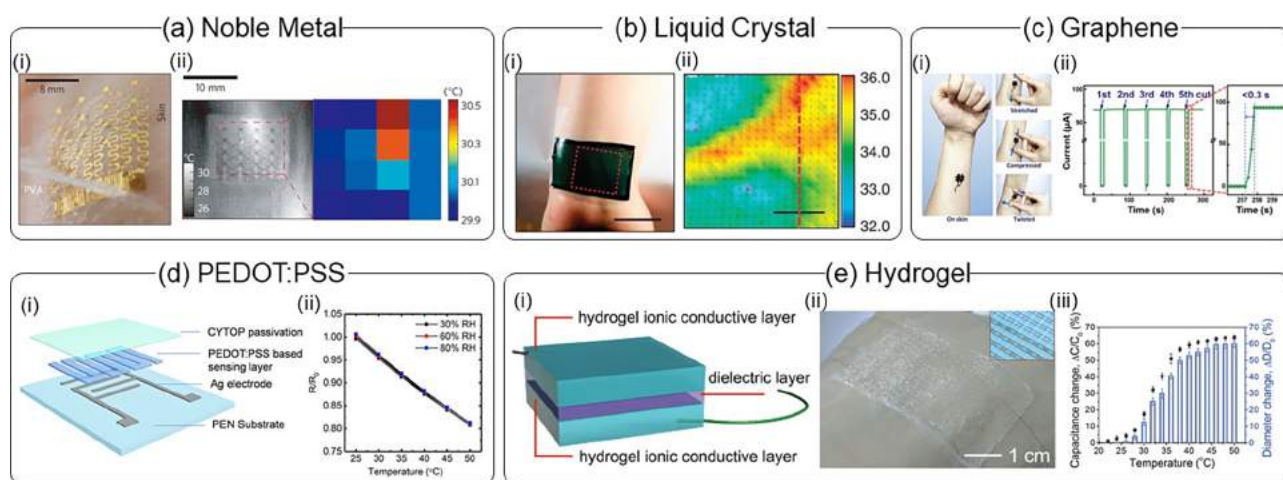


Figure 14. E-Tattoos for temperature sensing. (a) Noble-metal-based temperature sensing e-tattoo: (i) optical image of a 4×4 tattoo-like temperature sensor array mounted on human skin; (ii) infrared image of a human wrist temperature (left) and temperature mapping from the measurement (right). Reproduced with permission from ref 47. Copyright 2013 Springer Nature. (b) Liquid-crystal-based temperature sensing e-tattoo: (i) optical image of the e-tattoo attached on the wrist; (ii) temperature distribution on the wrist measured by a 26×26 sensor array. Reproduced with permission from ref 3. Copyright 2014 Springer Nature. (c) Graphene-based temperature sensing e-tattoo: (i) photographs of the graphene e-tattoo to the skin during stretching, pressing, and twisting; (ii) measured electric currents after multiple cuttings of the self-healable graphene e-tattoo. Reproduced with permission from ref 43. Copyright 2019 John Wiley and Sons. (d) PEDOT:PSS-based temperature sensor: (i) exploded schematic of the PEDOT:PSS temperature sensor; (ii) response of the resistance to temperatures at different humidities. Reproduced with permission from ref 158. Copyright 2020 Springer Nature. (e) Hydrogel-based temperature sensor: (i) schematic of hydrogel temperature e-tattoo; (ii) optical image of the e-tattoo attached to the skin of a human hand; (iii) the change of capacitance and the diameter of the e-tattoo in (ii). Reproduced with permission from ref 431. Copyright 2017 The Royal Society of Chemistry.

sensitive to mechanical strain and ion concentrations from sweat.

Optical signals are inherently contactless and therefore are an attractive option for human–machine interface. A touchless user interface can be as simple as a single photodetector. The shadow of a user's finger above the photodetector can be used to trigger an action and only requires ambient light. Furthermore, object proximity can be determined by including an IR LED and measuring the amount of reflected light. Hughes et al. utilized commercial optical proximity detectors using this principle encapsulated in PDMS to create a soft e-skin for object and touch detection.⁴¹⁸ Optical signals can also transfer information wirelessly. A stretchable array of MoS_2 photodetectors controlled a robotic hand by illuminating individual detectors (Figure 13e-i–e-iv).⁴¹⁹ Due to interlayer sliding of the multilayer MoS_2 , high stretchability ($\sim 50\%$ tensile strain) is achieved and leads to device imperceptibility. Various commands are sent to the robotic hand by illuminating different detectors. However, this type of optical signal transmission still requires line-of-sight and accurate alignment to individual photodetectors, and thus other bands of the electromagnetic spectrum (i.e., radio waves) will be more robust in most applications.

Despite significant progress in developing soft optoelectronics, these devices typically still rely on traditional, silicon-based ICs for control, signal processing, data acquisition, and wireless communication. Additionally, as soft displays stretch, their pixel densities inherently decrease. Finally, there are many more examples of stretchable optoelectronics being reported in the literature in nonwearable contexts.^{420,421} We are excited to see how these technologies can be applied to the field of e-tattoos.

4.1.6. Temperature Sensors. Skin temperature monitoring can offer valuable information for medical applications such as fever detection⁴²² and sports performance assessment.⁴²³

Moreover, skin temperature mapping can be employed to monitor blood flow in arteries.⁴²⁴ Skin temperature is typically characterized by measuring the change in electrical resistance of a temperature-sensitive material in contact with the skin. Traditional thermometers, such as digital thermometers and thermal imagers, are unsuitable for continuous health monitoring due to their limited spatial resolution or poor conformability with the human body. In contrast, the conformal nature of e-tattoos enables efficient heat transfer from the skin for accurate temperature sensing and mapping.

Temperature e-tattoos can be designed by leveraging the temperature-dependent electrical characteristics of various materials. Gold is one such material that exhibits a linear response of resistance over a range of temperatures, with a temperature coefficient of resistance of $0.0025 \text{ }^\circ\text{C}$. Webb et al. developed an e-tattoo temperature sensing system by integrating a 50 nm thick gold serpentine mesh into a $50 \text{ }\mu\text{m}$ thick PI substrate (Figure 14a-i).⁴⁷ This e-tattoo can be applied to the skin in a conformal manner (Figure 14a-ii, left), providing robust adhesion and millikelvin precision. As a result, the e-tattoo can measure subtle variations in skin temperature during mental and physical stimuli. Additionally, the device can be easily fabricated into a 4×4 sensor array, enabling spatial mapping of the temperature (Figure 14a-ii, right). This allows monitoring of the reactive hyperemia response without precise placement of a single device above the artery. In another work, Gao et al. developed an e-tattoo temperature array using thermochromic liquid crystal as the sensing material.⁵ This array consists of microencapsulated chiral nematic liquid crystals that undergo a phase change with increasing temperature, leading to a blue-shift in the peak of the reflected light (Figure 14b-i). Therefore, the temperature change can be directly monitored by a digital camera with a measurement precision of $\pm 50 \text{ mK}$, which is comparable to that of infrared cameras. The device is only $50 \text{ }\mu\text{m}$ thick, enabling a 26×26 temperature sensor array to conform to

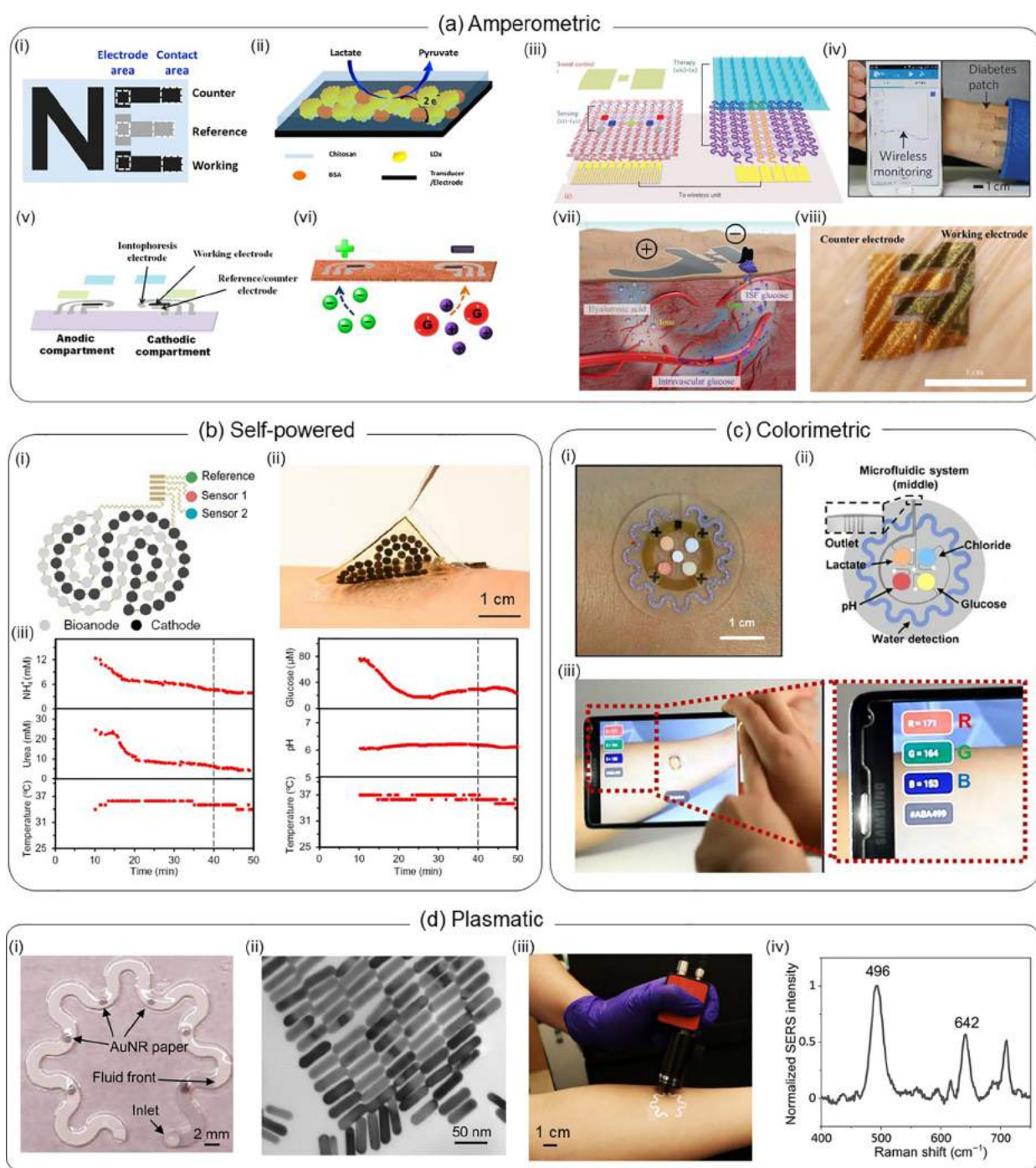


Figure 15. E-tattoo-based biochemical sensors. (a) Amperometric e-tattoo biochemical sensors: (i) schematic of the structure of a screen-printed e-tattoo biochemical sensor; (ii) schematic of lactate oxidation on enzyme-coated working electrode; (iii) schematic of graphene tattoo sensor consisting of sweat-controlling units, sweat-sensing units, and drug delivery units; (iv) tattoo sensor is attached to the skin and connected to a wireless electrochemical analyzer; (v) schematic of the structure of a screen-printed e-tattoo sensor for interstitial fluids analysis; (vi) schematic of the working mechanism of the iontophoresis for interstitial fluids extraction; (vii) schematic of the interstitial fluids glucose extraction with paper battery-induced hyaluronic acid delivery; (viii) nanostructured gold tattoo for interstitial glucose monitoring. Reproduced with permission from refs 102, 50, 443, and 450. Copyright 2013, 2015 American Chemical Society; 2017 AAAS. (b) Self-powered e-tattoo sweat sensor: (i) schematic of the design of the biofuel cell-sweat sensor; (ii) photograph of the biofuel cell powered sensor attaching to a healthy individual's arm; (iii) multiple analyte sensing in the sweat with the biofuel cell powered sensor in (i). Reproduced with permission from ref 121. Copyright 2020 AAAS. (c) Colorimetric sweat sensor: (i) photograph of the colorimetric sweat sensor on the skin; (ii) schematic of the structure of the sweat sensor; (iii) image capture with a smartphone for sweat analysis. Reproduced with permission from ref 451. Copyright 2016 AAAS. (d) Plasmatic sweat sensor: (i) photograph of the paperfluidic device with plasmatic sensors; (ii) transmission electron microscopy image of the gold nanorods in the SERS substrate; (iii) spectra collection with a portable Raman spectrometer; (iv) Raman spectrum of the sweat collected from the sensor in (iii). Reproduced with permission from ref 454. Copyright 2022 Springer Nature.

the wrist with minimal perturbation of the natural mechanical and thermal properties of the skin. The device array provided a three-dimensional temperature mapping of the wrist, including the blood vessels underneath (Figure 14b-ii).

Unfortunately, many temperature-sensitive materials (e.g., noble metals, conducting polymers) are also strain dependent. Therefore, decoupling the changes in resistance due to skin deformation and temperature changes is critical. To overcome this limitation, the structure of the e-tattoo can be designed such that strain is not concentrated in temperature-sensing components. Park et al. developed a temperature-sensing e-tattoo using an Al₂O₃-doped ZnO layer with embedded silver nanoparticles as the sensing layer. This layer was encapsulated by 1.2 μm thick PI layers.⁴²⁵ The temperature sensor was designed with a serpentine structure with a higher curvature than that of temperature sensing nodes, effectively reducing the strain concentration in the sensing nodes and enabling robust temperature sensing under strains.

In addition to standalone temperature sensing, e-tattoos can be multifunctional platforms with various sensing materials, including graphene,⁴²⁶ CNTs,⁴²⁷ silver nanowires,⁴²⁸ and silver nanoparticles.⁴²⁹ For example, a multifunctional e-tattoo platform was developed by Wang et al. utilizing a combination of graphene and silk fibroin (Figure 14c-i).⁴³ The graphene flakes dispersed in the matrices formed electrically conductive paths that vary with temperature, strain, and humidity. The device exhibited a sensitivity of 0.021/°C for temperature sensing. Notably, the silk fibroin can also form reversible hydrogen bonds for self-healing, allowing the mechanical properties and sensing performance to fully recover even after repeated cutting within 0.3 s (Figure 14c-ii).

Transparent e-tattoos can maintain the natural appearance of the user to protect their privacy. PEDOT:PSS exhibits high optical transparency and thermo-resistive behavior, making it a promising candidate for transparent e-tattoos for temperature sensing. Wang et al. developed a PEDOT:PSS temperature sensor by patterning using a dispenser (Figure 14d-i).¹⁵⁸ They cross-linked the hydrophilic part of the PSS unit with (3-glycidyloxypropyl) trimethoxysilane to make PEDOT:PSS water-stable. At last, the device was encapsulated with a fluorinated polymer layer. The device allowed reliable temperature sensing even in humid environments ranging from 30% to 80% room humidity (Figure 14d-ii). When it was mounted on and detached from the skin, the PEDOT:PSS temperature sensor showed a response time of 1.5 s and a recovery time of 6 s, respectively. A thermoresponsive ionic conductive hydrogel undergoes conformational changes with electrical resistance and transmittance variation, enabling temperature sensing in a transparent manner.⁴³⁰ Lei et al. developed a temperature-sensing e-tattoo through 3D printing of thermoresponsive *N,N*-dimethylacrylamide, followed by polymerization.⁴³¹ They further assembled the two hydrogels into a capacitive pressure sensor with a dielectric layer (Figure 14e-i). Although not transparent at room temperature, the transparency increased when attaching to human skin due to a hydrogel phase transition around 30 °C (Figure 14e-ii). Under thermal loading, the hydrogel electrodes underwent conformational changes, resulting in alterations in their effective area, inducing the change in capacitance and transmittance (Figure 14e-iii).

Despite the many advantages of temperature e-tattoos, there are also some potential limitations to consider. One main limitation is achieving robust sensing capabilities in varying environmental conditions. For example, the adhesion of e-

tattoos is affected by sweat or human motion, particularly in long-term and ambulatory applications. This makes temperature data acquisition more difficult than in a controlled condition, such as a laboratory setting. Additionally, e-tattoos cannot directly provide an assessment of core temperature, a parameter with much greater clinical relevance. Robust adhesion without compromising the sensitivity and the use of multiple sensors to retrieve heat capacity and transient temperature information may help obtain more accurate core body temperature.^{432,433}

4.2. Biochemical Sensors

The biophysical sensors above-described all require energy (e.g., electrical current, acoustic waves, light) to be transmitted into the body. Conversely, measurements can be made by analyzing biochemicals that get transmitted outside of the body. Biofluids such as sweat, interstitial fluids, tears, and saliva containing important biochemical information can be secreted due to the permeability of the skin.^{11,434–436} Biochemicals can also be secreted through wound exudate when the skin integrity is destroyed.^{437–439} E-Tattoos provide an attractive platform for continuous, noninvasive, and real-time monitoring of various biomarkers in these biofluids. Over the past decade, a variety of e-tattoos have been developed and applied to detect bacteria in saliva,⁴⁴⁰ glucose in tears,⁴⁴¹ electrolytes and lactate in sweat,^{102,442} glucose in interstitial fluids,⁴⁴³ and biomarkers in wound exudate.⁴⁴⁴ In this section, we discuss the applications of e-tattoos in the analysis of sweat, interstitial fluids, and wound exudate.

4.2.1. Body Fluid Analysis. Sweat and interstitial fluids are two crucial biofluids utilized for biochemical sensing. Sweat is the most accessible biofluid for chemical sensing because sweat glands are distributed across the entire body with densities ranging from tens (e.g., in the ears and lips) to hundreds (e.g., in the forehead and palms) of glands per square centimeter.¹¹ Conversely, biochemical analysis of interstitial fluids provides the closest correlations with that of blood. The conformability of e-tattoos enables efficient mass transfer at the interface for reliable analysis of the biomarkers. Additionally, biomarkers such as lactate can be sampled during exercise better as e-tattoos can maintain stable contact under deformation than rigid wearables. The first e-tattoo chemical sensor operates using amperometry and thus consists of a carbon working electrode, a carbon counter electrode, and an Ag/AgCl reference electrode (Figure 15a-i).¹⁰² The working electrode is typically functionalized with specific types of enzymes that selectively oxidize the target biochemicals in sweat, leading to an increase in current (Figure 15a-ii). To achieve high sensitivity, materials with large surface areas, such as carbon particles,⁴⁴² CNTs,³⁸⁹ graphene,⁵⁰ and liquid metal microparticles¹³² are typically used as working electrodes. These biosensors have been used to provide noninvasive and continuous monitoring of a wide range of biochemicals in sweat, including lactate,^{102,132} pH,^{445,446} sodium ions,⁴⁴² heavy metal ions,⁴⁴⁷ ammonium,²⁴³ glucose,^{50,132,443,449} and alcohol.²⁴² Additionally, biochemical sensors can be printed together with other devices to form multimodal sensors. For example, by printing a carbon electrochemical sensor together with an Ag/AgCl ECG electrode, a multimodal sensor was fabricated and capable of monitoring both the lactate level in sweat and ECG signals during exercise.⁴⁴⁸

The activity of the immobilized enzyme can be influenced by environmental factors, such as temperature, humidity, and pH, necessitating continuous correction over time for biochemical sensors. Lee et al. developed a closed-loop transparent graphene

hybrid (GP hybrid) patch with multiple sensors for glucose sensing, correction, and transdermal drug delivery.⁵⁰ The sensor array includes a gold-doped graphene electrode with functionalized glucose oxidase (GOx) for glucose sensing, a PANI-coated graphene electrode for pH sensing, a PEDOT:PSS-coated graphene electrode for humidity sensing, and a graphene strain sensor (Figure 15a-iii). The pH sensor corrects pH deviations in the GOx-based glucose sensor, enabling reliable glucose measurement for up to 6 h without further calibration. The patch can be conformally laminated onto human skin and then coupled with a portable analyzer that powers the e-tattoo and wirelessly transfers the data to mobile devices (Figure 15a-iv). The drug delivery system includes a microneedle array loaded with metformin, a gold mesh–graphene hybrid heater, and a graphene-based temperature sensor. The strain sensor detects hypoglycemia-induced tremors and triggers the breakdown of the thermally activated coating layer of the microneedles with the on-device heater, enabling closed-loop glucose sensing and drug delivery to control glucose level. In a following work, they further optimized the system by introducing porous sweat uptake and waterproof layers and shrinking the electrodes.⁴⁴⁹ The new design allowed for reliable glucose sensing even with sweat volumes down to 1 μL .

Interstitial fluids provide a more accurate representation of glucose levels⁴³⁴ because they are directly involved with biological material delivery to and from the cells. The biomarkers in interstitial fluids are generally extracted to the skin surface through reverse iontophoresis, which involves the application of a small current across the skin to induce electroosmotic flow of glucose to the cathode. Therefore, in situ monitoring of interstitial glucose can be achieved by incorporating reverse-iontophoresis electrodes on an enzyme-based amperometry biochemical sensor. Bandodkar et al. provided the first proof-of-concept demonstration of a tattoo sensor for noninvasive interstitial glucose monitoring.⁴⁴³ The device consists of anodic and cathodic contingents, each containing a carbon-Prussia-blue working electrode, an Ag/AgCl reference/counter electrode, and an Ag/AgCl iontophoresis electrode (Figure 15a-v). The working electrode of the cathodic contingent was modified with GOx for selective oxidation of the extracted glucose into hydrogen peroxide (Figure 15a-vi). The hydrogen peroxide can further oxidize the Prussia blue at the working electrode and lead to a rapid increase in the current. Therefore, the sensor allowed real-time and noninvasive detection of the rise of glucose after a meal. Continuous application of the current across the skin may cause skin irritation or pain in users, making it challenging to use iontophoresis-based sensors for long-term glucose sensing. Another issue is that the correlation between the concentration of glucose in sweat and interstitial fluids and the blood is still too low for clinical use. To address these issues, Chen et al. developed a method to directly extract intravascular blood glucose to the skin surface with paper-battery-enabled hyaluronic acid delivery into the interstitial fluids.⁴⁵⁰ The paper battery generated subcutaneous electrochemical twin channels (ETCs) and delivered hyaluronic acid into the interstitial fluids. Extra hyaluronic acid increased interstitial fluid osmotic pressure, disrupting the balance between interstitial fluid filtration and reabsorption and promoting glucose refiltration from the arterial ends into the interstitial fluids (Figure 15a-vii). The higher glucose concentration in the interstitial fluids also increased the flux of reverse iontophoresis and led to more extracted intravascular blood glucose to the skin

surface. Therefore, the correlation of the glucose concentration was greatly improved. The glucose in the extracted interstitial fluids was in situ analyzed by a nanostructured gold electrode on a 3 μm thick tattoo sensor (Figure 15a-viii) and demonstrated good agreement with matched results from a commercial glucometer during a 1-day period of glucose monitoring.

The above electrochemical sensors all require an external power supply, limiting the softness of the whole sensing system. To address this issue, Yu et al. developed a perspiration-powered integrated electronic skin termed PPES that is powered by the lactate in the sweat through a flexible biofuel cell array.¹²¹ The biofuel array consists of a CNT-coated GO-Ni foam anode and a Pt-Co nanoparticle-decorated CNT cathode (Figure 15b-i). The anode was modified with lactate oxidase (LOx), which can oxidize the lactate in the sweat into pyruvate. On the cathode, oxygen is reduced to water under the catalysis of Pt-Co nanoparticles, resulting in a maximum output power of 3.5 $\text{mW}\cdot\text{cm}^{-2}$. The PPES is only 11 μm in thickness and can be laminated on different body parts (Figure 15b-ii) for accurate and real-time sensing of multiple biomarkers in sweat, including urea, glucose, NH_4^+ , and pH during stationary cycling exercise (Figure 15b-iii). Although electrochemical sensors allow for real-time, accurate, and continuous sweat analysis, the biomarker-sensitive elements are prone to degradation after exposure to harsh environments or contamination, compromising the sensor performance. Additionally, although electrochemical sensors can be made ultrathin and soft, their reliance on batteries leads to large overall systems. Finally, the electrical output signals still require additional signal processing modules to convert back to the biochemical concentration in sweat.

Optical detection provides another attractive method for biochemical sensing owing to its ease of operation and simple readout. Optical detectors generally rely on chemical reactions between dye indicators and the chemicals in biofluids that change the color of the dyes. Therefore, simple quantitative assays can be achieved through image capture with a phone. Koh et al. developed a colorimetric biochemical sensing platform with dye indicators in a closed microfluidic system (Figure 15c-i).⁴⁵¹ The microfluidic system can directly and rapidly collect generated sweat before it evaporates or gets contaminated. There are four independent reservoirs filled with color-responsive materials that selectively react with lactate, H^+ , chloride, and glucose (Figure 15c-ii). The color change of each reservoir correlates with the concentration of the target biomarker and can be quantified through digital image capture with a smartphone (Figure 15c-iii). Additionally, the microfluidic channels are filled with water-responsive dyes, which can detect sweat rate and volume. In a following study, they developed a long-term sensing system by introducing a superabsorbent polymer-based active valve to control the overflow of the collected sweat and a passive valve with the tailed hydrophobic and hydrophilic surface to guide the flow of the sweat.⁴⁵² In a recent study, Yin et al. developed an electrochromic biochemical sensing system based on electrochemical redox/oxidization-induced color changes of PEDOT:PSS.⁴⁵³ The system consists of electrochemical sensors, a stretchable Ag_2O –Zn battery, 10 individually addressable electrochromic pixels, and a microcontroller unit. The electrochemical sensors can detect the concentration of the metabolites in sweat, where the current is correlated to the metabolite concentration. The current can be converted to voltage and sensed by the microcontroller unit to control the on-and-off of the electrochromic display. Therefore, the concentration of the

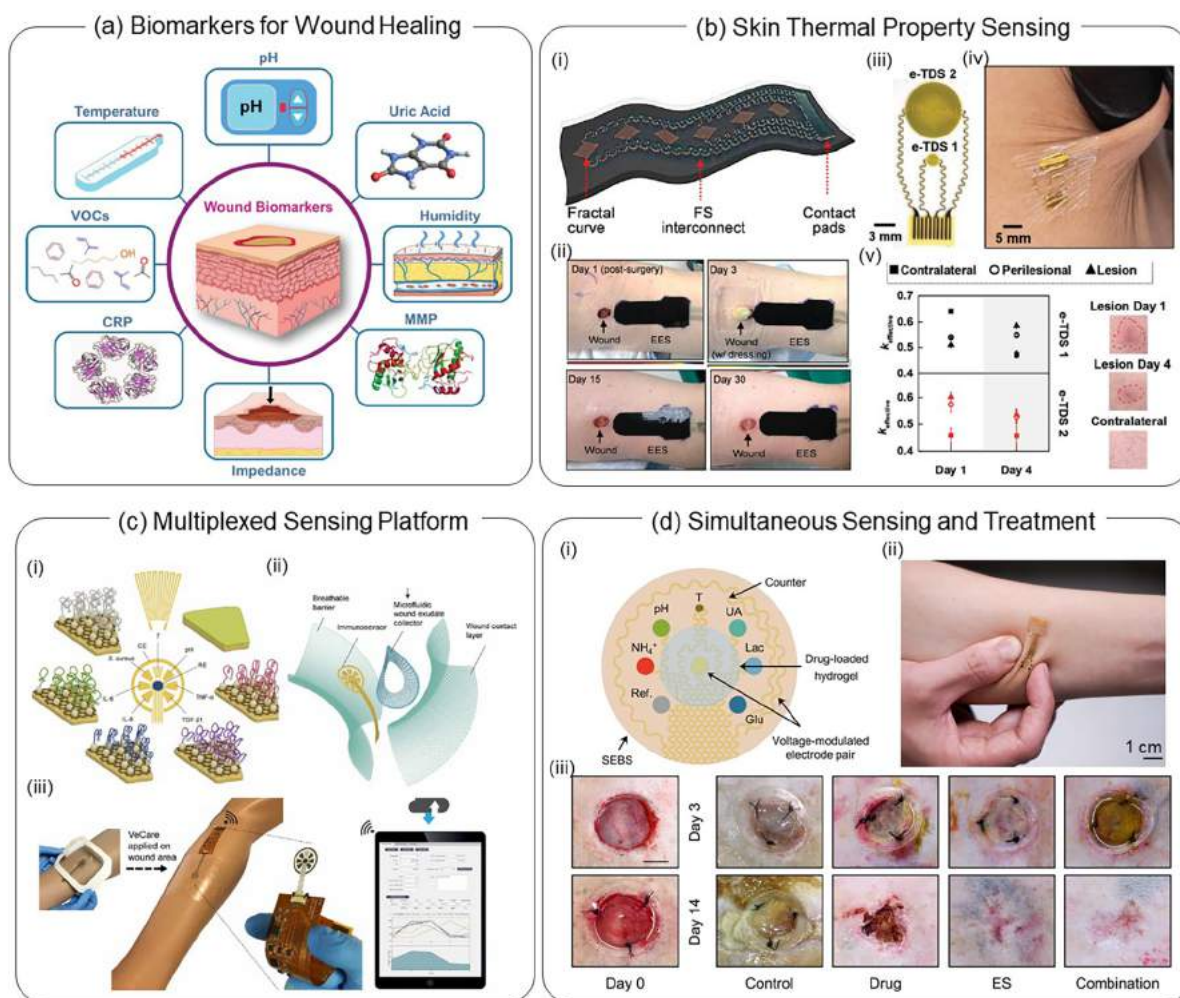


Figure 16. E-Tattoos for wound management. (a) Schematic of the representative biomarkers present in a wound. Reproduced with permission from ref 438. Copyright 2021 John Wiley and Sons. (b) Examples of monitoring the thermal properties of wound skin: (i) schematic of the design of the tattoo electronics integrated on a black silicone membrane for skin thermal properties monitoring; (ii) monitoring of the wound healing process with the e-tattoo for 30 days; (iii) schematic of the structure and (iv) photo of the e-TDS system for in-depth tissue thermal conductivity measurement; (v) measurement of skin thermal conductivity changes in different locations over time. Reproduced with permission from refs 49 and 455. Copyright 2014 and 2018 John Wiley and Sons. (c) Multiplexed wound sensing platform: (i) schematic of the sensing elements in the multiplexed sensing platform; (ii) schematic of the exploded view of the multiplexed sensing platform; (iii) multiplexed wound sensing platform attached on an artificial skin to demonstrate the wireless multiple biomarkers sensing. Reproduced with permission from ref 461. Copyright 2021 AAAS. (d) Multifunctional e-tattoo system for simultaneous wound sensing and treatment: (i) schematic of the structure of the multifunctional e-tattoo with wound sensing units, drug delivery unit, and electrical stimulation unit; (ii) e-tattoo system on human skin; (iii) accelerated wound healing process with combined electrical stimulation and drug delivery. Reproduced with permission from ref 444. Copyright 2023 AAAS.

metabolites can be readily read by the electrochromic display. The sensing and controlling units were powered with the printed battery, making the whole platform work without any wired or wireless connection to external devices.

Surface-enhanced Raman spectroscopy (SERS) provides another method for optical biofluid analysis.^{291,454} Recently, Mogera et al. developed a wearable sweat sensor using a paper-based microfluidic system with gold nanorod (Au NR) embedded chromatography paper as SERS substrates.⁴⁵⁴ The paper microfluidic sensor consists of a chromatography paper serpentine channel integrated between a double-sided adhesive layer with a sweat inlet and a PDMS encapsulation layer (Figure 15d-i). The Au NRs have a uniform size distribution (Figure 15d-ii) and can significantly enhance the scattering of uric acid in the sweat, allowing for sensitive and quantitative measurement of the sweat uric acid concentration. Additionally, the sweat volume and sweat rate can be quantified through the color

contrast between the wetted and dry regions. The device demonstrated good stretchability, and no delamination was found at 30% stretch. Therefore, the device can be easily applied and conformably laminated onto human skin (Figure 15d-iii) and analyzed with a hand-held Raman spectrometer to provide uric acid concentrations (Figure 15d-iv). Optical detection methods allow sweat analyte measurement without additional on-device rigid power and data converting units, which helps the conformal contact of the device onto the skin. However, the optical detection methods require special imaging modules or hand-held Raman spectrometers for accurate signal collection, which is a significant barrier for continuous background biochemical analysis. Additionally, due to the sensitivity to ambient light conditions and measurement focus and angle, optical detection methods tend to have issues with consistency. As discussed in section 3.1, color references on the e-tattoo can be used to overcome this issue.

4.2.2. Wound Sensing and Treatment. Wound healing is a complex and prolonged biological process that involves changes in a variety of biometrics such as skin temperature, pH, humidity, impedance, and chemical biomarkers (Figure 16a).⁴³⁸ Continuous monitoring of the progression of the wound (e.g., healing or deterioration) is necessary for informing proper treatment or corrective action. E-Tattoos, by conforming directly to the lesion, offer stable, long-term monitoring and stimulation of the wound for diagnosis and accelerating the healing process. Hattori et al. developed the first e-tattoo wound sensor and measured the temperature and thermal conductivity of the skin during the wound healing process.⁴⁹ The temperature sensors were designed with a fractal structure and connected with serpentine for global stretchability (Figure 16b-i). One of the sensors can be used as a heater with alternating current when measuring thermal conductivity. Thanks to its ultralow thickness ($\sim 11 \mu\text{m}$), the device allowed conformal and reversible bonding onto the skin via the vdW force for repeated application and removal. The device accurately monitored inflammation-induced temperature increases and thermal conductivity decreases during the wound healing process (Figure 16b-ii). In a following work, a thermal depth sensor (TDS) was developed for measuring the thermal properties of deep tissues and providing a more reliable thermal conductivity measurement insensitive to external environmental influences.⁴⁵⁵ The TDS consists of two gold coils encapsulated in PI with serpentine to pads for connection to an external circuit (Figure 16b-iii). The device is conformal and stretchable, as shown in Figure 16b-iv. It was found that a device with a coil radius of 3.5 mm allowed thermal conductivity sensing at depths up to 6 mm. The TDS demonstrated its ability to detect in vivo changes of thermal conductivities in the deep dermis and subcutaneous fat during the healing process of a cellulitis lesion (Figure 16b-v). In another work, they incorporated electronic components and an inductive coil for analogue signal conditioning and NFC-based wireless data and power transmission.¹⁵⁴ Thanks to the miniaturized design and battery-free operation, the device can continuously monitor changes in skin thermal conductivity for over a week.

Skin pH is another crucial biomarker for wound sensing. The pH of healthy skin is slightly acidic ($\text{pH} = 4\text{--}6$). When the skin barrier is breached, the pH increases to neutral or slightly basic due to the presence of enzymes and bacteria.⁴⁵⁶ During the healing process, the pH of the wound area reduces back to neutral and finally acidic after complete healing. Early reports showed that a potentiometric pH sensor consisting of a PANI-modified carbon working electrode and an Ag/AgCl reference electrode could be integrated into an adhesive bandage for monitoring the real-time changes of pH during wound healing.⁴⁵⁷ In another example, Tamayol et al. developed a colorimetric pH sensor with an alginate hydrogel microfiber loaded with pH-sensitive dyes.³⁷ The color of the microfiber changed with pH, enabling direct pH determination by image capture with a smartphone.

The onset of a wound is also typically accompanied by multiple distinct biomarkers. For example, tumor necrosis factor- α (TNF- α), interleukin-6 (IL-6), and IL-8 are reported to elevate in wound fluids obtained from nonhealing ulcers compared to healing ulcers.^{458–460} Consequently, simultaneous sensing of multiple biomarkers provides more comprehensive information about the wound environment. Gao et al. developed a sensing platform consisting of a gold temperature sensor, a PANI-coated gold pH sensor, and five graphene-coated gold

electrodes with different antibodies to detect interleukin-6 (IL-6), IL-8, transforming growth factor- $\beta 1$ (TGF- $\beta 1$), tumor necrosis factor- α (TNF- α), and the *Staphylococcus aureus* bacteria (Figure 16c-i).⁴⁶¹ The sensor array was further integrated with a microfluidic layer to guide the wound exudate to the sensing area without contamination (Figure 16c-ii). Thanks to a breathable substrate, the device can evaluate the wound environment, inflammation, and infection without obstructing the natural healing process (Figure 16c-iii).

Real-time wound sensing greatly enhances wound management by offering closed-loop feedback for various therapeutic procedures. Previous results show that the wound healing process can be greatly accelerated through a range of modalities, including drug delivery,¹⁰ ultrasonic,⁴⁶² thermal,⁴⁶³ and electrical stimulation.^{131,159} Song et al. recently developed a battery-free and wireless electrical stimulation tattoo for wound treatment.⁴⁶⁴ Notably, after the wound heals, the stimulation electrode gradually degrades with time in the regenerated skin, eliminating invasive procedures to remove the device. Pang et al. developed a smart, flexible e-tattoo for closed-loop wound sensing and treatment.¹⁰ The device contained a temperature sensor, UV-LEDs, and a UV-responsive antibacterial hydrogel. The temperature sensor can monitor the temperature of the wound area in real time and transmit the data to a smartphone over Bluetooth. When prolonged and elevated temperature (i.e., $40 \text{ }^\circ\text{C}$ for 6 h) associated with infection is detected, the UV LEDs were remotely controlled to turn on to trigger the release of the antibiotics in the hydrogel. Experiments showed that the wound area with on-demand treatment had significantly reduced bacteria density and temperature than the control area. In a recent work, Sani et al. developed a multimodal biochemical sensing system with integrated wound therapy capabilities. The sensor array consists of sensors to detect glucose, lactate, uric acid, ammonium ions, the pH of the wound exudate, and the temperature in the wound area (Figure 16d-i).⁴⁴⁴ The therapeutic portion is composed of a pair of electrical stimulation electrodes and an electroactive hydrogel containing antimicrobial drugs. The whole system is stretchable thanks to the serpentine interconnects and the elastomer substrate (Figure 16d-ii). An in vivo study showed that combined treatment of drug delivery with electrical stimulation exhibited substantially accelerated chronic wound healing in a rodent model (Figure 16d-iii). An in-depth overview of therapeutic e-tattoos will be expanded on in section 5.

Despite the significant progress of e-tattoos in the field of wound management, there are still several challenges that need to be addressed before adoption in clinical environments. First, high-quality sampling of the wound exudate remains challenging. The wound exudate is a mixture of proteins, cellular components, and other substances, which can easily adsorb onto the device surface and contaminate the device and the signal. Although this can be overcome by antifouling coating or sampling with microfluidic structures, it inherently increases the thickness of the device and requires an additional adhesive layer. Second, moisture from the wound can cause delamination of the device, therefore, achieving a stable device–skin interface for long-term monitoring of the wound biomarkers and wound treatment is still challenging.

5. E-TATTOO STIMULATORS

Unobstructive disease management and treatment for outpatients and the general population remain an outstanding challenge. Electrical, thermal stimulation, and transdermal drug

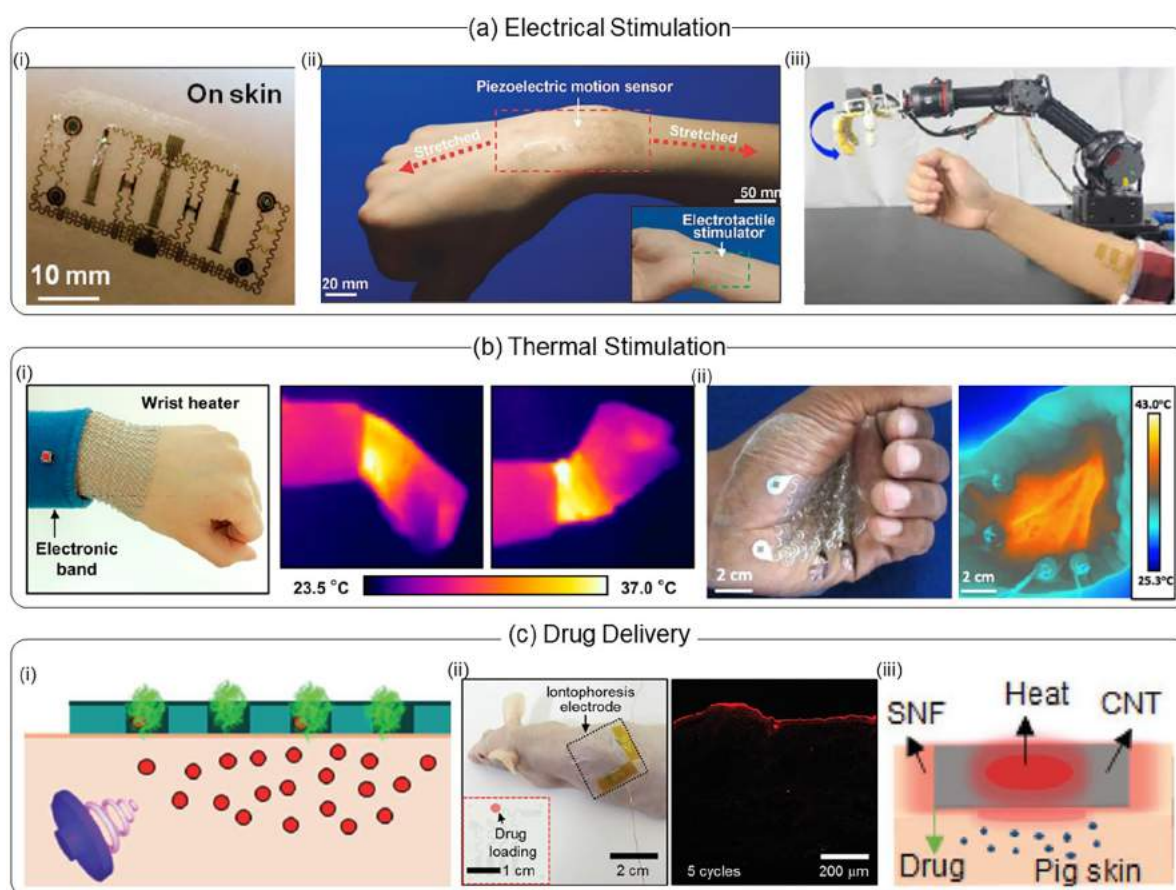


Figure 17. E-tattoo for stimulation. (a) Electrical stimulation e-tattoos: (i) photograph of the skin-mounted multifunctional e-tattoo with an electrical stimulator; (ii) images of a transparent graphene-based motion sensor and electro-tactile stimulator, positioned on the top and bottom of a human wrist, respectively; (iii) photograph of human–machine interaction facilitated by an AI-assisted M-bot system. Reproduced with permission from refs 51, 40, and 468. Copyright 2016, 2015 John Wiley and Sons, and 2022 AAAS. (b) Thermal stimulation e-tattoos: (i) optical image (left) of a large-area stretchable heater worn on the wrist and the corresponding infrared camera images during wrist movement downward and upward (center and right); (ii) photograph (left) and infrared image (right) of the skin-conformable palm heater during palm closing. Reproduced with permission from refs 473 and 237. Copyright 2015 American Chemical Society and 2018 MDPI. (c) Drug delivery e-tattoos: (i) schematic of ultrasound-pulse-induced drug delivery; (ii) photograph of the graphene iontophoresis electrode mounted on the mouse skin for drug delivery (left) and cross-sectional confocal microscope image of the transdermal drug delivery of doxorubicin (red, right); (iii) schematic of the dye (rhodamine B)-doped CNT/silk nanofiber e-tattoo on the pig skin for transdermal drug delivery. Reproduced with permission from refs 480, 476, and 223. Copyright 2017, 2015, and 2021 John Wiley and Sons.

delivery are promising methods for providing noninvasive, controllable therapeutics in ambulatory settings. Unfortunately, therapeutic devices based on conventional electronics have limited usability in daily life due to their bulkiness, discomfort, and lack of precise control. For wearable transdermal stimuli devices, it is essential to have intimate contact between the stimulating device and the skin to ensure efficient energy or drug transfer through the skin. In this regard, the ultrathin, conformable, and unobstructive nature of e-tattoos is conducive to achieving more effective transdermal stimulation.

Transdermal electrical stimulation is a noninvasive technique used in a variety of applications including pain relief,⁴⁶⁵ wound healing,⁴⁶⁶ inflammation treatment,¹²⁶ and producing an artificial sensation of touch.⁴⁶⁷ It relies on repetitive injections of electric current through the skin using electrodes to stimulate nerves and muscles. Xu et al. developed a transdermal stimuli e-tattoo platform with integrated EMG electrodes, strain sensors, and temperature sensors (Figure 17a-i).⁵¹ The concentric gold stimulation electrodes were designed with an inner disk ($r = 1$ mm) and an outer ring ($r = 2$ mm). They demonstrated a human–machine interface control system using the EMG

electrodes on the arm to signal a robot gripper to grasp a bottle. The electrical stimulation electrode located adjacent to the EMG electrode provides a feedback signal proportional to the gripping force of the subject to prevent dropping or crushing the water bottle. Unfortunately, the gold electrode is opaque and disrupts the natural appearance of the skin and may result in social stigma. To overcome this limitation and better protect the user's privacy, Lim et al. developed a transparent electrical stimulation system consisting of a motion sensor on the top side of the wrist and an electro-tactile stimulator on the bottom side of the forearm (Figure 17a-ii).⁴⁰ This system was similarly used to provide a closed-loop human–machine interface using the motion sensor to control a robotic arm and the electro-tactile stimulator to provide feedback. Yu further extended the capabilities of the human–machine interface system from object grasping to robot-assisted chemical contamination detection with an AI-powered interactive robotic system named M-bot (Figure 17a-iii).⁴⁶⁸ M-bot consists of four EMG electrodes and a pair of electro-tactile electrodes on a human subject and a range of e-skins on the robot, including tactile sensors, temperature sensors, and chemical sensors. All the

electrodes were fabricated by inkjet-printing customized nanomaterial inks, including silver nanowires, silver, graphene oxide, and CNTs. Using various machine learning algorithms, feedback is given to the user through the stimulation electrodes when the robot detects hazardous chemicals or is projected to collide with an object. Apart from human–machine interfaces, electrical stimulation e-tattoos have recently found applications in muscle-related chronic disease treatment,¹³² cardiac resynchronization therapy,⁴⁶⁹ virtual haptic feedback,⁴⁷⁰ and neuroprosthetic control.⁴⁷¹

Heating provides another method for stimulation through thermotherapy and is applied in pain alleviation⁴⁷² and muscle theranostics.⁵²⁶ High conformability is essential for efficient heat transfer. Noble metals stand out as one of the most widely employed materials for heating elements due to their exceptional conductivity, chemical stability, and biocompatibility. Choi et al. developed a silver nanowire e-tattoo heater that can conform to human joints for treating joint injury (Figure 17b-i).⁴⁷³ This heater exhibited outstanding mechanical reliability, featuring biaxial stretchability up to 100%, enabling stable heating performance during various wrist motions. Despite the effectiveness of noble metal-based heaters in joule heating, their widespread adoption is impeded by elevated material and fabrication costs. To address this issue, Stier et al. developed a cost-effective aluminum-based heater by cutting large-area aluminum/polymer laminates using the cut-and-paste method (Figure 17b-ii).²³⁷ The aluminum heating element exhibited notable stretchability of up to 70% thanks to the use of serpentine structures. Moreover, they integrated a temperature sensor into the heaters, incorporating a proportional-integral-derivative feedback unit to prevent the heaters from exceeding thermal safety thresholds.⁴⁷⁴ In recent years, e-tattoo heaters utilizing other materials, such as copper,⁴⁷⁵ liquid metal,¹²⁸ CNTs,¹⁰⁵ graphene,⁴⁰ and MXene,³²⁶ have also been developed and exhibited excellent heating performances.

For more intricate diseases, the timely delivery of therapeutic drugs is critical. This necessity serves as a strong motivation for the development of drug delivery devices that can be worn on the skin for extended periods with minimal obstruction. A variety of triggers, such as heat,^{10,476} pressure,⁴⁷⁷ ultrasound,⁴⁷⁸ and medical condition,⁴⁷⁹ can be employed to release drugs from the e-tattoos. Soto et al. developed a transdermal drug delivery e-tattoo comprising a polycarbonate membrane loaded with a microdose of the drug and a perfluorocarbon emulsion on a commercial tattoo substrate (Figure 17c-i).⁴⁸⁰ A piezoelectric transducer generates an ultrasonic pulse at a frequency of 2.25 MHz, inducing cavitation in the emulsion and resulting in the rapid ejection of microdoses from the patch pores. It was found that ultrasound-based drug delivery achieved a deeper penetration depth compared to methods relying solely on passive diffusion. Transdermal drug delivery can also be accomplished through electrical or thermal means. Choi et al. developed a graphene-based, transparent, ultrathin, and soft e-tattoo comprising a quantum dot LED, a strain sensor, a thermal actuator, and an iontophoresis electrode (Figure 17c-ii).⁴⁷⁶ By applying a voltage gradient across the skin, iontophoresis facilitates the transport of molecules through electrophoresis and electroosmosis while increasing the permeability of the skin. The penetration depth of the drug delivery can be controlled by programming the number of cycles of electrical stimulation. Gogurla et al. developed a CNT/porous silk nanofiber-based e-tattoo that releases drugs through thermal activation (Figure 17c-iii).²²³ To prevent tissue damage from direct heating, heat

was applied wirelessly through optical radiation. The high optical absorption of CNT enabled a 532 nm green laser to increase the temperature and resistance of the e-tattoo. Both electrical and optical heating were tested, with optical heating demonstrating a much deeper penetration depth and more efficient heating and cooling. The large surface-to-volume ratio of silk nanofibers also enhances the efficiency of drug delivery.

Despite their many advantages, transdermal stimulation e-tattoos face several limitations in ensuring their safe and reliable implementation. First, questions persist regarding the long-term safety of stimulation. Prolonged exposure facilitated by e-tattoos may result in unforeseen outcomes compared to acute exposure, given the intricate interactions with skin conditions and hormones. Second, the control of stimulation in e-tattoos is still in a nascent stage. While some stimulation e-tattoos incorporate limited feedback, they rely on basic sensors or machine learning algorithms to interpret highly complex human physiological and environmental conditions. Lastly, there is a need for improvement in stimulation performance. For example, although stimulation e-tattoos have demonstrated the ability to produce artificial sensations of touch, they currently lack the spatial resolution necessary to provide human-like sensations in prostheses and human–machine interfaces.

6. E-TATTOOS FOR ENERGY HARVESTING AND STORAGE

The advancement in e-tattoo capabilities introduces increased power consumption and storage requirements. While the sensing or stimulating e-tattoos have achieved ultrathin and wearable, batteries have not yet reached a comparable level of wearability, thereby mitigating some of these advantages. In addition to the mechanical limitations associated with conventional rigid batteries, the sustained operation of e-tattoos is contingent on the capacity of the battery. Over the past few years, a range of e-tattoo energy devices have been developed for energy harvesting, transmission, and storage. In this section, we discuss e-tattoo-based energy conversion and storage devices encompassing biofuel cells, mechanical energy harvesters, solar energy, thermal energy, wireless energy harvesters, rechargeable batteries, and supercapacitors.

6.1. Energy Harvesting E-Tattoos

There is a significant amount of energy generated by the human body and the external environment. Kinetic, thermal, mechanical, and chemical energy surrounding the body is estimated to range from millivolts during finger bending to tens of volts for footfalls.⁴⁸¹ Harvesting this energy could be employed for self-powered e-tattoos and can be accomplished through triboelectric,^{105,482,483} piezoelectric,⁴⁸⁴ thermoelectric,^{485–487} photo-voltaic,^{488–490} and biochemical^{48,491,492} mechanisms, which are discussed here.

6.1.1. Triboelectric Nanogenerators. TENGs convert mechanical energy into electrical energy through the coupling of triboelectrification and electrostatic induction. The surface electrostatic charge induces the flow of electrons to form a time-varying electric field. TENG offer a promising energy harvesting solution for powering on-body sensors and other electronics due to their high output voltage (\sim kV)^{493,494} and current (\sim mA).⁴⁹⁵ TENGs integrated on ultrathin, and soft substrates, such as PDMS,^{496–498} PVDF,⁴⁹⁹ and Ecoflex^{229,376} have been developed and utilized for energy harvesting from various resources. Wong et al. reported an e-tattoo TENG consisting of a 0.2 μ m thick copper layer sandwiched between a PI substrate and a

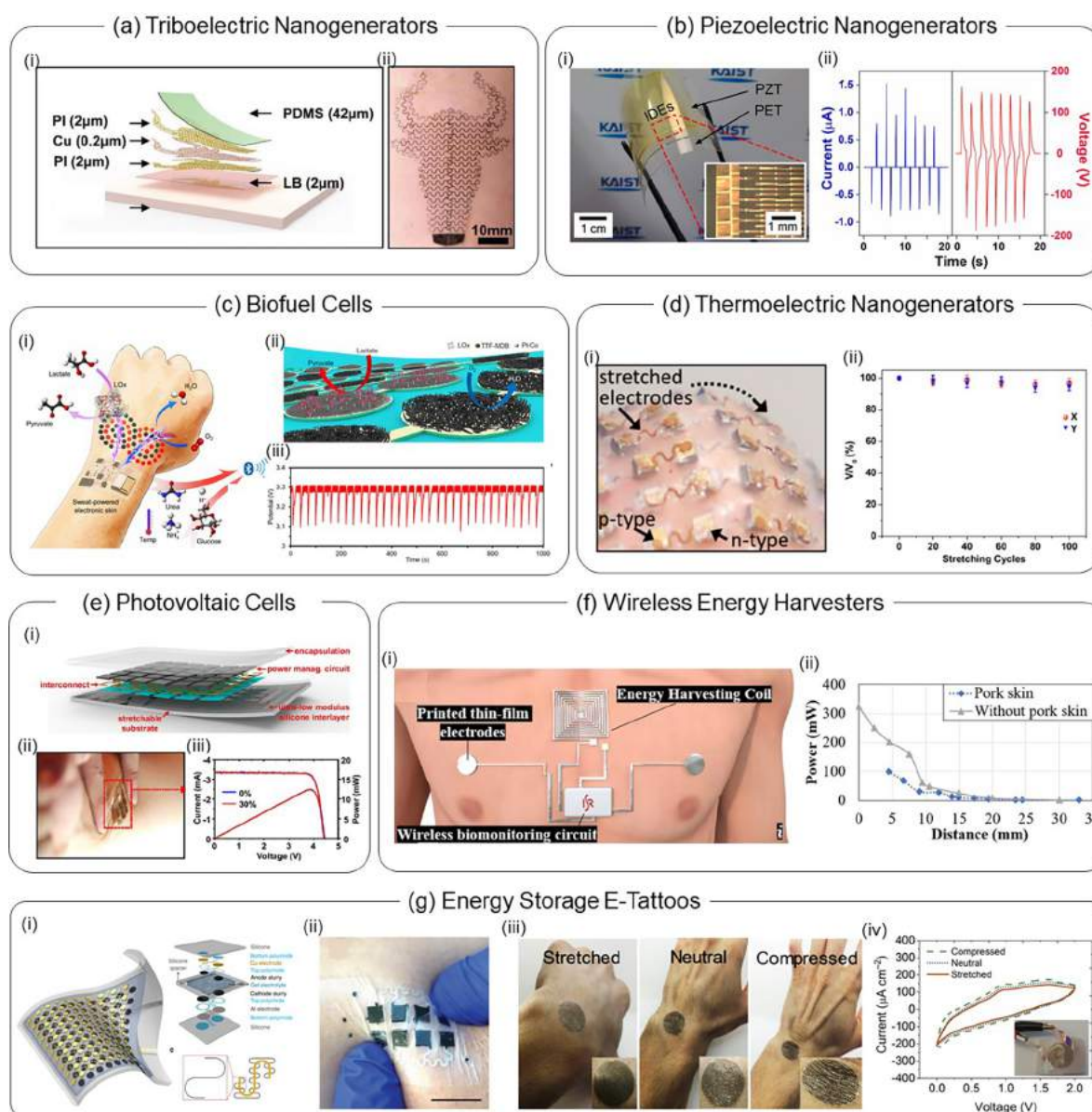


Figure 18. E-tattoo-based energy harvesting and energy storage devices. (a) Triboelectric nanogenerators: (i) schematic illustration of the structure of the tattoo TENG; (ii) An ox-pattern TENG on human skin. Reproduced with permission from ref 377. Copyright 2021 John Wiley and Sons. (b) Piezoelectric nanogenerators: (i) structure of the piezoelectric nanogenerators and the interdigitated electrodes; (ii) output voltage and currents. Reproduced with permission from 505. Copyright 2019 Elsevier. (c) Biofuel cells: (i) schematic of the biofuel cell tattoo supplying power to tattoo biochemical sensors; (iii) output performance of the tattoo biofuel cells. Reproduced with permission from ref 121. Copyright 2020 AAAS. (d) Thermoelectric nanogenerators: (i) photo of a 10×10 thermoelectric nanogenerator array; (ii) mechanical stability of the thermoelectric nanogenerator array. Reproduced with permission from ref 485. Copyright 2020 American Chemical Society. (e) Photovoltaic cells: (i) schematic of the structure of the photovoltaic cell; (ii) photovoltaic cell tattoo attached on the skin; (iii) current and power stability at 30% strain. Reproduced with permission from ref 531. Copyright 2016 National Academy of Sciences. (f) Wireless energy harvesters: (i) illustration of the working mechanism of the NFC for wireless energy harvesting; (ii) optical image of a liquid metal NFC; (iii) wireless detection of wrist motion. Reproduced with permission from ref 535. Copyright 2022 Springer Nature. (g) Energy storage e-tattoos: (i) rechargeable battery; (ii) supercapacitor, (iii,iv) hybrid energy harvesting and storage device. Reproduced with permission from refs 180, 543, and 544. Copyright 2013 Springer Nature, 2020 American Chemical Society, and 2021 John Wiley and Sons.

PDMS encapsulation layer (Figure 18a-i).³⁷⁷ The total thickness of the device is only $48.2 \mu\text{m}$, and an ox-pattern TENG can integrate onto human skin without any inconvenience or discomfort during daily body movements (Figure 18a-ii). The PDMS film acts as the negative triboelectric material and the clothing acts as the positive triboelectric material. When these opposite triboelectric materials interact, the triboelectric e-tattoo can generate an open-circuit voltage of up to 180 V and a

power density of up to $21.2 \text{ mW}\cdot\text{cm}^{-3}$. In another example, Gogurla et al. developed a $3 \mu\text{m}$ thick silk nanofiber/CNT/silk nanofiber sandwiched tattoo, with silk nanofiber serving as the triboelectric material and CNT as the charge-collecting electrode.¹⁰⁵ The device exhibited a maximum power density of $6 \text{ mW}\cdot\text{m}^{-2}$ when touching bare skin, allowing for lighting LEDs and a stopwatch. However, TENGs only produce power during dynamic movements such as bending, twisting, and

tapping, limiting their applications in continuous power harvesting for on-body e-tattoos. Additionally, the output power is still low for tattoo-like TENGs to provide continuous, long-term supply for e-tattoo sensors and stimulators.

6.1.2. Piezoelectric Nanogenerators. Piezoelectric nanogenerators (PENGs) convert biomechanical energy, such as body movements, heartbeats, and respiration into electricity. External mechanical stress or strain induces a change in electrical polarization inside the piezoelectric materials such as ZnO, PZT, BaTiO₃, PVDF, PVDF-TrFE, etc., generating an internal electric field.^{484,500–504} Khan et al. reported a flexible PENG with PZT and Cr/Au interdigitated electrodes on a PI film (Figure 18b-i).⁵⁰⁵ The device formed a stable contact on the hand skin under different deformations and delivered a maximum output voltage of 110 V with a static power consumption of only 1.15 nW (Figure 18b-ii). Like TENGs, PENGs also face challenges in dynamic energy harvesting and exhibit low output power.

6.1.3. Biofuel Cells. Biofuel cells harvest energy by oxidizing biologicals in sweat,⁵⁰⁶ saliva,⁵⁰⁷ and urine with enzymes.⁵⁰⁸ The process involves two half-reactions occurring at the bioanode and biocathode, respectively. In the bioanode, biochemicals such as glucose and lactate are oxidized by enzymes, releasing electrons that transfer to the biocathode through an external circuit, generating electrical currents. At the biocathode, oxygen or other oxidants are reduced, consuming the electrons from the bioanode, with water as a byproduct. Jia et al. demonstrated the first biofuel-cell e-tattoo using a CNT–tetrathiafulvalene composite, showing a power density ranging from 5 to 70 $\mu\text{W}\cdot\text{cm}^{-2}$ from perspiration lactate during physical activity.⁴⁸ In another work, a biofuel cell with a LOx-modified MCNT bioanode and a bilirubin oxidase (BOx)-modified MCNT biocathode converted lactate in sweat from the chest and lower back with outputs of 3.7 and 7.5 μW , respectively.⁴⁹² However, biofuel cells typically have low output energy, insufficient to power signal-processing circuitry and wireless data transmission units for on-body e-tattoos. To address this issue, Yu et al. designed an e-tattoo biofuel cell array with graphene oxide and CNT-coated nickel foam as the bioanode and Pt or Pt–Co nanoparticles-decorated CNT film as the biocathode (Figure 18c-i,c-ii).¹²¹ After further modification of the bioanodes with LOx, it readily oxidized the sweat lactate, enabling stable charging of a capacitor (Figure 18c-iii). Notably, the biofuel cell array exhibited a stable output power density of 3.5 $\text{mW}\cdot\text{cm}^{-2}$ during 60 h of continuous operation. One of the most promising advantages of biofuel cells over other energy harvesting systems is the availability of the energy source in the human body. However, limited power density, noncontinuous fuel availability, and system integration remain major obstacles for e-tattoo-based biofuel cells.

6.1.4. Thermoelectric Energy Harvesting. Thermoelectric generators (TEGs) convert body heat into electricity. Current TEG tattoos mainly use organic/inorganic hybrids,^{509,510} conductive polymers,^{511,512} and liquid metals^{513,514} as the active layer. For example, Yang et al. demonstrated a stretchable, 10×10 TEG array on an Ecoflex substrate using p-(Sb₂Te₃) and n-(Bi₂Te₃)-type thermoelectric couple arrays with serpentine interconnects between them (Figure 18d-i).⁴⁸⁵ The device exhibited an output power of $\sim 0.15 \text{ mW}\cdot\text{cm}^{-2}$ at $\Delta T = 19$ K, and no performance decay was observed after being stretched at 40% strain over 100 cycles (Figure 18d-ii). In another example, Kim et al. developed a Bi₂Te₃ and Sb₂Te₃-based TEG on glass fabric,⁵¹⁵ which demonstrated an output power density of $\sim 0.5 \text{ mW}\cdot\text{cm}^{-2}$ at $\Delta T = 19$ K. In a recent study, Tian et al.

used laser scribbling to pattern and sinter Bi₂Te₃ particles on a PI substrate to create a flexible TEG with a power factor of $1500 \mu\text{W}\cdot\text{m}^{-1}\cdot\text{K}^{-2}$.⁵¹⁶ When attached on human forearm, this TEG produced an output voltage of 1.97 mV. Besides, texture control during growth⁵¹⁷ or high-temperature sintering of nano-flakes^{518,519} have also been proposed to engineer thermoelectric materials. Stacked layers of 2D materials can slide under stretching, enabling inherently stretchable TEGs. A TEG composed of 100 stacked units of 1T-WS₂ (n-type) and 1T-NbSe₂ (p-type) demonstrated an output power of 38 nW at a temperature difference of 60 K.⁵²⁰ Other nanomaterials like CNTs^{521–523} and rGO⁵²⁴ have also been utilized for TEGs. For example, Wu et al. developed a flexible TEG by alternatively assembling p-type CNT and n-type CNT and then connecting these assemblies in series.⁵²³ The generator produced a high output voltage of 1.05 V and an outpower of 0.95 mW, sufficient to power an electrochromic device. In addition to inorganic materials, organic materials like PEDOT:PSS,⁵²⁵ as well as hybrids of inorganic and organic materials,⁵²⁶ have also been used to fabricate TEGs. In one example, a PEDOT:PSS-based TEG with 162 n-type and p-type thermoelectric elements generated an output voltage of 0.52 V and a maximum power output of 0.32 μW , enabling it to power organic field-effect transistor-based gas sensors.⁵²⁵ However, most of these TEGs are only flexible but not stretchable. More research is required to advance the form factors of TEGs to approach that of e-tattoos.

6.1.5. Photovoltaic Cells. Photovoltaic cells convert light energy into electricity through the process of photovoltaic effects. One advantage of photovoltaic cells over other mechanical energy harvesters is their production of direct current (DC) voltage, minimizing the circuit requirements and in-house power loss. Photovoltaic cells consist of a light-harvesting active layer, two carrier transport layers, and two electrodes. When light falls on the active layer, it generates electron–hole pairs, separated by the built-in potential, which are collected by the electrodes through the transport layers. Photoresponsive materials, including cadmium telluride, copper indium gallium diselenide (CIGS), perovskites, and polymers, have been used as active layers in photovoltaic cells.^{488,527–530} Metal nanowires, carbon nanomaterials, and conducting polymers are commonly used as electrodes due to their flexibility and transparency.⁵²⁷ Lee et al. demonstrated stretchable photovoltaic cell arrays (GaAs/InGaP) with serpentine Cu interconnects on the top of the elastomer substrate (Figure 18e-i,e-ii).⁵³¹ The photovoltaic cell maintained its output performance at 30% stretching without any significant loss in output voltage and current (Figure 18e-iii). In another example, Kaltenbrunner et al. reported a 2 μm thick organic solar cell using P3HT:PCBM/PEDOT:PSS/PET and a deposited Ca/Ag layer as the top electrode.⁵³² The device exhibited a compressive stretchability up to 50% on the prestretched elastomer substrate. Although tattoo photovoltaic cells can harvest energy more easily compared to mechanical and chemical mechanisms, they also have limited efficiency due to the ultrathin thickness of the light absorption layer. Additionally, it remains challenging for current photovoltaic cells to maintain their performance over the long-term, especially under sweaty conditions.

6.1.6. Wireless Energy Harvesting. E-Tattoos mainly utilize near-field inductive coupling and electric field coupling due to their close proximities to the power supply, enabling lower device profiles and higher efficiencies. Receiving coils commonly use noble metals,⁵³³ silver nanoparticles,⁵³⁴ liquid

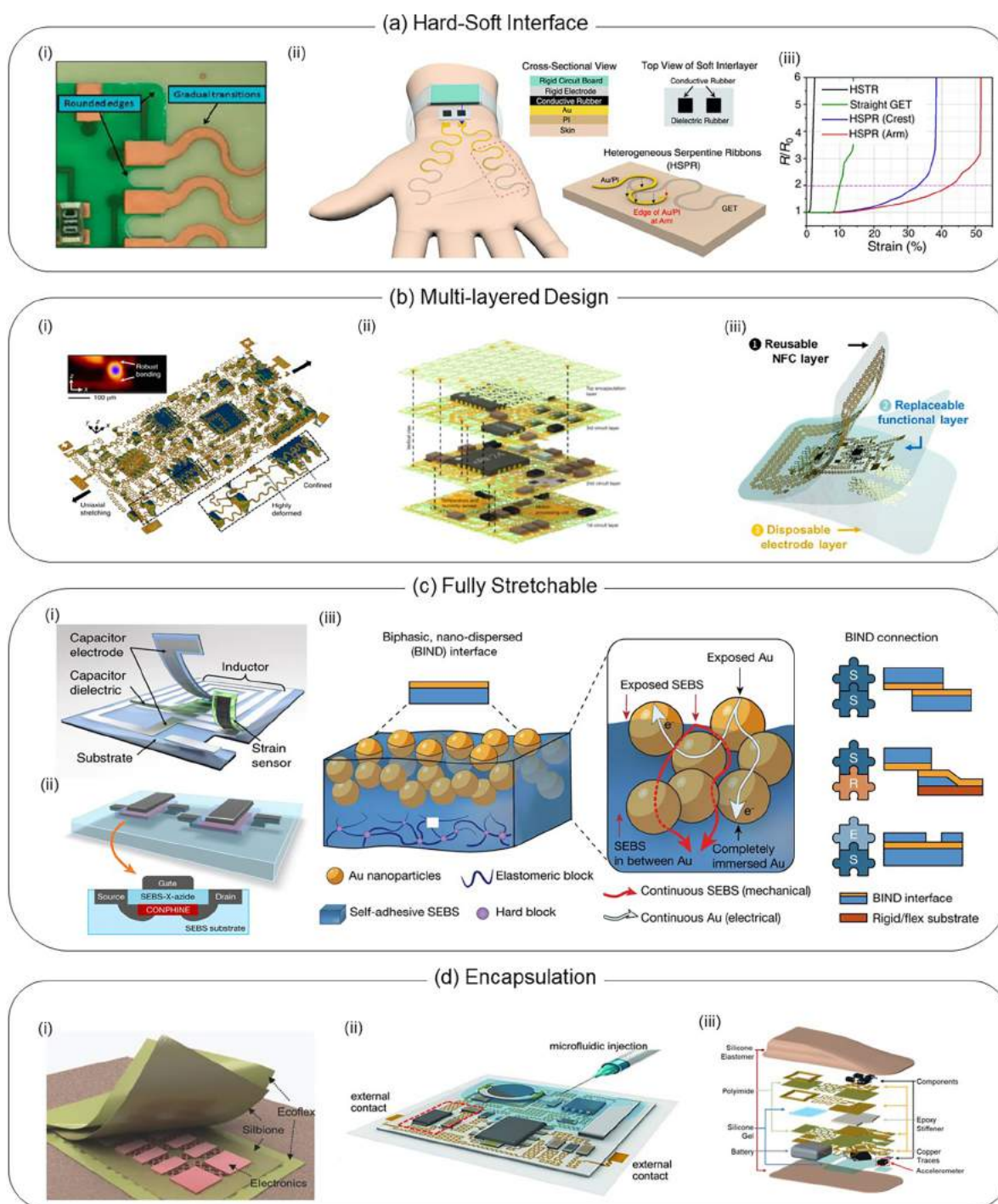


Figure 19. E-tattoo system integration and encapsulation strategies. (a) E-tattoo sensor to circuit board interface: (i) serpentine interconnects soldered to a rigid circuit board can be made more robust through gradually tapered serpentine width and rounded edges; (ii) heterogeneous serpentine ribbons (HSPR) referring to partially overlapped Au/PI serpentes as interconnects and graphene serpentes as electrodermal activity (EDA) sensors; (iii) stretchability comparison of three different HSPR configurations and a straight graphene e-tattoo. Reproduced with permission from refs 545 and 107. Copyright 2012 and 2022 Springer Nature. (b) Multilayered e-tattoo design: (i) robust VIAs for multilayer e-tattoo design; (ii) stacked multilayer network materials (SMNMs) for increased stretchability and breathability; (iii) reconfigurable and modular multilayer NFC e-tattoos. Reproduced with permission from refs 552, 553, and 400. Copyright 2018 Springer Nature, 2022 AAAS, and 2019 John Wiley and Sons. (c) Fully stretchable circuits and interconnects: (i) passive wireless tags fabricated with stretchable passive circuit components; (ii) high-density, intrinsically stretchable transistor array; (iii) universal stretchable interface achieved through adhesive and conductive bonding. Reproduced with permission from refs 555, 380, and 562. Copyright 2019, 2018, and 2023 Springer Nature. (d) Encapsulation strategies for strain isolation in e-tattoos: (i) multilayer encapsulation with a gradual change in stiffness; (ii) microfluidic matrix for strain isolation; (iii) intralayer encapsulation for strain isolation and environmental insulation. Reproduced with permission from refs 566, 567, and 568. Copyright 2015 John Wiley and Sons, 2014 AAAS, and 2019 Springer Nature.

metals,^{535,536} and graphene⁵³⁷ as the conductive circuit. Lin et al. found that liquid metal NFC can be digitally embroidered into textiles to power wearable devices (Figure 18f-i).⁵³⁵ Simulation results indicated that the liquid metal NFC exhibited a maximum transmitted power of 100 mW (Figure 18f-ii).⁵³⁵ As only a coil and some supporting electronics are required, receiving e-tattoos for wireless energy harvesting can be quite small and applicable to neonates. An NFC coil using 5 μm thick copper was developed and employed in the neonatal intensive care unit (NICU). The e-tattoo could harvest RF energy through bedding, blankets, and mattresses.³²⁵ This NFC coil was utilized to power ECG and PPG sensors for continuous and wireless monitoring of heart rate, respiration rate, peripheral arterial tone, SpO_2 , and blood pressure. Although the receiving coil can be made small and conformable, power-transmitting devices are generally large, limiting the power transfer system in wearable applications. Additionally, the inductive coupling of power is highly reliant on alignment between the transmitting and receiving coils. Despite efforts to integrate inductive transmission coils into clothing for ultimate imperceptibility, relative motion between the e-tattoo and clothing can severely degrade efficiency.

6.2. Energy Storage E-Tattoos

Harvested energy should be stored for continuous use. Batteries and supercapacitors are the two most widely used energy devices for e-tattoos,⁵³⁸ which will be discussed in this section.

6.2.1. Rechargeable Batteries. E-tattoo batteries have high energy density and can conformally attach to the skin to provide energy for e-tattoo sensors, signal processing units, and data transmission units. Xu et al. reported a stretchable battery that consists of an array of tiny storage units (LiCoO_2 cathode, $\text{Li}_4\text{Ti}_5\text{O}_{12}$ anode, and Al–Cu electrodes) connected by serpentine copper electrodes (Figure 18g-i).¹⁸⁰ The device exhibited high stretchability, showing only a slight decrease in the output power from ~ 5 mW to ~ 4.35 mW at 300% strain. Ag–Zn tattoo batteries were also used due to their high energy density, stable output voltage, and environmentally friendly nature.⁵³⁹ Berchmans et al. fabricated an Ag–Zn alkaline tattoo battery with screen printing, which showed a capacity density of $2.1 \text{ mAh}\cdot\text{cm}^{-2}$ and an output voltage of 1.5 V.⁵³⁹ Notably, this Ag–Zn battery used water-based electrolytes, making it safer than Li-ion batteries using flammable electrolytes.

6.2.2. Supercapacitors. Compared to batteries, supercapacitors exhibit much faster charging and discharging speed and longer life cycles.^{540,541} Luan et al. reported a supercapacitor with PEDOT:PSS decorated SWCNT film serving as positive and negative electrodes. The device has a low thickness of only $\sim 1 \mu\text{m}$ but a high-power density of $332 \text{ kW}\cdot\text{kg}^{-1}$.⁵⁴² Similarly, Giannakou et al. demonstrated a 3.7 μm thick supercapacitor using silver nanoparticles and nickel oxide as the electrode materials and a saturated magnesium perchlorate as the electrolyte.⁵⁴³ The supercapacitor exhibited a high areal capacitance of $87.2 \text{ mF}\cdot\text{cm}^{-2}$ and can be laminated on human skin with high conformability (Figure 18g-ii).⁵⁴³ Lv et al. fabricated a supercapacitor e-tattoo based on LOx-decorated CNT with Pt and polypyrrole electrodes. The e-tattoo can stably attach to the skin under different deformations (Figure 18g-iii) and exhibited a high output power density of $0.22 \text{ mW}\cdot\text{cm}^{-2}$ and an areal capacitance of $27.2 \text{ mF}\cdot\text{cm}^{-2}$ (Figure 18g-iv).⁵⁴⁴ Notably, this device can be integrated with a biofuel cell to store the energy harvested from sweat lactate.

Despite rapid growth in the research to develop energy harvesting and storage e-tattoos, several challenges still need to be addressed before they can be relied on for field operation. Integrating energy harvesting and energy storage with e-tattoos is a major challenge due to limited available materials, variations in geometry, thickness, working mechanisms, and flexibility. Consistent power generation is another challenge because mechanical harvesters depend on continuous external motion, biofuel cells depend on the availability of body fluids, and wireless power transfer methods depend on the availability of nearby transmitting devices. Additionally, energy densities for mechanical and biochemical energy harvesting are still not adequate to power many functions such as analogue-to-digital conversion or wireless transmission. Hybridizing multiple harvesting mechanisms under the same space, such as light, heat, and biomechanics can potentially increase the output power to meet next-generation e-tattoo's power requirements through multiple stages of power generation, resulting in more accumulated power.

7. SYSTEM INTEGRATION OF E-TATTOOS

Traditionally, e-tattoos have only referred to the components that interface directly with the human body (e.g., electrodes, transducers, optoelectronics). However, these sensors and stimulators cannot function alone and are always accompanied by additional hardware, such as wireless transceivers, amplifiers, processors, or driver circuits. Power must also be supplied wirelessly, from a battery, or harvested from the environment for operation. Lastly, the sensitive components need to be encapsulated to prevent damage from the external environment and reduce wear and tear. In this section, we will briefly discuss the integration of e-tattoos into complete standalone and stretchable systems.

7.1. Integration of Components

A full e-tattoo system must incorporate several important functions, including sensing or actuation, signal conditioning, ADC, data storage, transmission, or display, and power storage or generation. As most analogue signal processing and ADC circuitry still rely on traditional rigid electronics, the integration of the sensing/actuation module to the upstream electronics is particularly important. For e-tattoos that are fabricated with metallic interconnects, the process becomes easier as the interconnects can be directly soldered onto the contact pads of the rigid device. However, care must be taken to prevent stress build-up at the interface. This can be achieved with gradual tapering of the interconnects to match the width of the pads (Figure 19a-i).⁵⁴⁵ The taper angle is an important factor that can be varied to optimize the mechanical reliability of the interconnects by spreading the stress concentration at the joint. E-Tattoos made of nonmetallic materials would require an intermediary substrate to interface with upstream electronics. Conductive adhesives such as silver epoxy provide a robust, heat-free connection but are unsuitable for fine-pitch interconnects due to the risk of short-circuiting. Anisotropic conductive film (ACF) and z-axis conductive tape overcome this limitation and offer other advantages such as alleviating mechanical stresses by allowing some relative motion between the rigid and soft layers and enabling reusability as the adhesive is not permanent.^{546,547} E-Tattoos with submicrometer-thickness need a special kind of interface as the aforementioned methods involve a large strain mismatch. To address this issue, Jang et al. developed a heterogeneous serpentine ribbons

(HSPR) system that used submicrometer-thick gold-on-PI serpentines as intermediary interconnects between graphene electrodes and a millimeter-thick wristband of electronics (Figure 19a-ii).¹⁰⁷ All graphene-to-gold interfaces are held together through vdW forces. The resulting interface can withstand more than 40% tensile strain without fracture (Figure 19a-iii).

The upstream electronics can also be integrated on the e-tattoo and typically consist of discrete (e.g., capacitors, resistors, inductors) and integrated (e.g., amplifiers, microcontrollers) electrical components. The interconnects between these components are commonly thin metal sheets that have been patterned into appropriate designs.^{92,93,233} Copper is the metal that is used ubiquitously for this purpose due to its low cost, good conductivity, and solderability. The interconnects are patterned into serpentine structures to enable the circuit to stretch along with human skin.^{174,548} Some e-tattoo systems have also used intrinsically stretchable materials such as liquid metal as the interconnect material.^{549,550} As circuits become more complex with increased functionality, space becomes a major issue. Recent work has focused on creating multilayered e-tattoos where each layer is responsible for a specific function. Vertical stacking increases density while still preserving planar stretchability at the cost of increasing the total thickness of the device. Each layer is separated with an insulating substrate, and signals and power are transferred between layers through vertical interconnect accesses (VIAs). VIAs must be robust enough to withstand relative movement or displacement between layers under mechanical deformation. Conductive layer deposition has been used to realize multilayer stretchable electronics.⁵⁵¹ A more robust solution is to create VIAs using laser ablation and then perform selective soldering.⁵⁵² This method can create through, buried, and blind VIAs for more complex circuit designs. The authors used soft Ecoflex as the substrate to bond the circuit components and PI-coated copper interconnects. The final system can withstand up to 35% uniaxial tensile strain (Figure 19b-i). However, solid encapsulation strategies like this could highly restrict the deformation of serpentine interconnects as out-of-plane buckling is prevented, thereby posing a limit to the stretchability of the system. Stacked multilayer networks allow for out-of-plane buckling of their serpentine interconnects for better strain distribution. Therefore, they show much better elastic stretchability than the devices with solid encapsulation. In addition, there are many void areas in these stacked multilayer networks, making them more breathable than those with solid encapsulation.⁵⁵³ Figure 19b-ii illustrates a multilayered system fabricated using this method with the substrate layer highlighted in light green. The substrate is made using 50 μm thick PI patterned into a periodic triangular lattice of horseshoe microstructures. This mechanism allows for large uniaxial elastic stretchability of up to 37%, which is close to that of a freestanding serpentine interconnect. VIAs were patterned onto each layer, and layers were aligned by inserting silver pillars through alignment holes on the different layers. Soldering of the silver to the VIAs completes the interlayer connection. As multilayer e-tattoos segregate functionality into different layers, it is even possible to change the functionality of the e-tattoo by replacing specific layers.⁴⁰⁰ This opens up the possibility of having modular e-tattoos where the electrode or sensor layer can be disposed after use or replaced for other sensors, respectively, and the functional layers can be reused and replaced based on the desired signal to be measured (Figure 19b-iii). Each layer of the e-tattoo is made using the cut-and-paste method.⁵⁵⁴ Rigid

circuit components are connected by copper serpentine traces laminated onto a stretchable Tegaderm substrate. To assist in the disassembly of layers, the authors used detachable z-axis conductive tape as VIAs.

While the highest-performance devices still require rigid components, there has been increasing interest in realizing completely stretchable systems. Unfortunately, as seen in section 3.1, many passive components such as resistors and capacitors have inherent reliance on strain and deformation. While this allows body motion or touch to be sensed using various methods, variable value components are typically not desired for consistent circuit operation and therefore pose an outstanding challenge in the field. Niu et al. reported a method of using composite ink composed of silver flakes and elastomers as the conductive material embedded in SEBS substrate to fabricate stretchable inductors and capacitors.⁵⁵⁵ Stretchable, strain-sensitive resistors were manufactured using a thickness-gradient CNT network (Figure 19c-i). Semiconducting components such as transistors are the foundation of more complex components such as processors, amplifiers, and driver circuits. Correspondingly, stretchable transistors^{556–558} and memories^{559,560} have been a hot topic of research. A notable work by Wang et al. describes a high yield (94.4%) fabrication process for stretchable transistors using a variety of intrinsically stretchable polymers semiconductors with a device density of up to 347 transistors per square centimeter (Figure 19c-ii).³⁸⁰ However, current stretchable transistors using elastomers are unable to compete with the areal densities achievable by their silicon counterparts. Lastly, fully stretchable systems would also require stretchable self-adhesive interfaces for multilayer connections or connections with rigid components to reduce mechanical failure at the interface. Multiple approaches that emerged in recent years have tried to alleviate this problem by different approaches including fabricating stretchable-ACF (S-ACF)⁵⁶¹ and creating a universal interface for plug-and-play assembly of stretchable devices by using self-adhesive, biphasic, nanodispersed (BIND) materials (Figure 19c-iii).⁵⁶² This opens up the possibility of integrating e-tattoos into a fully flexible and stretchable system.

7.2. Encapsulation

E-Tattoos can provide clinical-grade health monitoring capabilities in ambulatory settings beyond the confines of traditional healthcare settings. For widespread practical use, however, e-tattoos must be mechanically robust in environments with varying temperatures, humidity, water exposure, electromagnetic interference, and mechanical stresses. Encapsulation protects the electronics from the external environment and provides mechanical support. PDMS and Ecoflex are two materials that are commonly used for encapsulation owing to their good biocompatibility, low Young's moduli, affordability, and easy manufacturability.⁵⁶³ Although it is important to match the stiffness of the encapsulation to that of the skin for maximum comfort,⁵⁶⁴ using a material that is too soft creates a stiffness mismatch with any rigid electronic components on the e-tattoo. To overcome this, multiple works have explored layered approaches where the electronics are encapsulated in progressively softer materials.⁵⁶⁵ Figure 19d-i illustrates such a scheme with the electronics encapsulated first with stiffer Silbione and then with Ecoflex.⁵⁶⁶ Another strategy is to mechanically decouple the electronics and encapsulating elastomer. This can be done by injecting a dielectric fluid with the electronics inside the encapsulation (Figure 19d-ii).⁵⁶⁷ This

strategy allows the free-standing serpentine interconnects to buckle, twist, and deform without constraint. The function of the encapsulating elastomer also dictates how stiff it should be designed. For example, the encapsulation for multilayered e-tattoos should decouple the deformation between layers. In Figure 19d-iii, the stiffer outer silicone elastomer provides robust insulation from the external environment and the softer inner silicone gel provides padding between the deformable layers. In areas of increased electronic component density, a stiffer epoxy resin can be used to provide enhanced mechanical stability to fragile electronic solder joints.⁵⁶⁸

8. CHALLENGES AND PROSPECTS

Our outlook on e-tattoos is inspired by the historical evolution of real tattoos. The very first tattoos were speculated to be used for therapeutic purposes, similar to acupuncture, as evident from tattoos found over osteoarthritic joints on an ancient corpse.⁵⁶⁹ Since then, tattoos have revolved around themes of stigmatization and self-expression. It is both fitting and incongruous, then, that e-tattoos now aim to provide medical sensing and stimulation in as inconspicuous a manner as possible. This review summarized developments in e-tattoos, focusing on materials and structural engineering for skin mimicry, manufacturing technologies, and transfer-to-skin techniques, sensor and stimulator applications, energy devices, and integration into practical wireless and wearable systems. Despite significant progress, several challenges remain for the widespread adoption of e-tattoos.

- (1) Lack of intrinsically stretchable high-performance conductors and semiconductors. Despite significant progress made in developing stretchable e-tattoos, the development of intrinsically stretchable high-performance e-tattoo conductors and semiconductors has been less than satisfactory. Recent efforts have shown that introducing defects such as wrinkles¹⁶⁹ and cracks,¹⁸⁹ as well as embedding the aligned metal nanowires into elastomers,⁹⁹ can effectively increase the stretchability of the films. However, the conductivity of these stretchable films is generally several times or orders of magnitude lower than that of their bulk counterparts. Additionally, although liquid metal exhibits intrinsic stretchability, it requires additional activation and is liable to form short circuits due to deformation-induced leakage. Furthermore, most of the currently used semiconductors, such as Si, GaN, and GaAs, are rigid, and their electronic performances degrade rapidly when stretched. Although some stretchable polymer semiconductors have been introduced through molecular-level design or morphology control, their carrier mobilities and on/off ratios are still far from sufficient for them to be used as data processing and transmission units for e-tattoos.
- (2) Skin interfacing. Although ultrathin and ultrasoft e-tattoos can adhere to the skin through vdW force, this interaction can be easily disrupted by biofluid secretion such as sweat and wound exudate, making it challenging to form a stable device–skin interface under humid skin conditions. Breathable or permeable e-tattoos that use porous substrates⁹⁶ or nanometer-thick substrates²¹³ have been developed to allow water to evaporate through the device. However, these substrates have reduced mechanical strength due to the pores or ultrathinness and are therefore difficult to transfer onto the skin. Additionally,

hairs on the skin act as an additional barrier between the e-tattoo and the skin, degrading signal quality and causing device delamination. Although hairs can be trimmed before device attachment, they will quickly regrow and are a significant obstacle to long-term signal recording. Finally, the ultrathinness and softness of e-tattoos make them difficult to remove from the skin without destroying the device. Therefore, most current e-tattoos are not reusable, increasing the amount of e-waste produced and the financial costs to the user.

- (3) Data quality under arbitrary motion in an uncontrolled environment. Most of the modalities used by e-tattoos are highly sensitive to motion. Such motion artifacts affect different sensor modalities to varying degrees. For example, biopotential signals are influenced by relative motion between the skin and the electrode due to changes in contact impedances as well as triboelectric charge generation.⁵⁷⁰ Bio-Z and optical sensors are impacted when the electrode or LED/photodetector relative positions change with motion, altering the path of electric current or photons through the tissue, respectively. SCGs and pressure sensors, in contrast, directly pick up motion in their signals. As the mass of the sensor adds inertia, the sensor's weight is a significant design consideration for minimizing the sensitivity to motion artifacts. Motion can also impact the connection between the e-tattoo sensors and upstream electronics, as this interface can become disconnected. In some cases, this can result in a partial or complete loss of signal, leading to inaccurate or unreliable measurements.
- (4) Tattoo-like actuators to provide haptic feedback. Haptic feedback involves the use of advanced actuators to stimulate mechanoreceptors or afferent nerves under the skin to create a sensation. An e-tattoo sensing system with haptic feedback can provide users with better immersive experiences, forming a closed-loop human–machine interface. However, while e-tattoo stimulators, such as electrical stimulators, can provide electrical feedback, there are currently no reports of e-tattoo actuators capable of providing haptic feedback. A haptic actuator is composed of a magnetic field generator, a magnet vibrator, a backbone, and a vibrator-supporting substrate. Despite of potential to design the haptic unit with a diameter as small as 5 mm, it is still a challenge to create tattoo actuators that are micrometers thick and can generate enough vibration force to stimulate the tactile sensation in human skin. Although haptic feedback commonly refers to vibrations or force feedback, there is emerging research to also leverage thermal feedback as a way to enhance the sensory experience.⁵⁷¹

Addressing the above challenges also presents new opportunities for e-tattoos, which are outlined as follows:

- (1) Scalable, low-cost, or on-body manufacture of e-tattoo systems. Because the thinness and softness of e-tattoos make reusability a significant challenge, minimizing the cost and improving the scalability of fabrication has practical significance. Current subtractive cut-and-paste and additive printing methods all require device transfer onto the skin and are challenging for ultrathin e-tattoos. Recent advancements in on-skin fabrication techniques^{132,141,258,268–271} have opened up new possibilities for fabricating transfer-free e-tattoos with well-defined

patterns. After the ink dries, a seamless device–skin interface with low contact impedance is formed. These transfer-free e-tattoos do not require any substrates or additional supporting layers, making them more breathable for sweaty skin. Furthermore, on-body printing techniques have the potential to directly print devices onto any part of the human body, including hairy sites. Moving forward, continued efforts should focus on developing fast-drying ink materials with high conductivity, stretchability, and biocompatibility, as well as improving printer resolution to achieve low-cost and high-resolution printing of e-tattoos.

- (2) Wearable and wireless ultrasound e-tattoos. Although great progress has been made toward conformal ultrasonic transducers, current wearable transducer arrays still rely on large desktop systems for pulse transmission and data acquisition. While these ultrasound patches can conformally adhere to the skin for long periods of time, they currently may not offer much more practicality or diagnostic information over, simple holders for conventional hand-held probes⁵⁷² due to the massiveness and nonportability of these desktop systems. Therefore, progress must be made toward making the whole system truly wearable (i.e., standalone) and wireless. Another unresolved challenge with wearable ultrasound e-tattoos is alignment over the target anatomy. With a standard B-mode image, the sonographer can manipulate the ultrasound probe with five degrees of freedom to best capture the target anatomy. However, with a wearable ultrasound e-tattoo, the patch cannot be moved and therefore can only rely on linear array scanning or beam steering to capture the anatomy. As the spatial resolution directly depends on the sample rate and number of transducers, ultrasound imaging is also inherently data-heavy. This makes wireless operation difficult as the data rates are limited to what the wireless protocol can support (e.g., ~200 kbps for BLE).⁵⁷³ However, overcoming these challenges will yield enormous diagnostic capabilities. Unlike other modalities, ultrasound is inherently robust against motion⁶² as the frequency of the ultrasonic signal is orders of magnitude greater than that of motion. Therefore, the long-term, mobile measurement capabilities of e-tattoos are very synergistic with the motion-resistance of ultrasound. Additionally, ultrasound provides direct measurements of anatomical and fluidic properties. Other modalities can only infer relative physiological changes happening inside the body, such as blood volume changes with PPG. One noteworthy application would be the measurement of cardiac function during dynamic cardiac stress tests as cardiac output, stroke volume, myocardium strain, and other metrics can be directly measured even during motion. An in-depth analysis of the applications of wearable ultrasound is provided by Tan et al.⁵⁷⁴
- (3) Self-powered e-tattoo systems. Self-powered e-tattoo systems can operate without an external power supply, allowing for wireless, long-term operation. Over the past few years, a plethora of energy harvesting e-tattoos have been reported, with diverse advantages and use cases. For example, TENGs show promise in self-powered motion-detection systems. Biofuel cells are capable of providing a continuous power supply when detecting sweat chemicals during intense physical activities. Perovskite solar cells, known for their high conversion efficiency, can power chemical sensors for the continuous monitoring of secreted biomarkers, even in the absence of vigorous exercise.⁵⁷⁵ TEGs can consistently generate power by harnessing energy from the human body, leveraging the temperature difference between the skin and the surrounding environment without requiring any movement, perspiration, or light. Due to the limited power output of current TEGs, they are more useful under cold environments. Future opportunities entail improving the power efficiency of these energy-harvesting devices, as well as enhancing their softness and stretchability to be compatible with the skin. It should be noted that not all energy harvesting devices need to be tattoo-like, in which case the interface between the energy harvesting devices and the e-tattoo sensors should be carefully designed.
- (4) Multimodal and multisite fusion, body area network. The biosignals that can be acquired by an e-tattoo are extremely site-specific. For instance, ECG and SCG signals can only be collected from the chest, EEG signals from the head and forehead, and EMG signals from the target muscle. Conformal, lightweight, and imperceptible e-tattoos offer a seamless way to monitor multiple sites across the body, enabling the collection of vast streams of relevant data. This network of e-tattoos can form a body area network (BAN) and the unique biosignals acquired from each site can be fused to provide improved diagnostic decisions. For instance, heart rate from ECG can be combined with EEG signals to measure stress.⁵⁷⁶ Future research in this area should focus on timing synchronization, efficient multidevice communication protocols, and interoperability between different e-tattoo systems. As such, e-tattoos have the potential to revolutionize the way we monitor and collect biosignals from the human body by providing a more accurate and holistic view of human health.
- (5) Closed-loop e-tattoos. To provide a comprehensive solution, e-tattoo sensing units should be integrated with therapeutic units for simultaneous signal recording and regulation through a closed-loop sensing and therapeutics platform. This closed-loop e-tattoo system can allow on-demand stimulation for precision treatment, increasing the treatment efficiency and decreasing the unnecessary disturbing of the human body. Another interesting direction is to integrate the decoding and feedback units into an e-tattoo sensing system to form a closed-loop human–machine interface or human–robot interface. The signals obtained by the sensors can be decoded and then activate the actuators to provide feedback on human skin to control the machine or the robot. Especially, the integration of e-tattoo haptic actuators into wearable electronics can stimulate the tactile sensation of the human body, thereby providing users with a more immersive and intuitive feedback experience. The advent of ultrathin magnets and new thermoelectric materials that offer both rapid cooling–heating speed and high flexibility and stretchability, along with the development of multimodal e-tattoo actuators for accurate sensation of the objects,⁵⁷¹ will revolutionize our interaction with devices, leading to a seamless user experience.

(6) Interactive e-tattoo and implantable. The integration of e-tattoos and implantable devices presents a unique opportunity to enhance their capabilities and applications. Implantable devices, such as pacemakers and neural implants, can benefit from e-tattoos that monitor and transmit data wirelessly, providing real-time feedback on a patient's condition as a full closed-loop platform. Conversely, e-tattoos can benefit from implantable devices that provide therapeutic aspects, as well as enhanced power and connectivity. This advantage enables complex functionalities such as electrotherapy stimulation after direct attachment on the targeted areas such as organs,⁵⁷⁷ nerves,⁵⁷⁸ or the brain.⁵⁷⁹ Recent studies demonstrated the combination of implantable devices and skin-interfaced devices that enable seamless and continuous monitoring and treatment of various health conditions, such as cardiovascular diseases,⁵⁷⁷ diabetes,⁵⁸⁰ and neurological disorders.⁵⁸¹ By integrating the data from these devices, clinicians could obtain a more comprehensive and accurate picture of a patient's health status and provide personalized treatment without external interventions. Moreover, the integration of e-tattoos with implants could also enhance human-machine interfaces, by enabling more intuitive and natural interactions between users and devices. Further research is needed to explore the technical and ethical challenges of e-tattoo-implantable interactions and to develop safe and effective integration strategies.

(7) Tattoo-specific integrated circuit (IC) design. Despite the excitement of ultrathin, skin-soft, and stretchable e-tattoos, their wearability must be carefully considered when integrating them with wireless circuitry. Integrating e-tattoos with commercially available COTS components is a convenient and cost-effective approach. When implementing simple functionalities, the COTS circuitry still can be implemented in a wearable form factor. However, certain applications, such as ultrasound measurement, necessitate complex and computing-expensive circuits to capture, digitize, and process a large amount of high-speed data. While the state-of-the-art sensors are wearable, integrating the bulky data control and acquisition circuitry into a wearable form factor poses a significant challenge. Thanks to the rapid development of semiconductor technology, ICs have been elevated to the next level in terms of power, area, and integration level. This advancement has significant benefits for wearable electronics, as IC technology allows for the integration of all necessary circuits for sensing, digitization, real-time processing, and data transmission within a small millimeter-scale size. Because of its compact size, ICs can be easily integrated into e-tattoos without causing obstructions.

We believe that with continuous interdisciplinary scientific collaborations, and the increasing involvement of physiologists and medical doctors, e-tattoos can gradually become a part of our everyday lives, reliably providing sensing, treatment, energy harvesting, and so on in an imperceptible and inexpensive way.

AUTHOR INFORMATION

Corresponding Author

Nanshu Lu – Department of Aerospace Engineering and Engineering Mechanics, Department of Electrical and

Computer Engineering, Department of Mechanical Engineering, Department of Biomedical Engineering, and Texas Materials Institute, The University of Texas at Austin, Austin, Texas 78712, United States; orcid.org/0000-0002-3595-3851; Email: nanshulu@utexas.edu

Authors

Hongbian Li – Department of Aerospace Engineering and Engineering Mechanics, The University of Texas at Austin, Austin, Texas 78712, United States; orcid.org/0000-0002-9806-3223

Philip Tan – Department of Electrical and Computer Engineering, The University of Texas at Austin, Austin, Texas 78712, United States

Yifan Rao – Department of Aerospace Engineering and Engineering Mechanics, The University of Texas at Austin, Austin, Texas 78712, United States; orcid.org/0000-0001-9941-8420

Sarnab Bhattacharya – Department of Electrical and Computer Engineering, The University of Texas at Austin, Austin, Texas 78712, United States

Zheliang Wang – Department of Aerospace Engineering and Engineering Mechanics, The University of Texas at Austin, Austin, Texas 78712, United States

Sangjun Kim – Department of Mechanical Engineering, The University of Texas at Austin, Austin, Texas 78712, United States

Susmita Gangopadhyay – Department of Electrical and Computer Engineering, The University of Texas at Austin, Austin, Texas 78712, United States

Hongyang Shi – Department of Electrical and Computer Engineering, The University of Texas at Austin, Austin, Texas 78712, United States; orcid.org/0000-0003-4135-3673

Matija Jankovic – Department of Electrical and Computer Engineering, The University of Texas at Austin, Austin, Texas 78712, United States; orcid.org/0009-0000-3146-7517

Heeyong Huh – Department of Aerospace Engineering and Engineering Mechanics, The University of Texas at Austin, Austin, Texas 78712, United States

Zhengjie Li – Department of Aerospace Engineering and Engineering Mechanics, The University of Texas at Austin, Austin, Texas 78712, United States; orcid.org/0000-0002-2918-2800

Pukar Maharjan – Department of Electrical and Computer Engineering, The University of Texas at Austin, Austin, Texas 78712, United States

Jonathan Wells – Department of Electrical and Computer Engineering, The University of Texas at Austin, Austin, Texas 78712, United States; orcid.org/0009-0007-9920-8299

Hyoyoung Jeong – Department of Electrical and Computer Engineering, University of California Davis, Davis, California 95616, United States

Yaoyao Jia – Department of Electrical and Computer Engineering, The University of Texas at Austin, Austin, Texas 78712, United States

Complete contact information is available at: <https://pubs.acs.org/10.1021/acs.chemrev.3c00626>

Author Contributions

CRediT: **Hongbian Li**: manuscript planning, coordinating, and polishing, introduction, materials for e-tattoos, biochemical sensors, challenges and prospects; **Philip Tan**: manuscript

polishing, photodetectors and displays, challenges and prospects; **Yifan Rao**: materials for e-tattoos, design strategies of e-tattoos; **Sarnab Bhattacharya**: system integration of e-tattoos, challenges and prospects; **Zheliang Wang**: properties of human skin and desirable properties of e-tattoo, design strategies of e-tattoos; **Sungjun Kim**: temperature sensors, e-tattoo stimulators; **Susmita Gangopadhyay**: manufacturing technologies of e-tattoos, transfer-on-skin technologies of e-tattoos; **Hongyang Shi**: pressure sensors; **Matija Jankovic**: bioimpedance sensors; **Heeyong Huh**: biopotential recording electrodes; **Zhengjie Li**: strain sensors; **Pukar Maharjan**: e-tattoos for energy harvesting and storage; **Jonathan Wells**: e-tattoos for energy harvesting and storage; **Hyoyoung Jeong**: challenges and prospects; **Yaoyao Jia**: challenges and prospects; **Nanshu Lu**: conceptualization, administration, funding acquisition. All authors participated in original draft writing, editing and revision.

Notes

The authors declare no competing financial interest.

Biographies

Hongbian Li received her Ph.D. degree from Nanjing University in China in 2008 and continued to work as a postdoc at Perking University in China. Then she joined the National Center for Nanoscience and Technology (NCNST), China, in 2011 and worked as an assistant professor, associate professor, and then professor from 2019. She joined Prof. Nanshu Lu's group as a research associate in 2022. Her research interests mainly focus on nanomaterials and nanostructures for bioelectronics.

Philip Tan is currently an Electrical and Computer Engineering Ph.D. candidate at the University of Texas at Austin. He also received his B.S. in Electrical and Computer Engineering at the University of Texas at Austin. His current research interests include wearable ultrasound, diffuse optical imaging, and cuffless blood pressure measurement.

Yifan Rao is a Ph.D. candidate in Engineering Mechanics at the University of Texas at Austin, working under the supervision of Prof. Nanshu Lu. Yifan's research interests focus on the mechanics and physics of low-dimensional materials. Yifan's work also encompasses other intriguing topics related to soft materials, thin film mechanics, interface mechanics, and small-scale mechanics. Before starting her Ph.D. program, Yifan Rao earned both her B.Eng. and M.S. degrees in engineering mechanics from Tongji University in China.

Sarnab Bhattacharya received his B. Tech. degree in Electronics and Electrical Communication Engineering from the Indian Institute of Technology, Kharagpur, and his M.S. in Electrical and Computer Engineering from the University of Texas at Austin. He joined Prof. Nanshu Lu's research group in 2021 and is currently pursuing his Ph.D. degree in Electrical and Computer Engineering. His research interest is wearable, continuous cardiovascular health monitoring.

Zheliang Wang received her Ph.D. degree in Mechanical Engineering from Johns Hopkins University. He joined Prof. Nanshu Lu's research group in 2022. His research interest is the numerical and analytical modeling of soft electronics.

Sangjun Kim obtained a B.S. degree in Mechanical Engineering from Inha University in 2016. From Korea Advanced Institute of Science and Technology, he received an M.S. degree in Mechanical Engineering. He then went on to earn a Ph.D. in Mechanical Engineering from the University of Texas at Austin, with Prof. Nanshu Lu serving as his advisor. His research focused on the mechanics and wireless power transfer of wearable devices.

Susmita Gangopadhyay got her bachelor's degree in Communication Engineering from Maulana Abul Kalam Azad University of Technology, India, and her M.S. degree in Electrical Engineering from State University of New York at Buffalo. She is currently a Ph.D. student in Prof. Nanshu Lu's group with a major in Electrical and Computer Engineering. Her research interest focuses on design and fabrication in printed electronics for effective electrophysiological signal monitoring.

Hongyang Shi received his Ph.D. degree in Electrical and Computer Engineering from Michigan State University (MSU), Michigan, USA, in 2022. He joined Prof. Nanshu Lu's research group as a postdoctoral researcher in August 2022. His research interest is soft robotic and haptic sensing.

Matija Jankovic is a second-year Ph.D. student in the Chandra Family Department of Electrical and Computer Engineering at the University of Texas at Austin. He obtained his B.Sc. degree in Engineering Science and Business Law from The University of Western Australia and his B.S. degree in Electrical Engineering from Texas A&M University in 2019 and 2021, respectively. Prior to joining the University of Texas, he worked as a technical advisor for a private intellectual property law firm, where he drafted and prosecuted patent applications in the areas of computer architecture, graphics architecture, system architecture, and software. His current research focuses on wearable sensing for human health monitoring, with a particular interest in whole-body hydration.

Heeyong Huh is a fourth-year Ph.D. student in the Department of Aerospace Engineering and Engineering Mechanics at the University of Texas at Austin. He obtained his Bachelor of Science degree in Mechanical Engineering from the same university. His current research focuses on wearable technology and human-robot interaction, with a particular interest in developing human-centered robot policies using wearable technology.

Zhengjie Li received his Bachelor's and Master's degrees in Engineering from Xi'an Jiaotong University, China, in 2018 and 2020. He is currently a Ph.D. student in the Aerospace Engineering and Engineering Mechanics Department at The University of Texas at Austin, working under Professor Nanshu Lu's supervision. His research interest is in the mechanics of conductive filler-doped polymer composites for capacitive pressure sensors.

Pukar Maharjan received his Ph.D. degree at Kwangwoon University in South Korea in 2021 and has since continued to work as a postdoctoral researcher at the same institution. In 2022, he joined the research group of Prof. Nanshu Lu as a postdoctoral researcher. His research interests are primarily focused on the development of bioelectronic devices using additive manufacturing techniques, including 3D printing. He is particularly interested in wearable energy harvesters and self-powered sensors.

Jonathan Wells received his B.S. degree in Electrical Engineering from The University of Texas at Tyler. He joined Prof. Nanshu Lu's research group in June 2019 and is currently pursuing his Ph.D. degree in Bioelectrical Engineering. His research interest is wearable wireless power transfer and powering wearable physiological sensors on the human body.

Hyoyoung Jeong is an assistant professor in the Department of Electrical and Computer Engineering at the University of California, Davis. He completed his Ph.D. at the University of Texas at Austin, where he developed a wireless stretchable electronic tattoo (e-tattoo) and unconventional freeform manufacturing schemes for flexible thin film wearable devices. Before his Ph.D., he worked for Samsung Advanced Institute of Technology (SAIT) for five years as a researcher and developer in the Mobile Healthcare Group. His work as a postdoctoral scholar focused on the development and characterization

of wireless soft wearable platforms for measuring and analyzing multimodal clinical-grade biopotentials. Currently, he focuses on personalized closed-loop wearable bioelectronics for health monitoring, diagnostics, and therapeutics.

Yaoyao Jia received her Ph.D. degree from Georgia Tech in 2019. From 2019 to 2021, she was an Assistant Professor in the Department of Electrical and Computer Engineering at North Carolina State University. Currently, she is an Assistant Professor in the Department of Electrical and Computer Engineering at the University of Texas at Austin and a Fellow of Silicon Laboratories Chair in Electrical Engineering. Her research primarily focuses on analogue and mixed-signal integrated circuits, energy harvesting, implantable biomedical devices, miniature neural interface implants, and wearable devices.

Nanshu Lu received her B.Eng. with honors from Tsinghua University, Beijing in 2005 and her Ph.D. from Harvard University in 2009. She spent two years working at the University of Illinois Urbana–Champaign (UIUC) as a Beckman postdoctoral fellow before she joined the Department of Aerospace Engineering and Engineering Mechanics at the University of Texas at Austin in 2011. She is currently the Frank and Kay Reese Professor at the University of Texas at Austin. Her research interests lie at the intersection of mechanics, materials, manufacture, and human or robot integration of soft electronics.

ACKNOWLEDGMENTS

N.L. acknowledges the supports from the U.S. Army Research Office under Cooperative Agreement W911NF-19-2-0333, the U.S. Office of Naval Research under grant N00014-20-1-2112, the U.S. Army Medical Research Acquisition Activity under contract HT942523C0039, and the U.S. National Science Foundation under grants 2133106 and 2219236. The views and conclusions contained in this review are those of the authors and should not be interpreted as representing the official policies, either expressed or implied, of the U.S. Army Research Office, the U.S. Office of Naval Research, the U.S. National Science Foundation, or the U.S. government.

ABBREVIATIONS

PEDOT:PSS = poly(3,4-ethylenedioxythiophene) polystyrene sulfonate
 PMMA = poly(methyl methacrylate)
 PDMS = polydimethylsiloxane
 PI = polyimide
 PANI = polyaniline
 EEG = electroencephalogram
 ECG = electrocardiogram
 EMG = electromyography
 EOG = electrooculography
 SCG = seismocardiography
 NIRS = near-infrared spectroscopy
 PPG = photoplethysmography
 P3HT = poly(3-hexylthiophene-2,5-diyl)
 SEBS = polystyrene-*block*-poly(ethylene-*ran*-butylene)-*block*-polystyrene
 WVTR = water vapor transmission rate
 LEG = laser-engraved graphene
 NFC = near-field communication
 GOx = glucose oxidase
 LOx = lactate oxidase
 TENG = triboelectric nanogenerator
 TEGs = Thermoelectric generators
 HRPS = hybrid response pressure sensors
 VIAS = vertical interconnect accesses

ACF = anisotropic conductive film
 vdW = van der Waals
 ADC = analog-to-digital converter

REFERENCES

- (1) Wu, H.; Yang, G. G.; Zhu, K. H.; Liu, S. Y.; Guo, W.; Jiang, Z.; Li, Z. Materials, Devices, and Systems of on-Skin Electrodes for Electrophysiological Monitoring and Human-Machine Interfaces. *Adv. Sci.* **2021**, *8*, 2001938.
- (2) Amjadi, M.; Kyung, K. U.; Park, I.; Sitti, M. Stretchable, Skin-Mountable, and Wearable Strain Sensors and Their Potential Applications: A Review. *Adv. Funct. Mater.* **2016**, *26*, 1678–1698.
- (3) Gao, L.; Zhang, Y. H.; Malyarchuk, V.; Jia, L.; Jang, K. I.; Chad Webb, R.; Fu, H. R.; Shi, Y.; Zhou, G. Y.; Shi, L. K.; et al. Epidermal Photonic Devices for Quantitative Imaging of Temperature and Thermal Transport Characteristics of the Skin. *Nat. Commun.* **2014**, *5*, 4938.
- (4) Jacques, S. L. Optical Properties of Biological Tissues: A Review. *Phys. Med. Biol.* **2013**, *58*, R37.
- (5) Xu, C. H.; Yang, Y. R.; Gao, W. Skin-Interfaced Sensors in Digital Medicine: From Materials to Applications. *Matter* **2020**, *2*, 1414–1445.
- (6) Lopez-Gordo, M. A.; Sanchez-Morillo, D.; Pelayo Valle, F. Dry EEG Electrodes. *Sensors* **2014**, *14*, 12847–12870.
- (7) Serhani, M. A.; El Kassabi, H. T.; Ismail, H.; Navaz, A. N. ECG Monitoring Systems: Review, Architecture, Processes, and Key Challenges. *Sensors* **2020**, *20*, 1796.
- (8) Zheng, M. D.; Crouch, M. S.; Eggleston, M. S. Surface Electromyography as a Natural Human–Machine Interface: A Review. *IEEE Sens. J.* **2022**, *22*, 9198–9214.
- (9) Chen, S. W.; Qi, J. M.; Fan, S. C.; Qiao, Z.; Yeo, J. C.; Lim, C. T. Flexible Wearable Sensors for Cardiovascular Health Monitoring. *Adv. Healthc. Mater.* **2021**, *10*, 2100116.
- (10) Pang, Q.; Lou, D.; Li, S. J.; Wang, G. M.; Qiao, B. B.; Dong, S. R.; Ma, L.; Gao, C. Y.; Wu, Z. H. Smart Flexible Electronics-Integrated Wound Dressing for Real-Time Monitoring and on-Demand Treatment of Infected Wounds. *Adv. Sci.* **2020**, *7*, 1902673.
- (11) Kim, J.; Campbell, A. S.; Esteban-Fernandez de Avila, B.; Wang, J. Wearable Biosensors for Healthcare Monitoring. *Nat. Biotechnol.* **2019**, *37*, 389–406.
- (12) Majumder, S.; Mondal, T.; Deen, M. J. Wearable Sensors for Remote Health Monitoring. *Sensors* **2017**, *17*, 130.
- (13) Wang, C.; He, K.; Li, J. F.; Chen, X. D. Conformal Electrodes for on-Skin Digitalization. *Smart Mater.* **2021**, *2*, 252–262.
- (14) Rodbard, D. Continuous Glucose Monitoring: A Review of Successes, Challenges, and Opportunities. *Diabetes Technol. Ther.* **2016**, *18*, S2-3.
- (15) Dunn, J.; Runge, R.; Snyder, M. Wearables and the Medical Revolution. *Per. Med.* **2018**, *15*, 429–448.
- (16) Ferguson, T.; Olds, T.; Curtis, R.; Blake, H.; Crozier, A. J.; Dankiw, K.; Dumuid, D.; Kasai, D.; O'Connor, E.; Virgara, R.; et al. Effectiveness of Wearable Activity Trackers to Increase Physical Activity and Improve Health: A Systematic Review of Systematic Reviews and Meta-Analyses. *Lancet. Digit. Health.* **2022**, *4*, e615–e626.
- (17) Luczak, T.; Burch, R.; Lewis, E.; Chander, H.; Ball, J. State-of-the-Art Review of Athletic Wearable Technology: What 113 Strength and Conditioning Coaches and Athletic Trainers from the USA Said About Technology in Sports. *Int. J. Sports Sci. Coach* **2020**, *15*, 26–40.
- (18) Yang, J. C.; Mun, J.; Kwon, S. Y.; Park, S.; Bao, Z. N.; Park, S. Electronic Skin: Recent Progress and Future Prospects for Skin-Attachable Devices for Health Monitoring, Robotics, and Prosthetics. *Adv. Mater.* **2019**, *31*, 1904765.
- (19) Yin, R. Y.; Wang, D. P.; Zhao, S. F.; Lou, Z.; Shen, G. Z. Wearable Sensors-Enabled Human-Machine Interaction Systems: From Design to Application. *Adv. Funct. Mater.* **2021**, *31*, 2008936.
- (20) Stoppa, M.; Chiolerio, A. Wearable Electronics and Smart Textiles: A Critical Review. *Sensors* **2014**, *14*, 11957–11992.

- (21) How Wearable Tech Is Shaping the Future of Skincare. *Beauty Business Journal* 2021, <https://beautybusinessjournal.com/how-wearable-tech-is-shaping-the-future-of-skincare/>.
- (22) Yetisen, A. K.; Martinez-Hurtado, J. L.; Unal, B.; Khademhosseini, A.; Butt, H. Wearables in Medicine. *Adv. Mater.* **2018**, *30*, 1706910.
- (23) Takei, K.; Honda, W.; Harada, S.; Arie, T.; Akita, S. Toward Flexible and Wearable Human-Interactive Health-Monitoring Devices. *Adv. Healthc. Mater.* **2015**, *4*, 487–500.
- (24) Wang, Y.; Haick, H.; Guo, S. Y.; Wang, C.; Lee, S.; Yokota, T.; Someya, T. Skin Bioelectronics Towards Long-Term, Continuous Health Monitoring. *Chem. Soc. Rev.* **2022**, *51*, 3759–3793.
- (25) Yang, Y.; Gao, W. Wearable and Flexible Electronics for Continuous Molecular Monitoring. *Chem. Soc. Rev.* **2019**, *48*, 1465–1491.
- (26) Luo, Y. F.; Abidian, M. R.; Ahn, J. H.; Akinwande, D.; Andrews, A. M.; Antonietti, M.; Bao, Z. N.; Berggren, M.; Berkey, C. A.; Bettinger, C. J.; et al. Technology Roadmap for Flexible Sensors. *ACS Nano* **2023**, *17*, 5211–5295.
- (27) Williams, N. X.; Franklin, A. D. Electronic Tattoos: A Promising Approach to Real-Time Theragnostics. *J. Dermatol. Skin. Sci.* **2020**, *2*, 5–16.
- (28) Kim, D. H.; Lu, N. S.; Ma, R.; Kim, Y. S.; Kim, R. H.; Wang, S. D.; Wu, J.; Won, S. M.; Tao, H.; Islam, A.; et al. Epidermal Electronics. *Science* **2011**, *333*, 838–843.
- (29) Yeo, W. H.; Kim, Y. S.; Lee, J.; Ameen, A.; Shi, L.; Li, M.; Wang, S.; Ma, R.; Jin, S. H.; Kang, Z.; et al. Multifunctional Epidermal Electronics Printed Directly onto the Skin. *Adv. Mater.* **2013**, *25*, 2773–2778.
- (30) Ameri, S. K.; Wang, L. Graphene Electronic Tattoo Sensors for Point-of-Care Personal Health Monitoring and Human-Machine Interfaces. *Emerging 2D Materials and Devices for the Internet of Things*; Elsevier, 2020; pp 59–86.
- (31) Liu, S. Y.; Rao, Y. F.; Jang, H.; Tan, P.; Lu, N. S. Strategies for Body-Conformable Electronics. *Matter* **2022**, *5*, 1104–1136.
- (32) Zhao, K.; Zhao, Y. B.; Qian, R.; Ye, C. Q. Recent Progress on Tattoo-like Electronics: From Materials and Structural Designs to Versatile Applications. *Chem. Eng. J.* **2023**, *477*, 147109.
- (33) Windmiller, J. R.; Bandothkar, A. J.; Valdés-Ramírez, G.; Parkhomovsky, S.; Martinez, A. G.; Wang, J. Electrochemical Sensing Based on Printable Temporary Transfer Tattoos. *Chem. Commun.* **2012**, *48*, 6794–6796.
- (34) Williams, N. X.; Noyce, S.; Cardenas, J. A.; Catenacci, M.; Wiley, B. J.; Franklin, A. D. Silver Nanowire Inks for Direct-Write Electronic Tattoo Applications. *Nanoscale* **2019**, *11*, 14294–14302.
- (35) Zucca, A.; Cipriani, C.; Sudha; Tarantino, S.; Ricci, D.; Mattoli, V.; Greco, F. Tattoo Conductive Polymer Nanosheets for Skin-Contact Applications. *Adv. Healthc. Mater.* **2015**, *4*, 983–990.
- (36) Guan, Y. S.; Thukral, A.; Zhang, S.; Sim, K.; Wang, X.; Zhang, Y. C.; Ershad, F.; Rao, Z.; Pan, F. J.; Wang, P.; et al. Assembled Rubbery Semiconducting Nanofilm for Fully Rubbery Integrated Electronics. *Sci. Adv.* **2020**, *6*, eabb3656.
- (37) Tamayol, A.; Akbari, M.; Zilberman, Y.; Comotto, M.; Leshia, E.; Serex, L.; Bagherifard, S.; Chen, Y.; Fu, G.; Ameri, S. K.; et al. Flexible pH-Sensing Hydrogel Fibers for Epidermal Applications. *Adv. Healthc. Mater.* **2016**, *5*, 711–719.
- (38) Park, M.; Park, Y. J.; Chen, X.; Park, Y. K.; Kim, M. S.; Ahn, J. H. MoS₂-Based Tactile Sensor for Electronic Skin Applications. *Adv. Mater.* **2016**, *28*, 2556–2562.
- (39) Yu, Y.; Zhang, J.; Liu, J. Biomedical Implementation of Liquid Metal Ink as Drawable ECG Electrode and Skin Circuit. *PLoS One* **2013**, *8*, e58771.
- (40) Lim, S.; Son, D.; Kim, J.; Lee, Y. B.; Song, J. K.; Choi, S.; Lee, D. J.; Kim, J. H.; Lee, M.; Hyeon, T.; et al. Transparent and Stretchable Interactive Human Machine Interface Based on Patterned Graphene Heterostructures. *Adv. Funct. Mater.* **2015**, *25*, 375–383.
- (41) Miyamoto, A.; Lee, S.; Cooray, N. F.; Lee, S.; Mori, M.; Matsuhisa, N.; Jin, H.; Yoda, L.; Yokota, T.; Itoh, A.; et al. Inflammation-Free, Gas-Permeable, Lightweight, Stretchable on-Skin Electronics with Nanomeshes. *Nat. Nanotechnol.* **2017**, *12*, 907–913.
- (42) Nawrocki, R. A.; Jin, H.; Lee, S.; Yokota, T.; Sekino, M.; Someya, T. Self-Adhesive and Ultra-Conformable, Sub-300 nm Dry Thin-Film Electrodes for Surface Monitoring of Biopotentials. *Adv. Funct. Mater.* **2018**, *28*, 1803279.
- (43) Wang, Q.; Ling, S. J.; Liang, X. P.; Wang, H. M.; Lu, H. J.; Zhang, Y. Y. Self-Healable Multifunctional Electronic Tattoos Based on Silk and Graphene. *Adv. Funct. Mater.* **2019**, *29*, 1808695.
- (44) Lee, S.; Franklin, S.; Hassani, F. A.; Yokota, T.; Nayeem, M. O. G.; Wang, Y.; Leib, R.; Cheng, G.; Franklin, D. W.; Someya, T. Nanomesh Pressure Sensor for Monitoring Finger Manipulation without Sensory Interference. *Science* **2020**, *370*, 966–970.
- (45) Chen, B. Z.; Kang, W.; Sun, J.; Zhu, R. T.; Yu, Y.; Xia, A. G.; Yu, M.; Wang, M.; Han, J. Y.; Chen, Y. X.; et al. Programmable Living Assembly of Materials by Bacterial Adhesion. *Nat. Chem. Biol.* **2022**, *18*, 289–294.
- (46) Xu, Y. D.; Su, Y. J.; Xu, X. C.; Arends, B.; Zhao, G. G.; Ackerman, D. N.; Huang, H. Y.; Reid, S. P.; Santarpia, J. L.; Kim, C.; et al. Porous Liquid Metal-Elastomer Composites with High Leakage Resistance and Antimicrobial Property for Skin-Interfaced Bioelectronics. *Sci. Adv.* **2023**, *9*, eadf0575.
- (47) Webb, R. C.; Bonifas, A. P.; Behnaz, A.; Zhang, Y. H.; Yu, K. J.; Cheng, H. Y.; Shi, M. X.; Bian, Z. G.; Liu, Z. J.; Kim, Y. S.; et al. Ultrathin Conformal Devices for Precise and Continuous Thermal Characterization of Human Skin. *Nat. Mater.* **2013**, *12*, 938–944.
- (48) Jia, W. Z.; Valdés-Ramírez, G.; Bandothkar, A. J.; Windmiller, J. R.; Wang, J. Epidermal Biofuel Cells: Energy Harvesting from Human Perspiration. *Angew. Chem., Int. Ed.* **2013**, *52*, 7233–7236.
- (49) Hattori, Y.; Falgout, L.; Lee, W.; Jung, S. Y.; Poon, E.; Lee, J. W.; Na, I.; Geisler, A.; Sadhwani, D.; Zhang, Y.; et al. Multifunctional Skin-Like Electronics for Quantitative, Clinical Monitoring of Cutaneous Wound Healing. *Adv. Healthc. Mater.* **2014**, *3*, 1597–1607.
- (50) Lee, H.; Choi, T. K.; Lee, Y. B.; Cho, H. R.; Ghaffari, R.; Wang, L.; Choi, H. J.; Chung, T. D.; Lu, N.; Hyeon, T.; et al. A Graphene-Based Electrochemical Device with Thermoresponsive Microneedles for Diabetes Monitoring and Therapy. *Nat. Nanotechnol.* **2016**, *11*, 566–572.
- (51) Xu, B. X.; Akhtar, A.; Liu, Y. H.; Chen, H.; Yeo, W. H.; Park, S. I.; Boyce, B.; Kim, H.; Yu, J.; Lai, H. Y.; et al. An Epidermal Stimulation and Sensing Platform for Sensorimotor Prosthetic Control, Management of Lower Back Exertion, and Electrical Muscle Activation. *Adv. Mater.* **2016**, *28*, 4462–4471.
- (52) Yokota, T.; Zalar, P.; Kaltenbrunner, M.; Jinno, H.; Matsuhisa, N.; Kitanosako, H.; Tachibana, Y.; Yukita, W.; Koizumi, M.; Someya, T. Ultraflexible Organic Photonic Skin. *Sci. Adv.* **2016**, *2*, e1501856.
- (53) Zhu, Z. J.; Li, R. Y.; Pan, T. R. Imperceptible Epidermal-Iontronic Interface for Wearable Sensing. *Adv. Mater.* **2018**, *30*, 1705122.
- (54) Wang, C. H.; Li, X. S.; Hu, H. J.; Zhang, L.; Huang, Z. L.; Lin, M. Y.; Zhang, Z. R.; Yin, Z. N.; Huang, B.; Gong, H.; et al. Monitoring of the Central Blood Pressure Waveform Via a Conformal Ultrasonic Device. *Nat. Biomed. Eng.* **2018**, *2*, 687–695.
- (55) Kim, Y.; Suh, J. M.; Liu, Y. P.; Yeon, H.; Qiao, K.; Kum, H. S.; Kim, C.; Lee, H. E.; Choi, C.; Kim, H.; et al. Chip-Less Wireless Electronic Skins by Remote Epitaxial Freestanding Compound Semiconductors. *Science* **2022**, *377*, 859–864.
- (56) Liu, Y.; Pharr, M.; Salvatore, G. A. Lab-on-Skin: A Review of Flexible and Stretchable Electronics for Wearable Health Monitoring. *ACS Nano* **2017**, *11*, 9614–9635.
- (57) Joodaki, H.; Panzer, M. B. Skin Mechanical Properties and Modeling: A Review. *Proc. Inst. Mech. Eng. H: J. Eng. Med.* **2018**, *232*, 323–343.
- (58) A, K.; A, L. Mechanical Behaviour of Skin: A Review. *J. Mater. Sci. Eng.* **2016**, *5*, 1000254.
- (59) Oxlund, H.; Manschot, J.; Viidik, A. The Role of Elastin in the Mechanical Properties of Skin. *J. Biomech.* **1988**, *21*, 213–218.
- (60) Silver, F. H.; Freeman, J. W.; DeVore, D. Viscoelastic Properties of Human Skin and Processed Dermis. *Skin. Res. Technol.* **2001**, *7*, 18–23.

- (61) Holzapfel, G. A. Biomechanics of Soft Tissue. *handbook of materials behavior models* **2001**, 3, 1057.
- (62) Wang, C. H.; Chen, X. Y.; Wang, L.; Makihata, M.; Liu, H. C.; Zhou, T.; Zhao, X. H. Bioadhesive Ultrasound for Long-Term Continuous Imaging of Diverse Organs. *Science* **2022**, 377, 517–523.
- (63) Li, S.; Lan, Y. Q.; Huang, Y.; Chen, Y. L.; Su, Y. W. A Universal Size Design Principle for Stretchable Inorganic Electronics to Work Consistently under Different Interface Conditions. *Adv. Funct. Mater.* **2023**, 33, 2210880.
- (64) Tchivaleva, L.; Zeng, H.; Markhvida, I.; McLean, D. I.; Lui, H.; Lee, T. K. Skin Roughness Assessment. *New Developments in Biomedical Engineering* **2010**, 341–358.
- (65) Pailler-Mattei, C.; Zahouani, H. Study of Adhesion Forces and Mechanical Properties of Human Skin in Vivo. *J. Adhes. Sci. Technol.* **2004**, 18, 1739–1758.
- (66) Pailler-Mattei, C.; Zahouani, H. Analysis of Adhesive Behaviour of Human Skin in Vivo by an Indentation Test. *Tribol. Int.* **2006**, 39, 12–21.
- (67) Baik, S.; Lee, H. J.; Kim, D. W.; Kim, J. W.; Lee, Y.; Pang, C. Bioinspired Adhesive Architectures: From Skin Patch to Integrated Bioelectronics. *Adv. Mater.* **2019**, 31, 1803309.
- (68) Meitl, M. A.; Zhu, Z. T.; Kumar, V.; Lee, K. J.; Feng, X.; Huang, Y. Y.; Adesida, L.; Nuzzo, R. G.; Rogers, J. A. Transfer Printing by Kinetic Control of Adhesion to an Elastomeric Stamp. *Nat. Mater.* **2006**, 5, 33–38.
- (69) Deng, J.; Yuk, H.; Wu, J. J.; Varela, C. E.; Chen, X. Y.; Roche, E. T.; Guo, C. F.; Zhao, X. H. Electrical Bioadhesive Interface for Bioelectronics. *Nat. Mater.* **2021**, 20, 229–236.
- (70) Li, J.; Celiz, A. D.; Yang, J.; Yang, Q.; Wamala, I.; Whyte, W.; Seo, B. R.; Vasilyev, N. V.; Vlassak, J. J.; Suo, Z.; et al. Tough Adhesives for Diverse Wet Surfaces. *Science* **2017**, 357, 378–381.
- (71) Wang, L.; Lu, N. Conformability of a Thin Elastic Membrane Laminated on a Soft Substrate with Slightly Wavy Surface. *J. Appl. Mech.* **2016**, 83, No. 041007.
- (72) Kabiri Ameri, S.; Ho, R.; Jang, H.; Tao, L.; Wang, Y. H.; Wang, L.; Schnyer, D. M.; Akinwande, D.; Lu, N. S. Graphene Electronic Tattoo Sensors. *ACS Nano* **2017**, 11, 7634–7641.
- (73) Wang, L.; Qiao, S. T.; Kabiri Ameri, S.; Jeong, H.; Lu, N. S. A Thin Elastic Membrane Conformed to a Soft and Rough Substrate Subjected to Stretching/Compression. *J. Appl. Mech.* **2017**, 84, 111003.
- (74) Buono, M.; Sjöholm, N. Effect of Physical Training on Peripheral Sweat Production. *J. Appl. Physiol.* **1988**, 65, 811–814.
- (75) Bandodkar, A. J.; Jeang, W. J.; Ghaffari, R.; Rogers, J. A. Wearable Sensors for Biochemical Sweat Analysis. *Annu. Rev. Anal. Chem.* **2019**, 12, 1–22.
- (76) Huang, Q.; Zheng, Z. Pathway to Developing Permeable Electronics. *ACS Nano* **2022**, 16, 15537–15544.
- (77) Yan, Z. C.; Xiong, J.; Wang, B.; Gao, M.; Yin, G. Q.; Hu, T.; Pan, T.; Wang, X. Z.; Lin, Y. Recent Advances in Breathable Electronics. *Nano Res.* **2023**, 16, 4130–4142.
- (78) Yang, J. W.; Zhang, Z. M.; Zhou, P. C.; Zhang, Y. J.; Liu, Y.; Xu, Y. M.; Gu, Y. H.; Qin, S. L.; Haick, H.; Wang, Y. Toward a New Generation of Permeable Skin Electronics. *Nanoscale* **2023**, 15, 3051–3078.
- (79) Yang, Y.; Cui, T. R.; Li, D.; Ji, S. R.; Chen, Z. K.; Shao, W. C.; Liu, H. F.; Ren, T. L. Breathable Electronic Skins for Daily Physiological Signal Monitoring. *Nanomicro Lett.* **2022**, 14, 161.
- (80) Zhang, J. H.; Li, Z. T.; Xu, J.; Li, J.; Yan, K.; Cheng, W.; Xin, M.; Zhu, T. S.; Du, J.; Chen, S. X.; et al. Versatile Self-Assembled Electrospun Micropyramid Arrays for High-Performance on-Skin Devices with Minimal Sensory Interference. *Nat. Commun.* **2022**, 13, 5839.
- (81) Gorzelanny, C.; Mess, C.; Schneider, S. W.; Huck, V.; Brandner, J. M. Skin Barriers in Dermal Drug Delivery: Which Barriers Have to Be Overcome and How Can We Measure Them? *Pharmaceutics* **2020**, 12, 684.
- (82) Phatale, V.; Vaiphei, K. K.; Jha, S.; Patil, D.; Agrawal, M.; Alexander, A. Overcoming Skin Barriers through Advanced Transdermal Drug Delivery Approaches. *J. Controlled Release* **2022**, 351, 361–380.
- (83) Halprin, K. M. Epidermal “Turnover Time”-a Re-Examination. *Br. J. Dermatol.* **1972**, 86, 14–19.
- (84) Matsukawa, R.; Miyamoto, A.; Yokota, T.; Someya, T. Skin Impedance Measurements with Nanomesh Electrodes for Monitoring Skin Hydration. *Adv. Healthc. Mater.* **2020**, 9, 2001322.
- (85) Lister, T.; Wright, P. A.; Chappell, P. H. Optical Properties of Human Skin. *J. Biomed. Opt.* **2012**, 17, No. 090901.
- (86) Kim, J.; Gutruf, P.; Chiarelli, A. M.; Heo, S. Y.; Cho, K.; Xie, Z. Q.; Banks, A.; Han, S.; Jang, K. I.; Lee, J. W.; et al. Miniaturized Battery-Free Wireless Systems for Wearable Pulse Oximetry. *Adv. Funct. Mater.* **2017**, 27, 1604373.
- (87) Pinti, P.; Aichelburg, C.; Gilbert, S.; Hamilton, A.; Hirsch, J.; Burgess, P.; Tachtsidis, I. A Review on the Use of Wearable Functional near-Infrared Spectroscopy in Naturalistic Environments. *Jpn. Psychol. Res.* **2018**, 60, 347–373.
- (88) Herneth, A. M.; Guccione, S.; Bednarski, M. Apparent Diffusion Coefficient: A Quantitative Parameter for in Vivo Tumor Characterization. *Eur. J. Radiol.* **2003**, 45, 208–213.
- (89) Lin, M.; Hu, H.; Zhou, S.; Xu, S. Soft Wearable Devices for Deep-Tissue Sensing. *Nat. Rev. Mater.* **2022**, 7, 850–869.
- (90) Kuhn, C.; Angehrn, F.; Sonnabend, O.; Voss, A. Impact of Extracorporeal Shock Waves on the Human Skin with Cellulite: A Case Study of a Unique Instance. *Clin. Interv. Aging* **2008**, 3, 201–210.
- (91) Wang, C. F.; Wang, C. H.; Huang, Z. L.; Xu, S. Materials and Structures toward Soft Electronics. *Adv. Mater.* **2018**, 30, 1801368.
- (92) Rogers, J. A.; Someya, T.; Huang, Y. G. Materials and Mechanics for Stretchable Electronics. *Science* **2010**, 327, 1603–1607.
- (93) Fan, J. A.; Yeo, W. H.; Su, Y. W.; Hattori, Y.; Lee, W.; Jung, S. Y.; Zhang, Y. H.; Liu, Z. J.; Cheng, H. Y.; Falgout, L.; et al. Fractal Design Concepts for Stretchable Electronics. *Nat. Commun.* **2014**, 5, 3266.
- (94) Amjadi, M.; Pichitpajongkit, A.; Lee, S.; Ryu, S.; Park, I. Highly Stretchable and Sensitive Strain Sensor Based on Silver Nanowire-Elastomer Nanocomposite. *ACS Nano* **2014**, 8, 5154–5163.
- (95) Yan, X.; Chen, S.; Zhang, G.; Shi, W.; Peng, Z.; Liu, Z.; Chen, Y.; Huang, Y.; Liu, L. Highly Breathable, Surface-Hydrophobic and Wet-Adhesive Silk Based Epidermal Electrode for Long-Term Electrophysiological Monitoring. *Compos. Sci. Technol.* **2022**, 230, 109751.
- (96) Zhou, W. X.; Yao, S. S.; Wang, H. Y.; Du, Q. C.; Ma, Y. W.; Zhu, Y. Gas-Permeable, Ultra-thin, Stretchable Epidermal Electronics with Porous Electrodes. *ACS Nano* **2020**, 14, 5798–5805.
- (97) Jung, D.; Lim, C.; Park, C.; Kim, Y.; Kim, M.; Lee, S.; Lee, H.; Kim, J. H.; Hyeon, T.; Kim, D. H. Adaptive Self-Organization of Nanomaterials Enables Strain-Insensitive Resistance of Stretchable Metallic Nanocomposites. *Adv. Mater.* **2022**, 34, 2200980.
- (98) Jung, D.; Kim, Y.; Lee, H.; Jung, S.; Park, C.; Hyeon, T.; Kim, D. H. Metal-Like Stretchable Nanocomposite Using Locally-Bundled Nanowires for Skin-Mountable Devices. *Adv. Mater.* **2023**, 35, 2303458.
- (99) Jung, D.; Lim, C.; Shim, H. J.; Kim, Y.; Park, C.; Jung, J.; Han, S. I.; Sunwoo, S. H.; Cho, K. W.; Cha, G. D.; et al. Highly Conductive and Elastic Nanomembrane for Skin Electronics. *Science* **2021**, 373, 1022–1026.
- (100) Wang, C. Y.; Xia, K. L.; Wang, H. M.; Liang, X. P.; Yin, Z.; Zhang, Y. Y. Advanced Carbon for Flexible and Wearable Electronics. *Adv. Mater.* **2019**, 31, 1801072.
- (101) Chae, S. H.; Lee, Y. H. Carbon Nanotubes and Graphene Towards Soft Electronics. *Nano Converg.* **2014**, 1, 15.
- (102) Jia, W. Z.; Bandodkar, A. J.; Valdes-Ramirez, G.; Windmiller, J. R.; Yang, Z. J.; Ramirez, J.; Chan, G.; Wang, J. Electrochemical Tattoo Biosensors for Real-Time Noninvasive Lactate Monitoring in Human Perspiration. *Anal. Chem.* **2013**, 85, 6553–6560.
- (103) Lu, N. S.; Lu, C.; Yang, S. X.; Rogers, J. A. Highly Sensitive Skin-Mountable Strain Gauges Based Entirely on Elastomers. *Adv. Funct. Mater.* **2012**, 22, 4044–4050.
- (104) Li, H.; Chang, S. L.; Li, M.; Hou, K. H.; Han, L.; Cao, A. Y.; Li, H. B.; Shang, Y. Y. Flexible and Stable Carbon Nanotube Film Strain

Sensors with Self-Derived Integrated Electrodes. *ACS Appl. Mater. Interfaces* **2021**, *13*, 55600–55610.

(105) Gogurla, N.; Kim, S. Self-Powered and Imperceptible Electronic Tattoos Based on Silk Protein Nanofiber and Carbon Nanotubes for Human-Machine Interfaces. *Adv. Energy Mater.* **2021**, *11*, 202100801.

(106) Htwe, Y. Z. N.; Mariatti, M. Printed Graphene and Hybrid Conductive Inks for Flexible, Stretchable, and Wearable Electronics: Progress, Opportunities, and Challenges. *J. Sci.: Adv. Mater. Devices* **2022**, *7*, 100435.

(107) Jang, H.; Sel, K.; Kim, E.; Kim, S.; Yang, X. X.; Kang, S.; Ha, K. H.; Wang, R.; Rao, Y. F.; Jafari, R.; Lu, N. Graphene E-Tattoos for Unobstructive Ambulatory Electrodermal Activity Sensing on the Palm Enabled by Heterogeneous Serpentine Ribbons. *Nat. Commun.* **2022**, *13*, 6604.

(108) Kireev, D.; Ameri, S. K.; Nederveld, A.; Kampfe, J.; Jang, H.; Lu, N. S.; Akinwande, D. Fabrication, Characterization and Applications of Graphene Electronic Tattoos. *Nat. Protoc.* **2021**, *16*, 2395–2417.

(109) Suk, J. W.; Kitt, A.; Magnuson, C. W.; Hao, Y. F.; Ahmed, S.; An, J.; Swan, A. K.; Goldberg, B. B.; Ruoff, R. S. Transfer of CVD-Grown Monolayer Graphene onto Arbitrary Substrates. *ACS Nano* **2011**, *5*, 6916–6924.

(110) Lee, C.; Wei, X. D.; Kysar, J. W.; Hone, J. Measurement of the Elastic Properties and Intrinsic Strength of Monolayer Graphene. *Science* **2008**, *321*, 385–388.

(111) Zheng, L.; Wang, X. W.; Jiang, H. J.; Xu, M. Z.; Huang, W.; Liu, Z. Recent Progress of Flexible Electronics by 2D Transition Metal Dichalcogenides. *Nano Res.* **2022**, *15*, 2413–2432.

(112) Feng, S. X.; Wang, X.; Wang, M. L.; Bai, C.; Cao, S. T.; Kong, D. S. Crumpled Mxene Electrodes for Ultrastretchable and High-Area-Capacitance Supercapacitors. *Nano Lett.* **2021**, *21*, 7561–7568.

(113) Hantanasirisakul, K.; Gogotsi, Y. Electronic and Optical Properties of 2D Transition Metal Carbides and Nitrides (Mxenes). *Adv. Mater.* **2018**, *30*, 1804779.

(114) Wang, Z.; Zhou, Z.; Li, C. L.; Liu, X. H.; Zhang, Y.; Pei, M. M.; Zhou, Z.; Cui, D. X.; Hu, D.; Chen, F.; Cao, W.-T. A Single Electronic Tattoo for Multisensory Integration. *Small Methods* **2023**, *7*, e2201566.

(115) Yoder, M. A.; Yan, Z.; Han, M. D.; Rogers, J. A.; Nuzzo, R. G. Semiconductor Nanomembrane Materials for High-Performance Soft Electronic Devices. *J. Am. Chem. Soc.* **2018**, *140*, 9001–9019.

(116) Kireev, D.; Okogbue, E.; Jayanth, R. T.; Ko, T. J.; Jung, Y.; Akinwande, D. Multipurpose and Reusable Ultra-thin Electronic Tattoos Based on PtSe₂ and PtTe₂. *ACS Nano* **2021**, *15*, 2800–2811.

(117) Cai, Z. Y.; Liu, B. L.; Zou, X. L.; Cheng, H. M. Chemical Vapor Deposition Growth and Applications of Two-Dimensional Materials and Their Heterostructures. *Chem. Rev.* **2018**, *118*, 6091–6133.

(118) Jang, H.; Dai, Z. H.; Ha, K. H.; Ameri, S. K.; Lu, N. S. Stretchability of PMMA-Supported CVD Graphene and of Its Electrical Contacts. *2D Mater.* **2020**, *7*, No. 014003.

(119) Coleman, J. N.; Lotya, M.; O'Neill, A.; Bergin, S. D.; King, P. J.; Khan, U.; Young, K.; Gaucher, A.; De, S.; Smith, R. J.; et al. Two-Dimensional Nanosheets Produced by Liquid Exfoliation of Layered Materials. *Science* **2011**, *331*, 568–571.

(120) Qiao, Y.; Wang, Y.; Tian, H.; Li, M.; Jian, J.; Wei, Y.; Tian, Y.; Wang, D. Y.; Pang, Y.; Geng, X.; et al. Multilayer Graphene Epidermal Electronic Skin. *ACS Nano* **2018**, *12*, 8839–8846.

(121) Yu, Y.; Nassar, N.; Xu, C. H.; Min, J. H.; Yang, Y. R.; Dai, A.; Doshi, R.; Huang, A.; Song, Y.; Gehlhar, R.; et al. Biofuel-Powered Soft Electronic Skin with Multiplexed and Wireless Sensing for Human-Machine Interfaces. *Sci. Robot* **2020**, *5*, eaaz7946.

(122) Weaver, C. L.; LaRosa, J. M.; Luo, X. L.; Cui, X. T. Electrically Controlled Drug Delivery from Graphene Oxide Nanocomposite Films. *ACS Nano* **2014**, *8*, 1834–1843.

(123) Huang, X.; Qi, X.; Boey, F.; Zhang, H. Graphene-Based Composites. *Chem. Soc. Rev.* **2012**, *41*, 666–686.

(124) Nicolosi, V.; Chhowalla, M.; Kanatzidis, M. G.; Strano, M. S.; Coleman, J. N. Liquid Exfoliation of Layered Materials. *Science* **2013**, *340*, 1226419.

(125) Cai, X.; Luo, Y.; Liu, B.; Cheng, H. M. Preparation of 2D Material Dispersions and Their Applications. *Chem. Soc. Rev.* **2018**, *47*, 6224–6266.

(126) Wang, X. L.; Zhang, Y. X.; Guo, R.; Wang, H. Z.; Yuan, B.; Liu, J. Conformable Liquid Metal Printed Epidermal Electronics for Smart Physiological Monitoring and Simulation Treatment. *J. Micromech. Microeng.* **2018**, *28*, No. 034003.

(127) Alberto, J.; Leal, C.; Fernandes, C.; Lopes, P. A.; Paisana, H.; de Almeida, A. T.; Tavakoli, M. Fully Untethered Battery-Free Biomonitoring Electronic Tattoo with Wireless Energy Harvesting. *Sci. Rep.* **2020**, *10*, 5539.

(128) Tang, L.; Shang, J.; Jiang, X. Multilayered Electronic Transfer Tattoo That Can Enable the Crease Amplification Effect. *Sci. Adv.* **2021**, *7*, eabe3778.

(129) Gao, Y.; Ota, H.; Schaler, E. W.; Chen, K.; Zhao, A.; Gao, W.; Fahad, H. M.; Leng, Y.; Zheng, A.; Xiong, F.; Zhang, C.; Tai, L.-C.; Zhao, P.; Fearing, R. S.; Javey, A.; et al. Wearable Microfluidic Diaphragm Pressure Sensor for Health and Tactile Touch Monitoring. *Adv. Mater.* **2017**, *29*, 1701985.

(130) Ding, L.; Hang, C.; Yang, S.; Qi, J.; Dong, R.; Zhang, Y.; Sun, H.; Jiang, X. In Situ Deposition of Skin-Adhesive Liquid Metal Particles with Robust Wear Resistance for Epidermal Electronics. *Nano Lett.* **2022**, *22*, 4482–4490.

(131) Lee, G. H.; Lee, Y. R.; Kim, H.; Kwon, D. A.; Kim, H.; Yang, C.; Choi, S. Q.; Park, S.; Jeong, J. W.; Park, S. Rapid Meniscus-Guided Printing of Stable Semi-Solid-State Liquid Metal Microgranular-Particle for Soft Electronics. *Nat. Commun.* **2022**, *13*, 2643.

(132) Lee, G. H.; Woo, H.; Yoon, C.; Yang, C.; Bae, J. Y.; Kim, W.; Lee, D. H.; Kang, H.; Han, S.; Kang, S. K.; et al. A Personalized Electronic Tattoo for Healthcare Realized by on-the-Spot Assembly of an Intrinsically Conductive and Durable Liquid-Metal Composite. *Adv. Mater.* **2022**, *34*, 2204159.

(133) Jiang, Y. W.; Zhang, Z. T.; Wang, Y. X.; Li, D. L.; Coen, C. T.; Hwaun, E.; Chen, G.; Wu, H. C.; Zhong, D. L.; Niu, S. M.; et al. Topological Supramolecular Network Enabled High-Conductivity, Stretchable Organic Bioelectronics. *Science* **2022**, *375*, 1411–1417.

(134) Mandala, H. S.; Kasteel, J. S.; McHail, D. G.; Rubinson, J. F.; Pancrazio, J. J.; Dumas, T. C. Improved Poly (3,4-Ethylenedioxythiophene) (PEDOT) for Neural Stimulation. *Neuromodulation* **2015**, *18*, 657–663.

(135) Wu, F.; Li, P.; Sun, K.; Zhou, Y.; Chen, W.; Fu, J.; Li, M.; Lu, S.; Wei, D.; Tang, X.; et al. Conductivity Enhancement of PEDOT:PSS Via Addition of Chloroplatinic Acid and Its Mechanism. *Adv. Electron. Mater.* **2017**, *3*, 1700047.

(136) Shi, H.; Liu, C.; Jiang, Q.; Xu, J. Effective Approaches to Improve the Electrical Conductivity of PEDOT:PSS: A Review. *Adv. Electron. Mater.* **2015**, *1*, 1500017.

(137) Shahrim, N. A.; Ahmad, Z.; Wong Azman, A.; Fachmi Buys, Y.; Sarifuddin, N. Mechanisms for Doped PEDOT:PSS Electrical Conductivity Improvement. *Mater. Adv.* **2021**, *2*, 7118–7138.

(138) Aguzin, A.; Dominguez-Alfaro, A.; Criado-Gonzalez, M.; Velasco-Bosom, S.; Picchio, M. L.; Casado, N.; Mitoudi-Vagourdi, E.; Minari, R. J.; Malliaras, G. G.; Mecerreyes, D. Direct Ink Writing of PEDOT Eutectogels as Substrate-Free Dry Electrodes for Electromyography. *Mater. Horiz.* **2023**, *10*, 2516–2524.

(139) Wang, Y.; Zhu, C. X.; Pfattner, R.; Yan, H. P.; Jin, L. H.; Chen, S. H.; Molina-Lopez, F.; Lissel, F.; Liu, J.; Rabiha, N. I.; et al. A Highly Stretchable, Transparent, and Conductive Polymer. *Sci. Adv.* **2017**, *3*, e1602076.

(140) Kayser, L. V.; Lipomi, D. J. Stretchable Conductive Polymers and Composites Based on PEDOT and PEDOT:PSS. *Adv. Mater.* **2019**, *31*, 1806133.

(141) Ershad, F.; Thukral, A.; Yue, J.; Comeaux, P.; Lu, Y.; Shim, H.; Sim, K.; Kim, N. I.; Rao, Z.; Guevara, R.; et al. Ultra-Conformal Drawn-on-Skin Electronics for Multifunctional Motion Artifact-Free Sensing and Point-of-Care Treatment. *Nat. Commun.* **2020**, *11*, 3823.

(142) Shin, M.; Song, J. H.; Lim, G. H.; Lim, B.; Park, J. J.; Jeong, U. Highly Stretchable Polymer Transistors Consisting Entirely of Stretchable Device Components. *Adv. Mater.* **2014**, *26*, 3706–3711.

- (143) Guan, Y.-S.; Ershad, F.; Rao, Z.; Ke, Z.; da Costa, E. C.; Xiang, Q.; Lu, Y.; Wang, X.; Mei, J.; Vanderslice, P.; Hochman-Mendez, C.; Yu, C. Elastic Electronics Based on Micromesh-Structured Rubbery Semiconductor Films. *Nat. Electron.* **2022**, *5*, 881–892.
- (144) Zhao, X. H.; Chen, X. Y.; Yuk, H.; Lin, S. T.; Liu, X. Y.; Parada, G. Soft Materials by Design: Unconventional Polymer Networks Give Extreme Properties. *Chem. Rev.* **2021**, *121*, 4309–4372.
- (145) Lim, C.; Hong, Y. J.; Jung, J.; Shin, Y.; Sunwoo, S. H.; Baik, S.; Park, O. K.; Choi, S. H.; Hyeon, T.; Kim, J. H.; et al. Tissue-Like Skin-Device Interface for Wearable Bioelectronics by Using Ultrasoft, Mass-Permeable, and Low-Impedance Hydrogels. *Sci. Adv.* **2021**, *7*, eabd3716.
- (146) Cheng, S.; Lou, Z.; Zhang, L.; Guo, H.; Wang, Z.; Guo, C.; Fukuda, K.; Ma, S.; Wang, G.; Someya, T.; et al. Ultrathin Hydrogel Films toward Breathable Skin-Integrated Electronics. *Adv. Mater.* **2023**, *35*, 2206793.
- (147) Yang, C. H.; Suo, Z. G. Hydrogel Ionotronics. *Nat. Rev. Mater.* **2018**, *3*, 125–142.
- (148) Yuk, H.; Zhang, T.; Parada, G. A.; Liu, X. Y.; Zhao, X. H. Skin-Inspired Hydrogel-Elastomer Hybrids with Robust Interfaces and Functional Microstructures. *Nat. Commun.* **2016**, *7*, 12028.
- (149) Gong, J. P.; Katsuyama, Y.; Kurokawa, T.; Osada, Y. Double-Network Hydrogels with Extremely High Mechanical Strength. *Adv. Mater.* **2003**, *15*, 1155–1158.
- (150) Guo, M. L.; Wu, Y. P.; Xue, S. S.; Xia, Y. M.; Yang, X.; Dzenis, Y.; Li, Z. Y.; Lei, W. W.; Smith, A. T.; Sun, L. Y. A Highly Stretchable, Ultra-Tough, Remarkably Tolerant, and Robust Self-Healing Glycerol-Hydrogel for a Dual-Responsive Soft Actuator. *J. Mater. Chem. A* **2019**, *7*, 25969–25977.
- (151) Liu, X.; Yuk, H.; Lin, S.; Parada, G. A.; Tang, T.-C.; Tham, E.; de la Fuente-Nunez, C.; Lu, T. K.; Zhao, X. 3D Printing of Living Responsive Materials and Devices. *Adv. Mater.* **2018**, *30*, 201704821.
- (152) Niu, W.; Tian, Q.; Liu, Z.; Liu, X. Solvent-Free and Skin-Like Supramolecular Ion-Conductive Elastomers with Versatile Processability for Multifunctional Ionic Tattoos and on-Skin Bioelectronics. *Adv. Mater.* **2023**, *35*, 2304157.
- (153) Ray, T. R.; Choi, J.; Bandothkar, A. J.; Krishnan, S.; Gutruf, P.; Tian, L.; Ghaffari, R.; Rogers, J. A. Bio-Integrated Wearable Systems: A Comprehensive Review. *Chem. Rev.* **2019**, *119*, 5461–5533.
- (154) Krishnan, S. R.; Su, C. J.; Xie, Z.; Patel, M.; Madhupathy, S. R.; Xu, Y.; Freudman, J.; Ng, B.; Heo, S. Y.; Wang, H.; et al. Wireless, Battery-Free Epidermal Electronics for Continuous, Quantitative, Multimodal Thermal Characterization of Skin. *Small* **2018**, *14*, e1803192.
- (155) Wong, T. H.; Yiu, C. K.; Zhou, J. K.; Song, Z.; Liu, Y. M.; Zhao, L.; Yao, K. M.; Park, W.; Yoo, W.; Song, E. M.; et al. Tattoo-Like Epidermal Electronics as Skin Sensors for Human Machine Interfaces. *Soft Sci.* **2021**, *1*, 10.
- (156) Niu, Z.; Dong, H.; Zhu, B.; Li, J.; Hng, H. H.; Zhou, W.; Chen, X.; Xie, S. Highly Stretchable, Integrated Supercapacitors Based on Single-Walled Carbon Nanotube Films with Continuous Reticulate Architecture. *Adv. Mater.* **2013**, *25*, 1058–1064.
- (157) Cao, J.; Yang, X. Y.; Rao, J. C.; Mitriashkin, A.; Fan, X.; Chen, R.; Cheng, H. L.; Wang, X. C.; Goh, J.; Leo, H. L.; Ouyang, J. Y.; et al. Stretchable and Self-Adhesive PEDOT: PSS Blend with High Sweat Tolerance as Conformal Biopotential Dry Electrodes. *ACS Appl. Mater. Interfaces.* **2022**, *14*, 39159–39171.
- (158) Wang, Y. F.; Sekine, T.; Takeda, Y.; Yokosawa, K.; Matsui, H.; Kumaki, D.; Shiba, T.; Nishikawa, T.; Tokito, S. Fully Printed PEDOT:PSS-Based Temperature Sensor with High Humidity Stability for Wireless Healthcare Monitoring. *Sci. Rep.* **2020**, *10*, 2467.
- (159) Cheng, J. H.; Shang, J.; Yang, S. J.; Dou, J. B.; Shi, X. H.; Jiang, X. Y. Wet-Adhesive Elastomer for Liquid Metal-Based Conformal Epidermal Electronics. *Adv. Funct. Mater.* **2022**, *32*, 2200444.
- (160) Matsuhisa, N.; Chen, X.; Bao, Z.; Someya, T. Materials and Structural Designs of Stretchable Conductors. *Chem. Soc. Rev.* **2019**, *48*, 2946–2966.
- (161) Sun, Y.; Rogers, J. A. Structural Forms of Single Crystal Semiconductor Nanoribbons for High-Performance Stretchable Electronics. *J. Mater. Chem.* **2007**, *17*, 832–840.
- (162) Yang, S.; Khare, K.; Lin, P. C. Harnessing Surface Wrinkle Patterns in Soft Matter. *Adv. Funct. Mater.* **2010**, *20*, 2550–2564.
- (163) Wang, S. D.; Song, J. Z.; Kim, D. H.; Huang, Y. G.; Rogers, J. A. Local Versus Global Buckling of Thin Films on Elastomeric Substrates. *Appl. Phys. Lett.* **2008**, *93*, No. 023126.
- (164) Yu, S. J.; Sun, Y. D.; Li, S. C.; Ni, Y. Harnessing Fold-to-Wrinkle Transition and Hierarchical Wrinkling on Soft Material Surfaces by Regulating Substrate Stiffness and Sputtering Flux. *Soft Matt.* **2018**, *14*, 6745–6755.
- (165) Jiang, H. Q.; Khang, D. Y.; Song, J. Z.; Sun, Y. G.; Huang, Y. G.; Rogers, J. A. Finite Deformation Mechanics in Buckled Thin Films on Compliant Supports. *Proc. Natl. Acad. Sci. U. S. A.* **2007**, *104*, 15607–15612.
- (166) Jiang, H. Q.; Sun, Y. G.; Rogers, J. A.; Huang, Y. G. Mechanics of Precisely Controlled Thin Film Buckling on Elastomeric Substrate. *Appl. Phys. Lett.* **2007**, *90*, 133119.
- (167) Xu, F.; Zhu, Y. Highly Conductive and Stretchable Silver Nanowire Conductors. *Adv. Mater.* **2012**, *24*, 5117–5122.
- (168) Das, A.; Banerji, A.; Mukherjee, R. Programming Feature Size in the Thermal Wrinkling of Metal Polymer Bilayer by Modulating Substrate Viscoelasticity. *ACS Appl. Mater. Interfaces* **2017**, *9*, 23255–23262.
- (169) Chen, G.; Matsuhisa, N.; Liu, Z. Y.; Qi, D. P.; Cai, P. Q.; Jiang, Y.; Wan, C. J.; Cui, Y. J.; Leow, W. R.; Liu, Z. J.; et al. Plasticizing Silk Protein for on-Skin Stretchable Electrodes. *Adv. Mater.* **2018**, *30*, 1800129.
- (170) Zang, J. F.; Ryu, S.; Pugno, N.; Wang, Q. M.; Tu, Q.; Buehler, M. J.; Zhao, X. H. Multifunctionality and Control of the Crumpling and Unfolding of Large-Area Graphene. *Nat. Mater.* **2013**, *12*, 321–325.
- (171) Lipomi, D. J.; Vosgueritchian, M.; Tee, B. C. K.; Hellstrom, S. L.; Lee, J. A.; Fox, C. H.; Bao, Z. N. Skin-Like Pressure and Strain Sensors Based on Transparent Elastic Films of Carbon Nanotubes. *Nat. Nanotechnol.* **2011**, *6*, 788–792.
- (172) Zhang, Y. H.; Wang, S. D.; Li, X. T.; Fan, J. A.; Xu, S.; Song, Y. M.; Choi, K. J.; Yeo, W. H.; Lee, W.; Nazaar, S. N.; et al. Experimental and Theoretical Studies of Serpentine Microstructures Bonded to Prestrained Elastomers for Stretchable Electronics. *Adv. Funct. Mater.* **2014**, *24*, 2028–2037.
- (173) Kim, D. H.; Liu, Z. J.; Kim, Y. S.; Wu, J.; Song, J. Z.; Kim, H. S.; Huang, Y. G.; Hwang, K.; Zhang, Y. W.; Rogers, J. A. Optimized Structural Designs for Stretchable Silicon Integrated Circuits. *Small* **2009**, *5*, 2841–2847.
- (174) Zhang, Y.; Xu, S.; Fu, H.; Lee, J.; Su, J.; Hwang, K. C.; Rogers, J. A.; Huang, Y. Buckling in Serpentine Microstructures and Applications in Elastomer-Supported Ultra-Stretchable Electronics with High Areal Coverage. *Soft Matter* **2013**, *9*, 8062–8070.
- (175) Yang, S. X.; Qiao, S. T.; Lu, N. S. Elasticity Solutions to Nonbuckling Serpentine Ribbons. *J. Appl. Mech.* **2017**, *84*, No. 021004.
- (176) Lu, N. S.; Yang, S. X. Mechanics for Stretchable Sensors. *Curr. Opin. Solid State Mater. Sci.* **2015**, *19*, 149–159.
- (177) Choi, C.; Choi, M. K.; Liu, S. Y.; Kim, M.; Park, O. K.; Im, C.; Kim, J.; Qin, X.; Lee, G. J.; Cho, K. W.; et al. Human Eye-Inspired Soft Optoelectronic Device Using High-Density MoS₂-Graphene Curved Image Sensor Array. *Nat. Commun.* **2017**, *8*, 1664.
- (178) Xu, L. Z.; Gutbrod, S. R.; Ma, Y. J.; Petrossians, A.; Liu, Y. H.; Webb, R. C.; Fan, J. A.; Yang, Z. J.; Xu, R. X.; Whalen, J. J., III; et al. Materials and Fractal Designs for 3D Multifunctional Integumentary Membranes with Capabilities in Cardiac Electrotherapy. *Adv. Mater.* **2015**, *27*, 1731–1737.
- (179) Zhang, Y.; Fu, H.; Su, Y.; Xu, S.; Cheng, H.; Fan, J. A.; Hwang, K. C.; Rogers, J. A.; Huang, Y. Mechanics of Ultra-Stretchable Self-Similar Serpentine Interconnects. *Acta Mater.* **2013**, *61* (20), 7816–7827.
- (180) Xu, S.; Zhang, Y.; Cho, J.; Lee, J.; Huang, X.; Jia, L.; Fan, J. A.; Su, Y.; Su, J.; Zhang, H.; et al. Stretchable Batteries with Self-Similar

Serpentine Interconnects and Integrated Wireless Recharging Systems. *Nat. Commun.* **2013**, *4*, 1543.

(181) Fu, H. R.; Xu, S.; Xu, R. X.; Jiang, J. Q.; Zhang, Y. H.; Rogers, J. A.; Huang, Y. G. Lateral Buckling and Mechanical Stretchability of Fractal Interconnects Partially Bonded onto an Elastomeric Substrate. *Appl. Phys. Lett.* **2015**, *106*, No. 091902.

(182) Liu, H. Z.; Li, H. G.; Wang, Z. C.; Wei, X.; Zhu, H. J.; Sun, M. Z.; Lin, Y.; Xu, L. Z. Robust and Multifunctional Kirigami Electronics with a Tough and Permeable Aramid Nanofiber Framework. *Adv. Mater.* **2022**, *34*, 2207350.

(183) Li, X.; Zhu, P.; Zhang, S.; Wang, X.; Luo, X.; Leng, Z.; Zhou, H.; Pan, Z.; Mao, Y. A Self-Supporting, Conductor-Exposing, Stretchable, Ultrathin, and Recyclable Kirigami-Structured Liquid Metal Paper for Multifunctional E-Skin. *ACS Nano* **2022**, *16*, 5909–5919.

(184) Sun, R. J.; Carreira, S. C.; Chen, Y.; Xiang, C. Q.; Xu, L. L.; Zhang, B.; Chen, M. D.; Farrow, I.; Scarpa, F.; Rossiter, J. Stretchable Piezoelectric Sensing Systems for Self-Powered and Wireless Health Monitoring. *Adv. Mater. Technol.* **2019**, *4*, 1900100.

(185) Morikawa, Y.; Yamagiwa, S.; Sawahata, H.; Numano, R.; Koida, K.; Kawano, T. Donut-Shaped Stretchable Kirigami: Enabling Electronics to Integrate with the Deformable Muscle. *Adv. Healthc. Mater.* **2019**, *8*, 1900939.

(186) Morikawa, Y.; Yamagiwa, S.; Sawahata, H.; Numano, R.; Koida, K.; Ishida, M.; Kawano, T. Ultrastretchable Kirigami Bioprobes. *Adv. Healthc. Mater.* **2018**, *7*, 1701100.

(187) Gao, J. Y.; Shang, K. Z.; Ding, Y. C.; Wen, Z. H. Material and Configuration Design Strategies Towards Flexible and Wearable Power Supply Devices: A Review. *J. Mater. Chem. A* **2021**, *9*, 8950–8965.

(188) Liu, Y. Q.; He, K.; Chen, G.; Leow, W. R.; Chen, X. D. Nature-Inspired Structural Materials for Flexible Electronic Devices. *Chem. Rev.* **2017**, *117*, 12893–12941.

(189) Feng, B.; Sun, T. M.; Wang, W. G.; Xiao, Y.; Huo, J. P.; Deng, Z. Y.; Bian, G. B.; Wu, Y. X.; Zou, G. S.; Wang, W. X.; et al. Venation-Mimicking, Ultrastretchable, Room-Temperature-Attachable Metal Tapes for Integrated Electronic Skins. *Adv. Mater.* **2023**, *35*, 2208568.

(190) Jiang, Z.; Chen, N.; Yi, Z.; Zhong, J.; Zhang, F.; Ji, S.; Liao, R.; Wang, Y.; Li, H.; Liu, Z.; et al. A 1.3-Micrometre-Thick Elastic Conductor for Seamless on-Skin and Implantable Sensors. *Nat. Electron.* **2022**, *5*, 784–793.

(191) Jeong, J. W.; Yeo, W. H.; Akhtar, A.; Norton, J. J. S.; Kwack, Y. J.; Li, S.; Jung, S. Y.; Su, Y. W.; Lee, W.; Xia, J.; et al. Materials and Optimized Designs for Human-Machine Interfaces Via Epidermal Electronics. *Adv. Mater.* **2013**, *25*, 6839–6846.

(192) Bae, W. G.; Kim, D.; Kwak, M. K.; Ha, L.; Kang, S. M.; Suh, K. Y. Enhanced Skin Adhesive Patch with Modulus-Tunable Composite Micropillars. *Adv. Healthc. Mater.* **2013**, *2*, 109–113.

(193) Pang, C.; Koo, J. H.; Nguyen, A.; Caves, J. M.; Kim, M. G.; Chortos, A.; Kim, K.; Wang, P. J.; Tok, J. B. H.; Bao, Z. N. Highly Skin-Conformal Microhair Sensor for Pulse Signal Amplification. *Adv. Mater.* **2015**, *27*, 634–640.

(194) Bartlett, M. D.; Croll, A. B.; King, D. R.; Paret, B. M.; Irschick, D. J.; Crosby, A. J. Looking Beyond Fibrillar Features to Scale Gecko-Like Adhesion. *Adv. Mater.* **2012**, *24*, 1078–1083.

(195) Bartlett, M. D.; Crosby, A. J. High Capacity, Easy Release Adhesives from Renewable Materials. *Adv. Mater.* **2014**, *26*, 3405–3409.

(196) Kim, T.; Park, J.; Sohn, J.; Cho, D.; Jeon, S. Bioinspired, Highly Stretchable, and Conductive Dry Adhesives Based on 1D-2D Hybrid Carbon Nanocomposites for All-in-One ECG Electrodes. *ACS Nano* **2016**, *10*, 4770–4778.

(197) O'Rourke, R. D.; Steele, T. W.; Taylor, H. Bioinspired Fibrillar Adhesives: A Review of Analytical Models and Experimental Evidence for Adhesion Enhancement by Surface Patterns. *J. Adhes. Sci. Technol.* **2016**, *30*, 362–391.

(198) Cadirov, N.; Booth, J. A.; Turner, K. L.; Israelachvili, J. N. Influence of Humidity on Grip and Release Adhesion Mechanisms for Gecko-Inspired Microfibrillar Surfaces. *ACS Appl. Mater. Interfaces* **2017**, *9*, 14497–14505.

(199) Choi, M. K.; Park, O. K.; Choi, C.; Qiao, S.; Ghaffari, R.; Kim, J.; Lee, D. J.; Kim, M.; Hyun, W.; Kim, S. J.; et al. Cephalopod-Inspired Miniaturized Suction Cups for Smart Medical Skin. *Adv. Healthc. Mater.* **2016**, *5*, 80–87.

(200) Qiao, S. T.; Wang, L.; Jeong, H.; Rodin, G. J.; Lu, N. S. Suction Effects in Cratered Surfaces. *J. R. Soc. Interface* **2017**, *14*, 20170377.

(201) Wang, L.; Ha, K. H.; Qiao, S. T.; Lu, N. S. Suction Effects of Crater Arrays. *Extreme Mech. Lett.* **2019**, *30*, 100496.

(202) Chun, S.; Kim, D. W.; Baik, S.; Lee, H. J.; Lee, J. H.; Bhang, S. H.; Pang, C. Conductive and Stretchable Adhesive Electronics with Miniaturized Octopus-Like Suckers against Dry/Wet Skin for Biosignal Monitoring. *Adv. Funct. Mater.* **2018**, *28*, 1805224.

(203) Pan, L.; Cai, P. Q.; Mei, L.; Cheng, Y.; Zeng, Y.; Wang, M.; Wang, T.; Jiang, Y.; Ji, B. H.; Li, D. C.; et al. A Compliant Ionic Adhesive Electrode with Ultralow Bioelectronic Impedance. *Adv. Mater.* **2020**, *32*, 2003723.

(204) Scognamiglio, F.; Travan, A.; Borgogna, M.; Donati, I.; Marsich, E.; Bosmans, J. W.; Perge, L.; Foulc, M. P.; Bouvy, N. D.; Paoletti, S. Enhanced Bioadhesivity of Dopamine-Functionalized Polysaccharidic Membranes for General Surgery Applications. *Acta Biomater* **2016**, *44*, 232–242.

(205) Ji, S.; Wan, C.; Wang, T.; Li, Q.; Chen, G.; Wang, J.; Liu, Z.; Yang, H.; Liu, X.; Chen, X. Water-Resistant Conformal Hybrid Electrodes for Aquatic Endurable Electrocardiographic Monitoring. *Adv. Mater.* **2020**, *32*, 2001496.

(206) Gonzalez, M. A.; Simon, J. R.; Ghoorchian, A.; Scholl, Z.; Lin, S. T.; Rubinstein, M.; Marszalek, P.; Chilkoti, A.; Lopez, G. P.; Zhao, X. H. Strong, Tough, Stretchable, and Self-Adhesive Hydrogels from Intrinsically Unstructured Proteins. *Adv. Mater.* **2017**, *29*, 1604743.

(207) Yuk, H.; Varela, C. E.; Nabzdyk, C. S.; Mao, X. Y.; Padera, R. F.; Roche, E. T.; Zhao, X. H. Dry Double-Sided Tape for Adhesion of Wet Tissues and Devices. *Nature* **2019**, *575*, 169–174.

(208) Mao, X. Y.; Yuk, H.; Zhao, X. H. Hydration and Swelling of Dry Polymers for Wet Adhesion. *J. Mech. Phys. Solids* **2020**, *137*, 103863.

(209) Chen, F.; Huang, Q. Y.; Zheng, Z. J. Permeable Conductors for Wearable and On-skin Electronics. *Small Structures* **2022**, *3*, 2100135.

(210) Smith, C. J.; Havenith, G. Body Mapping of Sweating Patterns in Male Athletes in Mild Exercise-Induced Hyperthermia. *Eur. J. Appl. Physiol.* **2011**, *111*, 1391–1404.

(211) Ameri, S. K.; Kim, M.; Kuang, I. A.; Perera, W. K.; Alshiekh, M.; Jeong, H.; Topcu, U.; Akinwande, D.; Lu, N. S. Imperceptible Electrooculography Graphene Sensor System for Human-Robot Interface. *npj 2D Mater. Appl.* **2018**, *2*, 19.

(212) Wang, Y. H.; Qiu, Y. T.; Ameri, S. K.; Jang, H.; Dai, Z. H.; Huang, Y. A.; Lu, N. S. Low-Cost, μm -Thick, Tape-Free Electronic Tattoo Sensors with Minimized Motion and Sweat Artifacts. *npj Flex. Electron.* **2018**, *2*, 6.

(213) Wang, Y.; Lee, S.; Wang, H. Y.; Jiang, Z.; Jimbo, Y.; Wang, C. Y.; Wang, B. H.; Kim, J. J.; Koizumi, M.; Yokota, T.; et al. Robust, Self-Adhesive, Reinforced Polymeric Nanofilms Enabling Gas-Permeable Dry Electrodes for Long-Term Application. *Proc. Natl. Acad. Sci. U. S. A.* **2021**, *118*, e2111904118.

(214) Yang, X. Q.; Li, L. H.; Wang, S. Q.; Lu, Q. F.; Bai, Y. Y.; Sun, F. Q.; Li, T.; Li, Y.; Wang, Z. H.; Zhao, Y. Y.; et al. Ultra-thin, Stretchable, and Breathable Epidermal Electronics Based on a Facile Bubble Blowing Method. *Adv. Electron. Mater.* **2020**, *6*, 2000306.

(215) Yao, Z. K.; Yang, Z.; Guo, H.; Ma, X. H.; Dong, Y. C.; Tang, C. Y. Highly Permeable and Highly Selective Ultra-thin Film Composite Polyamide Membranes Reinforced by Reactable Polymer Chains. *J. Colloid Interface Sci.* **2019**, *552*, 418–425.

(216) Cheon, S.; Kang, H.; Kim, H.; Son, Y.; Lee, J. Y.; Shin, H. J.; Kim, S. W.; Cho, J. H. High-Performance Triboelectric Nanogenerators Based on Electrospun Polyvinylidene Fluoride-Silver Nanowire Composite Nanofibers. *Adv. Funct. Mater.* **2018**, *28*, 1703778.

(217) Jiang, Z.; Nayeem, M. O. G.; Fukuda, K.; Ding, S.; Jin, H.; Yokota, T.; Inoue, D.; Hashizume, D.; Someya, T. Highly Stretchable Metallic Nanowire Networks Reinforced by the Underlying Randomly Distributed Elastic Polymer Nanofibers Via Interfacial Adhesion Improvement. *Adv. Mater.* **2019**, *31*, 1903446.

- (218) Liu, L.; Li, H. Y.; Fan, Y. J.; Chen, Y. H.; Kuang, S. Y.; Li, Z. B.; Wang, Z. L.; Zhu, G. Nanofiber-Reinforced Silver Nanowires Network as a Robust, Ultra-thin, and Conformable Epidermal Electrode for Ambulatory Monitoring of Physiological Signals. *Small* **2019**, *15*, 1900755.
- (219) Fan, Y. J.; Li, X.; Kuang, S. Y.; Kuang, Y.; Zhang, L.; Chen, Y. H.; Liu, L.; Zhang, K.; Ma, S. W.; Liang, F.; et al. Highly Robust, Transparent, and Breathable Epidermal Electrode. *ACS Nano* **2018**, *12*, 9326–9332.
- (220) Lu, L. J.; Yang, B.; Liu, J. Q. Flexible Multifunctional Graphite Nanosheet/Electrospun-Polyamide 66 Nanocomposite Sensor for ECG, Strain, Temperature and Gas Measurements. *Chem. Eng. J.* **2020**, *400*, 125928.
- (221) Gao, J. F.; Li, B.; Huang, X. W.; Wang, L.; Lin, L. W.; Wang, H.; Xue, H. G. Electrically Conductive and Fluorine Free Superhydrophobic Strain Sensors Based on SiO₂/Graphene-Decorated Electrospun Nanofibers for Human Motion Monitoring. *Chem. Eng. J.* **2019**, *373*, 298–306.
- (222) Pan, Q.; Tong, N. J.; He, N. F.; Liu, Y. X.; Shim, E.; Pourdeyhimi, B.; Gao, W. Electrospun Mat of Poly(Vinyl Alcohol)/Graphene Oxide for Superior Electrolyte Performance. *ACS Appl. Mater. Interfaces* **2018**, *10*, 7927–7934.
- (223) Gogurla, N.; Kim, Y.; Cho, S.; Kim, J.; Kim, S. Multifunctional and Ultra-thin Electronic Tattoo for on-Skin Diagnostic and Therapeutic Applications. *Adv. Mater.* **2021**, *33*, 2008308.
- (224) Ma, Z. J.; Huang, Q. Y.; Xu, Q.; Zhuang, Q. N.; Zhao, X.; Yang, Y. H.; Qiu, H.; Yang, Z. L.; Wang, C.; Chai, Y.; et al. Permeable Superelastic Liquid-Metal Fibre Mat Enables Biocompatible and Monolithic Stretchable Electronics. *Nat. Mater.* **2021**, *20*, 859–868.
- (225) Elsayes, A.; Sharma, V.; Yiannacou, K.; Koivikko, A.; Rasheed, A.; Sariola, V. Plant-Based Biodegradable Capacitive Tactile Pressure Sensor Using Flexible and Transparent Leaf Skeletons as Electrodes and Flower Petal as Dielectric Layer. *Adv. Sustain. Syst.* **2020**, *4*, 2000056.
- (226) Manvi, M.; Mruthyunjaya Swamy, K.B. Microelectronic Materials, Microfabrication Processes, Micromechanical Structural Configuration Based Stiffness Evaluation in Mems: A Review. *Microelectron. Eng.* **2022**, *263*, 111854.
- (227) Zhou, W. T.; Lin, R. Z.; Li, H. J.; Liu, R. Nano Foldaway Skin-Like E-Interface for Detecting Human Bioelectrical Signals. *ACS Appl. Mater. Interfaces* **2021**, *13*, 148–154.
- (228) Spanu, A.; Mascia, A.; Baldazzi, G.; Fenech-Salerno, B.; Torrisi, F.; Viola, G.; Bonfiglio, A.; Cosseddu, P.; Pani, D. Parylene C-Based, Breathable Tattoo Electrodes for High-Quality Bio-Potential Measurements. *Front Bioeng. Biotechnol.* **2022**, *10*, 820217.
- (229) He, J.; Xie, Z.; Yao, K.; Li, D.; Liu, Y.; Gao, Z.; Lu, W.; Chang, L.; Yu, X. Trampoline Inspired Stretchable Triboelectric Nanogenerators as Tactile Sensors for Epidermal Electronics. *Nano Energy* **2021**, *81*, 105590.
- (230) An, T.; Anaya, D. V.; Gong, S.; Yap, L. W.; Lin, F. E.; Wang, R.; Yuce, M. R.; Cheng, W. L. Self-Powered Gold Nanowire Tattoo Triboelectric Sensors for Soft Wearable Human-Machine Interface. *Nano Energy* **2020**, *77*, 105295.
- (231) Gong, S.; Yap, L. W.; Zhu, B. W.; Zhai, Q. F.; Liu, Y. Y.; Lyu, Q. X.; Wang, K. X.; Yang, M. J.; Ling, Y. Z.; Lai, D. T.; et al. Local Crack-Programmed Gold Nanowire Electronic Skin Tattoos for in-Plane Multisensor Integration. *Adv. Mater.* **2019**, *31*, 1903789.
- (232) Nyein, H. Y. Y.; Tai, L. C.; Ngo, Q. P.; Chao, M.; Zhang, G. B.; Gao, W.; Bariya, M.; Bullock, J.; Kim, H.; Fahad, H. M. A Wearable Microfluidic Sensing Patch for Dynamic Sweat Secretion Analysis. *ACS Sensors* **2018**, *3*, 944–952.
- (233) Martin, A.; Kim, J.; Kurniawan, J. F.; Sempionatto, J. R.; Moreto, J. R.; Tang, G. D.; Campbell, A. S.; Shin, A.; Lee, M. Y.; Liu, X.; et al. Epidermal Microfluidic Electrochemical Detection System: Enhanced Sweat Sampling and Metabolite Detection. *ACS Sensors* **2017**, *2*, 1860–1868.
- (234) Yang, S. X.; Chen, Y. C.; Nicolini, L.; Pasupathy, P.; Sacks, J.; Su, B.; Yang, R.; Sanchez, D.; Chang, Y. F.; Wang, P. L.; et al. Cut-and-Paste” Manufacture of Multiparametric Epidermal Sensor Systems. *Adv. Mater.* **2015**, *27*, 6423–6430.
- (235) Sun, T.; Hui, J. N.; Zhou, L.; Lin, B.; Sun, H. B.; Bai, Y. N.; Zhao, J. L.; Mao, H. J. A Low-Cost and Simple-Fabricated Epidermal Sweat Patch Based on “Cut-and-Paste” Manufacture. *Sens. Actuators B: Chemical* **2022**, *368*, 132184.
- (236) Ha, T.; Tran, J.; Liu, S. Y.; Jang, H.; Jeong, H.; Mitbender, R.; Huh, H.; Qiu, Y. T.; Duong, J.; Wang, R. L.; et al. A Chest-Laminated Ultra-thin and Stretchable E-Tattoo for the Measurement of Electrocardiogram, Seismocardiogram, and Cardiac Time Intervals. *Adv. Sci.* **2019**, *6*, 1900290.
- (237) Stier, A.; Halekote, E.; Mark, A.; Qiao, S. T.; Yang, S. X.; Diller, K.; Lu, N. S. Stretchable Tattoo-Like Heater with on-Site Temperature Feedback Control. *Micromachines* **2018**, *9*, 170.
- (238) Kireev, D.; Sel, K.; Ibrahim, B.; Kumar, N.; Akbari, A.; Jafari, R.; Akinwande, D. Continuous Cuffless Monitoring of Arterial Blood Pressure Via Graphene Bioimpedance Tattoos. *Nat. Nanotechnol.* **2022**, *17*, 864–870.
- (239) Unger, K.; Greco, F.; Coclite, A. M. Temporary Tattoo pH Sensor with pH-Responsive Hydrogel Via Initiated Chemical Vapor Deposition. *Adv. Mater. Technol.* **2022**, *7*, 2100717.
- (240) Zavanelli, N.; Yeo, W. H. Advances in Screen Printing of Conductive Nanomaterials for Stretchable Electronics. *ACS Omega* **2021**, *6*, 9344–9351.
- (241) Potts, S. J.; Phillips, C.; Jewell, E.; Clifford, B.; Lau, Y. C.; Claypole, T. High-Speed Imaging the Effect of Snap-Off Distance and Squeegee Speed on the Ink Transfer Mechanism of Screen-Printed Carbon Pastes. *J. Coatings Technol. Res.* **2020**, *17*, 447–459.
- (242) Kim, J.; Jeerapan, I.; Imani, S.; Cho, T. N.; Bandodkar, A.; Cinti, S.; Mercier, P. P.; Wang, J. Noninvasive Alcohol Monitoring Using a Wearable Tattoo-Based Iontophoretic-Biosensing System. *ACS Sensors* **2016**, *1*, 1011–1019.
- (243) Guinovart, T.; Bandodkar, A. J.; Windmiller, J. R.; Andrade, F. J.; Wang, J. A Potentiometric Tattoo Sensor for Monitoring Ammonium in Sweat. *Analyst* **2013**, *138*, 7031–7038.
- (244) De Guzman, K.; Al-Kharusi, G.; Levingstone, T.; Morrin, A. Robust Epidermal Tattoo Electrode Platform for Skin Physiology Monitoring. *Anal. Methods* **2019**, *11*, 1460–1468.
- (245) Zhao, C. S.; Zhou, Y. L.; Gu, S. Q.; Cao, S. T.; Wang, J. C.; Zhang, M. H.; Wu, Y. Z.; Kong, D. S. Fully Screen-Printed, Multicolor, and Stretchable Electroluminescent Displays for Epidermal Electronics. *ACS Appl. Mater. Interfaces* **2020**, *12*, 47902–47910.
- (246) Lemarchand, J.; Bridonneau, N.; Battaglini, N.; Carn, F.; Mattana, G.; Piro, B.; Zrig, S.; Noel, V. Challenges, Prospects, and Emerging Applications of Inkjet-Printed Electronics: A Chemist’s Point of View. *Angew. Chem., Int. Ed.* **2022**, *134*, e202200166.
- (247) Li, J.; Rossignol, F.; Macdonald, J. Inkjet Printing for Biosensor Fabrication: Combining Chemistry and Technology for Advanced Manufacturing. *Lab Chip* **2015**, *15*, 2538–2558.
- (248) Lohse, D. Fundamental Fluid Dynamics Challenges in Inkjet Printing. *Annu. Rev. Fluid Mech.* **2022**, *54*, 349–382.
- (249) Ferrari, L. M.; Sudha, S.; Tarantino, S.; Esposti, R.; Bolzoni, F.; Cavallari, P.; Cipriani, C.; Mattoli, V.; Greco, F. Ultraconformable Temporary Tattoo Electrodes for Electrophysiology. *Adv. Sci.* **2018**, *5*, 1700771.
- (250) Bihar, E.; Wustoni, S.; Pappa, A. M.; Salama, K. N.; Baran, D.; Inal, S. A Fully Inkjet-Printed Disposable Glucose Sensor on Paper. *npj Flex. Electron.* **2018**, *2*, 30.
- (251) Wang, S. Y.; Wu, X. L.; Lu, J. X.; Luo, Z. W.; Xie, H.; Zhang, X. B.; Lin, K. W.; Wang, Y. H. Inkjet-Printed Silver Nanowire Ink for Flexible Transparent Conductive Film Applications. *Nanomaterials* **2022**, *12*, 842.
- (252) Wawrzynek, E.; Baumbauer, C.; Arias, A. C. Characterization and Comparison of Biodegradable Printed Capacitive Humidity Sensors. *Sensors* **2021**, *21*, 6557.
- (253) Secor, E. B.; Prabhumirashi, P. L.; Puntambekar, K.; Geier, M. L.; Hersam, M. C. Inkjet Printing of High Conductivity, Flexible Graphene Patterns. *J. Phys. Chem. Lett.* **2013**, *4*, 1347–1351.

- (254) Gao, Y. H.; Shi, W.; Wang, W. C.; Leng, Y. P.; Zhao, Y. P. Inkjet Printing Patterns of Highly Conductive Pristine Graphene on Flexible Substrates. *Ind. Eng. Chem. Res.* **2014**, *53*, 16777–16784.
- (255) Wu, J. P.; Pang, H. M.; Ding, L.; Wang, Y.; He, X. K.; Shu, Q.; Xuan, S. H.; Gong, X. L. A Lightweight, Ultra-thin Aramid-Based Flexible Sensor Using a Combined Inkjet Printing and Buckling Strategy. *Chem. Eng. J.* **2021**, *421*, 129830.
- (256) Zhang, C.; McKeon, L.; Kremer, M. P.; Park, S. H.; Ronan, O.; Seral-Ascaso, A.; Barwich, S.; Coileáin, C. Ó.; McEvoy, N.; Nerl, H. C.; et al. Additive-Free Mxene Inks and Direct Printing of Micro-Supercapacitors. *Nat. Commun.* **2019**, *10*, 1795.
- (257) Gross, B. C.; Erkal, J. L.; Lockwood, S. Y.; Chen, C. P.; Spence, D. M. Evaluation of 3D Printing and Its Potential Impact on Biotechnology and the Chemical Sciences. *Anal. Chem.* **2014**, *86*, 3240–3253.
- (258) Zhu, Z.; Guo, S. Z.; Hirdler, T.; Eide, C.; Fan, X.; Tolar, J.; McAlpine, M. C. 3D Printed Functional and Biological Materials on Moving Freeform Surfaces. *Adv. Mater.* **2018**, *30*, 1707495.
- (259) Shi, G.; Lowe, S. E.; Teo, A. J.; Dinh, T. K.; Tan, S. H.; Qin, J.; Zhang, Y. B.; Zhong, Y. L.; Zhao, H. J. A Versatile PDMS Submicrobead/Graphene Oxide Nanocomposite Ink for the Direct Ink Writing of Wearable Micron-Scale Tactile Sensors. *Appl. Mater. Today* **2019**, *16*, 482–492.
- (260) Herren, B.; Saha, M. C.; Altan, M. C.; Liu, Y. Development of Ulstretchable and Skin Attachable Nanocomposites for Human Motion Monitoring Via Embedded 3D Printing. *Compos. B. Eng.* **2020**, *200*, 108224.
- (261) Wan, C.; Wu, Z.; Ren, M.; Tang, M.; Gao, Y.; Shang, X.; Li, T.; Xia, Z.; Yang, Z.; Mao, S.; et al. In Situ Formation of Conductive Epidermal Electrodes Using a Fully Integrated Flexible System and Injectable Photocurable Ink. *ACS Nano* **2023**, *17*, 10689–10700.
- (262) Secor, E. B. Principles of Aerosol Jet Printing. *Flex. Print. Electron.* **2018**, *3*, No. 035002.
- (263) Tonello, S.; Fapanni, T.; Bonaldo, S.; Giorgi, G.; Narduzzi, C.; Paccagnella, A.; Serpelloni, M.; Sardini, E.; Carrara, S. Amperometric Measurements by a Novel Aerosol Jet Printed Flexible Sensor for Wearable Applications. *IEEE Trans. Instrum. Meas.* **2023**, *72*, 7500512.
- (264) Parate, K.; Pola, C. C.; Rangnekar, S. V.; Mendivelso-Perez, D. L.; Smith, E. A.; Hersam, M. C.; Gomes, C. L.; Claussen, J. C. Aerosol-Jet-Printed Graphene Electrochemical Histamine Sensors for Food Safety Monitoring. *2D Materials* **2020**, *7*, No. 034002.
- (265) Patel, S.; Ershad, F.; Lee, J.; Chacon-Alberly, L.; Wang, Y.; Morales-Garza, M. A.; Haces-Garcia, A.; Jang, S.; Gonzalez, L.; Contreras, L.; et al. Drawn-on-Skin Sensors from Fully Biocompatible Inks toward High-Quality Electrophysiology. *Small* **2022**, *18*, 2107099.
- (266) Ershad, F.; Houston, M.; Patel, S.; Contreras, L.; Koirala, B.; Lu, Y.; Rao, Z.; Liu, Y.; Dias, N.; Haces-Garcia, A.; et al. Customizable, Reconfigurable, and Anatomically Coordinated Large-Area, High-Density Electromyography from Drawn-on-Skin Electrode Arrays. *PNAS Nexus* **2023**, *2*, pgac291.
- (267) Guo, R.; Sun, X. Y.; Yao, S. Y.; Duan, M. H.; Wang, H. Z.; Liu, J.; Deng, Z. S. Semi-Liquid-Metal-(Ni-Egain)-Based Ultraconformable Electronic Tattoo. *Adv. Mater. Technol.* **2019**, *4*, 1900183.
- (268) Luo, J.; Sun, C.; Chang, B.; Jing, Y.; Li, K.; Li, Y.; Zhang, Q.; Wang, H.; Hou, C. Mxene-Enabled Self-Adaptive Hydrogel Interface for Active Electroencephalogram Interactions. *ACS Nano* **2022**, *16*, 19373–19384.
- (269) Wang, C. Y.; Wang, H. Y.; Wang, B. H.; Miyata, H.; Wang, Y.; Nayeem, M. O. G.; Kim, J. J.; Lee, S.; Yokota, T.; Onodera, H.; et al. On-Skin Paintable Biogel for Long-Term High-Fidelity Electroencephalogram Recording. *Sci. Adv.* **2022**, *8*, eabd1396.
- (270) Huang, X. X.; Chen, C. W.; Ma, X. H.; Zhu, T. S.; Ma, W. C.; Jin, Q.; Du, R. C.; Cai, Y. F.; Zhang, M. H.; Kong, D. S.; et al. In Situ Forming Dual-Conductive Hydrogels Enable Conformal, Self-Adhesive and Antibacterial Epidermal Electrodes. *Adv. Funct. Mater.* **2023**, *33*, 2302846.
- (271) Hsieh, J. C.; He, W. L.; Venkatraghavan, D.; Koptelova, V. B.; Ahmad, Z. J.; Pyatnitskiy, I.; Wang, W. L.; Jeong, J.; Tang, K. K. W.; Harmer, C.; et al. Design of an Injectable, Self-Adhesive, and Highly Stable Hydrogel Electrode for Sleep Recording. *Device* **2023**, *1*, 100182.
- (272) Stanford, M. J.; Zhang, C.; Fowlkes, J. D.; Hoffman, A.; Ivanov, I. N.; Rack, P. D.; Tour, J. M. High-Resolution Laser-Induced Graphene. Flexible Electronics beyond the Visible Limit. *ACS Appl. Mater. & Interfaces* **2020**, *12*, 10902–10907.
- (273) Chyan, Y.; Ye, R. Q.; Li, Y.; Singh, S. P.; Arnusch, C. J.; Tour, J. M. Laser-Induced Graphene by Multiple Lasing: Toward Electronics on Cloth, Paper, and Food. *ACS Nano* **2018**, *12*, 2176–2183.
- (274) Yang, Y. R.; Song, Y.; Bo, X. J.; Min, J. H.; Pak, O. S.; Zhu, L. L.; Wang, M. Q.; Tu, J. B.; Kogan, A.; Zhang, H. X. A Laser-Engraved Wearable Sensor for Sensitive Detection of Uric Acid and Tyrosine in Sweat. *Nat. Biotechnol.* **2020**, *38*, 217–224.
- (275) Nair, V.; Yi, J.; Isheim, D.; Rotenberg, M.; Meng, L. Y.; Shi, F. Y.; Chen, X. Q.; Gao, X.; Prominski, A.; Jiang, Y. W.; et al. Laser Writing of Nitrogen-Doped Silicon Carbide for Biological Modulation. *Sci. Adv.* **2020**, *6*, eaaz2743.
- (276) Gao, Y.; Li, Q.; Wu, R.; Sha, J.; Lu, Y.; Xuan, F. Laser Direct Writing of Ultrahigh Sensitive SiC-Based Strain Sensor Arrays on Elastomer toward Electronic Skins. *Adv. Funct. Mater.* **2019**, *29*, 1806786.
- (277) Zhao, G. G.; Ling, Y.; Su, Y. J.; Chen, Z. Y.; Mathai, C. J.; Emeje, O.; Brown, A.; Alla, D. R.; Huang, J.; Kim, C. S.; et al. Laser-Scribed Conductive, Photoactive Transition Metal Oxide on Soft Elastomers for Janus on-Skin Electronics and Soft Actuators. *Sci. Adv.* **2022**, *8*, eabp9734.
- (278) Das, R.; Zeng, W.; Asci, C.; Del-Rio-Ruiz, R.; Sonkusale, S. Recent Progress in Electrospun Nanomaterials for Wearables. *APL Bioeng.* **2022**, *6*, No. 021505.
- (279) Garkal, A.; Kulkarni, D.; Musale, S.; Mehta, T.; Giram, P. Electrospinning Nanofiber Technology: A Multifaceted Paradigm in Biomedical Applications. *New J. Chem.* **2021**, *45*, 21508–21533.
- (280) Sun, B.; Long, Y. Z.; Zhang, H. D.; Li, M. M.; Duvail, J.; Jiang, X. Y.; Yin, H. L. Advances in Three-Dimensional Nanofibrous Macrostructures Via Electrospinning. *Prog. Polym. Sci.* **2014**, *39*, 862–890.
- (281) Taylor, G. I. Electrically Driven Jets. *Proceedings of the Royal Society of London. A. Mathematical and Physical Sciences* **1969**, *313*, 453–475.
- (282) Park, S. H.; Lee, H. B.; Yeon, S. M.; Park, J.; Lee, N. K. Flexible and Stretchable Piezoelectric Sensor with Thickness-Tunable Configuration of Electrospun Nanofiber Mat and Elastomeric Substrates. *ACS Appl. Mater. Interfaces* **2016**, *8*, 24773–24781.
- (283) Xu, Q.; Liu, H. J.; Zhong, X. R.; Jiang, B. F.; Ma, Z. J. Permeable Weldable Elastic Fiber Conductors for Wearable Electronics. *ACS Appl. Mater. Interfaces* **2020**, *12*, 36609–36619.
- (284) Sharifuzzaman, M.; Zahed, M. A.; Sharma, S.; Rana, S. S.; Chhetry, A.; Shin, Y. D.; Asaduzzaman, M.; Zhang, S.; Yoon, S.; Hui, X.; et al. β -Phase-Rich Laser-Induced Hierarchically Interactive Mxene Reinforced Carbon Nanofibers for Multifunctional Breathable Bioelectronics. *Adv. Funct. Mater.* **2022**, *32*, 2107969.
- (285) Huang, Z. L.; Lin, Y. Transfer Printing Technologies for Soft Electronics. *Nanoscale* **2022**, *14*, 16749–16760.
- (286) Tians, L. M.; Zimmerman, B.; Akhtar, A.; Yu, K. J.; Moore, M.; Wu, J.; Larsen, R. J.; Lee, J. W.; Li, J. H.; Liu, Y. H.; et al. Large-Area MRI-Compatible Epidermal Electronic Interfaces for Prosthetic Control and Cognitive Monitoring. *Nat. Biomed. Eng.* **2019**, *3*, 194–205.
- (287) Wang, Y. H.; Yin, L.; Bai, Y. Z.; Liu, S. Y.; Wang, L.; Zhou, Y.; Hou, C.; Yang, Z. Y.; Wu, H.; Ma, J. J.; et al. Electrically Compensated, Tattoo-Like Electrodes for Epidermal Electrophysiology at Scale. *Sci. Adv.* **2020**, *6*, eabd0996.
- (288) Taccola, S.; Poliziani, A.; Santonocito, D.; Mondini, A.; Denk, C.; Ide, A. N.; Oberparleiter, M.; Greco, F.; Mattoli, V. Toward the Use of Temporary Tattoo Electrodes for Impedancemetric Respiration Monitoring and Other Electrophysiological Recordings on Skin. *Sensors* **2021**, *21*, 1197.
- (289) Ferrari, L. M.; Keller, K.; Burtscher, B.; Greco, F. Temporary Tattoo as Unconventional Substrate for Conformable and Transferable

- Electronics on Skin and Beyond. *Multifunct. Mater.* **2020**, *3*, No. 032003.
- (290) Hwang, W.; Kim, J.; Park, S.; Kang, T. H.; Kim, S.; Lee, K.; Lee, M. G.; Kwak, R.; Choi, I. S.; Yi, H. A Breathable and Stretchable Metastructure for a Versatile Hybrid Electronic Skin Patch with Long-Term Skin Comfort. *Adv. Mater. Technol.* **2023**, *8*, 2200477.
- (291) Chung, M.; Skinner, W. H.; Robert, C.; Campbell, C. J.; Rossi, R. M.; Koutsos, V.; Radacsi, N. Fabrication of a Wearable Flexible Sweat pH Sensor Based on SERS-Active Au/TPU Electrospun Nanofibers. *ACS Appl. Mater. Interfaces* **2021**, *13*, 51504–51518.
- (292) Zhuang, M. Q.; Yin, L.; Wang, Y. H.; Bai, Y. Z.; Zhan, J.; Hou, C.; Yin, L. T.; Xu, Z. Y.; Tan, X. H.; Huang, Y. A. Highly Robust and Wearable Facial Expression Recognition Via Deep-Learning-Assisted, Soft Epidermal Electronics. *Research* **2021**, *2021*, 9759601.
- (293) Qiu, J. K.; Yu, T. H.; Zhang, W. F.; Zhao, Z. H.; Zhang, Y.; Ye, G.; Zhao, Y.; Du, X. J.; Liu, X.; Yang, L.; et al. A Bioinspired, Durable, and Nondisposable Transparent Graphene Skin Electrode for Electrophysiological Signal Detection. *ACS Mater. Lett.* **2020**, *2*, 999–1007.
- (294) Zhang, L.; Kumar, K. S.; He, H.; Cai, C. J.; He, X.; Gao, H. X.; Yue, S. Z.; Li, C. S.; Seet, R. C. S.; Ren, H.; et al. Fully Organic Compliant Dry Electrodes Self-Adhesive to Skin for Long-Term Motion-Robust Epidermal Biopotential Monitoring. *Nat. Commun.* **2020**, *11*, 4683.
- (295) Liu, Y.; Cheng, Y.; Shi, L. J.; Wang, R. R.; Sun, J. Breathable, Self-Adhesive Dry Electrodes for Stable Electrophysiological Signal Monitoring During Exercise. *ACS Appl. Mater. Interfaces* **2022**, *14*, 12812–12823.
- (296) Fang, Y. S.; Li, Y. Q.; Wang, X.; Zhou, Z. R.; Zhang, K.; Zhou, J.; Hu, B. Cryo-Transferred Ultra-thin and Stretchable Epidermal Electrodes. *Small* **2020**, *16*, 2000450.
- (297) Fang, Y. S.; Li, Y. Q.; Li, Y.; Ding, M. N.; Xie, J. J.; Hu, B. Solution-Processed Submicron Free-Standing, Conformal, Transparent, Breathable Epidermal Electrodes. *ACS Appl. Mater. Interfaces* **2020**, *12*, 23689–23696.
- (298) Castagnola, E.; Ansaldo, A.; Maggolini, E.; Ius, T.; Skrap, M.; Ricci, D.; Fadiga, L. Smaller, Softer, Lower-Impedance Electrodes for Human Neuroprosthesis: A Pragmatic Approach. *Front. Neuroeng.* **2014**, *7*, 8.
- (299) Choi, S.; Lee, H.; Ghaffari, R.; Hyeon, T.; Kim, D. H. Recent Advances in Flexible and Stretchable Bio-Electronic Devices Integrated with Nanomaterials. *Adv. Mater.* **2016**, *28*, 4203–4218.
- (300) Wu, W.; Haick, H. Materials and Wearable Devices for Autonomous Monitoring of Physiological Markers. *Adv. Mater.* **2018**, *30*, 1705024.
- (301) Goyal, K.; Borkholder, D. A.; Day, S. W. Dependence of Skin-Electrode Contact Impedance on Material and Skin Hydration. *Sensors* **2022**, *22*, 8510.
- (302) Khan, Y.; Pavinatto, F. J.; Lin, M. C.; Liao, A.; Swisher, S. L.; Mann, K.; Subramanian, V.; Maharbiz, M. M.; Arias, A. C. Inkjet-Printed Flexible Gold Electrode Arrays for Bioelectronic Interfaces. *Adv. Funct. Mater.* **2016**, *26*, 1004–1013.
- (303) Norton, J. J.; Lee, D. S.; Lee, J. W.; Lee, W.; Kwon, O.; Won, P.; Jung, S. Y.; Cheng, H.; Jeong, J. W.; Akce, A.; et al. Soft, curved electrode systems capable of integration on the auricle as a persistent brain-computer interface. *Proc. Natl. Acad. Sci. U. S. A.* **2015**, *112*, 3920–3925.
- (304) Niu, H. R.; Li, M.; Yang, L. N.; Xu, B. C.; Li, M. Y.; Wang, H. F.; Guo, Q. Q.; Meng, Z. S.; Liu, Y. J.; Chen, D. Low-Cost, Large-Area, Multifunctional Stretchable E-Tattoos Inspired by Dough Figurines for Wearable Human-Machine Interfaces. *Adv. Mater. Technol.* **2022**, *7*, 2100907.
- (305) Liu, H.; Dong, W.; Li, Y.; Li, F.; Geng, J.; Zhu, M.; Chen, T.; Zhang, H.; Sun, L.; Lee, C. An Epidermal s-EMG Tattoo-like Patch as a New Human-Machine Interface for Patients with Loss of Voice. *Microsyst. Nanoeng.* **2020**, *6*, 16.
- (306) Gao, N.; Yu, J. R.; Tian, Q. Y.; Shi, J. F.; Zhang, M.; Chen, S.; Zang, L. Application of PEDOT:PSS and Its Composites in Electrochemical and Electronic Chemosensors. *Chemosensors* **2021**, *9*, 79.
- (307) Tan, P.; Wang, H. F.; Xiao, F. R.; Lu, X.; Shang, W. H.; Deng, X. B.; Song, H. F.; Xu, Z.; Yao, C.; Cao, J. F.; et al. Solution-processible, Soft, Self-adhesive, and Conductive Polymer Composites for Soft Electronics. *Nat. Commun.* **2022**, *13*, 358.
- (308) Fan, X.; Nie, W. Y.; Tsai, H.; Wang, N. X.; Huang, H. H.; Cheng, Y. J.; Wen, R. J.; Ma, L. J.; Yan, F.; Xia, Y. G. PEDOT:PSS for Flexible and Stretchable Electronics: Modifications, Strategies, and Applications. *Adv. Sci.* **2019**, *6*, 1900813.
- (309) Ferrari, L. M.; Ismailov, U.; Badier, J. M.; Greco, F.; Ismailova, E. Conducting polymer tattoo electrodes in clinical electro- and magneto-encephalography. *npj Flexible Electronics* **2020**, *4*, 4.
- (310) Bareket, L.; Inzelberg, L.; Rand, D.; David-Pur, M.; Rabinovich, D.; Brandes, B.; Hanein, Y. Temporary-Tattoo for Long-Term High Fidelity Biopotential Recordings. *Sci. Rep.* **2016**, *6*, 25727.
- (311) Du, X. J.; Jiang, W. C.; Zhang, Y.; Qiu, J. K.; Zhao, Y.; Tan, Q. S.; Qi, S. Y.; Ye, G.; Zhang, W. F.; Liu, N. Transparent and Stretchable Graphene Electrode by Intercalation Doping for Epidermal Electrophysiology. *ACS Appl. Mater. Interfaces* **2020**, *12*, 56361–56371.
- (312) Zhao, Y.; Zhang, S.; Yu, T. H.; Zhang, Y.; Ye, G.; Cui, H.; He, C. Z.; Jiang, W. C.; Zhai, Y.; Lu, C. M.; et al. Ultra-Conformal Skin Electrodes with Synergistically Enhanced Conductivity for Long-Time and Low-Motion Artifact Epidermal Electrophysiology. *Nat. Commun.* **2021**, *12*, 4880.
- (313) Lee, S. M.; Byeon, H. J.; Lee, J. H.; Baek, D. H.; Lee, K. H.; Hong, J. S.; Lee, S. H. Self-Adhesive Epidermal Carbon Nanotube Electronics for Tether-Free Long-Term Continuous Recording of Biosignals. *Sci. Rep.* **2014**, *4*, 6074.
- (314) Jeong, J. W.; Kim, M. K.; Cheng, H.; Yeo, W. H.; Huang, X.; Liu, Y.; Zhang, Y.; Huang, Y.; Rogers, J. A. Capacitive Epidermal Electronics for Electrically Safe, Long-Term Electrophysiological Measurements. *Adv. Healthc. Mater.* **2014**, *3*, 642–648.
- (315) Webster, J. G. Reducing Motion Artifacts and Interference in Biopotential Recording. *IEEE Trans. Biomed. Eng.* **1984**, *BME-31*, 823–826.
- (316) Anderer, P.; Roberts, S.; Schlogl, A.; Gruber, G.; Klosch, G.; Herrmann, W.; Rappelsberger, P.; Filz, O.; Barbanoj, M. J.; Dorffner, G.; et al. Artifact Processing in Computerized Analysis of Sleep EEG - a Review. *Neuropsychobiology* **1999**, *40*, 150–157.
- (317) Bhattacharya, S.; Nikbakht, M.; Alden, A.; Tan, P.; Wang, J.; Alhalimi, T. A.; Kim, S.; Wang, P.; Tanaka, H.; Tandon, A.; et al. A Chest-Conformable, Wireless Electro-Mechanical E-Tattoo for Measuring Multiple Cardiac Time Intervals. *Adv. Electron. Mater.* **2023**, *9*, 2201284.
- (318) Namkoong, M.; Guo, H.; Rahman, M. S.; Wang, D.; Pfeil, C. J.; Hager, S.; Tian, L. Moldable and Transferrable Conductive Nanocomposites for Epidermal Electronics. *Npj Flex Electron* **2022**, *6*, 41.
- (319) Han, L.; Lu, X.; Wang, M. H.; Gan, D. L.; Deng, W. L.; Wang, K. F.; Fang, L. M.; Liu, K. Z.; Chan, C. W.; Tang, Y. H.; et al. A Mussel-Inspired Conductive, Self-Adhesive, and Self-Healable Tough Hydrogel as Cell Stimulators and Implantable Bioelectronics. *Small* **2017**, *13*, 1601916.
- (320) Kumar, P. Ultra-thin 2D Nanomaterials for Electromagnetic Interference Shielding. *Adv. Mater. Interfaces* **2019**, *6*, 1901454.
- (321) Iqbal, A.; Sambyal, P.; Koo, C. M. 2D Mxenes for Electromagnetic Shielding: A Review. *Adv. Funct. Mater.* **2020**, *30*, 2000883.
- (322) Liang, C. B.; Gu, Z. J.; Zhang, Y. L.; Ma, Z. L.; Qiu, H.; Gu, J. W. Structural Design Strategies of Polymer Matrix Composites for Electromagnetic Interference Shielding: A Review. *Nanomicro. Lett.* **2021**, *13*, 181.
- (323) Sun, B.; McCay, R. N.; Goswami, S.; Xu, Y.; Zhang, C.; Ling, Y.; Lin, J.; Yan, Z. Gas-Permeable, Multifunctional on-Skin Electronics Based on Laser-Induced Porous Graphene and Sugar-Templated Elastomer Sponges. *Adv. Mater.* **2018**, *30*, 1804327.
- (324) Chen, Y.; Zhou, G.; Yuan, X.; Li, C.; Liu, L.; You, H. Substrate-Free, Ultra-Conformable PEDOT:PSS E-Tattoo Achieved by Energy Regulation on Skin. *Biosens. Bioelectron.* **2022**, *206*, 114118.
- (325) Chung, H. U.; Kim, B. H.; Lee, J. Y.; Lee, J.; Xie, Z.; Ibler, E. M.; Lee, K.; Banks, A.; Jeong, J. Y.; Kim, J.; et al. Binodal, Wireless

Epidermal Electronic Systems with in-Sensor Analytics for Neonatal Intensive Care. *Science* **2019**, *363*, eaau0780.

(326) Song, D. K.; Ye, G.; Zhao, Y.; Zhang, Y.; Hou, X. C.; Liu, N. An All-in-One, Bioderived, Air-Permeable, and Sweat-Stable Mxene Epidermal Electrode for Muscle Theranostics. *ACS Nano* **2022**, *16*, 17168–17178.

(327) Zhang, Y. J.; Tao, T. H. Skin-Friendly Electronics for Acquiring Human Physiological Signatures. *Adv. Mater.* **2019**, *31*, 1905767.

(328) Teplan, M. Fundamentals of EEG Measurement. *Meas. Sci. Rev.* **2002**, *2*, 1–11.

(329) Shin, J. H.; Kwon, J.; Kim, J. U.; Ryu, H.; Ok, J.; Kwon, S. J.; Park, H.; Kim, T. I. Wearable EEG Electronics for a Brain-AI Closed-Loop System to Enhance Autonomous Machine Decision-Making. *npj Flex. Electron.* **2022**, *6*, 32.

(330) Kusche, R.; Klimach, P.; Ryschka, M. A Multichannel Real-Time Bioimpedance Measurement Device for Pulse Wave Analysis. *IEEE Trans. Biomed. Circuits Syst.* **2018**, *12*, 614–622.

(331) Tang, X. C.; Jankovic, M.; Jafari, R. A Non-Invasive Radial Arterial Compliance Measuring Method Using Bio-Impedance. *Annu. Int. Conf. IEEE Eng. Med. Biol. Soc.* **2021**, 2330–2334.

(332) Cho, M. C.; Kim, J. Y.; Cho, S. A Bio-Impedance Measurement System for Portable Monitoring of Heart Rate and Pulse Wave Velocity Using Small Body Area. *IEEE Int. Symp. Circ. S* **2009**, *2009*, 3106–3109.

(333) Sel, K.; Osman, D.; Jafari, R. Non-Invasive Cardiac and Respiratory Activity Assessment from Various Human Body Locations Using Bioimpedance. *IEEE Open J. Eng. Med. Biol.* **2021**, *2*, 210–217.

(334) Grimnes, S.; Martinsen, O. G. *Bioimpedance and Bioelectricity Basics*, 2nd ed.; Academic Press, 2008; pp 1–471.

(335) Ibrahim, B.; Jafari, R. Cuffless Blood Pressure Monitoring from an Array of Wrist Bio-Impedance Sensors Using Subject-Specific Regression Models: Proof of Concept. *IEEE Trans. Biomed. Circuits Syst.* **2019**, *13*, 1723–1735.

(336) Ibrahim, B.; Jafari, R. Cuffless Blood Pressure Monitoring from a Wristband with Calibration-Free Algorithms for Sensing Location Based on Bio-Impedance Sensor Array and Autoencoder. *Sci. Rep.* **2022**, *12*, 319.

(337) Sel, K.; Osman, D.; Huerta, N.; Edgar, A.; Pettigrew, R. I.; Jafari, R. Continuous Cuffless Blood Pressure Monitoring with a Wearable Ring Bioimpedance Device. *npj Digit. Med.* **2023**, *6*, 59.

(338) Osman, D.; Jankovic, M.; Sel, K.; Pettigrew, R. I.; Jafari, R. Blood Pressure Estimation Using a Single Channel Bio-Impedance Ring Sensor. *Annu. Int. Conf. IEEE Eng. Med. Biol. Soc.* **2022**, 4286–4290.

(339) Levit, B.; Krebsbach, P.; Bar-Haim, C.; Hernandez-Sosa, G.; Hanein, Y. Printed Soft Skin Electrodes for Seamless Bio-Impedance Measurements. *Flex. Print. Electron.* **2023**, *8*, No. 015020.

(340) Sel, K.; Brown, A.; Jang, H.; Krumholz, H. M.; Lu, N.; Jafari, R. A Wrist-Worn Respiration Monitoring Device Using Bio-Impedance. *Annu. Int. Conf. IEEE Eng. Med. Biol. Soc.* **2020**, 3989–3993.

(341) Widlund, T.; Yang, S. X.; Hsu, Y. Y.; Lu, N. S. Stretchability and Compliance of Freestanding Serpentine-Shaped Ribbons. *Int. J. Solids Struct.* **2014**, *51*, 4026–4037.

(342) Huang, X.; Cheng, H.; Chen, K.; Zhang, Y.; Zhang, Y.; Liu, Y.; Zhu, C.; Ouyang, S.; Kong, G. W.; Yu, C.; Huang, Y.; Rogers, J. A.; et al. Epidermal Impedance Sensing Sheets for Precision Hydration Assessment and Spatial Mapping. *IEEE Trans. Biomed. Eng.* **2013**, *60*, 2848–2857.

(343) Chortos, A.; Liu, J.; Bao, Z. N. Pursuing Prosthetic Electronic Skin. *Nat. Mater.* **2016**, *15*, 937–950.

(344) Nie, P.; Wang, R. R.; Xu, X. J.; Cheng, Y.; Wang, X.; Shi, L. J.; Sun, J. High-Performance Piezoresistive Electronic Skin with Bionic Hierarchical Microstructure and Microcracks. *ACS Appl. Mater. Interfaces* **2017**, *9*, 14911–14919.

(345) Yan, C. Y.; Wang, J. X.; Kang, W. B.; Cui, M. Q.; Wang, X.; Foo, C. Y.; Chee, K. J.; Lee, P. S. Highly Stretchable Piezoresistive Graphene-Nanocellulose Nanopaper for Strain Sensors. *Adv. Mater.* **2014**, *26*, 2022–2027.

(346) Wang, Y.; Lee, S.; Yokota, T.; Wang, H.; Jiang, Z.; Wang, J. B.; Koizumi, M.; Someya, T. A Durable Nanomesh on-Skin Strain Gauge for Natural Skin Motion Monitoring with Minimum Mechanical Constraints. *Sci. Adv.* **2020**, *6*, eabb7043.

(347) Gong, S.; Lai, D. T.; Wang, Y.; Yap, L. W.; Si, K. J.; Shi, Q.; Jason, N. N.; Sridhar, T.; Uddin, H.; Cheng, W. Tattolike Polyaniline Microparticle-Doped Gold Nanowire Patches as Highly Durable Wearable Sensors. *ACS Appl. Mater. Interfaces* **2015**, *7*, 19700–19708.

(348) Sun, Z.; Yang, S.; Zhao, P.; Zhang, J.; Yang, Y.; Ye, X.; Zhao, X.; Cui, N.; Tong, Y.; Liu, Y.; et al. Skin-Like Ultrasensitive Strain Sensor for Full-Range Detection of Human Health Monitoring. *ACS Appl. Mater. Interfaces* **2020**, *12*, 13287–13295.

(349) Kim, T.; Shin, Y.; Kang, K.; Kim, K.; Kim, G.; Byeon, Y.; Kim, H.; Gao, Y.; Lee, J. R.; Son, G.; et al. Ultrathin Crystalline-Silicon-Based Strain Gauges with Deep Learning Algorithms for Silent Speech Interfaces. *Nat. Commun.* **2022**, *13*, 5815.

(350) Qiu, A.; Li, P.; Yang, Z.; Yao, Y.; Lee, I.; Ma, J. A Path Beyond Metal and Silicon: Polymer/Nanomaterial Composites for Stretchable Strain Sensors. *Adv. Funct. Mater.* **2019**, *29*, 1806306.

(351) Dong, T.; Sun, Y.; Zhu, Z.; Wu, X.; Wang, J.; Shi, Y.; Xu, J.; Chen, K.; Yu, L. Monolithic Integration of Silicon Nanowire Networks as a Soft Wafer for Highly Stretchable and Transparent Electronics. *Nano Lett.* **2019**, *19*, 6235–6243.

(352) Huang, S.; Zhang, B.; Shao, Z.; He, L.; Zhang, Q.; Jie, J.; Zhang, X. Ultraminiaturized Stretchable Strain Sensors Based on Single Silicon Nanowires for Imperceptible Electronic Skins. *Nano Lett.* **2020**, *20*, 2478–2485.

(353) Wang, B.; Wu, K.; Hjort, K.; Guo, C. F.; Wu, Z. G. High-Performance Liquid Alloy Patterning of Epidermal Strain Sensors for Local Fine Skin Movement Monitoring. *Soft Robot.* **2019**, *6*, 414–421.

(354) Wang, X.; Liu, X. H.; Schubert, D. W. Highly Sensitive Ultrathin Flexible Thermoplastic Polyurethane/Carbon Black Fibrous Film Strain Sensor with Adjustable Scaffold Networks. *Nanomicro. Lett.* **2021**, *13*, 64.

(355) Cai, L.; Song, L.; Luan, P. S.; Zhang, Q.; Zhang, N.; Gao, Q. Q.; Zhao, D.; Zhang, X.; Tu, M.; Yang, F.; et al. Super-Stretchable, Transparent Carbon Nanotube-Based Capacitive Strain Sensors for Human Motion Detection. *Sci. Rep.* **2013**, *3*, 3048.

(356) Cheng, Y.; Zhou, Y.; Wang, R.; Chan, K. H.; Liu, Y.; Ding, T.; Wang, X.-Q.; Li, T.; Ho, G. W. An Elastic and Damage-Tolerant Dry Epidermal Patch with Robust Skin Adhesion for Bioelectronic Interfacing. *ACS Nano* **2022**, *16*, 18608–18620.

(357) Wei, Y. H.; Qiao, Y. C.; Jiang, G. Y.; Wang, Y. F.; Wang, F. W.; Li, M. R.; Zhao, Y. F.; Tian, Y.; Gou, G. Y.; Tan, S. Y.; et al. A Wearable Skinlike Ultra-Sensitive Artificial Graphene Throat. *ACS Nano* **2019**, *13*, 8639–8647.

(358) Yamada, T.; Hayamizu, Y.; Yamamoto, Y.; Yomogida, Y.; Izadi-Najafabadi, A.; Futaba, D. N.; Hata, K. A Stretchable Carbon Nanotube Strain Sensor for Human-Motion Detection. *Nat. Nanotechnol.* **2011**, *6*, 296–301.

(359) Kim, H. J.; Thukral, A.; Yu, C. J. Highly Sensitive and Very Stretchable Strain Sensor Based on a Rubbery Semiconductor. *ACS Appl. Mater. Interfaces* **2018**, *10*, 5000–5006.

(360) Liu, S. Q.; Zhang, R. M.; Chen, S.; Wu, Y. H.; Liu, H. Z.; Wang, P. P.; Deng, Z. F.; Liu, L. A Compliant, Self-Adhesive and Self-Healing Wearable Hydrogel as Epidermal Strain Sensor. *J. Mater. Chem. C* **2018**, *6*, 4183–4190.

(361) Wang, Z. Y.; Xu, X. R.; Xu, Y. T.; Lin, W. E.; Peng, Z. C. A Ternary Heterogeneous Hydrogel with Strength Elements for Resilient, Self-Healing, and Recyclable Epidermal Electronics. *npj Flex. Electron.* **2022**, *6*, 51.

(362) Zhang, Q.; Wang, Q.; Wang, G.; Zhang, Z.; Xia, S.; Gao, G. Ultrathin and Highly Tough Hydrogel Films for Multifunctional Strain Sensors. *ACS Appl. Mater. Interfaces* **2021**, *13*, 50411–50421.

(363) Luo, N. Q.; Dai, W. X.; Li, C. L.; Zhou, Z. Q.; Lu, L. Y.; Poon, C. C. Y.; Chen, S. C.; Zhang, Y. T.; Zhao, N. Flexible Piezoresistive Sensor Patch Enabling Ultralow Power Cuffless Blood Pressure Measurement. *Adv. Funct. Mater.* **2016**, *26*, 1178–1187.

- (364) Xu, H. C.; Gao, L. B.; Wang, Y. J.; Cao, K.; Hu, X. K.; Wang, L.; Mu, M.; Liu, M.; Zhang, H. Y.; Wang, W. D.; et al. Flexible Waterproof Piezoresistive Pressure Sensors with Wide Linear Working Range Based on Conductive Fabrics. *Nanomicro Lett.* **2020**, *12*, 159.
- (365) Zhao, C. D.; Fang, Y. Q.; Chen, H.; Zhang, S. N.; Wan, Y. J.; Riaz, M. S.; Zhang, Z.; Dong, W. J.; Diao, L.; Ren, D. Y.; et al. Ultra-thin Mo₂S₃ Nanowire Network for High-Sensitivity Breathable Piezoresistive Electronic Skins. *ACS Nano* **2023**, *17*, 4862–4870.
- (366) Kim, H.; Choi, S.; Lee, B.; Seo, J.; Lee, S.; Yoon, J.; Hong, Y. Nonpatterned Soft Piezoresistive Films with Filamentous Conduction Paths for Mimicking Multiple-Resolution Receptors of Human Skin. *ACS Appl. Mater. Interfaces* **2022**, *14*, 55088–55097.
- (367) Luo, Z. B.; Chen, J.; Zhu, Z. F.; Li, L.; Su, Y.; Tang, W.; Omisore, O. M.; Wang, L.; Li, H. High-Resolution and High-Sensitivity Flexible Capacitive Pressure Sensors Enhanced by a Transferable Electrode Array and a Micropillar-PVDF Film. *ACS Appl. Mater. Interfaces* **2021**, *13*, 7635–7649.
- (368) Lin, L.; Dautta, M.; Hajiaghajani, A.; Escobar, A. R.; Tseng, P.; Khine, M. Paint-on Epidermal Electronics for on-Demand Sensors and Circuits. *Adv. Electron. Mater.* **2021**, *7*, 2000765.
- (369) Yang, J.; Luo, S.; Zhou, X.; Li, J. L.; Fu, J. T.; Yang, W. D.; Wei, D. P. Flexible, Tunable, and Ultrasensitive Capacitive Pressure Sensor with Microconformal Graphene Electrodes. *ACS Appl. Mater. Interfaces* **2019**, *11*, 14997–15006.
- (370) Kang, M.; Kim, J.; Jang, B.; Chae, Y.; Kim, J. H.; Ahn, J. H. Graphene-Based Three-Dimensional Capacitive Touch Sensor for Wearable Electronics. *ACS Nano* **2017**, *11*, 7950–7957.
- (371) Yu, P. T.; Li, X.; Li, H. Y.; Fan, Y. J.; Cao, J. W.; Wang, H. L.; Guo, Z. H.; Zhao, X. J.; Wang, Z. L.; Zhu, G. All-Fabric Ultra-thin Capacitive Sensor with High Pressure Sensitivity and Broad Detection Range for Electronic Skin. *ACS Appl. Mater. Interfaces* **2021**, *13*, 24062–24069.
- (372) Laurila, M. M.; Peltokangas, M.; Montero, K. L.; Verho, J.; Haapala, M.; Oksala, N.; Vehkaoja, A.; Mäntysalo, M. Self-Powered, High Sensitivity Printed E-Tattoo Sensor for Unobtrusive Arterial Pulse Wave Monitoring. *Nano Energy* **2022**, *102*, 107625.
- (373) Lozano Montero, K.; Laurila, M. M.; Peltokangas, M.; Haapala, M.; Verho, J.; Oksala, N.; Vehkaoja, A.; Mäntysalo, M. Self-Powered, Ultra-thin, and Transparent Printed Pressure Sensor for Biosignal Monitoring. *ACS Appl. Electron. Mater.* **2021**, *3*, 4362–4375.
- (374) Cao, Y. Q.; Figueroa, J.; Li, W.; Chen, Z. Q.; Wang, Z. L.; Sepúlveda, N. Understanding the Dynamic Response in Ferroelectric Nanogenerators to Enable Self-Powered Tactile Systems and Human-Controlled Micro-Robots. *Nano Energy* **2019**, *63*, 103852.
- (375) Yi, Z. R.; Liu, Z. X.; Li, W. B.; Ruan, T.; Chen, X.; Liu, J. Q.; Yang, B.; Zhang, W. M. Piezoelectric Dynamics of Arterial Pulse for Wearable Continuous Blood Pressure Monitoring. *Adv. Mater.* **2022**, *34*, 2110291.
- (376) Liu, Y. M.; Wang, L. Y.; Zhao, L.; Yao, K. M.; Xie, Z. Q.; Zi, Y. L.; Yu, X. G. Thin, Skin-Integrated, Stretchable Triboelectric Nanogenerators for Tactile Sensing. *Adv. Electron. Mater.* **2020**, *6*, 1901174.
- (377) Wong, T. H.; Liu, Y. M.; Li, J.; Yao, K. M.; Liu, S. T.; Yiu, C. K.; Huang, X. C.; Wu, M. G.; Park, W.; Zhou, J. K.; et al. Triboelectric Nanogenerator Tattoos Enabled by Epidermal Electronic Technologies. *Adv. Funct. Mater.* **2022**, *32*, 2111269.
- (378) Liu, R.; Lai, Y.; Li, S.; Wu, F.; Shao, J.; Liu, D.; Dong, X.; Wang, J.; Wang, Z. L. Ultrathin, Transparent, and Robust Self-Healing Electronic Skins for Tactile and Non-Contact Sensing. *Nano Energy* **2022**, *95*, 107056.
- (379) Peng, X.; Dong, K.; Zhang, Y.; Wang, L.; Wei, C.; Lv, T.; Wang, Z. L.; Wu, Z. Sweat-Permeable, Biodegradable, Transparent and Self-Powered Chitosan-Based Electronic Skin with Ultrathin Elastic Gold Nanofibers. *Adv. Funct. Mater.* **2022**, *32*, 2112241.
- (380) Wang, S. H.; Xu, J.; Wang, W. C.; Wang, G. J. N.; Rastak, R.; Molina-Lopez, F.; Chung, J. W.; Niu, S.; Feig, V. R.; Lopez, J.; et al. Skin Electronics from Scalable Fabrication of an Intrinsically Stretchable Transistor Array. *Nature* **2018**, *555*, 83–88.
- (381) Huang, Y. C.; Liu, Y.; Ma, C.; Cheng, H.-C.; He, Q. Y.; Wu, H.; Wang, C.; Lin, C. Y.; Huang, Y.; Duan, X. F. Sensitive Pressure Sensors Based on Conductive Microstructured Air-Gap Gates and Two-Dimensional Semiconductor Transistors. *Nat. Electron.* **2020**, *3*, 59–69.
- (382) Park, Y. J.; Sharma, B. K.; Shinde, S. M.; Kim, M. S.; Jang, B.; Kim, J. H.; Ahn, J. H. All MoS₂-Based Large Area, Skin-Attachable Active-Matrix Tactile Sensor. *ACS Nano* **2019**, *13*, 3023–3030.
- (383) Xu, H. C.; Gao, L. B.; Zhao, H. T.; Huang, H. L.; Wang, Y. J.; Chen, G.; Qin, Y. X.; Zhao, N. J.; Xu, D. D.; Duan, L.; et al. Stretchable and Anti-Impact Iontronic Pressure Sensor with an Ultrabroad Linear Range for Biophysical Monitoring and Deep Learning-Aided Knee Rehabilitation. *Microsyst. Nanoeng.* **2021**, *7*, 92.
- (384) Liu, Q. X.; Liu, Z. G.; Li, C. G.; Xie, K. W.; Zhu, P.; Shao, B. Q.; Zhang, J. M.; Yang, J. L.; Zhang, J.; Wang, Q.; et al. Highly Transparent and Flexible Iontronic Pressure Sensors Based on an Opaque to Transparent Transition. *Adv. Sci.* **2020**, *7*, 2000348.
- (385) Ha, K. H.; Zhang, W. Y.; Jang, H.; Kang, S.; Wang, L.; Tan, P.; Hwang, H.; Lu, N. Highly Sensitive Capacitive Pressure Sensors over a Wide Pressure Range Enabled by the Hybrid Responses of a Highly Porous Nanocomposite. *Adv. Mater.* **2021**, *33*, 2103320.
- (386) Yu, J. B.; Hou, X. J.; Cui, M.; Zhang, S. N.; He, J.; Geng, W. P.; Mu, J. L.; Chou, X. J. Highly Skin-Conformal Wearable Tactile Sensor Based on Piezoelectric-Enhanced Triboelectric Nanogenerator. *Nano Energy* **2019**, *64*, 103923.
- (387) Wang, H. L.; Guo, Z. H.; Pu, X.; Wang, Z. L. Ultralight Iontronic Triboelectric Mechanoreceptor with High Specific Outputs for Epidermal Electronics. *Nanomicro Lett.* **2022**, *14*, 86.
- (388) Hu, H. J.; Zhu, X.; Wang, C. H.; Zhang, L.; Li, X. S.; Lee, S.; Huang, Z. L.; Chen, R. M.; Chen, Z. Y.; Wang, C. F.; et al. Stretchable Ultrasonic Transducer Arrays for Three-Dimensional Imaging on Complex Surfaces. *Sci. Adv.* **2018**, *4*, eaar3979.
- (389) Sempionatto, J. R.; Lin, M.; Yin, L.; De la Paz, E.; Pei, K.; Sonaard, T.; de Loyola Silva, A. N.; Khorshed, A. A.; Zhang, F.; Tostado, N.; Xu, S.; Wang, J.; et al. An Epidermal Patch for the Simultaneous Monitoring of Haemodynamic and Metabolic Biomarkers. *Nat. Biomed. Eng.* **2021**, *5*, 737–748.
- (390) Ruth, S. R. A.; Feig, V. R.; Tran, H.; Bao, Z. N. Microengineering Pressure Sensor Active Layers for Improved Performance. *Adv. Funct. Mater.* **2020**, *30*, 2003491.
- (391) Fan, W. J.; He, Q.; Meng, K. Y.; Tan, X. L.; Zhou, Z. H.; Zhang, G. Q.; Yang, J.; Wang, Z. L. Machine-Knitted Washable Sensor Array Textile for Precise Epidermal Physiological Signal Monitoring. *Sci. Adv.* **2020**, *6*, eaay2840.
- (392) Meng, K. Y.; Chen, J.; Li, X. S.; Wu, Y. F.; Fan, W. J.; Zhou, Z. H.; He, Q.; Wang, X.; Fan, X.; Zhang, Y. X.; et al. Flexible Weaving Constructed Self-Powered Pressure Sensor Enabling Continuous Diagnosis of Cardiovascular Disease and Measurement of Cuffless Blood Pressure. *Adv. Funct. Mater.* **2019**, *29*, 1806388.
- (393) Guo, H.; Chen, J.; Tian, L.; Leng, Q.; Xi, Y.; Hu, C. Airflow-Induced Triboelectric Nanogenerator as a Self-Powered Sensor for Detecting Humidity and Airflow Rate. *ACS Appl. Mater. Interfaces* **2014**, *6*, 17184–17189.
- (394) Barsotti, J.; Rapisarda, A. G.; Hirata, I.; Greco, F.; Cacialli, F.; Mattoli, V. Ultra-thin, Ultra-Conformable, and Free-Standing Tattooable Organic Light-Emitting Diodes. *Adv. Electron. Mater.* **2021**, *7*, 2001145.
- (395) Lu, Q.; Yang, Z. C.; Meng, X.; Yue, Y. F.; Ahmad, M. A.; Zhang, W. J.; Zhang, S. S.; Zhang, Y. Q.; Liu, Z. H.; Chen, W. A Review on Encapsulation Technology from Organic Light Emitting Diodes to Organic and Perovskite Solar Cells. *Adv. Funct. Mater.* **2021**, *31*, 2100151.
- (396) Wijshoff, R. W. C. G. R.; Mischi, M.; Veen, J.; van der Lee, A. M.; Aarts, R. M. Reducing Motion Artifacts in Photoplethysmograms by Using Relative Sensor Motion Phantom Study. *J. Biomed. Optics* **2012**, *17*, 117007.
- (397) Lee, G. H.; Kang, H.; Chung, J. W.; Lee, Y.; Yoo, H.; Jeong, S.; Cho, H.; Kim, J. Y.; Kang, S. G.; Jung, J. Y.; et al. Stretchable Ppg Sensor with Light Polarization for Physical Activity-Permissible Monitoring. *Sci. Adv.* **2022**, *8*, eabm3622.
- (398) Lo, L. W.; Zhao, J.; Wan, H.; Wang, Y.; Chakrabarty, S.; Wang, C. An Inkjet-Printed Pedot:Pss-Based Stretchable Conductor for

Wearable Health Monitoring Device Applications. *ACS Appl. Mater. Interfaces* **2021**, *13*, 21693–21702.

(399) Li, H.; Ma, Y.; Liang, Z.; Wang, Z.; Cao, Y.; Xu, Y.; Zhou, H.; Lu, B.; Chen, Y.; Han, Z.; et al. Wearable Skin-Like Optoelectronic Systems with Suppression of Motion Artifacts for Cuff-Less Continuous Blood Pressure Monitor. *Natl. Sci. Rev.* **2020**, *7*, 849–862.

(400) Jeong, H.; Wang, L.; Ha, T.; Mitbender, R.; Yang, X.; Dai, Z.; Qiao, S.; Shen, L.; Sun, N.; Lu, N. Modular and Reconfigurable Wireless E-Tattoos for Personalized Sensing. *Adv. Mater. Technol.* **2019**, *4*, 1900117.

(401) Lee, H.; Kim, E.; Lee, Y.; Kim, H.; Lee, J.; Kim, M.; Yoo, H.-J.; Yoo, S. Toward All-Day Wearable Health Monitoring: An Ultralow-Power, Reflective Organic Pulse Oximetry Sensing Patch. *Sci. Adv.* **2018**, *4*, eaas9530.

(402) Jinno, H.; Yokota, T.; Koizumi, M.; Yukita, W.; Saito, M.; Osaka, I.; Fukuda, K.; Someya, T. Self-Powered Ultraflexible Photonic Skin for Continuous Bio-Signal Detection Via Air-Operation-Stable Polymer Light-Emitting Diodes. *Nat. Commun.* **2021**, *12*, 2234.

(403) Han, D.; Khan, Y.; Ting, J.; Zhu, J.; Combe, C.; Wadsworth, A.; McCulloch, I.; Arias, A. C. Pulse Oximetry Using Organic Optoelectronics under Ambient Light. *Adv. Mater. Technol.* **2020**, *5*, 1901122.

(404) Han, D.; Kim, H.; Lee, S.; Seo, M.; Yoo, S. Realization of Efficient Semitransparent Organic Photovoltaic Cells with Metallic Top Electrodes: Utilizing the Tunable Absorption Asymmetry. *Opt. Express* **2010**, *18*, A513–A521.

(405) Kim, J.; Salvatore, G. A.; Araki, H.; Chiarelli, A. M.; Xie, Z.; Banks, A.; Sheng, X.; Liu, Y.; Lee, J. W.; Jang, K. I.; et al. Battery-Free, Stretchable Optoelectronic Systems for Wireless Optical Characterization of the Skin. *Sci. Adv.* **2016**, *2*, e1600418.

(406) Jacobson, H. The Informational Capacity of the Human Eye. *Science* **1951**, *113*, 292–293.

(407) Bonaque-González, S.; Trujillo-Sevilla, J. M.; Velasco-Ocaña, M.; Casanova-González, O.; Sicilia-Cabrera, M.; Roqué-Velasco, A.; Ceruso, S.; Oliva-García, R.; Martín-Hernández, J.; Gomez-Cardenas, O.; et al. The Optics of the Human Eye at 8.6 μm Resolution. *Sci. Rep.* **2021**, *11*, 23334.

(408) Choi, M.; Bae, S.-R.; Hu, L.; Hoang, A. T.; Kim, S. Y.; Ahn, J.-H. Full-Color Active-Matrix Organic Light-Emitting Diode Display on Human Skin Based on a Large-Area MoS₂ Backplane. *Sci. Adv.* **2020**, *6*, eabb5898.

(409) Choi, M. K.; Yang, J.; Kang, K.; Kim, D. C.; Choi, C.; Park, C.; Kim, S. J.; Chae, S. I.; Kim, T. H.; Kim, J. H.; et al. Wearable Red-Green-Blue Quantum Dot Light-Emitting Diode Array Using High-Resolution Intaglio Transfer Printing. *Nat. Commun.* **2015**, *6*, 7149.

(410) Lee, Y.; Chung, J. W.; Lee, G. H.; Kang, H.; Kim, J. Y.; Bae, C.; Yoo, H.; Jeong, S.; Cho, H.; Kang, S. G.; et al. Standalone Real-time Health Monitoring Patch Based on a Stretchable Organic Optoelectronic System. *Sci. Adv.* **2021**, *7*, eabg9180.

(411) Zhang, Z. T.; Wang, W. C.; Jiang, Y. W.; Wang, Y. X.; Wu, Y. L.; Lai, J. C.; Niu, S. M.; Xu, C. Y.; Shih, C. C.; Wang, C.; et al. High-Brightness All-Polymer Stretchable Led with Charge-Trapping Dilution. *Nature* **2022**, *603*, 624–630.

(412) Koo, J. H.; Jeong, S.; Shim, H. J.; Son, D.; Kim, J.; Kim, D. C.; Choi, S.; Hong, J.-I.; Kim, D. H. Wearable Electrocardiogram Monitor Using Carbon Nanotube Electronics and Color-Tunable Organic Light-Emitting Diodes. *ACS Nano* **2017**, *11*, 10032–10041.

(413) Davis, A.; Deane, G.; Diffey, B. Possible Dosimeter for Ultraviolet Radiation. *Nature* **1976**, *261*, 169–170.

(414) Huang, X. Y.; Chalmers, A. N. Review of Wearable and Portable Sensors for Monitoring Personal Solar UV Exposure. *Ann. Biomed. Eng.* **2021**, *49*, 964–978.

(415) Araki, H.; Kim, J.; Zhang, S.; Banks, A.; Crawford, K. E.; Sheng, X.; Gutruf, P.; Shi, Y.; Pielak, R. M.; Rogers, J. A. Materials and Device Designs for an Epidermal UV Colorimetric Dosimeter with near Field Communication Capabilities. *Adv. Funct. Mater.* **2017**, *27*, 1604465.

(416) Shi, Y.; Manco, M.; Moyal, D.; Huppert, G.; Araki, H.; Banks, A.; Joshi, H.; McKenzie, R.; Seewald, A.; Griffin, G.; et al. Soft, Stretchable, Epidermal Sensor with Integrated Electronics and

Photochemistry for Measuring Personal UV Exposures. *PLoS One* **2018**, *13*, No. e0190233.

(417) Kim, Y.; Suh, J. M.; Shin, J.; Liu, Y.; Yeon, H.; Qiao, K.; Kum, H. S.; Kim, C.; Lee, H. E.; Choi, C.; et al. Chip-Less Wireless Electronic Skins by Remote Epitaxial Freestanding Compound Semiconductors. *Science* **2022**, *377*, 859–864.

(418) Hughes, D.; Lammie, J.; Correll, N. A Robotic Skin for Collision Avoidance and Affective Touch Recognition. *IEEE Robot. Autom. Lett.* **2018**, *3*, 1386–1393.

(419) Zhang, W. F.; Liu, Y. L.; Pei, X.; Yuan, Z. H.; Zhang, Y.; Zhao, Z. H.; Hao, H.; Long, R.; Liu, N. Stretchable MoS₂ Artificial Photoreceptors for E-Skin. *Adv. Funct. Mater.* **2022**, *32*, 2107524.

(420) Sekitani, T.; Someya, T. Stretchable, Large-Area Organic Electronics. *Adv. Mater.* **2010**, *22*, 2228–2246.

(421) Lee, Y.; Cho, H.; Yoon, H.; Kang, H.; Yoo, H.; Zhou, H.; Jeong, S.; Lee, G. H.; Kim, G.; Go, G. T.; et al. Advancements in Electronic Materials and Devices for Stretchable Displays. *Adv. Mater. Technol.* **2023**, *8*, 2201067.

(422) Smarr, B. L.; Aschbacher, K.; Fisher, S. M.; Chowdhary, A.; Dilchert, S.; Puldon, K.; Rao, A.; Hecht, F. M.; Mason, A. E. Feasibility of Continuous Fever Monitoring Using Wearable Devices. *Sci. Rep.* **2020**, *10*, 21640.

(423) Li, R. T.; Kling, S. R.; Salata, M. J.; Cupp, S. A.; Sheehan, J.; Voos, J. E. Wearable Performance Devices in Sports Medicine. *Sports Health: A Multidisciplinary Approach* **2016**, *8*, 74–78.

(424) Mistry, K. K.; Mahapatra, A. Design and Simulation of a Thermo Transfer Type Memes Based Micro Flow Sensor for Arterial Blood Flow Measurement. *Microsys. Technol.* **2012**, *18*, 683–692.

(425) Park, M.; Do, K.; Kim, J.; Son, D.; Koo, J. H.; Park, J.; Song, J. K.; Kim, J. H.; Lee, M.; Hyeon, T.; et al. Oxide Nanomembrane Hybrids with Enhanced Mechano- and Thermo-Sensitivity for Semitransparent Epidermal Electronics. *Adv. Healthc. Mater.* **2015**, *4*, 992–997.

(426) Kireev, D.; Kampfe, J.; Hall, A.; Akinwande, D. Graphene Electronic Tattoos 2.0 with Enhanced Performance, Breathability and Robustness. *npj 2D Mater. Appl.* **2022**, *6*, 46.

(427) Zhu, C. X.; Chortos, A.; Wang, Y.; Pfattner, R.; Lei, T.; Hinckley, A. C.; Pochorovski, I.; Yan, X. Z.; To, J. W. F.; Oh, J. Y.; et al. Stretchable Temperature-Sensing Circuits with Strain Suppression Based on Carbon Nanotube Transistors. *Nat. Electron.* **2018**, *1*, 183–190.

(428) Cui, Z.; Poblete, F. R.; Zhu, Y. Tailoring the Temperature Coefficient of Resistance of Silver Nanowire Nanocomposites and Their Application as Stretchable Temperature Sensors. *ACS Appl. Mater. Interfaces* **2019**, *11*, 17836–17842.

(429) Joh, H.; Lee, S. W.; Seong, M.; Lee, W. S.; Oh, S. J. Engineering the Charge Transport of Ag Nanocrystals for Highly Accurate, Wearable Temperature Sensors through All-Solution Processes. *Small* **2017**, *13*, 1700247.

(430) Park, T. H.; Park, S.; Yu, S.; Park, S.; Lee, J.; Kim, S.; Jung, Y.; Yi, H. Highly Sensitive on-Skin Temperature Sensors Based on Biocompatible Hydrogels with Thermoresponsive Transparency and Resistivity. *Adv. Healthc. Mater.* **2021**, *10*, 2100469.

(431) Lei, Z. Y.; Wang, Q. K.; Wu, P. Y. A Multifunctional Skin-Like Sensor Based on a 3D Printed Thermo-Responsive Hydrogel. *Mater. Horiz.* **2017**, *4*, 694–700.

(432) Yamamoto, Y.; Yamamoto, D.; Takada, M.; Naito, H.; Arie, T.; Akita, S.; Takei, K. Efficient Skin Temperature Sensor and Stable Gel-Less Sticky Ecg Sensor for a Wearable Flexible Healthcare Patch. *Adv. Healthc. Mater.* **2017**, *6*, 1700495.

(433) Zhang, Y. H.; Webb, R. C.; Luo, H. Y.; Xue, Y. G.; Kurniawan, J.; Cho, N. H.; Krishnan, S.; Li, Y.; Huang, Y.; Rogers, J. A. Theoretical and Experimental Studies of Epidermal Heat Flux Sensors for Measurements of Core Body Temperature. *Adv. Healthc. Mater.* **2016**, *5*, 119–127.

(434) Kim, J.; Campbell, A. S.; Wang, J. Wearable Non-Invasive Epidermal Glucose Sensors: A Review. *Talanta* **2018**, *177*, 163–170.

(435) Yu, Y.; Nyein, H. Y. Y.; Gao, W.; Javey, A. Flexible Electrochemical Bioelectronics: The Rise of in Situ Bioanalysis. *Adv. Mater.* **2020**, *32*, 1902083.

- (436) Min, J. H.; Sempionatto, J. R.; Teymourian, H.; Wang, J.; Gao, W. Wearable Electrochemical Biosensors in North America. *Biosens. Bioelectron.* **2021**, *172*, 112750.
- (437) Patel, S.; Ershad, F.; Zhao, M.; Isseroff, R. R.; Duan, B.; Zhou, Y. B.; Wang, Y.; Yu, C. J. Wearable Electronics for Skin Wound Monitoring and Healing. *Soft Sci.* **2022**, *2*, 9.
- (438) Tang, N.; Zheng, Y. B.; Cui, D. X.; Haick, H. Multifunctional Dressing for Wound Diagnosis and Rehabilitation. *Adv. Healthc. Mater.* **2021**, *10*, 2101292.
- (439) Wang, C.; Shirzaei Sani, E.; Gao, W. Wearable Bioelectronics for Chronic Wound Management. *Adv. Funct. Mater.* **2022**, *32*, 2111022.
- (440) Mannoor, M. S.; Tao, H.; Clayton, J. D.; Sengupta, A.; Kaplan, D. L.; Naik, R. R.; Verma, N.; Omenetto, F. G.; McAlpine, M. C. Graphene-Based Wireless Bacteria Detection on Tooth Enamel. *Nat. Commun.* **2012**, *3*, 763.
- (441) Senior, M. Novartis Signs up for Google Smart Lens. *Nat. Biotechnol.* **2014**, *32*, 856.
- (442) Bandodkar, A. J.; Molinnus, D.; Mirza, O.; Guinovart, T.; Windmiller, J. R.; Valdes-Ramirez, G.; Andrade, F. J.; Schoning, M. J.; Wang, J. Epidermal Tattoo Potentiometric Sodium Sensors with Wireless Signal Transduction for Continuous Non-Invasive Sweat Monitoring. *Biosens. Bioelectron.* **2014**, *54*, 603–609.
- (443) Bandodkar, A. J.; Jia, W. Z.; Yardimci, C.; Wang, X.; Ramirez, J.; Wang, J. Tattoo-Based Noninvasive Glucose Monitoring: A Proof-of-Concept Study. *Anal. Chem.* **2015**, *87*, 394–398.
- (444) Shirzaei Sani, E.; Xu, C.; Wang, C.; Song, Y.; Min, J.; Tu, J.; Solomon, S. A.; Li, J.; Banks, J. L.; Armstrong, D. G.; Gao, W. A Stretchable Wireless Wearable Bioelectronic System for Multiplexed Monitoring and Combination Treatment of Infected Chronic Wounds. *Sci. Adv.* **2023**, *9*, eadf7388.
- (445) Bandodkar, A. J.; Hung, V. W.; Jia, W. Z.; Valdes-Ramirez, G.; Windmiller, J. R.; Martinez, A. G.; Ramirez, J.; Chan, G.; Kerman, K.; Wang, J. Tattoo-Based Potentiometric Ion-Selective Sensors for Epidermal pH Monitoring. *Analyst* **2013**, *138*, 123–128.
- (446) Pal, A.; Nadiger, V. G.; Goswami, D.; Martinez, R. V. Conformal, Waterproof Electronic Decals for Wireless Monitoring of Sweat and Vaginal pH at the Point-of-Care. *Biosens. Bioelectron.* **2020**, *160*, 112206.
- (447) Kim, J.; de Araujo, W. R.; Samek, I. A.; Bandodkar, A. J.; Jia, W. Z.; Brunetti, B.; Paixão, T. R. L. C.; Wang, J. Wearable Temporary Tattoo Sensor for Real-Time Trace Metal Monitoring in Human Sweat. *Electrochem. Commun.* **2015**, *51*, 41–45.
- (448) Imani, S.; Bandodkar, A. J.; Mohan, A. M. V.; Kumar, R.; Yu, S. F.; Wang, J.; Mercier, P. P. A Wearable Chemical-Electrophysiological Hybrid Biosensing System for Real-Time Health and Fitness Monitoring. *Nat. Commun.* **2016**, *7*, 11650.
- (449) Lee, H.; Song, C.; Hong, Y. S.; Kim, M.; Cho, H. R.; Kang, T.; Shin, K.; Choi, S. H.; Hyeon, T.; Kim, D. H. Wearable/Disposable Sweat-Based Glucose Monitoring Device with Multistage Transdermal Drug Delivery Module. *Sci. Adv.* **2017**, *3*, e1601314.
- (450) Chen, Y. H.; Lu, S. Y.; Zhang, S. S.; Li, Y.; Qu, Z.; Chen, Y.; Lu, B. W.; Wang, X. Y.; Feng, X. Skin-Like Biosensor System Via Electrochemical Channels for Noninvasive Blood Glucose Monitoring. *Sci. Adv.* **2017**, *3*, e1701629.
- (451) Koh, A.; Kang, D.; Xue, Y. G.; Lee, S.; Pielak, R. M.; Kim, J.; Hwang, T.; Min, S.; Banks, A.; Bastien, P.; Manco, M. C.; et al. Soft, Wearable Microfluidic Device for the Capture, Storage, and Colorimetric Sensing of Sweat. *Sci. Transl. Med.* **2016**, *8*, 366ra165.
- (452) Kim, S. B.; Zhang, Y.; Won, S. M.; Bandodkar, A. J.; Sekine, Y.; Xue, Y.; Koo, J.; Harshman, S. W.; Martin, J. A.; Park, J. M.; et al. Super-Absorbent Polymer Valves and Colorimetric Chemistries for Time-Sequenced Discrete Sampling and Chloride Analysis of Sweat Via Skin-Mounted Soft Microfluidics. *Small* **2018**, *14*, 1703334.
- (453) Yin, L.; Cao, M.; Kim, K. N.; Lin, M.; Moon, J.-M.; Sempionatto, J. R.; Yu, J.; Liu, R.; Wicker, C.; Trifonov, A.; et al. A Stretchable Epidermal Sweat Sensing Platform with an Integrated Printed Battery and Electrochromic Display. *Nat. Electron.* **2022**, *5*, 694–705.
- (454) Mogera, U.; Guo, H.; Namkoong, M.; Rahman, M. S.; Nguyen, T.; Tian, L. M. Wearable Plasmonic Paper-Based Microfluidics for Continuous Sweat Analysis. *Sci. Adv.* **2022**, *8*, eabn1736.
- (455) Madhvapathy, S. R.; Patel, M.; Krishnan, S.; Wei, C.; Li, Y.; Xu, S.; Feng, X.; Huang, Y.; Rogers, J. A. Epidermal Electronic Systems for Measuring the Thermal Properties of Human Skin at Depths of up to Several Millimeters. *Adv. Funct. Mater.* **2018**, *28*, 1802083.
- (456) Dargaville, T. R.; Farrugia, B. L.; Broadbent, J. A.; Pace, S.; Upton, Z.; Voelcker, N. H. Sensors and Imaging for Wound Healing: A Review. *Biosens. Bioelectron.* **2013**, *41*, 30–42.
- (457) Guinovart, T.; Valdés-Ramírez, G.; Windmiller, J. R.; Andrade, F. J.; Wang, J. Bandage-Based Wearable Potentiometric Sensor for Monitoring Wound pH. *Electroanalysis* **2014**, *26*, 1345–1353.
- (458) Wallace, H. J.; Stacey, M. C. Levels of Tumor Necrosis Factor-Alpha (Tnf-Alpha) and Soluble Tnf Receptors in Chronic Venous Leg Ulcers—Correlations to Healing Status. *J. Invest. Dermatol.* **1998**, *110*, 292–296.
- (459) Trengove, N. J.; Bielefeldt-Ohmann, H.; Stacey, M. C. Mitogenic Activity and Cytokine Levels in Non-Healing and Healing Chronic Leg Ulcers. *Wound Repair Regen* **2000**, *8*, 13–25.
- (460) Edsberg, L. E.; Wyffels, J. T.; Brogan, M. S.; Fries, K. M. Analysis of the Proteomic Profile of Chronic Pressure Ulcers. *Wound Repair Regen* **2012**, *20*, 378–401.
- (461) Gao, Y. J.; Nguyen, D. T.; Yeo, T.; Lim, S. B.; Tan, W. X.; Madden, L. E.; Jin, L.; Long, J. Y. K.; Aloweni, F. A. B.; Liew, Y. J. A.; et al. A Flexible Multiplexed Immunosensor for Point-of-Care in Situ Wound Monitoring. *Sci. Adv.* **2021**, *7*, eabg9614.
- (462) Lyu, W.; Ma, Y. J.; Chen, S. Y.; Li, H. B.; Wang, P.; Chen, Y.; Feng, X. Flexible Ultrasonic Patch for Accelerating Chronic Wound Healing. *Adv. Healthc. Mater.* **2021**, *10*, 2100785.
- (463) Zhang, L. J.; Jiang, X. X.; Jiang, W.; Li, S.; Chi, Y. X.; Liu, H.; Zhang, M. Y.; Li, J. Y.; Fang, M.; Pan, B.; et al. Infrared Skin-Like Active Stretchable Electronics Based on Organic–Inorganic Composite Structures for Promotion of Cutaneous Wound Healing. *Adv. Mater. Technol.* **2019**, *4*, 1900150.
- (464) Song, J. W.; Ryu, H.; Bai, W. B.; Xie, Z. Q.; Vázquez-Guardado, A.; Nandoliya, K.; Avila, R.; Lee, G.; Song, Z.; Kim, J.; et al. Bioresorbable, Wireless, and Battery-Free System for Electrotherapy and Impedance Sensing at Wound Sites. *Sci. Adv.* **2023**, *9*, eade4687.
- (465) Zeng, C.; Li, H.; Yang, T.; Deng, Z. H.; Yang, Y.; Zhang, Y.; Lei, G. H. Electrical Stimulation for Pain Relief in Knee Osteoarthritis: Systematic Review and Network Meta-Analysis. *Osteoarthritis and Cartilage* **2015**, *23*, 189–202.
- (466) Nguyen, N.; Lin, Z. H.; Barman, S. R.; Korupalli, C.; Cheng, J. Y.; Song, N. X.; Chang, Y.; Mi, F. L.; Song, H. L.; Sung, H. W.; et al. Engineering an Integrated Electroactive Dressing to Accelerate Wound Healing and Monitor Noninvasively Progress of Healing. *Nano Energy* **2022**, *99*, 107393.
- (467) Ying, M.; Bonifas, A. P.; Lu, N. S.; Su, Y. W.; Li, R.; Cheng, H. Y.; Ameen, A.; Huang, Y. G.; Rogers, J. A. Silicon Nanomembranes for Fingertip Electronics. *Nanotechnology* **2012**, *23*, 344004.
- (468) Yu, Y.; Li, J. H.; Solomon, S. A.; Min, J. H.; Tu, J. B.; Guo, W.; Xu, C. H.; Song, Y.; Gao, W. All-Printed Soft Human-Machine Interface for Robotic Physicochemical Sensing. *Sci. Robot.* **2022**, *7*, eabn0495.
- (469) Sunwoo, S. H.; Han, S. I.; Kang, H.; Cho, Y. S.; Jung, D.; Lim, C.; Lim, C.; Cha, M. J.; Lee, S. P.; Hyeon, T.; et al. Stretchable Low-Impedance Nanocomposite Comprised of Ag-Au Core-Shell Nanowires and Pt Black for Epicardial Recording and Stimulation. *Adv. Mater. Technol.* **2020**, *5*, 1900768.
- (470) Yao, K. M.; Zhou, J. K.; Huang, Q. Y.; Wu, M. G.; Yiu, C. K.; Li, J.; Huang, X. C.; Li, D. F.; Su, J. Y.; Hou, S. L.; et al. Encoding of Tactile Information in Hand Via Skin-Integrated Wireless Haptic Interface. *Nat. Mach. Intell.* **2022**, *4*, 893–903.
- (471) Gu, G. Y.; Zhang, N. B.; Xu, H. P.; Lin, S. T.; Yu, Y.; Chai, G. H.; Ge, L. S.; Yang, H. L.; Shao, Q. W.; Sheng, X. J.; et al. A Soft Neuroprosthetic Hand Providing Simultaneous Myoelectric Control and Tactile Feedback. *Nat. Biomed. Eng.* **2023**, *7*, 589–598.

- (472) Dehghan, M.; Farahbod, F. The Efficacy of Thermotherapy and Cryotherapy on Pain Relief in Patients with Acute Low Back Pain, a Clinical Trial Study. *J. Clin. Diagn. Res. JCDR* **2014**, *8*, LC01.
- (473) Choi, S.; Park, J.; Hyun, W.; Kim, J.; Kim, J.; Lee, Y. B.; Song, C.; Hwang, H. J.; Kim, J. H.; Hyeon, T.; et al. Stretchable Heater Using Ligand-Exchanged Silver Nanowire Nanocomposite for Wearable Articular Thermotherapy. *ACS Nano* **2015**, *9*, 6626–6633.
- (474) Roselli, R. J.; Diller, K. R. *Biotransport: Principles and Applications*; Springer, 2011.
- (475) Lee, J.; Sul, H.; Lee, W.; Pyun, K. R.; Ha, I.; Kim, D.; Park, H.; Eom, H.; Yoon, Y.; Jung, J.; et al. Stretchable Skin-Like Cooling/Heating Device for Reconstruction of Artificial Thermal Sensation in Virtual Reality. *Adv. Funct. Mater.* **2020**, *30*, 1909171.
- (476) Choi, M. K.; Park, I.; Kim, D. C.; Joh, E.; Park, O. K.; Kim, J.; Kim, M.; Choi, C.; Yang, J.; Cho, K. W.; et al. Thermally Controlled, Patterned Graphene Transfer Printing for Transparent and Wearable Electronic/Optoelectronic System. *Adv. Funct. Mater.* **2015**, *25*, 7109–7118.
- (477) Derakhshandeh, H.; Aghabaglou, F.; Mccarthy, A.; Mostafavi, A.; Wiseman, C.; Bonick, Z.; Ghanavati, I.; Harris, S.; Kreikemeier-Bower, C.; Moosavi Basri, S. M.; et al. A Wirelessly Controlled Smart Bandage with 3D-Printed Miniaturized Needle Arrays. *Adv. Funct. Mater.* **2020**, *30*, 1905544.
- (478) Soto, F.; Jeerapan, I.; Silva-López, C.; Lopez-Ramirez, M. A.; Chai, I.; Xiaolong, L.; Lv, J.; Kurniawan, J. F.; Martin, I.; Chakravarthy, K.; et al. Noninvasive Transdermal Delivery System of Lidocaine Using an Acoustic Droplet-Vaporization Based Wearable Patch. *Small* **2018**, *14*, 1803266.
- (479) Joo, H.; Lee, Y.; Kim, J.; Yoo, J. S.; Yoo, S.; Kim, S.; Arya, A. K.; Kim, S.; Choi, S. H.; Lu, N.; et al. Soft Implantable Drug Delivery Device Integrated Wirelessly with Wearable Devices to Treat Fatal Seizures. *Sci. Adv.* **2021**, *7*, eabd4639.
- (480) Soto, F.; Mishra, R. K.; Chrostowski, R.; Martin, A.; Wang, J. Epidermal Tattoo Patch for Ultrasound-Based Transdermal Microballistic Delivery. *Adv. Mater. Technol.* **2017**, *2*, 1700210.
- (481) Zou, Y.; Bo, L.; Li, Z. Recent Progress in Human Body Energy Harvesting for Smart Bioelectronic System. *Fundam. Res.* **2021**, *1*, 364.
- (482) Fan, F. R.; Tian, Z. Q.; Wang, Z. L. Flexible Triboelectric Generator. *Nano Energy* **2012**, *1*, 328.
- (483) Ha, M.; Lim, S.; Cho, S.; Lee, Y.; Na, S.; Baig, C.; Ko, H. Skin-Inspired Hierarchical Polymer Architectures with Gradient Stiffness for Spacer-Free, Ultra-thin, and Highly Sensitive Triboelectric Sensors. *ACS Nano* **2018**, *12*, 3964–3974.
- (484) Wang, Z. L.; Song, J. Piezoelectric Nanogenerators Based on Zinc Oxide Nanowire Arrays. *Science* **2006**, *312*, 242–246.
- (485) Yang, Y.; Hu, H. J.; Chen, Z. Y.; Wang, Z. Y.; Jiang, L. M.; Lu, G. X.; Li, X. J.; Chen, R. M.; Jin, J.; Kang, H. C.; et al. Stretchable Nanolayered Thermoelectric Energy Harvester on Complex and Dynamic Surfaces. *Nano Lett.* **2020**, *20*, 4445–4453.
- (486) Du, Y.; Xu, J. Y.; Paul, B.; Eklund, P. Flexible Thermoelectric Materials and Devices. *Appl. Mater. Today* **2018**, *12*, 366–388.
- (487) Zeng, M. X.; Zavanelli, D.; Chen, J. H.; Saeidi-Javash, M.; Du, Y. P.; LeBlanc, S.; Snyder, G. J.; Zhang, Y. L. Printing Thermoelectric Inks toward Next-Generation Energy and Thermal Devices. *Chem. Soc. Rev.* **2022**, *51*, 485–512.
- (488) Li, C.; Cong, S.; Tian, Z.; Song, Y.; Yu, L.; Lu, C.; Shao, Y.; Li, J.; Zou, G.; Rummeli, M. H.; et al. Flexible perovskite solar cell-driven photo-rechargeable lithium-ion capacitor for self-powered wearable strain sensors. *Nano Energy* **2019**, *60*, 247.
- (489) Park, S.; Heo, S. W.; Lee, W.; Inoue, D.; Jiang, Z.; Yu, K.; Jinno, H.; Hashizume, D.; Sekino, M.; Yokota, T.; et al. Self-Powered Ultra-Flexible Electronics Via Nano-Grating-Patterned Organic Photovoltaics. *Nature* **2018**, *561*, 516–521.
- (490) Wangatia, L. M.; Yang, S.; Zabihi, F.; Zhu, M.; Ramakrishna, S. Biomedical Electronics Powered by Solar Cells. *Curr. Opin. Biomed. Eng.* **2020**, *13*, 25–31.
- (491) Banerjee, S.; Slaughter, G. A Tattoo-Like Glucose Abiotic Biofuel Cell. *J. Electroanal. Chem.* **2022**, *904*, 115941.
- (492) Bandodkar, A. J.; You, J. M.; Kim, N. H.; Gu, Y.; Kumar, R.; Mohan, A. M. V.; Kurniawan, J.; Imani, S.; Nakagawa, T.; Parish, B.; et al. Soft, Stretchable, High Power Density Electronic Skin-Based Biofuel Cells for Scavenging Energy from Human Sweat. *Energy Environ. Sci.* **2017**, *10*, 1581–1589.
- (493) Hou, X. J.; Zhong, J. X.; Yang, C. J.; Yang, Y.; He, J.; Mu, J. L.; Geng, W. P.; Chou, X. J. A High-Performance, Single-Electrode and Stretchable Piezo-Triboelectric Hybrid Patch for Omnidirectional Biomechanical Energy Harvesting and Motion Monitoring. *J. Materiomics* **2022**, *8*, 958.
- (494) Stanford, M. G.; Li, J. T.; Chyan, Y.; Wang, Z.; Wang, W.; Tour, J. M. Laser-Induced Graphene Triboelectric Nanogenerators. *ACS Nano* **2019**, *13*, 7166–7174.
- (495) Menge, H. G.; Huynh, N. D.; Hwang, H. J.; Han, S.; Choi, D.; Park, Y. T. Designable Skin-Like Triboelectric Nanogenerators Using Layer-by-Layer Self-Assembled Polymeric Nanocomposites. *ACS Energy Lett.* **2021**, *6*, 2451–2459.
- (496) Chen, X.; Song, Y.; Chen, H.; Zhang, J.; Zhang, H. An Ultra-thin Stretchable Triboelectric Nanogenerator with Coplanar Electrode for Energy Harvesting and Gesture Sensing. *J. Mater. Chem. A* **2017**, *5*, 12361–12368.
- (497) Jiang, Y.; Dong, K.; Li, X.; An, J.; Wu, D. Q.; Peng, X.; Yi, J.; Ning, C.; Cheng, R. W.; Yu, P. T.; et al. Stretchable, Washable, and Ultra-thin Triboelectric Nanogenerators as Skin-Like Highly Sensitive Self-Powered Haptic Sensors. *Adv. Funct. Mater.* **2021**, *31*, 2005584.
- (498) Liu, Y. M.; Zhao, L.; Wang, L. Y.; Zheng, H. Y.; Li, D. F.; Avila, R.; Lai, K. W. C.; Wang, Z. K.; Xie, Z. Q.; Zi, Y. L.; et al. Skin-Integrated Graphene-Embedded Lead Zirconate Titanate Rubber for Energy Harvesting and Mechanical Sensing. *Adv. Mater. Technol.* **2019**, *4*, 1900744.
- (499) Wang, X. Y.; Ling, X.; Hu, Y.; Hu, X. R.; Zhang, Q.; Sun, K.; Xiang, Y. Electronic Skin Based on PLLA/TFT/PVDF-TrFE Array for Multi-Functional Tactile Sensing and Visualized Restoring. *Chem. Eng. J.* **2022**, *434*, 134735.
- (500) Park, K. I.; Son, J. H.; Hwang, G. T.; Jeong, C. K.; Ryu, J.; Koo, M.; Choi, I.; Lee, S. H.; Byun, M.; Wang, Z. L.; et al. Highly-Efficient, Flexible Piezoelectric PZT Thin Film Nanogenerator on Plastic Substrates. *Adv. Mater.* **2014**, *26*, 2514–2520.
- (501) Shin, S. H.; Kim, Y. H.; Lee, M. H.; Jung, J.-Y.; Nah, J. Hemispherically Aggregated BaTiO₃ Nanoparticle Composite Thin Film for High-Performance Flexible Piezoelectric Nanogenerator. *ACS Nano* **2014**, *8*, 2766–2773.
- (502) He, S.; Guo, Y.; Guo, R.; Fu, X.; Guan, L.; Liu, H. Piezoelectric Nanogenerators Based on Self-Poled Two-Dimensional Li-Doped ZnO Microdisks. *J. Electron. Mater.* **2019**, *48*, 2886.
- (503) Lu, L. J.; Ding, W. Q.; Liu, J. Q.; Yang, B. Flexible PVDF Based Piezoelectric Nanogenerators. *Nano Energy* **2020**, *78*, 105251.
- (504) Jin, C. R.; Hao, N. J.; Xu, Z.; Trase, I.; Nie, Y.; Dong, L.; Closson, A.; Chen, Z.; Zhang, J. X. J. Flexible Piezoelectric Nanogenerators Using Metal-Doped ZnO-PVDF Films. *Sens. Actuators A Phys.* **2020**, *305*, 111912.
- (505) Khan, M. B.; Kim, D. H.; Han, J. H.; Saif, H.; Lee, H.; Lee, Y.; Kim, M.; Jang, E.; Hong, S. K.; Joe, D. J.; et al. Performance Improvement of Flexible Piezoelectric Energy Harvester for Irregular Human Motion with Energy Extraction Enhancement Circuit. *Nano Energy* **2019**, *58*, 211–219.
- (506) Yu, Y.; Zhai, J. F.; Xia, Y.; Dong, S. J. Single Wearable Sensing Energy Device Based on Photoelectric Biofuel Cells for Simultaneous Analysis of Perspiration and Illuminance. *Nanoscale* **2017**, *9*, 11846–11850.
- (507) Falk, M.; Pankratov, D.; Lindh, L.; Arnebrant, T.; Shleev, S. Miniature Direct Electron Transfer Based Enzymatic Fuel Cell Operating in Human Sweat and Saliva. *Fuel Cells* **2014**, *14*, 1050–1056.
- (508) Shitanda, I.; Fujimura, Y.; Takarada, T.; Suzuki, R.; Aikawa, T.; Itagaki, M.; Tsujimura, S. Self-Powered Diaper Sensor with Wireless Transmitter Powered by Paper-Based Biofuel Cell with Urine Glucose as Fuel. *ACS Sensors* **2021**, *6*, 3409–3415.
- (509) Malik, Y. T.; Akbar, Z. A.; Seo, J. Y.; Cho, S.; Jang, S. Y.; Jeon, J. W. Self-Healable Organic-Inorganic Hybrid Thermoelectric Materials

- with Excellent Ionic Thermoelectric Properties. *Adv. Energy Mater.* **2022**, *12*, 2103070.
- (510) Wang, L.; Zhang, Z.; Geng, L.; Yuan, T.; Liu, Y.; Guo, J.; Fang, L.; Qiu, J.; Wang, S. Solution-Printable Fullerene/TiS₂ Organic/Inorganic Hybrids for High-Performance Flexible N-Type Thermoelectrics. *Energy & Environ. Sci.* **2018**, *11*, 1307–1317.
- (511) Prunet, G.; Pawula, F.; Fleury, G.; Cloutet, E.; Robinson, A. J.; Hadziioannou, G.; Pakdel, A. A Review on Conductive Polymers and Their Hybrids for Flexible and Wearable Thermoelectric Applications. *Mater. Today Phys.* **2021**, *18*, 100402.
- (512) Bharti, M.; Singh, A.; Samanta, S.; Aswal, D. K. Conductive Polymers for Thermoelectric Power Generation. *Prog. Mater. Sci.* **2018**, *93*, 270–310.
- (513) Zadan, M.; Malakooti, M. H.; Majidi, C. Soft and Stretchable Thermoelectric Generators Enabled by Liquid Metal Elastomer Composites. *ACS Appl. Mater. Interfaces* **2020**, *12*, 17921–17928.
- (514) Suarez, F.; Parekh, D. P.; Ladd, C.; Vashae, D.; Dickey, M. D.; Öztürk, M. C. Flexible Thermoelectric Generator Using Bulk Legs and Liquid Metal Interconnects for Wearable Electronics. *Appl. Energy* **2017**, *202*, 736–745.
- (515) Kim, S. J.; We, J. H.; Cho, B. J. A Wearable Thermoelectric Generator Fabricated on a Glass Fabric. *Energy Environ. Sci.* **2014**, *7*, 1959–1965.
- (516) Tian, Y.; Florenciano, I.; Xia, H. Y.; Li, Q. Y.; Baysal, H. E.; Zhu, D. M.; Ramunni, E.; Meyers, S.; Yu, T. Y.; Baert, K.; et al. Facile Fabrication of Flexible and High-Performing Thermoelectrics by Direct Laser Printing on Plastic Foil. *Adv. Mater.* **2023**, 2307945.
- (517) Zheng, Z. H.; Shi, X. L.; Ao, D. W.; Liu, W. D.; Li, M.; Kou, L. Z.; Chen, Y. X.; Li, F.; Wei, M.; Liang, G. X.; et al. Harvesting Waste Heat with Flexible Bi₂Te₃ Thermoelectric Thin Film. *Nat. Sustain.* **2023**, *6*, 180–191.
- (518) Saeidi-Javash, M.; Kuang, W. Z.; Dun, C. C.; Zhang, Y. L. 3D Conformal Printing and Photonic Sintering of High-Performance Flexible Thermoelectric Films Using 2D Nanoplates. *Adv. Funct. Mater.* **2019**, *29*, 1901930.
- (519) Lee, D.; Park, W.; Kang, Y. A.; Lim, H. T.; Park, S.; Mun, Y.; Kim, J.; Jang, K. S. Substrate-Free Thermoelectric 25 μm -Thick Ag₂Se Films with High Flexibility and in-Plane zT of 0.5 at Room Temperature. *ACS Appl. Mater. Interfaces* **2023**, *15*, 3047–3053.
- (520) Oh, J. Y.; Lee, J. H.; Han, S. W.; Chae, S. S.; Bae, E. J.; Kang, Y. H.; Choi, W. J.; Cho, S. Y.; Lee, J. O.; Baik, H. K.; et al. Chemically Exfoliated Transition Metal Dichalcogenide Nanosheet-Based Wearable Thermoelectric Generators. *Energy & Environ. Sci.* **2016**, *9*, 1696–1705.
- (521) Kim, S.; Mo, J. H.; Jang, K. S. Solution-Processed Carbon Nanotube Bucky papers for Foldable Thermoelectric Generators. *ACS Appl. Mater. Interfaces* **2019**, *11*, 35675–35682.
- (522) Hong, S. H.; Lee, T. C.; Liu, C. L. All-Solution-Processed Polythiophene/Carbon Nanotube Nanocomposites Integrated on Biocompatible Silk Fibroin Substrates for Wearable Thermoelectric Generators. *ACS Applied Energy Materials* **2023**, *6*, 2602–2610.
- (523) Wu, B.; Guo, Y.; Hou, C. Y.; Zhang, Q. H.; Li, Y. G.; Wang, H. Z. From Carbon Nanotubes to Highly Adaptive and Flexible High-Performance Thermoelectric Generators. *Nano Energy* **2021**, *89*, 106487.
- (524) Zeng, W.; Tao, X. M.; Lin, S. P.; Lee, C.; Shi, D. L.; Lam, K. H.; Huang, B. L.; Wang, Q. M.; Zhao, Y. Defect-Engineered Reduced Graphene Oxide Sheets with High Electric Conductivity and Controlled Thermal Conductivity for Soft and Flexible Wearable Thermoelectric Generators. *Nano Energy* **2018**, *54*, 163–174.
- (525) Zheng, C. Z.; Xiang, L. Y.; Jin, W. L.; Shen, H. G.; Zhao, W. R.; Zhang, F. J.; Di, C. A.; Zhu, D. B. A Flexible Self-Powered Sensing Element with Integrated Organic Thermoelectric Generator. *Adv. Mater. Technol.* **2019**, *4*, 1900247.
- (526) Li, C. C.; Jiang, F. X.; Liu, C. C.; Wang, W. F.; Li, X. J.; Wang, T. Z.; Xu, J. K. A Simple Thermoelectric Device Based on Inorganic/Organic Composite Thin Film for Energy Harvesting. *Chem. Eng. J.* **2017**, *320*, 201–210.
- (527) Li, X. Y.; Li, P. C.; Wu, Z. B.; Luo, D. Y.; Yu, H. Y.; Lu, Z. H. Review and Perspective of Materials for Flexible Solar Cells. *Mater. Rep. Energy* **2021**, *1*, 100001.
- (528) Carlson, D. E.; Wronski, C. R. Amorphous Silicon Solar Cell. *Appl. Phys. Lett.* **1976**, *28*, 671–673.
- (529) Docampo, P.; Ball, J. M.; Darwich, M.; Eperon, G. E.; Snaith, H. J. Efficient Organometal Trihalide Perovskite Planar-Heterojunction Solar Cells on Flexible Polymer Substrates. *Nat. Commun.* **2013**, *4*, 2761.
- (530) Li, Y. W.; Xu, G. Y.; Cui, C. H.; Li, Y. F. Flexible and Semitransparent Organic Solar Cells. *Adv. Energy Mater.* **2018**, *8*, 1701791.
- (531) Lee, J. W.; Xu, R.; Lee, S.; Jang, K.-I.; Yang, Y.; Banks, A.; Yu, K. J.; Kim, J.; Xu, S.; Ma, S.; et al. Soft, Thin Skin-Mounted Power Management Systems and Their Use in Wireless Thermography. *Proc. Natl. Acad. Sci. U. S. A.* **2016**, *113*, 6131–6136.
- (532) Kaltenbrunner, M.; White, M. S.; Glowacki, E. D.; Sekitani, T.; Someya, T.; Sariciftci, N. S.; Bauer, S. Ultra-thin and Lightweight Organic Solar Cells with High Flexibility. *Nat. Commun.* **2012**, *3*, 770.
- (533) Kim, J.; Banks, A.; Cheng, H.; Xie, Z.; Xu, S.; Jang, K. I.; Lee, J. W.; Liu, Z.; Gutruf, P.; Huang, X.; et al. Epidermal Electronics with Advanced Capabilities in near-Field Communication. *Small* **2015**, *11*, 906–912.
- (534) Jeong, Y. R.; Lee, G.; Park, H.; Ha, J. S. Stretchable, Skin-Attachable Electronics with Integrated Energy Storage Devices for Biosignal Monitoring. *Acc. Chem. Res.* **2019**, *52*, 91–99.
- (535) Lin, R. Z.; Kim, H. J.; Achavananthadith, S.; Xiong, Z.; Lee, J. K. W.; Kong, Y. L.; Ho, J. S. Digitally-Embroidered Liquid Metal Electronic Textiles for Wearable Wireless Systems. *Nat. Commun.* **2022**, *13*, 2190.
- (536) Jeong, Y. R.; Kim, J.; Xie, Z. Q.; Xue, Y. G.; Won, S. M.; Lee, G.; Jin, S. W.; Hong, S. Y.; Feng, X.; Huang, Y. G.; et al. A Skin-Attachable, Stretchable Integrated System Based on Liquid Gains for Wireless Human Motion Monitoring with Multi-Site Sensing Capabilities. *NPG Asia Materials* **2017**, *9*, e443.
- (537) Scidà, A.; Haque, S.; Treossi, E.; Robinson, A.; Smerzi, S.; Ravesi, S.; Borini, S.; Palermo, V. Application of Graphene-Based Flexible Antennas in Consumer Electronic Devices. *Mater. Today* **2018**, *21*, 223.
- (538) Li, J.; Yang, P.; Li, X.; Jiang, C.; Yun, J.; Yan, W.; Liu, K.; Fan, H. J.; Lee, S. W. Ultrathin Smart Energy-Storage Devices for Skin-Interfaced Wearable Electronics. *ACS Energy Lett.* **2023**, *8*, 1–8.
- (539) Berchmans, S.; Bandodkar, A. J.; Jia, W.; Ramirez, J.; Meng, Y. S.; Wang, J. An Epidermal Alkaline Rechargeable Ag–Zn Printable Tattoo Battery for Wearable Electronics. *J. Mater. Chem. A* **2014**, *2*, 15788–15795.
- (540) An, T.; Gong, S.; Ling, Y.; Dong, D.; Zhao, Y.; Cheng, W. Dynamically Functioning and Highly Stretchable Epidermal Supercapacitor Based on Vertically Aligned Gold Nanowire Skins. *EcoMat* **2020**, *2*, e12022.
- (541) Joshi, S. R.; Pratap, A.; Gogurla, N.; Kim, S. Ultrathin, Breathable, Permeable, and Skin-Adhesive Charge Storage Electronic Tattoos Based on Biopolymer Nanofibers and Carbon Nanotubes. *Adv. Electron. Mater.* **2023**, *9*, 2201095.
- (542) Luan, P. S.; Zhang, N.; Zhou, W. Y.; Niu, Z. Q.; Zhang, Q.; Cai, L.; Zhang, X.; Yang, F.; Fan, Q.; Zhou, W. B.; et al. Epidermal Supercapacitor with High Performance. *Adv. Funct. Mater.* **2016**, *26*, 8178–8184.
- (543) Giannakou, P.; Tas, M. O.; Le Borgne, B.; Shkunov, M. Water-Transferred, Inkjet-Printed Supercapacitors toward Conformal and Epidermal Energy Storage. *ACS Appl. Mater. Interfaces* **2020**, *12*, 8456–8465.
- (544) Lv, J.; Yin, L.; Chen, X. H.; Jeerapan, I.; Silva, C. A.; Li, Y.; Le, M.; Lin, Z. H.; Wang, L. W.; Trifonov, A.; et al. Wearable Biosupercapacitor: Harvesting and Storing Energy from Sweat. *Adv. Funct. Mater.* **2021**, *31*, 2102915.
- (545) Vanfleteren, J.; Gonzalez, M.; Bossuyt, F.; Hsu, Y. Y.; Vervust, T.; De Wolf, I.; Jablonski, M. Printed Circuit Board Technology Inspired Stretchable Circuits. *MRS Bull.* **2012**, *37*, 254–260.

- (546) Kim, J. H.; Lee, T. I.; Kim, T. S.; Paik, K. W. The Effect of Anisotropic Conductive Films Adhesion on the Bending Reliability of Chip-in-Flex Packages for Wearable Electronics Applications. *IEEE Trans. Compon. Packaging Manuf. Technol.* **2017**, *7*, 1583–1591.
- (547) Yim, M. J.; Li, Y.; Moon, K. S.; Paik, K. W.; Wong, C. P. Review of Recent Advances in Electrically Conductive Adhesive Materials and Technologies in Electronic Packaging. *J. Adhes. Sci. Technol.* **2008**, *22*, 1593–1630.
- (548) Pan, T. S.; Pharr, M.; Ma, Y. J.; Ning, R.; Yan, Z.; Xu, R.; Feng, X.; Huang, Y. G.; Rogers, J. A. Experimental and Theoretical Studies of Serpentine Interconnects on Ultra-thin Elastomers for Stretchable Electronics. *Adv. Funct. Mater.* **2017**, *27*, 1702589.
- (549) Guo, R.; Sun, X. Y.; Yao, S. Y.; Duan, M. H.; Wang, H. Z.; Liu, J.; Deng, Z. S. Semi-Liquid-Metal-(Ni-Eggin)-Based Ultraconformable Electronic Tattoo. *Adv. Mater. Technol.* **2019**, *4*, 1900183.
- (550) Yin, L. D.; Deng, P. F.; Ma, J. J.; Shen, Y. X.; Ren, J. H.; Zhang, S. C.; Huang, Y. Large-Area, Fully Conformable, μm -Thick E-Tattoo for High-Fidelity in Situ Personal Health Monitoring. *2019 IEEE 19th International Conference on Nanotechnology (IEEE-NANO) 2019*, 211–214.
- (551) Guo, L.; DeWeerth, S. P. High-Density Stretchable Electronics: Toward an Integrated Multilayer Composite. *Adv. Mater.* **2010**, *22*, 4030–4033.
- (552) Huang, Z. L.; Hao, Y. F.; Li, Y.; Hu, H. J.; Wang, C. H.; Nomoto, A.; Pan, T. S.; Gu, Y.; Chen, Y. M.; Zhang, T. J.; et al. Three-Dimensional Integrated Stretchable Electronics. *Nat. Electron.* **2018**, *1*, 473–480.
- (553) Song, H. L.; Luo, G. Q.; Ji, Z. Y.; Bo, R. H.; Xue, Z. G.; Yan, D. J.; Zhang, F.; Bai, K.; Liu, J. X.; Cheng, X.; et al. Highly-Integrated, Miniaturized, Stretchable Electronic Systems Based on Stacked Multilayer Network Materials. *Sci. Adv.* **2022**, *8*, eabm3785.
- (554) Yang, X. X.; Huang, Y. F.; Dai, Z. H.; Barber, J.; Wang, P. L.; Lu, N. S. Cut-and-Paste” Method for the Rapid Prototyping of Soft Electronics. *Sci. China Technol. Sci.* **2019**, *62*, 199–208.
- (555) Niu, S. M.; Matsuhisa, N.; Beker, L.; Li, J. X.; Wang, S. H.; Wang, J. C.; Jiang, Y. W.; Yan, X. Z.; Yun, Y. J.; Burnett, W.; et al. A Wireless Body Area Sensor Network Based on Stretchable Passive Tags. *Nat. Electron.* **2019**, *2*, 361–368.
- (556) Wang, W. C.; Wang, S. H.; Rastak, R.; Ochiai, Y.; Niu, S. M.; Jiang, Y. W.; Arunachala, P. K.; Zheng, Y.; Xu, J.; Matsuhisa, N.; et al. Strain-Insensitive Intrinsically Stretchable Transistors and Circuits. *Nat. Electron.* **2021**, *4*, 143–150.
- (557) Liang, J. J.; Li, L.; Chen, D.; Hajagos, T.; Ren, Z.; Chou, S. Y.; Hu, W.; Pei, Q. B. Intrinsically Stretchable and Transparent Thin-Film Transistors Based on Printable Silver Nanowires, Carbon Nanotubes and an Elastomeric Dielectric. *Nat. Commun.* **2015**, *6*, 7647.
- (558) Cai, L.; Zhang, S. M.; Miao, J. S.; Yu, Z. B.; Wang, C. Fully Printed Stretchable Thin-Film Transistors and Integrated Logic Circuits. *ACS Nano* **2016**, *10*, 11459–11468.
- (559) Xiang, L.; Wang, Y. R.; Xia, F.; Liu, F.; He, D. L.; Long, G. H.; Zeng, X. W.; Liang, X. L.; Jin, C. H.; Wang, Y. W.; et al. An Epidermal Electronic System for Physiological Information Acquisition, Processing, and Storage with an Integrated Flash Memory Array. *Science Advances* **2022**, *8*, eabp8075.
- (560) Son, D.; Koo, J. H.; Song, J. K.; Kim, J.; Lee, M.; Shim, H. J.; Park, M.; Lee, M.; Kim, J. H.; Kim, D. H. Stretchable Carbon Nanotube Charge-Trap Floating-Gate Memoryand Logic Devices for Wearable Electronics. *ACS Nano* **2015**, *9*, 5585–5593.
- (561) Hwang, H.; Kong, M.; Kim, K.; Park, D.; Lee, S.; Park, S.; Song, H. J.; Jeong, U. Stretchable Anisotropic Conductive Film (S-ACF) for Electrical Interfacing in High-Resolution Stretchable Circuits. *Sci. Adv.* **2021**, *7*, eabh0171.
- (562) Jiang, Y.; Ji, S. B.; Sun, J.; Huang, J. P.; Li, Y. H.; Zou, G. J.; Salim, T.; Wang, C. X.; Li, W. L.; Jin, H. R.; et al. A Universal Interface for Plug-and-Play Assembly of Stretchable Devices. *Nature* **2023**, *614*, 456–462.
- (563) Wang, Z. X.; Volinsky, A. A.; Gallant, N. D. Crosslinking Effect on Polydimethylsiloxane Elastic Modulus Measured by Custom-Built Compression Instrument. *J. Appl. Polym. Sci.* **2014**, *131*, 41050.
- (564) Li, C. H.; Guan, G. Y.; Reif, R.; Huang, Z. H.; Wang, R. K. Determining Elastic Properties of Skin by Measuring Surface Waves from an Impulse Mechanical Stimulus Using Phase-Sensitive Optical Coherence Tomography. *J. R. Soc. Interface* **2012**, *9*, 831–841.
- (565) Kim, J.; Shim, H. J.; Yang, J.; Choi, M. K.; Kim, D. C.; Kim, J.; Hyeon, T.; Kim, D. H. Ultrathin Quantum Dot Display Integrated with Wearable Electronics. *Adv. Mater.* **2017**, *29*, 1700217.
- (566) Lee, C. H.; Ma, Y.; Jang, K. I.; Banks, A.; Pan, T.; Feng, X.; Kim, J. S.; Kang, D.; Raj, M. S.; McGrane, B. L.; et al. Soft Core/Shell Packages for Stretchable Electronics. *Adv. Funct. Mater.* **2015**, *25*, 3698–3704.
- (567) Xu, S.; Zhang, Y. H.; Jia, L.; Mathewson, K. E.; Jang, K. I.; Kim, J.; Fu, H. R.; Huang, X.; Chava, P.; Wang, R. H.; et al. Soft Microfluidic Assemblies of Sensors, Circuits, and Radios for the Skin. *Science* **2014**, *344*, 70–74.
- (568) Lee, K.; Ni, X. Y.; Lee, J. Y.; Arafa, H.; Pe, D. J.; Xu, S.; Avila, R.; Irie, M.; Lee, J. H.; Easterlin, R. L.; et al. Mechano-Acoustic Sensing of Physiological Processes and Body Motions Via a Soft Wireless Device Placed at the Suprasternal Notch. *Nat. Biomed. Eng.* **2020**, *4*, 148–158.
- (569) Vassileva, S.; Hristakieva, E. Medical Applications of Tattooing. *Clin. Dermatol.* **2007**, *25*, 367–374.
- (570) Takeshita, T.; Yoshida, M.; Takei, Y.; Ouchi, A.; Hinoki, A.; Uchida, H.; Kobayashi, T. Relationship between Contact Pressure and Motion Artifacts in ECG Measurement with Electrostatic Flocked Electrodes Fabricated on Textile. *Sci. Rep.* **2019**, *9*, 5897.
- (571) Huang, Y.; Zhou, J.; Ke, P.; Guo, X.; Yiu, C. K.; Yao, K.; Cai, S.; Li, D.; Zhou, Y.; Li, J.; et al. A Skin-Integrated Multimodal Haptic Interface for Immersive Tactile Feedback. *Nat. Electron.* **2023**, *6*, 1041.
- (572) Li, L. L.; Zhao, L.; Hassan, R.; Ren, H. L. Review on Wearable System for Positioning Ultrasound Scanner. *Machines* **2023**, *11*, 325.
- (573) Dian, F. J.; Yousefi, A.; Lim, S. A Practical Study on Bluetooth Low Energy (BLE) Throughput. *IEEE 9th Annual Information Technology, Electronics and Mobile Communication Conference (IEMCON); IEEE, 2018*; pp 768–771.
- (574) Tan, P.; Lu, N. S. Seeing inside a Body in Motion. *Science* **2022**, *377*, 466–467.
- (575) Min, J. H.; Demchyshyn, S.; Sempionatto, J. R.; Song, Y.; Hailegnaw, B.; Xu, C. H.; Yang, Y. R.; Solomon, S.; Putz, C.; Lehner, L. E.; et al. An Autonomous Wearable Biosensor Powered by a Perovskite Solar Cell. *Nat. Electron.* **2023**, *6*, 630–641.
- (576) Ahn, J. W.; Ku, Y.; Kim, H. C. A Novel Wearable EEG and ECG Recording System for Stress Assessment. *Sensors* **2019**, *19*, 1991.
- (577) Choi, Y. S.; Jeong, H.; Yin, R. T.; Avila, R.; Pfenniger, A.; Yoo, J.; Lee, J. Y.; Tzavelis, A.; Lee, Y. J.; Chen, S. W.; et al. A Transient, Closed-Loop Network of Wireless, Body-Integrated Devices for Autonomous Electrotherapy. *Science* **2022**, *376*, 1006–1012.
- (578) Mickle, A. D.; Won, S. M.; Noh, K. N.; Yoon, J.; Meacham, K. W.; Xue, Y.; McIlvried, L. A.; Copits, B. A.; Saminen, V. K.; Crawford, K. E.; et al. A Wireless Closed-Loop System for Optogenetic Peripheral Neuromodulation. *Nature* **2019**, *565*, 361–365.
- (579) Jeong, H.; Yoo, J. Y.; Ouyang, W.; Greane, A.; Wiebe, A. J.; Huang, I.; Lee, Y. J.; Lee, J. Y.; Kim, J.; Ni, X.; et al. Closed-Loop Network of Skin-Interfaced Wireless Devices for Quantifying Vocal Fatigue and Providing User Feedback. *Proc. Natl. Acad. Sci. U. S. A.* **2023**, *120*, e2219394120.
- (580) Luo, X. J.; Yu, Q.; Liu, Y. Q.; Gai, W. X.; Ye, L.; Yang, L.; Cui, Y. Closed-Loop Diabetes Minipatch Based on a Biosensor and an Electroosmotic Pump on Hollow Biodegradable Microneedles. *ACS Sens.* **2022**, *7*, 1347–1360.
- (581) Topalovic, U.; Barclay, S.; Ling, C.; Alzuhair, A.; Yu, W.; Hokhikyan, V.; Chandrakumar, H.; Rozgic, D.; Jiang, W.; Basir-Kazeruni, S.; et al. A Wearable Platform for Closed-Loop Stimulation and Recording of Single-Neuron and Local Field Potential Activity in Freely Moving Humans. *Nat. Neurosci.* **2023**, *26*, 517–527.